सत्यमेव जयते

[illegible]IAN AGRICULTURAL
[illegible]TITUTE, NEW DELHI

19210

I.A.R.I. 6.
GIPNLK—H-3 I.A.[illegible]—15,000

CANADIAN JOURNAL OF RESEARCH

VOLUME 17
1939

SECTION A

CANADA

19210
IARI

Published by the
NATIONAL
RESEARCH COUNCIL
of CANADA

19210

Canadian Journal of Research

Issued by THE NATIONAL RESEARCH COUNCIL OF CANADA

VOL. 17, SEC. A. JANUARY, 1939 NUMBER 1

LIBRARY

VIBRATIONS ON POWER LINES IN A STEADY WIND

VI. FORCED VIBRATIONS OF UNIFORM STRINGS AND OF STRINGS WITH STRENGTHENED ENDS UNDER THE ACTION OF UNIFORM PERIODIC FORCES[1]

BY R. RUEDY[2]

Abstract

A study of the complete equation expressing the action of a driving force, periodic in time but constant throughout the length of the string and opposed by a damping force proportional to the velocity, leads to formulae suitable for the practical calculation of the shape of standing waves that are produced by a plane wave of sound or by a steady wind. At resonance the amplitude at the midpoint of a uniform string set into a plane wave of sound is proportional to the diameter, to the square root of the intensity of the wave (G erg per sq. cm. per sec.), and inversely proportional to the order of the overtone and to the square root of the frequency. Damping causes the lag between force and motion to differ from point to point, particularly near the nodes, so that even at resonance the wave pattern is not rigorously stationary. On the average, the lag increases from the value zero, obtained when the ratio ν/ν_0 between applied frequency and fundamental frequency is zero, to $\pm\pi/2$ when $\nu/\nu_0 = 1$, increases again from $-\pi/2$ through 0 at $\nu/\nu_0 = 2$, to $\pi/2$ at $\nu/\nu_0 = 3$, and so on.

Action of a Constant Periodic Force upon a Damped String of Uniform Cross Section

When a string that has a cross section of radius a is placed in the field of a plane sound wave of frequency ν and intensity G erg per sec. per sq. cm., the air vibrating in a direction normal to the long axis of the string, each unit length of the string is subject to a lateral force

$$Y = 0.0074\nu a^2\sqrt{G}\epsilon^{-2\pi i\nu t}.$$

The intensity G is equal to the product ps of the sound pressure p and the velocity s of the vibrating air, where p and s denote root mean square values. In ordinary conversation the intensities are of the order of the erg at a distance of a few feet from the source; this intensity corresponds to a pressure variation of 1 dyne per cm., or one-millionth of atmospheric pressure. A sound intensity corresponding to a pressure amplitude of 1 dyne per sq. cm. at a frequency of 1,000 cycles per sec. is sometimes used as a reference point in the measurement of loudness. The pressure variations that occur in speech or music are below 1/100 atm. at the ear.

---

[1] *Manuscript received January 4, 1939.*
Contribution from the Research Plans and Publications Section, National Research Laboratories, Ottawa, Canada.

[2] *Research Investigator, National Research Laboratories, Ottawa.*

Somewhat stronger lateral forces are exerted upon a string when a steady wind of velocity U cm. per sec. blows at a right angle against the wire, and the amplitudes obtained in winds with a speed of 500 to 1200 cm. per sec., a range most favourable to the production of vibrations, become visible to the unaided eye. As shown by theory and confirmed by experiments, the amplitude of the alternating force acting in a direction at right angles to both the uniform wind and the string, as though it were produced by an electrodynamic effect, is equal to

$$G = 1.46\rho a \frac{U^2}{2} ,$$

where ρ is the density of the air (1.25×10^{-3} at 10° C.) and U does not normally exceed 12 metres per sec. for winds that can be called steady. Since the frequency of vibration is $\nu = \dfrac{U}{10a}$,

$$G = 0.09a^3\nu^2 ;$$

the alternating force exerted upon a wire by a steady wind increases, therefore, more rapidly with the radius of the wire and the frequency of the sound than do the forces obtained in the field of a plane wave.

The equation of motion of a string of mass ρ_0 per unit length set into vibration by a force $F\epsilon^{-2\pi i\nu t}$ dyne per cm. that is periodic in time but at any moment constant throughout the length $l = 2L$ of the string, and opposed by a frictional force proportional to the velocity but independent of the actual frequency, $R(x)\,\partial y/\partial t$ dyne per unit length, is

$$\frac{\partial^2 y}{\partial t^2} = \frac{S}{\rho_0}\frac{\partial^2 y}{\partial x^2} + \frac{F}{\rho_0}\epsilon^{-2\pi i\nu t} - \frac{R}{m}\frac{\partial y}{\partial t} .$$

On the assumption that F and R are constant, a solution exists in the form

$$y = Y(x)T(t) = Y(x)\epsilon^{-2\pi i\nu t},$$

so that

$$\frac{d^2Y}{dx^2} + \frac{4\pi^2\nu^2 + 4\pi i\nu k}{c^2} Y + f = \frac{d^2Y}{dx^2} + \frac{w^2}{c^2} Y + f = 0,$$

where

$$f = F/S \text{ and } 2k = R/m.$$

In accordance with the theory of linear differential equations, the solution consists of the complementary function $A \cos wx/c$ obtained when F is zero, and a particular integral. A particular integral of the present equation is found by assuming Y to be a constant, namely, according to the equation, equal to $-fc^2/w^2$, with

$$w^2 = 4\pi^2\nu^2 + 4\pi i\nu k = 4\pi^2\nu^2\left(1 + \frac{ik}{\pi\nu}\right),$$

and for the small values of $2k = R/m$ normally encountered there follows

$$w = 2\pi\nu\left(1 + \frac{ik}{2\pi\nu}\right) = \omega + ik.$$

A complete solution satisfying the boundary conditions $Y = 0$ at $x = -L$ and at $x = +L = l/2$ is

$$Y(x) = \frac{F}{\rho_0 w^2}\,\frac{\cos\frac{w}{c}x - \cos\frac{wl}{2c}}{\cos\frac{wl}{2c}},$$

so that

$$Y(x) = \frac{F}{4\pi^2\rho_0\nu^2\left(1 + \frac{ik}{\nu\pi}\right)}\left\{\frac{\cos\left(\frac{\nu}{\nu_0}\frac{\pi}{2} + \frac{ik}{4\nu_0}\right)\frac{x}{L}}{\cos\left(\frac{\nu}{\nu_0}\frac{\pi}{2} + \frac{ik}{4\nu_0}\right)} - 1\right\}$$

for a small value of k. The solution has the form $Y(x) = A\cos(bx + d) - F/b^2S$. A pure harmonic wave shape is not to be expected since the external force is not proportional to the displacement along the freely vibrating stretched wire.

Discussion of the Equation

When $k = 0$, the expression for the amplitude reduces to the formula given in treatises on sound

$$Y(x) = \frac{F}{4\rho_0\pi^2\nu^2}\left\{\frac{\cos\frac{\nu}{\nu_0}\frac{\pi}{2}\frac{x}{L}}{\cos\frac{\nu}{\nu_0}\frac{\pi}{2}} - 1\right\} = \frac{F}{4\pi^2\rho_0\nu^2}\,\frac{\cos\frac{\nu}{\nu_0}\frac{\pi}{2}\frac{x}{L}}{\cos\frac{\nu}{\nu_0}\frac{\pi}{2}} - \frac{F}{4\pi^2\rho_0\nu^2};$$

it corresponds to a single yet slightly distorted wave that instead of having its equilibrium position along $Y = 0$ is symmetrical, at a given frequency, with respect to the straight line $Y = -F/4\rho_0\pi^2\nu^2$. The excursions in the negative direction are therefore deeper than the displacements in the positive direction. The amplitude at the centre reduces to zero when ν/ν_0 is a multiple of four. The amplitudes tend to become infinite throughout the length of the string whenever the applied frequency is an odd multiple of the fundamental frequency ν_0. Since, according to the Fourier development,

$$1 = \frac{4}{\pi}\left(\sin\pi\frac{x}{l} + \frac{1}{3}\sin 3\pi\frac{x}{l} + \frac{1}{5}\sin 5\pi\frac{x}{l} + \cdots\right)$$

for any value of x between 0 and l, a constant force F has no components that correspond to an even number of loops, and none of the even multiples of the fundamental frequency can be expected to produce resonance.

In order to arrive at results that apply to actual measurements it is necessary to include the damping force, at least at or near the resonance frequencies, where ν/ν_0 is an odd multiple of $\pi/2$, so that

$$Y(x) = \frac{\left(1 - \frac{ik}{\nu\pi}\right) F}{4\rho_0\pi^2\nu^2\left(1 + \frac{k^2}{\pi^2\nu^2}\right)} \left(\frac{\sin \frac{\nu}{\nu_0} \frac{\pi}{2} \frac{x}{L} \sinh \frac{k}{4\nu_0} \frac{x}{L} + i \cos \frac{\nu}{\nu_0} \frac{\pi}{2} \frac{x}{L} \cosh \frac{k}{4\nu_0} \frac{x}{L}}{\pm \sinh \frac{k}{4\nu_0}} - 1 \right),$$

where the plus sign applies to multiples of $\pi/2$, $5\pi/2$, $9\pi/2$, etc., and the minus sign to $3\pi/2$, $7\pi/2$, $11\pi/2$, etc. Providing that, as usually obtains, $k/4\nu_0 < 0.03$, and therefore $(1 + ik/2\pi\nu)^2$ is closely equal to $\left(1 + \frac{ik}{\nu\pi}\right)$, the amplitude is

$$Y(x) = \frac{F}{\pm 4\rho_0\pi^2\nu_0^2 \frac{\nu^2}{\nu_0^2}} \frac{\cos \frac{\nu}{\nu_0} \frac{\pi}{2} \frac{x}{L}}{\frac{k}{4\nu_0}} \epsilon^{i(\phi + \phi_1)} \quad \text{(at resonance)}$$

$$\tan \phi = -\frac{k}{\pi\nu}$$

$$\tan \phi_1 = \frac{1}{\frac{k}{4\nu_0} \frac{x}{L} \tan \frac{\pi}{2} \frac{x}{L}} .$$

For arbitrary values of ν the expression containing the trigonometric functions in the formula for the wave shape may be written in the form

$$\frac{r_1}{r_2} \epsilon^{i(\phi_1 - \phi_2)} = \frac{\cos\left(\frac{\nu}{\nu_0}\frac{\pi}{2} + i\frac{k}{4\nu_0}\right)\frac{x}{L} - \cos\left(\frac{\nu}{\nu_0}\frac{\pi}{2} + i\frac{k}{4\nu_0}\right)}{\cos\left(\frac{\nu}{\nu_0}\frac{\pi}{2} + i\frac{k}{4\nu_0}\right)}$$

where

$$\begin{aligned} r_1^2 &= \cos^2 \frac{\nu}{\nu_0}\frac{\pi}{2}\frac{x}{L} + \cos^2 \frac{\nu}{\nu_0}\frac{\pi}{2} + \sinh^2 \frac{k}{4\nu_0}\frac{x}{L} + \sinh^2 \frac{k}{4\nu_0} \\ &\quad - 2\cos\frac{\nu}{\nu_0}\frac{\pi}{2} \cos\frac{\nu}{\nu_0}\frac{\pi}{2}\frac{x}{L} \cosh\frac{k}{4\nu_0} \cosh\frac{k}{4\nu_0}\frac{x}{L} \\ &\quad - 2\sin\frac{\nu}{\nu_0}\frac{\pi}{2} \sin\frac{\nu}{\nu_0}\frac{\pi}{2}\frac{x}{L} \sinh\frac{k}{4\nu_0} \sinh\frac{k}{4\nu_0}\frac{x}{L} \\ &= \sin^2\frac{\nu}{\nu_0}\frac{\pi}{4}\left(\frac{x}{L} + 1\right) \sin^2\frac{\nu}{\nu_0}\frac{\pi}{4}\left(\frac{x}{L} - 1\right) \\ &\quad + \sin^2\frac{\nu}{\nu_0}\frac{\pi}{4}\left(\frac{x}{L} + 1\right) \sinh^2\frac{k}{8\nu_0}\left(\frac{x}{L} - 1\right) \\ &\quad + \sin^2\frac{\nu}{\nu_0}\frac{\pi}{4}\left(\frac{x}{L} - 1\right) \sinh^2\frac{k}{8\nu_0}\left(\frac{x}{L} + 1\right) \\ &\quad + \sinh^2\frac{k}{8\nu_0}\left(\frac{x}{L} + 1\right) \sinh^2\frac{k}{8\nu_0}\left(\frac{x}{L} - 1\right) \end{aligned}$$

$$r_2^2 = \cos^2\frac{\nu}{\nu_0}\frac{\pi}{2}\cosh^2\frac{k}{4\nu_0} + \sin^2\frac{\nu}{\nu_0}\frac{\pi}{2}\frac{x}{L}\sinh^2\frac{k}{4\nu_0}\frac{x}{L}$$

$$= \cos^2\frac{\nu}{\nu_0}\frac{\pi}{2} + \sinh^2\frac{k}{4\nu_0},$$

with slight simplifications when ν/ν_0 is an even or an odd number. Moreover

$$\tan\phi_1 = -\frac{\sin\frac{\nu}{\nu_0}\frac{\pi}{2}\sinh\frac{k}{4\nu_0} - \sin\frac{\nu}{\nu_0}\frac{\pi}{2}\frac{x}{L}\sinh\frac{k}{4\nu_0}\frac{x}{L}}{\cos\frac{\nu}{\nu_0}\frac{\pi}{2}\cosh\frac{k}{4\nu_0} - \cos\frac{\nu}{\nu_0}\frac{\pi}{2}\frac{x}{L}\cosh\frac{k}{4\nu_0}\frac{x}{L}}$$

$$\tan\phi_2 = -\tan\frac{\nu}{\nu_0}\frac{\pi}{2}\tanh\frac{k}{4\nu_0}.$$

In particular, when $\frac{\nu}{\nu_0} = 1, 3, 5 \ldots$

$$\tan\phi_1 = -\tan\frac{\nu}{\nu_0}\frac{\pi}{2}\frac{x}{L}\tanh\frac{k}{4\nu_0}\frac{x}{L} \mp \frac{\sinh\frac{k}{4\nu_0}}{\cos\frac{\nu}{\nu_0}\frac{\pi}{2}\frac{x}{L}\cosh\frac{k}{4\nu_0}\frac{x}{L}},$$

and when $\frac{\nu}{\nu_0} = 2, 4 \ldots$

$$\tan\phi_2 = \frac{\sin\frac{\nu}{\nu_0}\frac{\pi}{2}\frac{x}{L}\sinh\frac{k}{4\nu_0}\frac{x}{L}}{\pm\cos\frac{\nu}{\nu_0}\frac{\pi}{2}\cosh\frac{k}{4\nu_0} - \cos\frac{\nu}{\nu_0}\frac{\pi}{2}\frac{x}{L}\cosh\frac{k}{4\nu_0}\frac{x}{L}}.$$

$$\tan\phi_2 = \mp\infty \qquad \text{or } \phi_2 = \pm\frac{\pi}{2} \qquad \text{when } \frac{\nu}{\nu_0} \doteq 1, 3, 5 \ldots$$

$$\tan\phi_2 = 0 \qquad \text{or } \phi_2 = 0 \qquad \text{when } \frac{\nu}{\nu_0} \doteq 2, 4 \ldots$$

$$\tan(\phi_1 - \phi_2) = 1/\tan\phi_1 \qquad \text{for } \frac{\nu}{\nu_0} \doteq 1, 3, 5 \ldots$$

$$\tan(\phi_1 - \phi_2) = \tan\phi_1 \qquad \text{for } \frac{\nu}{\nu_0} \doteq 2, 4 \ldots$$

When, as is usually the case, k is smaller than 0.1 the development in series of the sinh and cosh functions may be confined to the first terms; there follows $\left(\text{except when } x/L = 0 \text{ and } \cos\frac{\nu}{\nu_0}\frac{\pi}{2} = 0\right)$,

$$\frac{r_1}{r_2} = \left\{\frac{\cos\frac{\nu}{\nu_0}\frac{\pi}{2}\frac{x}{L}}{\cos\frac{\nu}{\nu_0}\frac{\pi}{2}} - 1\right\}\frac{1}{\sqrt{\cosh^2\frac{k}{4\nu_0} + \tan^2\frac{\nu}{\nu_0}\frac{\pi}{2}\frac{x}{L}\sinh^2\frac{k}{4\nu_0}\frac{x}{L}}}$$

$$\tan\phi_1 = -\frac{k}{4\nu_0}\,\frac{\sin\dfrac{\nu}{\nu_0}\dfrac{\pi}{2} - \dfrac{x}{L}\sin\dfrac{\nu}{\nu_0}\dfrac{\pi}{2}\dfrac{x}{L}}{\cos\dfrac{\nu}{\nu_0}\dfrac{\pi}{2} - \cos\dfrac{\nu}{\nu_0}\dfrac{\pi}{2}\dfrac{x}{L}}$$

$$\tan\phi_2 = -\frac{k}{4\nu_0}\tan\frac{\nu}{\nu_0}\frac{\pi}{2}$$

or, finally, with $\tan\phi = \dfrac{k}{\nu\pi}$, a small quantity,

$$Y(x) = \frac{F}{4\rho_0\pi^2\nu_0^2\nu^2/\nu_0^2}\,\frac{r_1}{r_2}\,\epsilon^{i(\phi+\phi_1-\phi_2)}\left\{\frac{\cos\dfrac{\nu}{\nu_0}\dfrac{\pi}{2}\dfrac{x}{L}}{\cos\dfrac{\nu}{\nu_0}\dfrac{\pi}{2}} - 1\right\}$$

for the amplitudes off resonance. The frequency appears in the formula in the ratio ν/ν_0, so that the same solution holds for all strings, regardless of their fundamental frequency. As to the phase difference,

$$\tan(\phi + \phi_1 - \phi_2) \doteq \tan\phi + \tan(\phi_1 - \phi_2)$$

or

$$\tan(\phi + \phi_1 - \phi_2) \doteq -\frac{k}{4\nu_0}\left\{\frac{2}{\dfrac{\nu}{\nu_0}\dfrac{\pi}{2}} + \frac{\sin\dfrac{\nu}{\nu_0}\dfrac{\pi}{2} - \dfrac{x}{L}\sin\dfrac{\nu}{\nu_0}\dfrac{\pi}{2}\dfrac{x}{L}}{\cos\dfrac{\nu}{\nu_0}\dfrac{\pi}{2} - \cos\dfrac{\nu}{\nu_0}\dfrac{\pi}{2}\dfrac{x}{L}} - \tan\frac{\nu}{\nu_0}\frac{\pi}{2}\right\}$$

(off resonance).

In other words, the amplitudes produced off resonance by a uniform alternating force along a uniform string with viscous damping are equal to the amplitudes of the undamped string multiplied by a correction factor that is virtually equal to unity, and a lag factor that varies from point to point. Owing to the factor $k/4\nu_0$, the lag or phase difference is small, with two exceptions. Large phase angles are obtained along the entire string in the neighbourhood of the resonance frequencies $\nu/\nu_0 = 1$, $\nu/\nu_0 = 3$, etc., where $\tan\dfrac{\nu}{\nu_0}\dfrac{\pi}{2}$ increases without limit. The average lag increases from the value zero, obtained when the ratio ν/ν_0 is nearly equal to zero, to $\pm\pi/2$ when ν/ν_0 is about unity, increases again from $-\pi/2$ to zero at $\nu/\nu_0 = 2$, and to $\pi/2$ at $\nu/\nu_0 = 3$; then the same changes are repeated. The phase angle is also large, regardless of the frequency, at those points of the string for which

$$\cos\frac{\nu}{\nu_0}\frac{\pi}{2} = \cos\frac{\nu}{\nu_0}\frac{\pi}{2}\frac{x}{L}.$$

Several series of solutions exist for this equation. By virtue of the relation $\cos a = \cos(2\pi - a) = \cos(4\pi - a)$, etc. where a stands for $\nu/\nu_0 \times \pi/2$, the equation is satisfied by values of x/L such that, for instance,

$$2\pi - \frac{\nu}{\nu_0}\frac{\pi}{2} = \frac{\nu}{\nu_0}\frac{\pi}{2}\frac{x}{L}$$

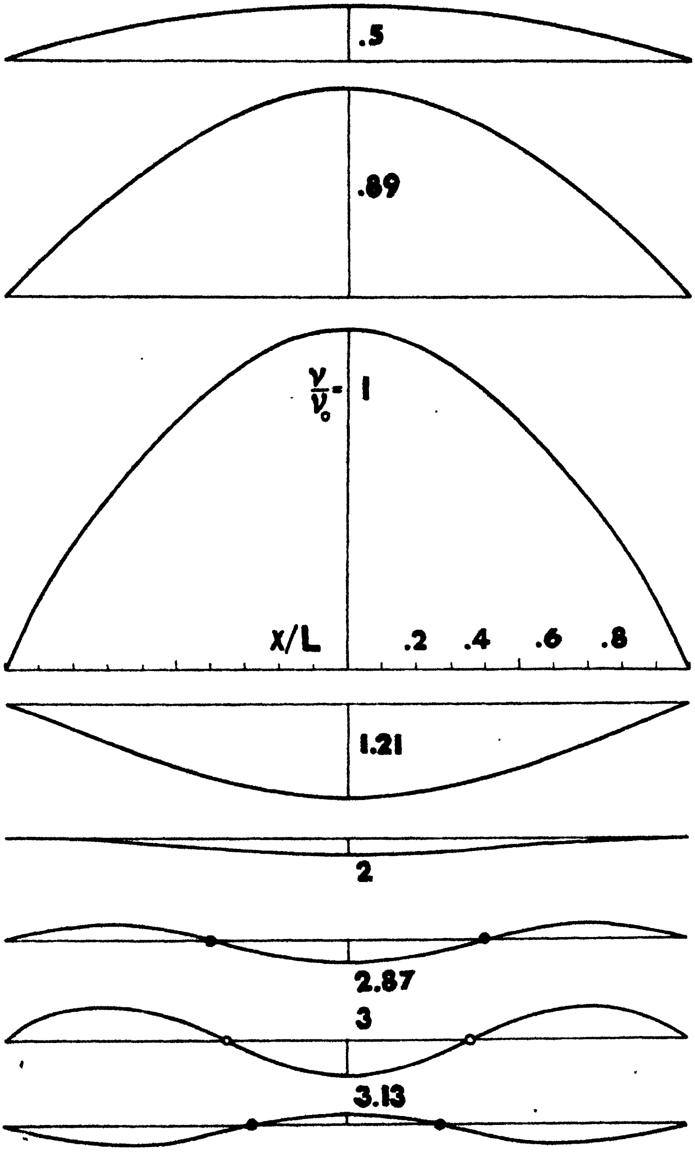

FIG. 1. *Shapes of standing waves of a damped string stretched between rigid supports when driven by a uniform force $F/4\rho_0\pi^2\nu_0^2$ of frequency ν. The fundamental frequency of the string is ν_0. Phase differences along the string are neglected. The amplitudes at resonance are inversely proportional to $k/4\nu_0$, and the curves shown for $\nu/\nu_0 = 1$, $\nu/\nu_0 = 3$, $\nu/\nu_0 = 5$, correspond to the large and constant value $k/4\nu_0 = 0.1$. Points at which the phase difference attains large values and changes rapidly are marked by circles.*

or

$$4 - \frac{\nu}{\nu_0} = \frac{\nu}{\nu_0}\frac{x}{L},$$

providing that a positive fraction less than unity is obtained for x/L; in other words, ν/ν_0 must exceed 2 and be less than 4. Another group of points is deduced from the relation $\cos a = \cos(2\pi + a)$ or

$$\frac{\nu}{\nu_0} - 4 = \frac{\nu}{\nu_0}\frac{x}{L}.$$

With this choice the solutions x/L lie near the nodes of the string, and since the phase difference varies rapidly in their neighbourhood, the wave pattern fails to become completely stationary, a conclusion that is in agreement with careful measurements of the amplitudes of ordinary strings as well as of power lines.

Fig. 1 shows the shapes of steady state motion of a damped string stretched between rigid supports and driven by a uniform force $F/4\rho_0\pi^2\nu_0^2$, of frequency ν. The fundamental frequency of the string is ν_0. Phase differences are disregarded, but the points at which rapid increases and decreases in phase angle occur are marked by circles. The amplitudes at resonance are computed on the assumption that $k/4\nu_0 = 0.1$; normally, this fraction is much smaller. Fig. 2 represents the tan of the angle by which the motion lags behind the force for various ratios ν/ν_0, the fraction $k/4\nu_0$ being equal to unity. The tan of the phase angle is proportional to $k/4\nu_0$.

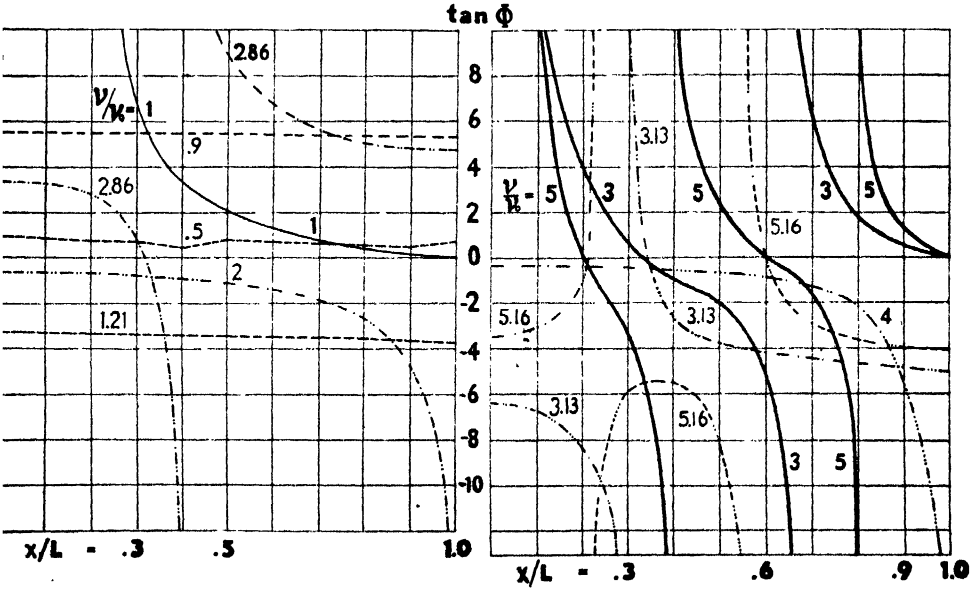

FIG. 2. *The tan of the total phase angle* ($\phi_1 + \phi_1 - \phi_2$) *in the steady motion of a damped string with fixed ends. For the frequencies off resonance the tan is proportional to* $k/4\nu_0$; *for the resonance frequency the tan is about inversely proportional to* $k/4\nu_0$ *and quite large. The curves are based on the assumption that* $\frac{k}{4\nu_0} = 1$.

Practical Applications

For viscous motion of the air the damping coefficient of a string of diameter $d = 2a$ is given by a formula derived by Stokes

$$k = \frac{4\sqrt{\pi \rho \eta \nu}}{\rho_0 d},$$

where η is the viscosity of the air (1.77×10^{-5} at 10° C.), ρ its density (1.25×10^{-3} at 10° C.), and ρ_0 the density of the material from which the string is made. For quiet air at about 10° C.

$$k = \frac{0.0033\sqrt{\nu}}{\rho_0 d}.$$

It may be considered as approximately independent of the frequency, particularly at high frequencies. With this coefficient the formula for the greatest amplitude at the midpoint becomes

$$Y(0)_r \doteqdot \frac{\nu_0 F}{\pi^2 \rho_0 \nu^2 k} \doteqdot \frac{300\nu_0 F d}{\pi^2 \nu^{5/2}}.$$

When F is the force acting in a plane wave of sound at right angles to the string

$$Y(0)_r \doteqdot \frac{0.0723 d\sqrt{G}}{\nu^{1/2}} \frac{\nu_0}{\nu} \text{ cm} \doteqdot \frac{d\sqrt{G}}{14\nu^{1/2}} \frac{\nu_0}{\nu}.$$

For sounds of ordinary intensity G and frequency, the motion of a thin string, produced by resonance in the field of a plane sound wave, is too small to be detected even with a microscope. A thin stretched wire might nevertheless be used for exploring the distribution of the intensity in front of a loudspeaker emitting low frequencies in great strength.

When the string is exposed to a steady wind, the amplitude at the midpoint becomes equal to

$$Y(0)_r \doteqdot 0.9d \frac{\nu_0}{\sqrt{\nu}} \text{ cm.}$$

With wires that are one or several centimetres thick and tuned to frequencies of a few cycles per second, as is the case with power lines, the amplitude at the centre exceeds 1 mm. even if the external force creates a frequency of as many as 50 cycles per sec. Measurements give amplitudes of several millimetres.

The amplitudes of a wire stretched out in a magnetic field and traversed by an alternating current may be obtained in a similar way.

Response of a Strengthened Damped String to a Uniform Alternating Force

When the radius a of the cross section of a string of length $l = 2L$ increases according to the law $a_0(1 \pm \lambda x/L)^{m/2}$, on both sides of a midpoint taken as the origin, the mass per unit length increases as $\rho_0(1 \pm \lambda x/L)^m$, and the force exerted in a transverse direction upon unit length of a string by a sound field of intensity G ergs per sec. per sq. cm. is

$$F = 0.0074\nu a^2(1 \pm \lambda x/L)^m \sqrt{G}\epsilon^{-2\pi i\nu t}$$

Apart from the time function the equation of motion of the string is, with $\eta = y/L$ and $\xi = 1 + x/L$,

$$\frac{d^2\eta}{d\xi^2} + \omega^2 \frac{L^2}{4\lambda^2} \frac{\rho_0}{S} \xi^m = \frac{F}{S} \xi^m .$$

The solution of the equation without second member is known. A particular solution of the complete equation is $F\lambda^2\nu_0^2/\pi^2\nu^2 S$, and since

$$\frac{d^2}{d\xi^2}\left(\xi^{1/2} J_{\frac{\pm 1}{m+2}}\left(\frac{2\sqrt{b}}{m+2}\, \xi^{\frac{m+2}{2}}\right)\right) = - b\xi^{m+1/2} J_{\frac{\pm 1}{m+2}}\left(\frac{2\sqrt{b}}{m+2}\, \xi^{\frac{m+2}{2}}\right),$$

a complete solution satisfying the boundary conditions that $\eta = y/L$ is equal to zero at the ends, where $\xi = 1 + \lambda$, but not at $\xi = 1$, or at the centre, is

$$\eta = \frac{\lambda^2}{\pi^2} \frac{\nu_0^2}{\nu^2} \frac{F}{S} \left[\frac{\xi^{1/2} J_{-\frac{1}{m+2}}\left(\frac{\pi/\lambda}{m+2} \frac{\nu}{\nu_0}\, \xi^{\frac{m+2}{2}}\right)}{(1+\lambda)^{1/2} J_{-\frac{1}{m+2}}\left(\frac{\pi/\lambda}{m+2} \frac{\nu}{\nu_0}\, (1+\lambda)^{\frac{m+2}{2}}\right)} - 1 \right].$$

For the sake of brevity a corresponding term proportional to $\sqrt{\xi}\, J_{1/(m+2)}$ has been omitted from numerator and denominator. In the present example, terms in $J_{+1/(m+2)}$ need not be included because a constant force can be represented as a sum of products of ξ by $J_{-1/(m+2)}$ alone, indeed, since

$$x^{\mu} = \sum_{r=1}^{\infty} \frac{2 J_{\mu}(j_r x)}{j_r J_{\mu+1}(j_r)} \qquad \text{where } J_{\mu}(j_r) = 0,$$

$$\xi^{-1/2} = \sum_{r=1}^{\infty} \frac{2 J_{-\frac{1}{m+2}}\left(j_r \xi^{\frac{m+2}{2}}\right)}{j_r J_{\frac{m+1}{m+2}}(j_r)}$$

$$1 = \sum_{r=1}^{\infty} \frac{2 \xi^{1/2} J_{-\frac{1}{m+2}}\left(j_r \xi^{\frac{m+2}{2}}\right)}{j_r J_{\frac{m+1}{m+2}}(j_r)}$$

$$\xi^m = \sum_{r=1}^{\infty} \frac{2 \xi^m \xi^{1/2} J_{-\frac{1}{m+2}}\left(j_r \xi^{\frac{m+2}{2}}\right)}{j_r J_{\frac{m+1}{m+2}}(j_r)}$$

The amplitude at the centre reduces to zero at the frequencies for which

$$J_{-\frac{1}{m+2}}\left(\frac{\pi/\lambda}{m+2} \frac{\nu}{\nu_0}\right) = (1+\lambda)^{1/2} J_{-\frac{1}{m+2}}\left(\frac{\pi/\lambda}{m+2} \frac{\nu}{\nu_0}\, (1+\lambda)^{\frac{m+2}{2}}\right).$$

Since both $(1 + \lambda)^{1/2}$ and $(1 + \lambda)^{(m+2)/2}$ exceed unity, a series of such solutions exist. When ν is a real quantity the amplitude becomes infinite throughout the length of the string for the ratio

$$\frac{\nu}{\nu_0} = \lambda(m+2)(1+\lambda)^{\frac{2}{m+2}} \frac{j_r}{\pi},$$

where j_r is a root of $J_{-1/(m+2)}$.

In order to take the damping force into account, a very important factor from the practical point of view, a complex value $w = \nu + ik/2\pi$ is put in the place of ν, and since for $m = 2$ the factor $\pi/\lambda(m + 2)$ varies between 0.785, for $Q = 4$, and 0.26, for $Q = 16$, the asymptotic formulae for the Bessel functions are suitable for frequencies above the thirtieth overtone. For other frequencies, advantage is taken of the relation

$$J_\mu(x+iy) = \sum_{s=0}^{\infty} J_{\mu-s}(x)J_s(iy) + \sum_{s=1}^{\infty} (-1)^s J_{\mu+s}(x)J_s(iy)$$

or

$$\begin{aligned} J_\mu(x+iy) &= J_\mu(x)J_0(iy) + J_1(iy)\big(J_{\mu+1}(x) - J_{\mu-1}(x)\big) \\ &\quad + J_2(iy)\big(J_{\mu+2}(x) - J_{\mu-2}(x)\big) \end{aligned}$$

where, in the present problem,

$$\begin{aligned} x &= \frac{\pi}{\lambda(m+2)} \frac{\nu}{\nu_0} \xi^{\frac{m+2}{2}} \\ y &= \frac{k}{2\lambda(m+2)\nu_0} \xi^{\frac{m+2}{2}}, \end{aligned}$$

and k is a small quantity. A solution that is sufficiently accurate for practical purposes is

$$\eta = \frac{\lambda^2}{\pi^2} \frac{\nu_0^2}{w^2} \frac{F}{S}\left(\frac{N}{D} - 1\right) = \frac{\lambda^2(1-ik/2\pi)}{\pi^2\nu^2/\nu_0^2} \frac{F}{S}\left(\frac{N}{D} - 1\right),$$

where

$$\frac{N}{\xi^{1/2}} = J_{-\frac{1}{m+2}}(x)J_0(y) - 2J_1(y)dJ_{-\frac{1}{m+2}}(x)/dr$$

$$\begin{aligned} \frac{D}{(1+\lambda)^{1/2}} &= J_{-\frac{1}{m+2}}\left(\frac{\pi/\lambda}{m+2} \frac{\nu}{\nu_0} (1+\lambda)^{\frac{m+2}{2}}\right) J_0\left(\frac{ik}{2\lambda(m+2)\nu_0} (1+\lambda)^{\frac{m+2}{2}}\right) \\ &\quad + \left(J_{\frac{m+1}{m+2}}\left(\frac{\pi/\lambda}{m+2} \frac{\nu}{\nu_0} (1+\lambda)^{\frac{m+2}{2}}\right)\right. \\ &\quad \left. - J_{-\frac{m+1}{m+2}}\left(\frac{\pi/\lambda}{m+2} \frac{\nu}{\nu_0} (1+\lambda)^{\frac{m+2}{2}}\right)\right) J_1\left(\frac{ik}{2\lambda(m+2)\nu_0} (1+\lambda)^{\frac{m+2}{2}}\right). \end{aligned}$$

At resonance the first term of the denominator vanishes with

$$J_{-\frac{1}{m+2}}\left(\frac{\pi/\lambda}{m+2} \frac{\nu}{\nu_0} (1+\lambda)^{\frac{m+2}{2}}\right) = 0,$$

and the second term is small, so that N/D is much larger than unity. When the square and higher terms of $k/4\lambda\nu_0$ are neglected, there follows

$$\frac{(1+\lambda)^{1/2}N}{\xi^{1/2}D} = \frac{J_{\frac{-1}{m+2}}(x) - 2J_1(y)dJ_{\frac{-1}{m+2}}(x)/dx}{\frac{ik(1+\lambda)^{\frac{m+2}{2}}}{4\lambda(m+2)\nu_0}\left(J_{\frac{m+1}{m+2}}\left(\frac{\pi/\lambda}{m+2}\frac{\nu}{\nu_0}(1+\lambda)^{\frac{m+2}{2}}\right) - J_{-\frac{m+3}{m+2}}\left(\frac{\pi/\lambda}{m+2}\frac{\nu}{\nu_0}(1+\lambda)^{\frac{m+2}{2}}\right)\right)},$$

and for the amplitude at the centre

$$\eta_0 = \frac{\lambda^2}{\pi^2}\frac{\nu^2}{\nu_0^2}\frac{F}{S}\,\frac{J_{\frac{-1}{m+2}}\left(\frac{\pi/\lambda}{m+2}\frac{\nu}{\nu_0}\right)\epsilon^{-i\pi/2}}{\frac{k(1+\lambda)^{\frac{m+3}{2}}}{4\lambda(m+2)\nu_0}\left(J_{\frac{m+1}{m+2}}\left(\frac{\pi/\lambda}{m+2}\frac{\nu}{\nu_0}(1+\lambda)^{\frac{m+2}{2}}\right) - J_{-\frac{m+3}{m+2}}\left(\frac{\pi/\lambda}{m+2}\frac{\nu}{\nu_0}(1+\lambda)^{\frac{m+2}{2}}\right)\right)}.$$

The functions $J_{5/4}$ and $J_{-5/4}$ required for dealing with the vibrations when $m = 2$ have been computed for variables up to 8, and are represented in Figs. 3 and 4. For larger variables the asymptotic expansions are suitable. For other values of m, no tables for the functions in the denominator are

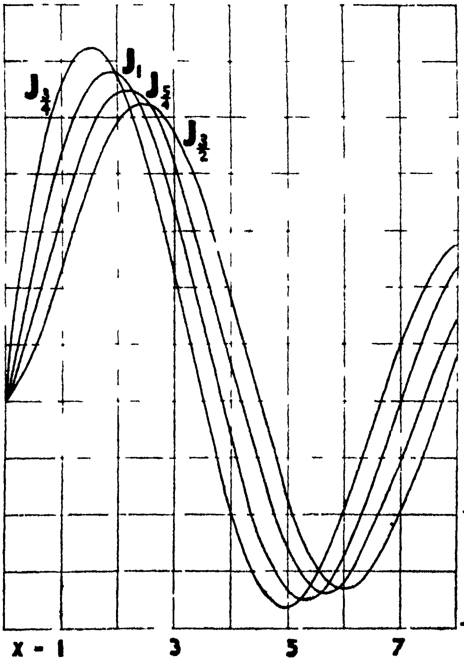

FIG. 3. *The Bessel function $J_{5/4}(x)$, with $J_{3/4}$, $J_{4/4}$, and $J_{6/4}(x)$ for comparison.*

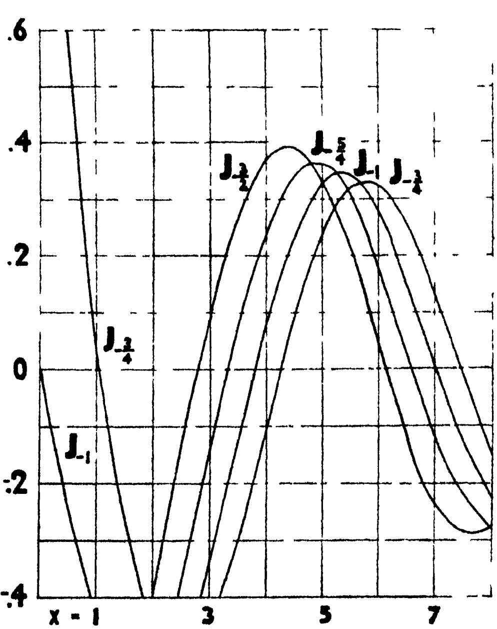

FIG. 4. *The Bessel function $J_{-5/4}(x)$, with $J_{-6/4}$ and $J_{-3/4}$ for comparison.*

available, and a comparison with the uniform string can therefore be made only from case to case for a given ν/ν_0 and a given λ.

Response of a Strengthened String to Arbitrary Non-uniform Alternating Forces

When the force acting upon unit length of the string at the point x is $R(\xi)\epsilon^{-2\pi i\nu t}$, the equation of motion of the string

$$\frac{d^2\eta}{d\xi^2} + \frac{\pi^2\nu^2}{\lambda^2\nu_0^2}\,\xi^m\eta = -\frac{LF(\xi)}{S\lambda^2} - i\,\frac{\omega}{\lambda^2}\,\frac{R(\xi)}{S}$$

can be solved either by using Lagrange's method of the variation of the constants of integration, or by means of an analysis into normal modes of motion. Both methods use the solutions obtained when the right-hand side of the equation is zero, with or without regard to the boundary conditions.

In a few cases the solutions are obtained in finite form. Since, for instance,

$$\int z^{\mu+1}J_\mu(z)dz = z^{\mu+1}J_{\mu+1}(z)$$

and

$$\int z^{\mu}J_{\mu-1}(z)dz = z^{\mu}J_\mu(z)\,,$$

there follows, with $\mu = \dfrac{1}{m+2}$ and $z = \alpha\xi^{\frac{m+2}{2}}$,

$$\int \xi^{m+1}\sqrt{\xi}\,J_{\frac{1}{m+2}}\left(\alpha\xi^{\frac{m+2}{2}}\right) = \frac{2}{\alpha\,(m+2)}\,\xi^{\frac{m+3}{m+2}}J_{\frac{m+3}{m+2}}\left(\alpha\xi^{\frac{m+2}{2}}\right)$$

$$\int \xi^{m+1}\sqrt{\xi}\,J_{-\frac{1}{m+2}}\left(\alpha\xi^{\frac{m+2}{2}}\right) = \frac{-2}{\alpha\,(m+2)}\,\xi^{\frac{m+3}{m+2}}J_{-\frac{m+3}{m+2}}\left(\alpha\xi^{\frac{m+2}{2}}\right)$$

When the external force varies as ξ^{m+1}, the expressions occurring in Lagrange's solutions of the equation of forced motion

$$\eta = c_1\eta_1 + \frac{\pi}{m+2}\,\frac{\eta_1}{\sin\dfrac{\pi}{m+2}}\int \eta_2R(\xi) + c_2\eta_2 - \frac{\pi}{m+2}\,\frac{\eta_2}{\sin\dfrac{\pi}{m+2}}\int \eta_1R(\xi)$$

where

$$\eta_1 = \sqrt{\xi}\,J_{\frac{1}{m+2}}\left(\alpha\xi^{\frac{m+2}{2}}\right)$$

$$\eta_2 = \sqrt{\xi}\,J_{-\frac{1}{m+2}}\left(\alpha\xi^{\frac{m+2}{2}}\right)$$

are readily integrated. The boundary conditions are introduced and the complete solution follows.

Canadian Journal of Research

Issued by The National Research Council of Canada

VOL. 17, SEC. A. FEBRUARY, 1939 NUMBER 2

THE DIFFUSION OF WATER VAPOUR THROUGH VARIOUS BUILDING MATERIALS[1]

By J. D. Babbitt[2]

Abstract

A method of measuring the diffusion coefficient of water vapour through solids is outlined, and a table of the coefficients for various materials used in building construction is given. The method of employing these coefficients to calculate the vapour pressure gradient through a typical wall is shown, and this is applied to estimate the resistance to water vapour necessary to prevent condensation.

Introduction

The importance of a thorough knowledge of the cause and mechanism of moisture condensation in walls and roofs of buildings has become increasingly evident during the past few years through the report of numerous structural defects from this cause and also as a result of recent experimental work (6, 9). The experiments of Teesdale at the Forest Products Research Laboratory at Madison, Wisconsin, and those of Rowley at Minneapolis have shown conclusively that the condensation of moisture arises from the migration of water vapour from the warm interior of the building through the interior portions of the wall until it reaches a point in the wall where the temperature is below the dew-point. Here, condensation occurs, so that water and ice accumulate; this results directly in a loss in the insulation of the wall and indirectly in structural deterioration through dry rot, etc. The solution of this problem, as pointed out by both Teesdale and Rowley and subsequently by numerous other writers, lies in preventing the migration of the moisture from the warm side of the wall to the point of condensation; that is to say, the interior of the wall, which usually consists of plaster on some form of plaster base (with perhaps some added insulation either of wallboard type or in the nature of a fill), must be made so impervious to water vapour that there will never be an accumulation of sufficient water vapour within the wall to allow condensation. Since it is obvious that walls as present constructed do not offer sufficient resistance to the passage of water vapour, it is necessary to add some type of vapour barrier on the interior portion of the wall to prevent moisture movement. The three types of material which are, at present, advocated as vapour barriers are (cf. Teesdale):—

---

[1] *Manuscript received January 27, 1939.*

Contribution from the Division of Physics, National Research Laboratories, Ottawa, Canada. Published as N.R.C. No. 786.

[2] *Physicist, National Research Laboratories, Ottawa.*

1. Asphalt-impregnated and surface-coated sheathing paper, glossy surfaced, weighing 35 to 50 lb. per roll of 500 sq. ft.
2. Laminated sheathing paper made of two or more sheets of kraft paper cemented together with asphalt.
3. Double-faced reflective insulation mounted on paper.

These materials have been tested by both Teesdale and Rowley and there is no doubt that, when they are suitably applied, the vapour diffusion through them is so small that the possibility of the condensation of moisture under any circumstances is negligible.

To show that the use of some material impervious to water vapour on the interior part of the wall would stop all condensation was the first step towards the solution of this problem. But now it is essential to continue the investigation until the mechanism of moisture movement through buildings is as clearly understood as that of heat transfer. The following three factors affect the movement of moisture through any structure:

1. The temperature distribution through the wall. This, of course, is dependent on inside and outside temperatures and on the thermal resistance of the various parts of the wall.
2. The moisture content of the air on both the interior and exterior of the structure.
3. Resistance of the various parts of the wall to vapour movement.

It is essential to point out that in the calculation of the possibility of condensation in a wall the permeability of the exterior portions of the wall plays a role only a little less important than that of the interior portions. The important point is that the moisture should escape through the exterior portions of the wall more quickly than it enters the interior portions, as then there will be no possibility of an accumulation of sufficient moisture for condensation. Therefore, an alternative method of preventing moisture is to make the exterior portion of the wall extremely pervious to moisture by leaving holes or cracks to the outside. This method, however, is not desirable, as it allows water in the form of rain to enter the wall. Hence the established method of preventing condensation is to make the interior so impervious to moisture that the exterior can be made wind and rain proof without any possibility of condensation.

When the three factors listed above are known it is possible to calculate accurately the distribution of moisture through a wall under equilibrium conditions. Since the temperature distribution can be determined from a knowledge of the inside and outside temperatures and the thermal conductivities of the materials constituting the wall, a table of dew-points is sufficient to show the probability of condensation, once the moisture distribution through the wall has been obtained. An indication of this procedure has been presented by Miller (5). Unfortunately, however, the resistance of various building materials to water vapour is very imperfectly known. Some work has been done on various packaging materials, and this has been summarized by Carson (2); there are some excellent measurements on paints (3, 10); a few measurements on wood (4, 7); and some miscellaneous measurements given by Miller (5); but there are no generally accepted data for the great mass of material used for constructional purposes.

In this paper the results of some measurements made at the National Research Laboratories, Ottawa, will be presented, and some indication given of their application to diffusion problems.

Explanation of Diffusion Coefficient

In a preliminary paper (1) the significance of the diffusion coefficient and the method by which it is measured were explained; these points will therefore be outlined only briefly here. To treat the transfer of water vapour as a diffusion phenomenon is a somewhat questionable procedure, as there is undoubted evidence that the phenomenon of water vapour transfer is a more complicated process than simple diffusion. Almost all materials that are used for building purposes are hygroscopic, *i.e.*, they absorb a definite weight of water if exposed to an atmosphere of a definite relative humidity. The relation between the amount of moisture absorbed and the relative humidity is different for different materials, and in no case is a simple linear relation obtained. It has been quite definitely established that in the movement of moisture through hygroscopic materials a much more intimate relation exists between the water and the material than in pure diffusion. This is strikingly emphasized by the fact that there is no connection between the permeability of a substance to air, which is a case of pure diffusion, and its permeability to water vapour. Rubber has been shown to be 50 times more permeable to water vapour than to hydrogen, and since lighter gases diffuse much more rapidly than heavier ones there must be some additional action in the case of water. However, it is not the intention to deal with the mechanism of water vapour transfer in this paper, but rather to present some measurements of the rate of transfer and to show how these may be applied to practical cases.

In order to obtain a working basis for the treatment of moisture transfer it is essential, notwithstanding the remarks above, to treat the transfer of vapour as a diffusion phenomenon and to make use of the various relations that have been found to hold for such phenomena. In fact, the errors introduced by the use of this assumption are, for all conditions that exist in practice, much smaller than errors introduced by other unavoidable factors, such as variations in materials, methods of construction, etc. It is only when high humidities, (greater than 80% relative humidity) occur that the departure from the laws of diffusion becomes of sufficient magnitude to influence the results unduly (2, 8, 3).

In this paper, therefore, the work will be presented as based on the assumption that the transfer of moisture is a diffusion process and as such obeys Fick's law. For this purpose the law is used in the following form:

$$W = \frac{dAt}{X}(P_1 - P_2),$$

where W is the weight of water vapour diffusing in time t through a material of thickness X and area A when the vapour pressures on the two sides of the material are P_1 and P_2 respectively. The quantity d is the coefficient of diffusion or the diffusivity. It may be defined as the amount of water vapour passing through unit area of the material in unit time when unit vapour pressure difference is maintained per unit thickness. In the treatment of non-homogeneous materials it is advantageous to consider the diffusance $D = \frac{d}{X}$ instead of the diffusivity. To facilitate the calculation of the diffusion through composite structures, the concept of the resistivity and resistance, the reciprocals of the diffusivity and the diffusance respectively, are convenient.

Fick's law is similar in form to Fourier's equation for the transfer of heat, so that once the assumption is made that Fick's law does satisfactorily explain water vapour diffusion then all the mathematical analysis that has been developed for thermal applications becomes available. The calculation of the humidity gradient through a wall is then similar in method to the determination of temperature gradient through the wall.

Experimental

The Measurement of the Diffusion Coefficient.

On the assumption that the transfer of water vapour through a solid material obeys Fick's law, it is a simple matter to evaluate the coefficient d. It is necessary only to determine the weight of moisture that passes through a sample of the material per hour when different constant relative humidities are maintained on the two sides of the sample.

In this investigation the diffusion coefficient has been measured by an application of the cell method: that is to say, the material, the coefficient of which is to be measured, is placed over the top of the dish or cell so as to completely shut off the interior of the cell from the external atmosphere. The cell is filled with calcium chloride, an aqueous solution of sulphuric acid, or some other desiccant, so as to give the desired vapour pressure within the cell. The whole arrangement (cell plus sample) is then placed in an enclosure maintained at a constant temperature and humidity. The gain in weight of the cell, after equilibrium has been attained, is then equal to the weight of water diffusing through the specimen. Two types of cells used in this research are shown in Figs. 1 and 2. The first, Fig. 1, used for thick samples, consists of a straight-walled glass vessel similar to a crystallizing dish, and the specimen is placed flush with the upper edge of the vessel. The edges of the specimen are covered with a layer of wax before being placed in the cell so as to prevent any possibility of edge loss, and after it has been inserted in the dish the space between the edge of the sample and the wall of the vessel is sealed with wax. The second, Fig. 2, is constructed from duralumin and is so made that samples of any thickness up to 1 in. may be tested. The sample rests on a horizontal rim and is firmly pressed against this by a screw cap. This surface is first coated with wax and heated to receive the specimen. If the thickness of the sample is comparable to the width of the rim the edges of the sample must also be sealed with wax. The area of the duralumin cells used was about 45 sq. cm., and that of the glass vessels, about 70 sq. cm.

In accordance with the suggestion made by Carson (2), a solid desiccant (calcium chloride) was used in the cells, and these were so filled that the surface of the desiccant was almost touching the lower surface of the specimen. In this way, the air space between the desiccant and the lower surface of the sample was made as small as possible, so that the error introduced by assuming that the vapour pressure at the lower surface of the sample was equal to that of the desiccant was negligible.

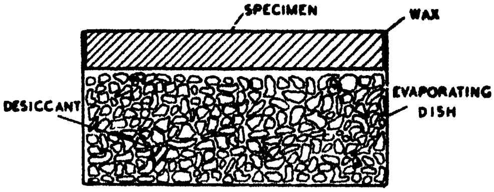

FIG. 1. *Cell used for thick samples.*

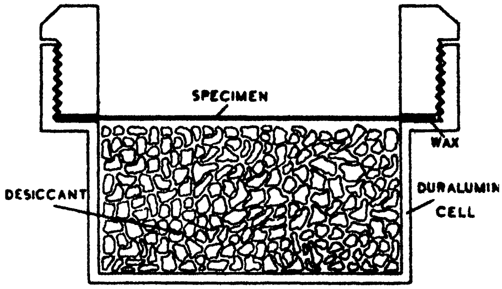

FIG. 2. *Cell used for samples of any thickness up to 1 in.*

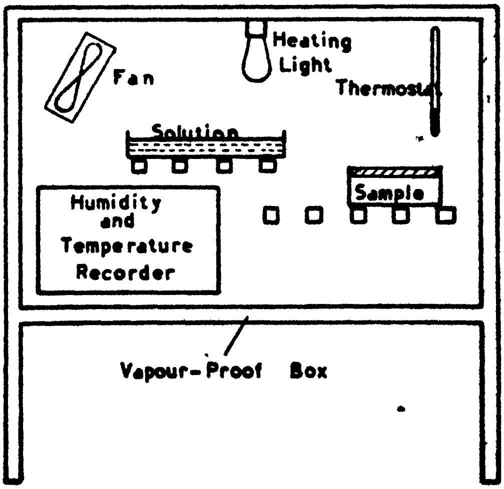

FIG. 3. *Arrangement of apparatus in humidity chamber.*

The arrangement of the apparatus in the constant humidity chamber is shown in Fig. 3. This chamber had the internal dimensions 1 ft. by 2 ft. by 2 ft. and was constructed of five-ply wood, which was painted on the inside with three coats of aluminium paint. A small fan with 8-in. blades was so placed as to blow a stream of air across the surface of a flat tray containing a saturated aqueous solution, and from this on to the measuring cells. In this way the air in contact with the upper surface of the samples was kept at a humidity corresponding to that of the solution. The temperature within the chamber was kept constant by means of a thermostat controlling a 100 watt lamp. The temperature and relative humidity were recorded on a recording humidograph. This arrangement is slightly different from that described in a previous paper (1), but it was found essential to place the tray containing the solution directly between the fan and the samples in order to obtain the correct humidity conditions.

In most of the experiments reported here the temperature of the box was held constant at a temperature in the vicinity of 90° F. This temperature was chosen mainly for convenience; most of the measurements were taken during the summer months when it would have been impossible to maintain a lower temperature without some method of cooling. As it has been found by a number of investigators (cf. Carson (2)) that, except for high temperatures or humidities, the rate of transpiration of moisture is governed by the vapour pressure difference irrespective of the temperature, the error introduced by transposing the measured coefficients to room temperatures is not great. The humidity in the chamber was maintained constant by means of a saturated sodium chloride solution. According to the International Critical Tables this corresponds to a relative humidity of 75% at 91° F. The humidity was checked as closely as possible by means of a small piece of fibreboard which was left exposed to the atmosphere in the chamber. The moisture absorption curve for this material had previously been determined, so that the increase of weight of the fibreboard when left in the chamber enabled the humidity to be roughly checked. It was found, within the errors of the experiment, to be 75% relative humidity.

In the determination of the vapour transmissions the cells were weighed every 24 hr. The increase in weight was then plotted against the time. When a straight line was obtained the slope was measured; this gave the vapour transmission per hour. Since most of the materials were hygroscopic, a considerable time was required before the material was in equilibrium with the moisture in the atmosphere. During this time the weight of the cell increased either more quickly or more slowly than under equilibrium conditions, the rate depending on whether the sample was dry or damp when placed in the cell. A typical curve for a sample composed of five pieces of Presdwood is shown in Fig. 4. This sample was dry when placed in the apparatus; considerable time was therefore required before equilibrium was attained. In the case of thin materials or non-hygroscopic material, equilibrium is attained

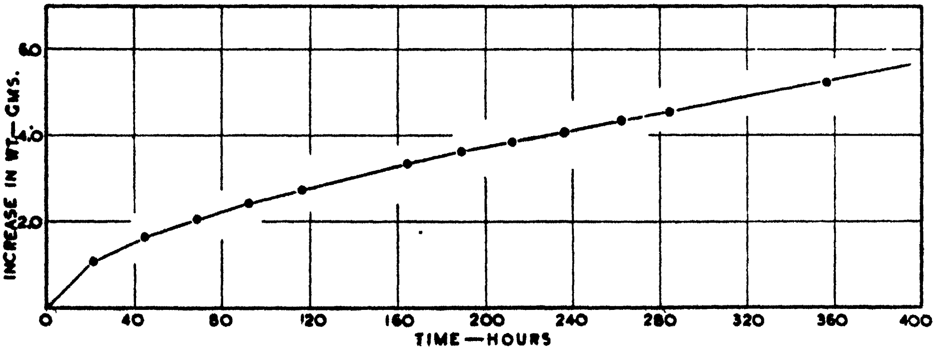

FIG. 4. *Showing how the weight of a sample consisting of five thicknesses of Presdwood varies with time.*

almost immediately, so that the final linear curve relating increase of weight with time passes through the origin.

Discussion of Results

The diffusion coefficients obtained by the above method are given in Table I. In cases of those non-homogeneous materials where the impedance to moisture is obtained mostly from a special part of the material (*e.g.*, a surface layer) and is not proportional to the thickness, the diffusance, D, is given instead of the diffusivity, d. The units used are grams per 24 hr. per sq. meter per vapour pressure difference of 1 mm. of mercury per cm. in the case of d, and grams per 24 hr. per sq. meter per vapour pressure difference of 1 mm. of mercury across the material in the case of D.

TABLE I

DIFFUSION COEFFICIENTS

Temperature = 91.0° F.
External vapour pressure = 27.2 mm. of Hg. = 75% relative humidity
Internal vapour pressure = 0.0 mm. of Hg.

Material	Thickness cm.	Diffusance D gm./24 hr./sq.m./mm. Hg.	Diffusivity d gm./24 hr./sq.m./ $\frac{\text{mm.Hg.}}{\text{cm.}}$
Fibreboard	1.25	19.7	24.8
Fibreboard; asphalt on one surface; applied by rolling	1.25	2.6	
Fibreboard; a glossy coating of asphalt on one surface; applied by dipping	1.6	5.6	
Fibreboard, laminated; two ½ in. samples cemented together with asphalt	2.5	0.89	
Fibreboard, laminated; 6 layers of fibreboard with 5 layers of asphalt	1.34	0.075	
Fibreboard	2.69	12.0	32.2
Fibreboard (above sample reduced in thickness)	2.04	14.1	28.7
Fibreboard (above sample reduced in thickness)	1.52	18.3	27.8
Fibreboard (above sample reduced in thickness)	1.03	24.2	24.8
Fibreboard (above sample reduced in thickness)	0.51	43.3	22.2
Wood (Spruce)	1.43	1.13	1.62
Wood (Spruce)	1.22	1.31	1.60
Wood (Spruce)	1.03	1.28	1.32
Wood (Spruce)	0.82	1.60	1.31
Wood (Spruce)	0.59	2.35	1.39
Wood (Spruce)	0.41	3.36	1.37
Wood (Pine)	2.03	0.61	1.25
Wood (Pine)	1.64	0.82	1.34
Wood (Pine)	1.26	1.12	1.41
Wood (Pine)	0.80	1.80	1.43
Wood (Pine)	0.43	3.13	1.34
Wood (Pine) A	1.29	2.10	2.71
Wood (Pine) A 1 coat aluminium paint		1.11	
Wood (Pine) A 2 coats aluminium paint		0.30	
Wood (Pine)A 3 coats aluminium paint		0.23	

TABLE I—*Concluded*

DIFFUSION COEFFICIENTS—*Concluded*

Temperature = 91.0° F.
External vapour pressure = 27.2 mm. of Hg. = 75% relative humidity
Internal vapour pressure = 0.0 mm. of Hg.

Material	Thickness, cm.	Diffusance D gm./24 hr./sq. m./mm. Hg.	Diffusivity d $\frac{\text{gm./24 hr./sq. m./mm. Hg.}}{\text{cm.}}$
Wood (Pine) B	1.29	2.17	2.80
Wood (Pine) B 1 coat white enamel paint		1.25	
Wood (Pine) B 2 coats white enamel paint		0.60	
Wood (Pine) B 3 coats white enamel paint		0.47	
Kraft paper (1 sheet)	0.010	51.8	
Kraft paper (2 sheets)		32.9	
Kraft paper (3 sheets)		24.7	
Kraft paper (4 sheets)		19.6	
Kraft paper (5 sheets)		16.5	
Kraft paper (5 sheets)		20.1	
Kraft paper (5 sheets)		19.0	
Kraft paper (7 sheets)		14.0	
Kraft paper (7 sheets)		11.8	
Kraft paper (8 sheets)		11.8	
Kraft paper (8 sheets)		10.2	
Black vulcanized rubber (Hardness 40)	0.201	0.060	0.012
Plasticized rubber hydrochloride	0.004	0.124	0.00049
30-30-30 paper A.	0.018	0.595	
30-30-30 paper B.	0.018	0.581	
Duplex Scutan 6-6 (Asphalt between two sheets of kraft paper)	0.018	0.307	
Scutan 0-14 (Kraft paper infused with asphalt on one surface) A.	0.018	2.79	
Scutan 0-14, B.	0.018	5 18	
Scutan 14—Kraft paper infused with asphalt on both surfaces, A	0.018	4.50	
Scutan 14, B.	0.018	5.11	
Black building paper, A black shiny paper completely infused with asphalt	0.044	0.122	
Asphalt felt, 15 lb., A felt building paper having soft dull appearance	0.081	4.38	
Pressed corkboard A	2.3	1.54	3.55
Pressed corkboard B	2.5	1.76	4.39
Plaster	3.4	8.81	30.2
Plaster board (Plaster between sheets of heavy paper)	0.94	22.8	
Rock wool (density 7 lb./cu. ft.)	9.0		152.0
Masonite Presdwood (Tempered)	0.33	3.17	
Masonite Presdwood	0.33	7.04	
Masonite Presdwood (5 thicknesses)		2.03	
Masonite Presdwood (7 thicknesses)		1.59	

No great accuracy is claimed for the results given in this table. Because of the practical application to which the results are to be put, no very great accuracy is required. The variation in the diffusion coefficient of different samples of the same material, and variations in the methods of construction in buildings are so large that too great a refinement in the measurements is quite uncalled for. It is for this reason also that there need be no hesitation in using Fick's law for such measurements. Notwithstanding this, it was found that measurements on any one sample could be repeated accurately to two figures. But when different specimens were used the results were not so consistent. This was especially noticeable in the case of wood, which, as is quite evident, does not have a homogeneous structure. In all the specimens of wood tested, the moisture flow was transverse to the grain, but no precautions were taken to distinguish whether the flow was radial or tangential to the annual rings. The measurements recorded in this paper indicate that the flow of moisture through wood is a very complicated phenomenon. This bears out previous work (4, 7). It is quite definitely established that the moisture gradient in wood through which moisture is moving in a transverse direction departs quite substantially from a straight line, so that the use of Fick's law is quite unwarranted. This probably accounts for a great deal of the variations in the results obtained for wood under various conditions of measurement. In building construction, wood is always employed in the form of boards that are joined together with a tongue and groove, or an over-lap, or are simply butted together. In any case, cracks are bound to exist between the individual pieces, and it is exceedingly probable that by far the greater amount of moisture passes through these cracks; consequently, the amount passing through the wood itself is negligible. Thus, while the figures for wood are interesting for purposes of comparison, the diffusion coefficients in this case have little practical value. Before any reliable estimate can be made of the vapour transmission through a wooden wall, it will be necessary to obtain accurate data on the vapour transmission through cracks. These data are not yet available, so that one can only roughly estimate the vapour resistance of a wooden wall.

The resistance of wood, fibreboard and kraft paper have been measured at various thicknesses; the relation between the resistance and thickness for these three materials is shown in Figs. 5, 6, and 7, respectively. In these

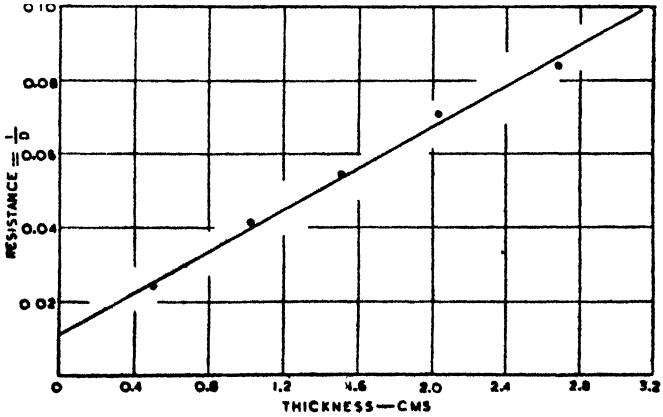

FIG. 5. *Fibreboard: Variation of resistance with thickness.*

figures the resistance of the material has been plotted against the thickness. The resistance is the reciprocal of the diffusance $\left(R = \frac{1}{D}\right)$, and, according to Fick's law, should vary linearly with thickness. In all three figures it is seen that the points approach more or less closely to a straight line. Only in the case of wood does this line appear to pass through the origin. When the curve does not pass through the origin it indicates that there is a surface resistance to moisture transfer; in other words, even if the thickness of the material were zero there would remain some resistance. This means that an additional resistance exists in the air space in contact with the surface of the material, so that the vapour pressure drop across the sample is less than the total vapour drop between the desiccant and the external atmosphere [cf. (1) and (2)]. The effect, however, is insignificant for our purposes. That the curve for wood appears to pass through the origin may be due to the relatively greater resistance of wood.

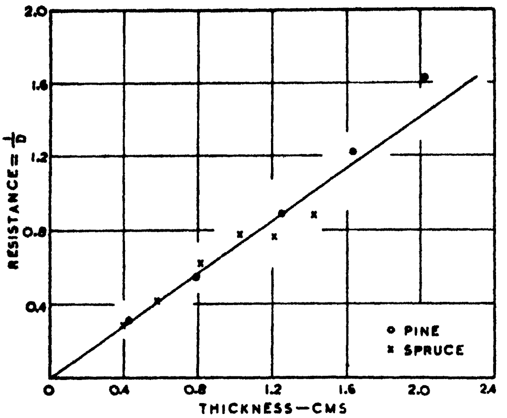

FIG. 6. *Wood: Variation of resistance with thickness.*

In Table II some results of previous measurements are reproduced for purposes of comparison. The results for rubber and plasticized rubber hydrochloride are included to show that the present results compare favour-

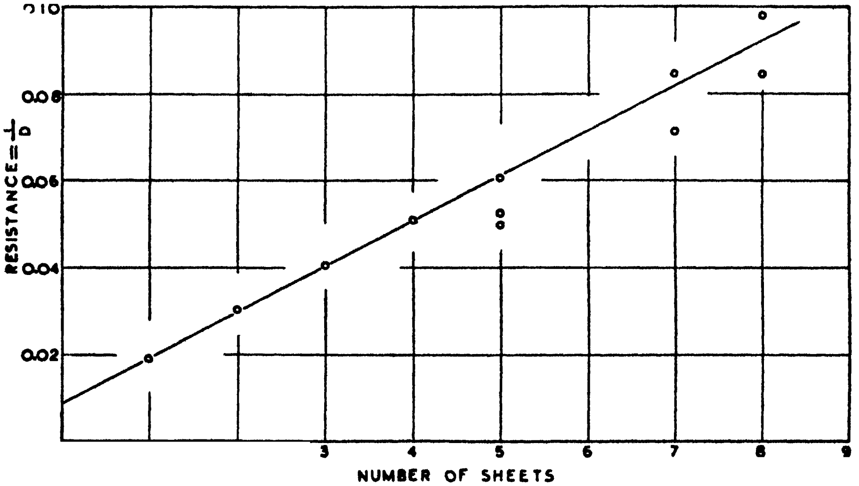

FIG. 7. *Kraft paper: relation between number of sheets of paper and resistance.*

ably with those of Taylor, Herrmann, and Kemp (8). Results from the very excellent paper on wood by Stillwell (7) have not been included since it is too difficult to extract a representative result. The reader is referred to the original paper, which gives an interesting theoretical discussion of moisture transfer through wood. Also, none of the data obtained by Wray and his co-workers (3, 10) on paint films are shown in Table II, as, to be of value, they would have to be reproduced in full. Here again reference should be made to the original papers. The results given by Miller (5) have been reproduced in full.

TABLE II

PREVIOUS MEASUREMENTS

Material	Thickness	Temp., ° F.	V.P. difference, mm. of Hg.	*d*	*D*	Ref.
Rubber (soft vulcanized)	0.0354 cm.	77.0	Various	0.0158 to 0.0185		(8)
Plasticized rubber hydrochloride	0.0029 cm.	77.0	18.0 - 0.0	0.00036	0.126	(8)
Wood (Scots pine)	From 1 to 5 cm.	104.0	Av. up to 20 mm.	17.6		(4)
Wood (Western yellow pine)	0.635 cm.	80.6	25.4 - 0.0	1.48		(10)
Plaster base and plaster	0.75 in.				9.71	(5)
Fir sheathing	0.75 in.				1.94	(5)
Vapour barrier					0.53	(5)
Waterproof paper					32.4	(5)
Pine lap siding					3.24	(5)
Paint film					2.26	(5)
Celotex	0.75 in.				8.25	(5)
Brick masonry	4.0 in.				0.71	(5)

It has been necessary to change the units in nearly all cases. Miller, in his paper, has given very little indication of how his results were obtained. For some materials they differ widely from the present measurements. His figure for a vapour barrier is especially interesting. It is taken from a paper published by the Engineering Division of the Kimberley-Clark Corporation, entitled "The Practical Aspects of Condensation in the Building Industry." In this paper the statement is made that "Information now available leads to the recommendation that within the United States vapour seals are needed only in locations North of the Ohio River and that the seal or barrier used should transmit water vapour no faster than 0.40 gm./sq. m./hr. under a vapour pressure of 18 mm. of mercury." This is the figure quoted by Miller when the units are suitably changed. Unfortunately the Kimberley-Clark Corporation do not give the data on which this figure is based. In the following section of this paper, further considerations will be given to this question of a vapour barrier, and an endeavour made to estimate what value of vapour resistance is required before any material may be considered to constitute a vapour barrier.

Use of Diffusion Coefficients

In his paper (5), L. G. Miller has indicated how the diffusion coefficient of a material may be used to calculate the possibility of condensation in a wall. It is the intention now to extend this method and to apply the coefficients presented in this paper. It is especially desirable to indicate how the vapour barrier conception works in practice.

As indicated by Miller the possibility of moisture condensation is related to the temperature gradient through the wall. The fundamental equation for heat transfer, from which the temperature gradient can be determined, is:

$$H = \frac{kAt}{x}(T_1 - T_2)$$

where H is the quantity of heat transmitted in time t through a cross section of material of area A and thickness x when a temperature difference $T_1 - T_2$ is maintained across the material. The term k is the coefficient of conductivity. The method of applying this equation to a composite wall structure in order to obtain the over-all transmission is well known and is given in any standard book on heat transfer. The point to be emphasized is that Fourier's equation above is identical in form with Fick's law governing the vapour transfer, so that the same treatment may be applied to Fick's law to find the vapour gradient through the wall as is used with Fourier's law to obtain the temperature gradient. When these two gradients are known, the possibility of condensation can be immediately estimated. The dew-point at various positions in the wall can be plotted, and if at some point in the wall the existing temperature is below the dew-point corresponding to the humidity at this point, condensation will occur.

In order to carry through a calculation of the temperature and humidity gradients through a wall it is necessary to assume some typical conditions of temperature and humidity existing on the two sides of the wall. For the inside conditions a temperature of 70° F. with a relative humidity of 40% would seem to be a suitable choice. (This corresponds to a vapour pressure of 7.5 mm. of mercury). The temperature of 70° is an average indoor winter temperature, and one would seldom find a relative humidity greater than 40% when there is zero weather outside. The choice of suitable external conditions is not nearly so easy. In Canada, temperatures of −20° F. are quite common and in many cities temperatures much lower than this have been recorded. Except in extreme cases, however, these conditions do not last for a sufficient length of time to establish equilibrium conditions in a building, so that for our purpose it is not necessary to assume a temperature as low as −20°. However, to make the conditions more severe than would commonly be met in practice, we shall assume an external temperature of −10° F. and shall take the external vapour pressure as being 75% relative humidity at this temperature. (Vapour pressure = 0.42 mm. of mercury.)

For our purpose a typical wood frame wall will be considered. This consists of siding, building paper, sheathing, a 4 in. air space filled with rock wool, and a finishing of plaster base and plaster on the inside. This type of wall, containing 4 in. of rock wool, furnishes just the conditions that are most conducive to moisture condensation, since, as has been pointed out by many authors, the high degree of insulation afforded by the rock wool maintains the inside surface of the sheathing at a lower temperature than it would have if the insulation were less. Table III gives the data necessary to calculate the temperature gradient through such a wall, and indicates the method of computation.

TABLE III

—	C, B.T.U. /hr./sq. ft./°F.	$R = \frac{1}{C}$	Temp. drop, °F.	Actual temp., °F.	Saturated vapour pressure, mm. Hg
External surface coefficient	6.00	0.17	0.8	−9.2	0.6
Siding, building paper, sheathing	0.50	2.00	9.2	0.0	1.0
Air space + rock wool	0.07	14.28	65.1	65.1	15.8
Wood lath + plaster	2.50	0.40	1.8	66.9	16.9
Internal surface coefficient	1.65	0.61	2.7	69.6	18.8

Over-all resistance = 17.46

Over-all transmission $= \frac{1}{17.46} = 0.057$ B.T.U./hr./sq. ft./°F.

Total temperature drop across the wall = 70° + 10° = 80°

Total heat transmitted through 1 sq. ft. = 0 057 × 80 = 4.56 B.T.U./hr.

The first column gives the conductance, C, of the material. The third column gives the temperature drop across the different sections of the wall; this is obtained by multiplying the total heat transmitted (4.56 B.T.U.) by the value of R in Column 2. The fourth column gives the actual temperature of the inside surface of these different sections. In the last column the saturated vapour pressures corresponding to the temperatures in the preceding column are given. The temperature gradient through the wall has been drawn in Fig. 8, and the saturated vapour pressure is also indicated. The saturated vapour pressure is not linear but is concave upwards.

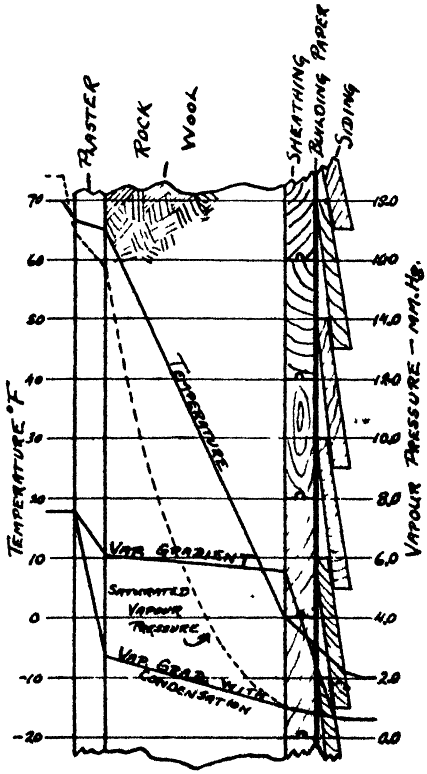

FIG. 8. *Temperature and vapour gradient through a wall with no vapour barrier.*

The next step is to calculate the vapour pressure drop through the wall, but here the difficulty of assessing the resistance of the wood sheathing and siding to moisture movement is encountered. As has been indicated previously, it is impossible, on the basis of the data at present available, to estimate, with any degree of accuracy, the vapour flow through the joints and cracks in the wood. In any case the individual joints will vary so greatly that anything but a very rough guess would be impossible. One thing is certain, and that is that the vapour resistance will be much less than that indicated by the flow through the wood itself. A study of Table I shows that a representative value of D for an inch of wood would be 0.50, but this figure is plainly much too low for a built-up wall. After considerable thought the conclusion was reached that if the resistance of the outer portion of the wall, *i.e.*, the sheathing, building paper, and paint, were taken equal to the measured value of the building paper alone, too great an error would not be introduced. In this way some allowance is made for the joints in the paper and the assumption is implicitly made that the resistance of the paint is not great, owing to weathering and cracking. The coefficients for the other portions of the wall may be used as measured since there the medium has no joints but is continuous. Table IV indicates the calculations involved in determining the vapour pressure drop through the wall.

TABLE IV

—	D	$R = \frac{1}{D}$	Vapour drop, mm. Hg.	Actual pressure, mm. Hg.
Siding, building paper, sheathing	4.4	0.23	5.2	5.6
Air space + rock wool*	42.8	0 02	0.5	6.1
Plaster + plaster base (¾-in.)	15 9	0.06	1.4	7.5
		0.31		

Over-all moisture transmittance $= \frac{1}{0.31} = 3.2$ gm./24 hr./sq.m./mm.Hg.
Total vapour pressure drop across wall $= 7.5 - 0.4 = 7.1$ mm. Hg.
Total moisture transmitted per sq. m. $= 3.2 \times 7.1 = 22.6$ gm./24 hr.

* *The factor used for rock wool is about 2½ times that given in Table I to allow for the fact that the bats are not continuous.*

The vapour gradient as given by the figures in the last column has been plotted in Fig. 8, where the saturated vapour pressure through the wall is also shown. Now, it is impossible for the actual vapour pressure at any point in a wall to exceed the saturated vapour pressure corresponding to the temperature at that point, because in that case condensation will occur until the vapour pressure has decreased to the saturated value. It is seen in the figure that the calculated vapour gradient is above the saturated vapour pressure in the outer portions of the rock wool, and it will be observed that for the inner surface of the sheathing the curve representing the vapour gradient is 4.6 mm. of mercury above the saturated vapour pressure corresponding to the temperature of the sheathing. Under these conditions condensation will certainly occur. Since the vapour pressure gradient through the wall was calculated on the assumption that there was no condensation but a steady flow of moisture from the interior to the exterior, it must now be modified to allow for condensation. The vapour pressure in the wall can never be higher than the saturated vapour pressure. It is clear from the figure that the vapour pressure at the inner surface of the sheathing can never be greater than 1.0 mm. of mercury, which is the saturated vapour pressure corresponding to the temperature at this point. In the calculation of the vapour gradient given above, it was implicitly assumed that continuity of flow held, that is to say, that the amount of moisture leaving the wall at the exterior surface was exactly equal to, and neither greater nor less than, the amount of moisture entering the interior surface. When condensation takes place, this assumption is obviously untrue, and the vapour pressure gradient must adjust itself to allow for the condensation. It is necessary, therefore, to recalculate the vapour gradient on the assumption that moisture can move from the inside of a building to a point of condensation independently of any conditions existing beyond this point. Table V indicates the calculation of the vapour gradient from the interior to the surface of the sheathing under these conditions.

TABLE V

—	D	$R = \frac{1}{D}$	Vapour drop	Vapour pressure
Air space + rock wool	42.8	0.023	1.7	2.7
Plaster + plaster base	15.9	0.063	4.8	7.5
		0.086	6.5	

Over-all moisture transmittance $= \frac{1}{0.086} =$ 11.63 gm./24 hr./sq.m./mm. Hg.

Vapour pressure drop = 7.5 − 1.0 = 6.5 mm. Hg.

Total moisture transmitted per sq. m. = 11.63 × 6.5 = 75.6 gm./24 hr.

Under these conditions 75.6 gm. of moisture per sq. m. would move each day from the interior of the house to the point of condensation at the inside of the sheathing. However, the water (in this case it would be in the form of ice) would not accumulate quite so quickly as this, since there would be a tendency for some of it to continue to migrate towards the outside. The following calculation shows the amount of moisture transmitted.

	D	$R = \frac{1}{D}$
Siding, building paper, sheathing	4.38	0.228

Vapour drop = 1.0 − 0.4 = 0.6 mm. Hg.

Total moisture transmitted = 4.38 × 0.6 = 2.6 gm./24 hr./sq. m.

Hence under the conditions outlined above, moisture would accumulate at a rate of approximately $75.6 - 2.6 = 73$ gm. per day per sq. m.

It is interesting at this point to note that, owing to the curvature of the saturated vapour pressure curve, it is possible for condensation to occur at points in the rock wool other than at the surface of the sheathing. For if the vapour pressure gradient in the rock wool has a greater slope than that of the saturated vapour pressure curve at the sheathing, then the curve of vapour pressure gradient must meet the saturated vapour pressure curve before the sheathing is reached. The movement of vapour then adjusts itself so that the gradient is tangent to the saturated curve at some point and follows the saturated curve from there to the surface of the sheathing. Since beyond the point of tangency the slope of the gradient steadily decreases (corresponding to the saturated vapour) there would be a tendency for moisture to accumulate at this point.

Now, it is obvious from the above that to prevent the accumulation of moisture it will be necessary to reduce the flow through the inner portion of the wall until it is equal to or less than that through the outer portions; that is to say, the resistance must be increased by the addition of a vapour barrier. The accumulation of moisture could be prevented just as well by decreasing the resistance of the outer portion of the wall. This could be done by providing vents through which the moisture could easily diffuse. Many people have advocated the use of a combination of the two methods, but since we are primarily interested in the mechanism of vapour barriers we shall confine ourselves to this aspect of the problem. We, therefore, assume that conditions remain the same on the outside of the rock wool, so that our problem is to reduce the flow of moisture through the inside of the wall to 2.6 gm. per 24 hr. per sq. m. Hence the vapour barrier must reduce the flow from 75.6 gm. to 2.6 gm., *i.e.*, by a factor of $\frac{75.6}{2.6} = 29$. Therefore the vapour barrier must

TABLE VI

—	D	$R = \frac{1}{D}$	Vapour drop	Vapour pressure
Siding, building paper, sheathing	4.4	0.23	0.58	1.0
Air space + rock wool	42.8	0.02	0.06	1.1
Vapour barrier	0.4	2.50	6.32	7.4
Plaster + plaster base	15.9	0.06	0.16	7.5
		2.81	7.12	

Over-all moisture transmittance $= \frac{1}{2.81} = 0.36$ gm./24 hr./sq. m./mm. Hg.

Total vapour drop across wall $= 7.5 - 0.4 = 7.1$ mm. Hg.

Total moisture transmitted per sq. m. $= 0.36 \times 7.1 = 2.5$ gm./24 hr.

increase the resistance of the wall by a factor of 29. Since the present resistance of the interior of the wall is 0.086, the wall required must have a resistance of 0.086 × 29 = 2.5. This is approximately the resistance that is required in the vapour barrier. It represents a diffusance of 0.4 gm. per 24 hr. per sq. m. per mm. of mercury. The corresponding value given by the Kimberley-Clark Corporation was 0.53. When the assumptions in the calculations and the inaccuracies in the data are taken into account, these two values may be taken as being roughly equivalent. Any material having a diffusance in the neighbourhood of these figures may be considered as a vapour barrier when used under conditions such as those specified above.

It now remains to calculate the vapour gradient through the wall constructed with such a vapour barrier ($D = 0.4$). Table VI gives this calculation.

The vapour gradient through the wall, given in the last column, has been plotted in Fig. 9 along with the temperature and saturated vapour pressure. It is evident from this that there is now no possibility of moisture condensation.

The calculations above have been given to show how the diffusion coefficients can be applied to any wall to determine the possibility of moisture condensation. The figure obtained for a vapour barrier applies only to the one type of wall and only to the conditions outlined. It is hoped, however, that this presentation has in some degree clarified some of the points that have so long obscured the problem of moisture condensation.

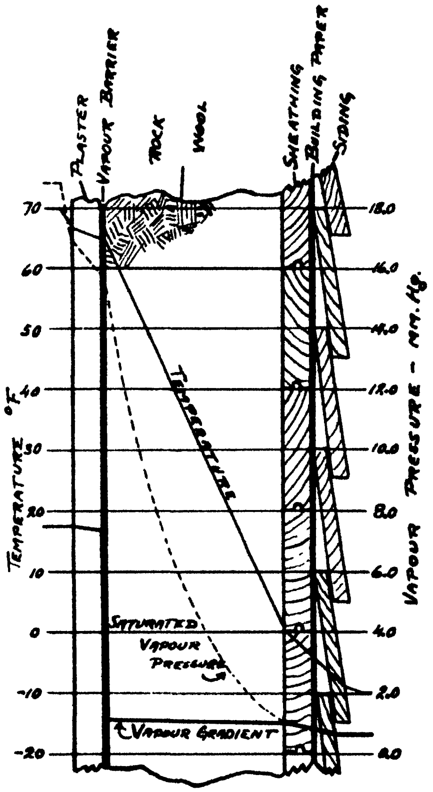

FIG. 9. *Showing vapour gradient through a wall in which vapour barrier is placed.*

Acknowledgment

The author wishes to express his indebtedness to C. St. Jacques and W. G. Martin, laboratory assistants at the National Research Council. The former has constructed the apparatus involved in these measurements, and the latter has done much of the routine weighing.

References

1. Babbitt, J. D. Heating, Piping, Air Conditioning, 10 : 751-755. 1938.
2. Carson, F. T. Natl. Bur. Standards, Misc. Pub. M127. 1937.
3. Edwards, J. D. and Wray, R. I. Ind. Eng. Chem. 28 : 549-553. 1936.
4. Martley, J. F. Forest Products Research, Dept. Sci. Ind. Research, Brit. Tech. Paper, No. 2. 1926.
5. Miller, L. G. Heating and Ventilating, 35 : 56-58. 1938.
6. Rowley, F. B., Algren, A. B., and Lund, C. E. Heating, Piping, Air Conditioning, 10 : 49-60. 1938.
7. Stillwell, S. T. C. Forest Products Research, Dept. Sci. Ind. Research, Brit. Tech. Paper, No. 1, 1926.
8. Taylor, R. L., Herrmann, D. B., and Kemp, A. R. Ind. Eng. Chem. 28 : 1255-1263. 1936.
9. Teesdale, L. C. Condensation in walls and attics. Forest Products Laboratory, Madison, Wis. Oct. 1937.
10. Wray, R. I. and Van Worst, A. R. Ind. Eng. Chem. 25 : 842-847. 1933.

Canadian Journal of Research

Issued by THE NATIONAL RESEARCH COUNCIL OF CANADA

VOL. 17, SEC. A. MARCH, 1939 NUMBER 3

LIBRARY

THE ELASTIC EXTENSIBILITY OF MUSCLE[1]

BY GEORGE W. F. BRISBIN[2] AND FRANK ALLEN[3]

Abstract

Measurements of the extensibility of muscles and other tissues were first made, as far as the authors are aware, by Wertheim in 1846. He proposed for them a hyperbolic law of elasticity of the form: $y^2 = ax^2 + bx$. Further measurements were made at much later dates by Marey and by Howell, who did not attach to them any mathematical law of elasticity.

The present writers have investigated the elasticity of muscles again, and have found that their own data, as well as those of previous investigators, conform to the logarithmic law,

$$E = k \log W + c,$$

where E is the extension, W the stretching force, and k and c are constants.

This law is found to hold for muscles both striped and plain, and for nerve tissue. It seems to be true for all tissues except bone which, according to Wertheim, follows Hooke's law of elasticity for inorganic elastic matter.

One of the earliest, if not the first, quantitative investigations of the extensibility of the principal tissues chiefly of the human body was made in 1846 by Wertheim (15). His researches were very extensive and comprised numerous experiments on the comparative elasticities of bone, nerve, tendon, vein, and muscle from both human and canine sources, some of which were obtained immediately after death and others about five hours later. From his paper nothing can be gathered concerning the methods which he used to apply the stress to the tissues. Since, after death, chemical changes of a complex nature occur in all tissues, subsequent investigators have preferred to work with materials taken from the living animal.

Wertheim found that his measurements, when plotted with the stretching weights as abscissae and the corresponding extensions as ordinates, formed not a straight but a curved line which appeared to be approximately a hyperbola of the form given by the equation:

$$y^2 = ax^2 + bx,$$

where y represents extensions of the tissue in millimetres, x the stress in kilograms per square millimetre of its cross section, and a and b are constants. Since of necessity there is no extension when there is no stress, or $y = 0$ when $x = 0$, the vertex of the curve occurs at the origin of co-ordinates. From

---

[1] *Manuscript received December 1, 1938.*
Contribution from the Department of Physics, University of Manitoba, Winnipeg, Canada.

[2] *Demonstrator in Zoology, University of Manitoba.*

[3] *Professor of Physics, University of Manitoba.*

the graph Wertheim obtained numerical values of the constants, which have an extraordinary range in magnitude for different tissues as the following equations show:

$$\begin{array}{lrl} \text{Muscle,} & y^2 = & 14{,}549{,}333\,x^2 + 23{,}863\,x \\ \text{Vein,} & y^2 = & 1{,}174{,}780\,x^2 + 193{,}970\,x \\ \text{Artery,} & y^2 = & 257{,}747{,}000\,x^2 + 5{,}784{,}200\,x. \end{array}$$

With constants of such great magnitude, the equation could be forced to agree with the curve. As the constants are concerned chiefly with changes in the physiological properties that occur in tissues when being stretched, they have probably small numerical values. It is difficult to believe that the enormous magnitudes of the constants in Wertheim's equations have any physiological significance whatever.

The writers have replotted a number of Wertheim's series of measurements for the extensibility of muscle and nerve with logarithms of the stress as abscissae and extensions as ordinates, and three of them are shown in Fig. 1. The data from which they are plotted are reproduced in Table I. The letters *A*, *B*, and *C* on the graphs refer to corresponding letters in the table. The graphs consist of two or three rectilinear parts with abrupt changes of slope which are represented by the equation:

TABLE I

ELASTICITY OF MUSCLES AND NERVES. MEASUREMENTS OF WERTHEIM

Tissue	Weight, gm.	log W	Extension, mm.
A. Nerve—Tibial Posterior	150	2.18	7.38
	300	2.48	13.23
	450	2.65	19.40
	600	2.78	25.20
	750	2.88	30.64
	900	2.95	35.91
	1050	3.02	36.91
B. Nerve—Tibial Posterior	100	2	10.25
	200	2.30	16.13
	300	2.48	20.91
	400	2.60	24.62
	500	2.70	28.74
	700	2.85	33.40
C. Muscle—Stemomastod (dog)	8.4	0.92	7.40
	16.8	1.23	15.18
	25.2	1.40	22.88
	33.9	1.53	30.82
	42.5	1.63	36.22
	51.1	1.71	41.99
	59.7	1.78	48.46

1. *For convenience in plotting in the same figure, the characteristics of the logs in C have been increased by 1.*
2. *The weight is expressed in grams per square millimetre of cross section of the tissue.*

$$E = k \log W + c,$$

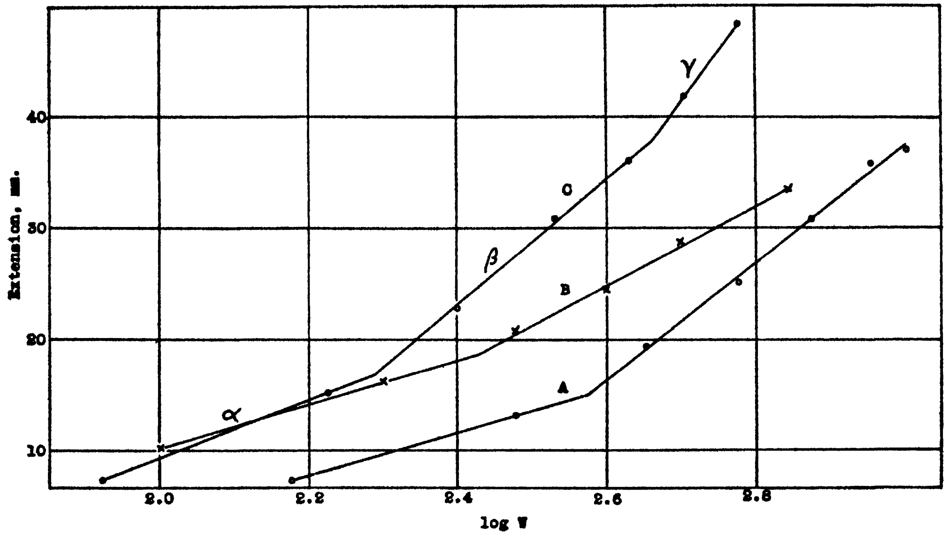

FIG. 1. *Wertheim's measurements of the elasticity of (A) nerve, (B) nerve, (C) muscle. The characteristics of log W for graph C have been increased by unity for convenience in plotting. Its real position is far to the left of the others.*

where E, replacing y in Wertheim's equation, is the extension, W, replacing X, is the stress, and k and c are constants, which have different numerical values in the different linear parts.

It may be remarked that Wertheim found the extensibility of bone to follow Hooke's law of elasticity for inorganic materials, which states that the elongation, or strain, is proportional to the stress, or, in symbols, $E = kW$.

Wertheim's measurements on any one tissue were few in number, especially for the smaller values of the stress. The lowest or α part of each graph therefore consists of only two points. The second or β parts, however, have from three to five points which satisfactorily demonstrate their rectilinear character. The third or γ part of one graph again has only two points. Since these graphs are found to be linear in form, Wertheim's proposed hyperbolic law of elasticity of organic tissues is evidently erroneous, and it can therefore be replaced by the simpler logarithmic law.

Wertheim measured the elasticity of human muscles (Sartorius) taken from subjects from 1 to 74 years of age, and from the measurements he computed the values of various constants:

Age	Value of a	Value of b	Coefficient of elasticity	Cohesion
1 (male)	607700	13832	1.271	0.070
21 (F)	1351875	8219	0.857	0.040
30 (M)	7960000	38860	0.352	0.026
74 (M)	14549333	23863	0.261	0.017

From these values it is clear that as age progresses both the elasticity and cohesion of muscles are greatly diminished. If the ages are plotted as abscissae and values of the coefficients of elasticity and of the cohesion as ordinates, the shape of the curves indicates that the diminution follows an exponential law. This is confirmed, since exponential and logarithmic curves are closely related, by plotting logarithms of ages as abscissae, when the exponential curves become approximately straight lines. In the curves for the coefficient of elasticity, however, the second value, for the age of 21, departs widely from the graphs; this may be due to the fact that the subject was female, whereas the other three were male. Though the data are few and inconclusive, it may be tentatively assumed that the elasticity and cohesion of human muscles diminish in magnitude as the logarithms of the ages increase; or, in symbols,

$$E = -k \log A + c,$$

where E represents either the coefficient of elasticity or the cohesion, A the age of the subject, and k and c are constants. The negative sign indicates that the properties of the muscles diminish with age.

These measurements on human muscles are of a kind perhaps never repeated and the likelihood of confirmation or correction is probably not soon to be expected. It would seem, however, that the elasticity and cohesion of the muscles drop to half their value at about 25 years of age, or one-third of a lifetime. By extrapolation of the graphs to the zero base line, the interesting conclusion is suggested that could human life be prolonged to the age of 200 years, the elasticity of muscles would vanish, and in half a century more not even cohesion would remain. Since vital functions rest upon elasticity, it is at least clear that the rapid diminution of this property is one of the chief relentless foes of longevity.

Following the researches of Wertheim came the investigations of Marey (12, p. 284), which are quoted by Howell (10, p. 22), who showed that as the stress to which a living muscle was subjected was increased, the resulting extension diminished. His measurements, when plotted with the increments of elongation as ordinates and the stretching weights as abscissae, form a curve which is concave to the horizontal axis up to the limit of elasticity. When this critical value was exceeded, however, the muscle began to lengthen by increasing extensions for equal increments of weight up to the point of rupture.

In his treatise on physiology, Howell (10, p. 21) gives two diagrams in which the elasticity of a rubber band is compared with that of the gastrocnemius muscle of a frog for equal stretching forces. The rubber band, following Hooke's law of elasticity, shows equal extensions for equal increments of weight, while the muscle, under the same conditions of stretching, gives decreasing extensions. Since Howell's diagrams are drawn to scale, the writers measured, on that for the muscle, the elastic extensions corresponding to the nine weights used. They are given in Table II, and are plotted in two ways in Fig. 2. When extensions of the muscle are plotted against weights as abscissae, which are indicated on the upper part of the figure, the resulting broken line has a curved form. But when the elongations are plotted against the logarithms of the weights, the graph is perfectly straight, as indicated by the continuous line, for eight of the points, while the ninth marks the beginning of a second linear part as in the graphs in Fig. 1. The equation representing the straight line is of the logarithmic type, precisely the same as before.

As part of a general plan of investigation of the responses to stimulation of different kinds of organs of the body which has been directed by one of the writers (Allen), Brisbin has conducted a series of researches on the elastic extensibility of muscles. His experiments were performed under conditions which, as far as possible, maintained the tissue under examination in its normal state. But in an investigation of this nature several factors may detrimentally influence the elasticity of the tissue. The complex chemical constitution of the fluids within the muscle substance undergoes alterations when the muscle is isolated which may affect its elasticity. Its properties are also influenced by changes in temperature as well as by the composition of the medium in which the muscle is immersed during the experiment.

TABLE II

Elasticity of muscles*

Weight, gm.	log *W*	Extension, mm.
20	1.30	0.19
23	1.36	0.36
26	1.42	0.50
29	1.46	0.63
32	1.51	0.75
35	1.54	0.86
38	1.58	0.96
41	1.61	1.05
44	1.64	1.16

**From "Text-book of Physiology" Howell. 12th ed. p. 21.*

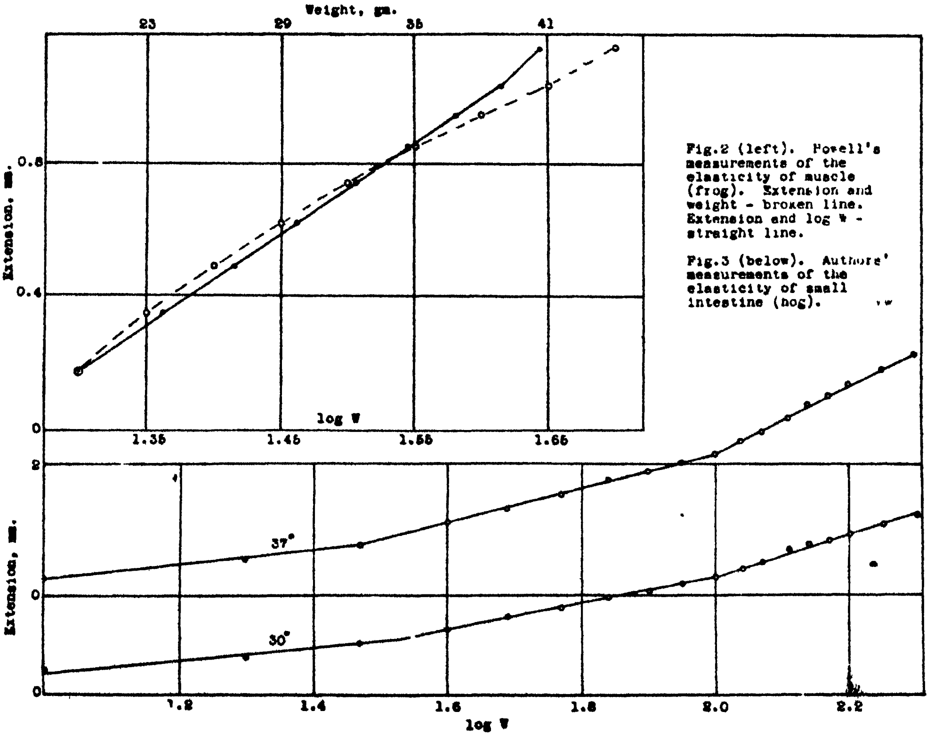

Fig.2 (left). Howell's measurements of the elasticity of muscle (frog). Extension and weight - broken line. Extension and log W - straight line.

Fig.3 (below). Authors' measurements of the elasticity of small intestine (hog).

It seems probable that the conditions governing a stretching muscle are similar to those prevailing during contraction. When a muscle shortens and doubtless also when it lengthens, the resting or equilibrium arrangement of the molecules or structural particles must rapidly change to other configurations appropriate to the new state. It was formerly concluded by Gasser and Hill (8) that the change of shape must be made against the hysteresis of the molecular system of the muscle and the viscosity of the muscle substance itself. An excited muscle is much less extensible than an unexcited one. In the former condition the new elastic state is produced and disappears more quickly than in the latter. A resting muscle when stretched and then released reaches equilibrium more rapidly than an active one, that is, an excited one was considered to be both more viscous and less extensible than one at rest. The basis of muscular contraction and extension was believed to consist of the two factors, elasticity and viscosity. In developing these views Levin and Wyman (11) concluded that the phenomena of muscular contraction could be accounted for on the assumption that the muscle is a complex system formed of two elements or mechanisms, one consisting of a free-elastic portion comparable to an undamped spring, and the other of a viscous-elastic portion comparable to a highly damped spring. The second portion was considered probably to be the contractile mechanism. Upon stimulation the latter elements were believed suddenly to change their elastic properties and thereupon to shorten and to stretch the free-elastic elements until a new condition of equilibrium is reached which is not directly proportional to the intensity of stimulation but follows an exponential law. Such a law is closely related to a logarithmic law. If the muscle consisted only of a structure with a free-elastic movement like a spring, as Weber assumed it to be, it might be expected when stretched to follow Hooke's law of elasticity. The presence of a viscous-elastic portion, or other complicating mechanism, however, indicates that the law of elasticity will likewise be complex, as the investigations of Wertheim and of the writers show it to be.

The most recent conclusions of Hill (9, p. 184) have radically altered these views by indicating that viscosity as a significant element in the process of muscular contraction must be entirely set aside. But the conclusion is maintained that "an active striated muscle is still a two-component system, consisting of an undamped purely elastic element in series with a contractile element governed by a characteristic equation" which, since it refers to the speed of contraction under stimulation, need not be considered here.

The measurements which are graphically shown in the figures of this communication, indicate that muscular elasticity, as far as elongation is concerned, is governed by a single logarithmic law. The fact that the graphs consist of several intersecting straight lines of different slopes may be interpreted as indicative of the existence of two components or processes which control the elasticity of muscles. The writers would prefer to consider the muscle not as two-component mechanisms, but as a single contractile-elastic system governed by two processes, one of which tends to enhance or facilitate and the other to reduce or partially inhibit the elastic response to stretching or contracting forces. In physical terms these conditions may be thus stated: as the stress on a muscle is uniformly increased, the strain is not proportional to it according to Hooke's law of elasticity, but it varies as if it were controlled by two opposing processes, the ratio of their magnitudes changing at certain critical values of the stress which are those where the slopes of the graphs abruptly change. The nature of these controlling processes, which must be inherent in the muscle substance itself, cannot yet be suggested.

A somewhat analogous idea (Saunderson) was advanced many years ago that "the excitatory process in a muscle is made up of two antagonistic component processes, one of which is associated with shortening the other with relaxation". The possibility has also been suggested (J. von Kries, 1892) that a muscle is re-excited by the very effort which it makes in contracting or striving to contract.

While the most recent work has been undertaken from the point of view of contraction, it seemed appropriate to study more fully the process of extension also. For this purpose the following experimental procedure was devised. A light celluloid cylinder, containing a normal saline solution in which the muscle preparation or other elastic tissue was immersed, was fixed in position on a massive stand. The ends of the muscle were held firmly without tearing in aluminium clamps, the upper of which was attached to a rigid support on the stand and the lower to a fine steel rod which passed freely through a hole in the base of the cylinder. The aperture was made water-tight by a large drop of medium grade oil which offered no resistance to the movement of the rod. The lower end of the rod carried a light scale-pan on which weights were placed to stretch the muscle. The extension of the muscle was measured with a micrometer microscope, reading to 0.005 mm., by observing the sharp point of a fine steel needle affixed horizontally to the base of the scale-pan.

TABLE III

ELASTICITY OF MUSCLES. SMALL INTESTINE (HOG)

Weight, gm.	log W	Extension mm. 30° C.	Extension mm. 37° C.
10	1	0.40	0.28
20	1.30	0.57	0.55
30	1.48	0.79	0.80
40	1.60	1.00	1.14
50	1.70	1.20	1.34
60	1.78	1.33	1.55
70	1.85	1.47	1.77
80	1.90	1.58	1.90
90	1.95	1.68	2.02
100	2	1.80	2.15
110	2.04	1.92	2.34
120	2.08	2.05	2.50
130	2.11	2.20	2.70
140	2.15	2.26	2.90
150	2.18	2.33	3.02
160	2.20	2.42	3.18
180	2.26	2.57	3.44
200	2.30	2.74	3.65

With this apparatus two series of measurements were obtained on the elasticity of pieces of the small intestine of the hog at temperatures of 30° and 37° C. The data are given in Table III, and they are plotted as before in

Fig. 3, in conjunction with Fig. 2. Each graph consists of three linear parts which conform to the logarithmic law of elasticity. The parts of the graph for 37° are more sharply differentiated than those for the lower temperature.

In arranging an experiment with the same apparatus on the gastrocnemius muscle of a frog, the following procedure was adopted. After pithing the specimen from which the muscle was to be taken, a short time was allowed to elapse before the muscle was removed, so as to permit any condition of shock due to the operation to subside. After removal the muscle was placed firmly between the clamps, and an initial weight of 20 gm. was placed in the scale-pan which was allowed to act upon the muscle for two minutes before measurements were taken. The microscope was focused on the sharp point of the needle on the scale-pan and the zero reading made. Additional weights of 10 gm. at a time up to 200 gm. were added at intervals of one minute, and the corresponding extensions of the muscle were measured by means of the micrometer. The temperature of the saline bath was maintained approximately constant within 1° C. while a series of readings was taken.

It may be remarked that in these experiments various initial weights were sometimes employed, but they were found to have no observable effect upon the elastic property of the muscles. The time during which the stress acted upon the muscle before the reading of its extension was made also appeared to be devoid of influence upon the character of its extensibility.

A group of five series of measurements on the gastrocnemius muscle was obtained, the data for which are given in Table IV and plotted in Fig. 4,

TABLE IV

ELASTICITY OF MUSCLES. GASTROCNEMIUS MUSCLE (FROG)

Weight, gm.	log *W*	Extension mm. 12° C.	Extension mm. 17° C.	Extension mm. 26° C.	Extension mm. 30° C.	Extension mm. 35° C.
10	1	0.25	0.18	0.35	0.30	0.19
20	1.30	0.50	0.42	0.67	0.57	0.44
30	1.48	0.75	0.73	1.00	0.80	0.75
40	1.60	1.02	0.92	1.22	1.37	0.91
50	1.70	1.27	1.08	1.52	1.70	1.10
60	1.78	1.47	1.25	1.77	1.95	1.25
70	1.85	1.58	1.43	2.00	2.20	1.37
80	1.90	1.70	1.52	2.22	2.47	1.51
90	1.95	1.88	1.61	2.45	2.73	1.66
100	2	2.00	1.72	2.67	2.90	1.75
110	2.04	2.13	1.83	2.85	3.10	1.83
120	2.08	2.25	1.91	3.00	3.30	1.90
130	2.11	2.36	2.00	3.14	3.47	2.01
140	2.15	2.43	2.08	3.36	3.72	2.08
150	2.18	2.57	2.14	3.50	3.87	2.17
160	2.20	2.62	2.24	3.62	4.12	2.25
170	2.23	—	—	—	4.30	—
180	2.26	2.78	2.35	3.84	—	2.36
190	2.28	—	—	—	4.52	—
200	2.30	2.90	2.44	4.05	—	2.50
210	2.32	—	—	—	4.80	—

with total extensions as ordinates and logarithms of weights as abscissae. Each series was taken with a different muscle and at a different temperature ranging from 12° to 35° C. The graphs are plotted to the same scale, but, to afford comparison without confusion, the ordinates for four of them are displaced upwards as indicated by the zero marks. Each graph consists of three linear parts which conform to the equation:

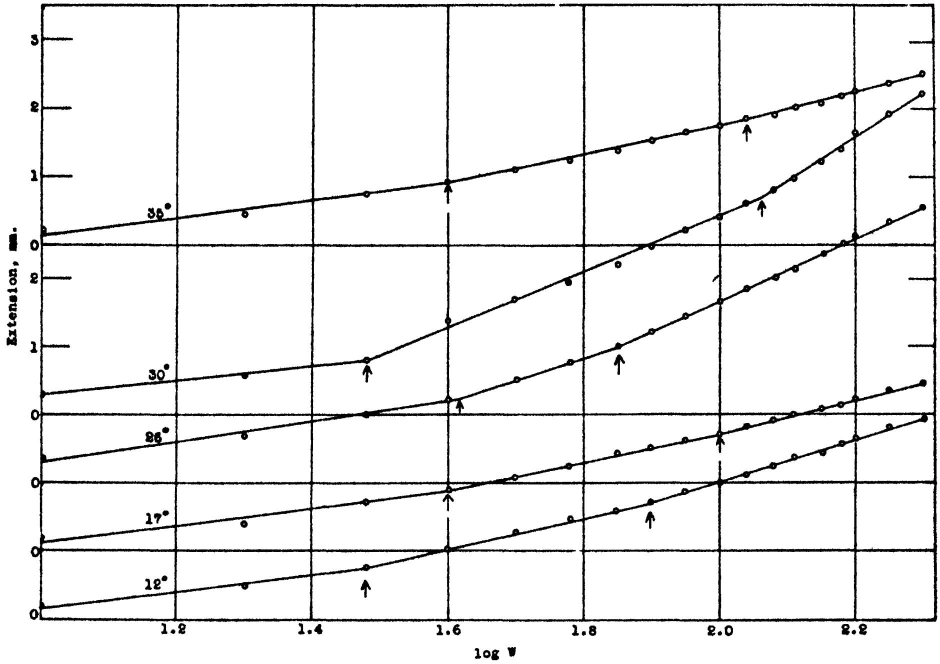

FIG. 4. *Elasticity of gastrocnemius muscle of frog at various temperatures.*

$$E = k \log W + c,$$

where E is the extension of the muscle produced by the weight W, and k and c are constants, which differ in numerical value for each part.

The influence of temperature upon the degree of elasticity is clearly shown, the graph for 30° having the best defined character as regards its linear parts.

From the positions of the intersection points of the parts of the graphs, it will be noticed that as the temperature of the muscle rises from 12° to 26°, it maintains the uniformity of its elastic properties for increasingly large stresses. At 30° this progression is reversed for the first point but not for the second. At 35° the graph approaches a straight line throughout its length; this indicates almost complete uniformity of elasticity for all values of the stress.

In the contraction of isolated muscles, the temperature has a marked effect. The gastrocnemius muscle of the frog loses its irritability at or slightly below 0° C., a maximum contraction is obtained at from 5° to 9° C., while a further rise in temperature to 15° or 18° causes a decrease in contraction. Beyond this point the contraction again increases to a second maximum at from 26° to 30°. A still further rise in temperature causes a diminution of contraction with a loss of irritability at 37° C.

In the present experiments on the stretching of muscles it was found that for temperatures ranging from 26° to 30°, the extension was from 3.4 to 6.05 mm.; for temperatures above 30° the extension fell to 2.5 mm., that is, a decrease in extension was shown. For temperatures from 12° to 17° the extension ranged from 2.44 to 2.9 mm., that is, a decrease in extension again occurs. The elasticity of the muscle at temperatures of 5° and 9° was also measured in this series of experiments, but the graphs are not given here. The extension was found to reach its first maximum value between these temperatures. It appears, therefore, that the relation between temperature and contraction applies also to temperature and extension.

During the summer of 1937 one of the writers (Brisbin) was enabled to continue the investigation at the Marine Biological Station, Wood's Hole, Mass., U.S.A., where he used the muscles of *Cancer irroratus* (Rock Crab), of *Callinectes sapidus* (Blue Crab) and of *Homarus americanus* (Lobster). In each case either the first or second pereiopodal or walking muscles were selected for the experiments on elasticity, the corresponding muscle in each species being always selected. A different specimen was used for each temperature which varied from 4° C. to 35° C. The measurements are given in Tables V, VI, and VII, and are plotted respectively in Figs. 5, 6, and 7.

TABLE V

ELASTICITY OF MUSCLES. *Cancer irroratus* (ROCK CRAB)

Weight, gm.	log *W*	Extension mm. 4° C.	Extension mm. 8° C.	Extension mm. 12° C.	Extension mm. 16° C.	Extension mm. 20° C.	Extension mm. 23° C.	Extension mm. 27° C.	Extension mm. 29° C.	Extension mm. 35° C.
20	1.30	0.51	0.85	—	0.69	0.33	0.65	0.25	1.10	0.82
30	1.48	0.82	1.40	0.68	1.03	0.58	0.80	0.77	1.55	1.27
40	1.60	1.04	1.90	1.07	1.40	0.90	1.05	1.10	1.90	1.42
50	1.70	1.38	2.15	1.50	1.63	1.05	1.11	1.25	1.96	1.60
60	1.78	1.67	2.55	1.77	1.86	1.23	1.20	1.45	2.11	1.75
70	1.85	1.89	2.95	1.93	2.11	1.29	1.20	1.50	2.21	1.82
80	1.90	2.09	3.07	2.05	2.36	1.33	1.40	1.79	2.40	1.90
90	1.95	2.25	3.35	2.27	2.49	1.38	1.57	1.83	2.57	2.06
100	2	2.45	3.55	2.53	2.65	1.40	1.64	2.04	2.75	2.12
110	2.04	2.60	3.76	2.80	2.78	1.49	1.75	2.08	2.85	2.20
120	2.08	2.76	3.94	3.01	—	1.61	1.84	2.27	2.92	2.26
130	2.11	2.89	—	—	3.08	—	1.91	2.34		2.32
140	2.15	3.01	4.05	3.23	—	1.78	2.02			2.34
150	2.18		—	—	3.52	—	2.06			Rupture
160	2.20		4.22	3.57	—	1.97	Rupture			
170	2.23		—	—	3.80					
180	2.26		4.47	3.80	—					
190	2.28		—		4.05					
200	2.30		4.53							
220	2.34		4.72							
240	2.38		4.95							
260	2.41		5.21							

In every case the total extension is plotted and not merely the increment of length for each additional weight. Increments, if desired, are easily obtained by subtracting successive values in the tables. It may be remarked that the same apparatus previously employed was used in the manner described above.

In Figs. 5, 6, and 7, the graphs are all plotted to the same vertical and horizontal scales. But in order to exhibit without confusion in the same figure the group obtained with each species of muscle at the different temperatures, the individual graphs are displaced vertically as in drawing Fig. 4. Though all zeros are not indicated on the figure, each graph has a separate zero value.

In Fig. 5 are shown nine graphs for the elasticity of muscles of as many specimens of Rock Crab at the different temperatures indicated. The initial weight was 10 gm., except for the temperatures 12° and 20°, where it was 20 gm., and the time elapsing after the weight was added and before the reading was taken was 1 min., except for 4° where it was 1.5 min., for 27° where it was 0.5 min., and for 20° where it was 2 min. The graphs consist of from two to four linear parts which conform to the logarithmic law of elasticity. The values of the initial weight and time intervals evidently have no apparent influence upon the form of the graph. All the measure-

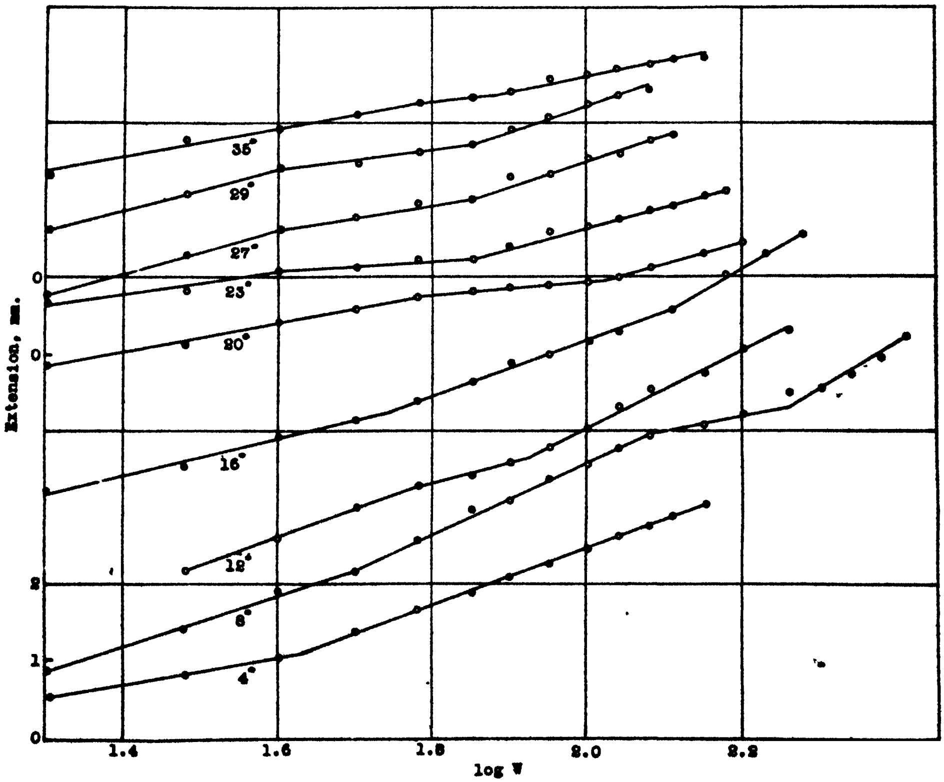

FIG. 5. *Elasticity of pereiopodal muscles of Rock Crab at various temperatures.*

ments lie on the graphs with remarkable precision. For in this and in the following two figures no point is away from the graph by an amount exceeding the very small quantity of 0.2 mm. By a comparison of the extensions for stresses of 140 gm. in Table V, it is seen that the value for 8° is the largest and that for 20° is the smallest. The extension rises to a maximum at 8° C. falls to a minimum at 20°, rises to a second but smaller maximum at 29°, and again falls to a minimum at 35°, the graph for which is nearly a single straight line. While a different muscle was used at each temperature, it is probable at least that at 8° the elastic properties of muscle of this species reach their most pronounced character. This temperature is probably near that of the water in which the crab lives. It is noteworthy that with two of these muscles, which were used at temperatures of 23° and 35°, the logarithmic law of elasticity held up to the point of rupture. In no other case was the point of rupture attained.

TABLE VI

ELASTICITY OF MUSCLES. *Callinectes sapidus* (BLUE CRAB)

Weight, gm.	log W	Extension mm. 7° C.	Extension mm. 14° C.	Extension mm. 22° C.	Extension mm. 27° C.	Extension mm. 30° C.	Extension mm. 34° C.
20	1.30	0.95	—	0.78	—	1.36	—
30	1.48	1.69	0.36	1.35	0.96	2.30	0.50
40	1.60	2.14	0.64	1.65	1.60	2.47	0.76
50	1.70	2.58	0.78	1.90	1.98	2.65	1.12
60	1.78	2.82	0.98	2.08	2.31	2.75	1.35
70	1.85	3.02	1.19	2.48	2.54	2.92	1.69
80	1.90	3.27	1.42	2.71	2.66	3.05	1.88
90	1.95	3.49	1.60	2.93	2.79	3.33	2.10
100	2	3.62	1.76	3.27	2.95	3.55	2.34
110	2.04	3.95	1.84	3.50	3.22	3.78	2.52
120	2.08	—	1.93	3.62	3.39	3.94	2.62
130	2.11	4.15	—	—	—	—	—
140	2.15	—	2.14	3.80	3.71	4.12	2.73
150	2.18	4.41	—	—	—	—	—
160	2.20	—	2.34	3.95	4.11	4.35	2.87
170	2.23	4.64	—	—	—	—	—
180	2.26	—	2.50	4.12	4.42	4.61	3.02
190	2.28	4.89	—	—	—	—	—
200	2.30	—	2.78	4.30	4.74	4.75	3.32
210	2.32	5.18	—	—	—	—	—
220	2.34	—	2.93	4.45	4.97	4.90	3.61
240	2.38	5.39	3.10	4.62	—	5.10	3.88
250	2.40	—	—	—	5.18	—	—
260	2.41	—	3.27	4.84	—	5.35	4.23
270	2.43	5.50	—	—	—	—	—
280	2.45	—	3.41	—	5.48	5.51	4.40
290	2.46	—	—	5.06	—	—	—
300	2.48	—	3.58	—	—	—	—
310	2.49	—		—	5.75	—	4.75
320	2.51	5.80		5.34	—	—	
330	2.52	—		—	—	5.92	
370	2.57	6.08		5.82	—	—	
380	2.58	—				6.28	

In Fig. 6 are shown six graphs for measurements of the elasticity of the muscles of the Blue Crab. These also in all cases conform to the logarithmic law of elasticity. For the same temperatures they differ in shape from those in the preceding figure. The graph for 7° is almost a single straight line, while that for 22° has the most pronounced character as far as the number and distinctness of the linear parts show. In half of the graphs the initial weight was 10 gm. and in the remainder 20 gm., and the time elapsing between successive readings, after each additional stretching weight was applied, was either 1 or 1 5 min., and the increments of weight were 10 gm. up to stresses of 120 gm Beyond this value the increments of stress were increased to 20 gm. up to 240 gm. and the time intervals were two minutes; for stresses in excess of 240 gm. the increments, as the table shows, were 30 gm., and in some cases, 50 gm , with slightly increased time intervals. None of these variations, however, show any want of conformity with the logarithmic law of elasticity. From the corresponding values in the table it appears that the extension of muscles in this species of crab is a maximum at 7°, a minimum at 14°, rises gradually to a second maximum at 30°, and declines towards a minimum again at 34°. This characteristic behaviour of the muscles of the Blue Crab is parallel with that of the Rock Crab, though the number of temperatures

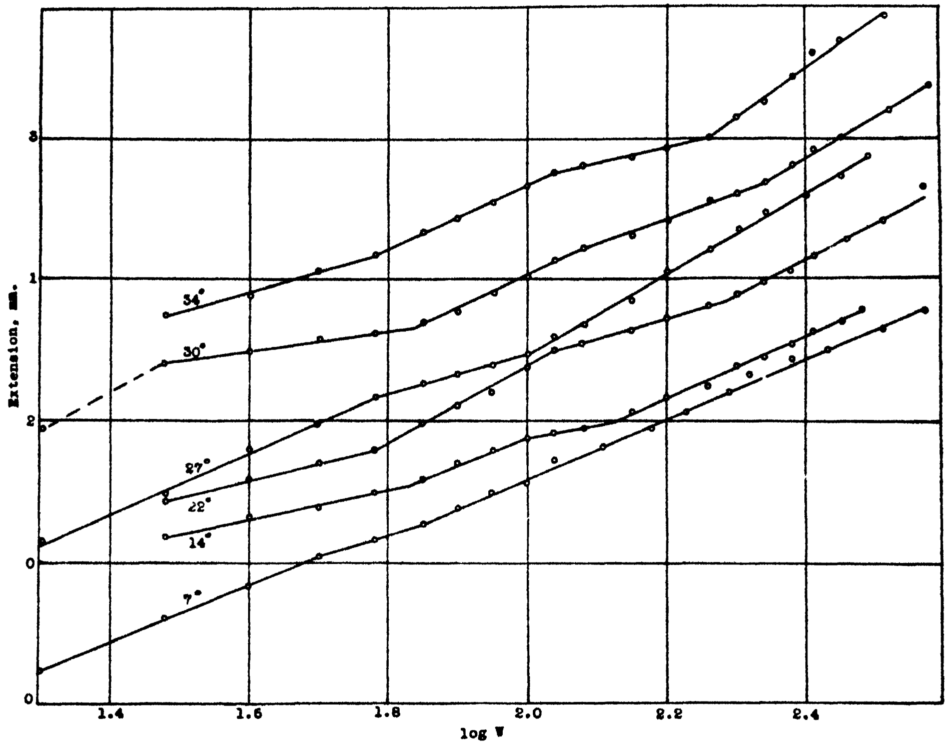

FIG. 6. *Elasticity of pereiopodal muscles of Blue Crab.*

upon which these conclusions are based is smaller in the former than in the latter case.

In Fig. 7 are shown nine graphs for measurements of the elasticity of the muscles of the Lobster. In all cases again they conform to the logarithmic law of elasticity, while the number of linear parts in the graphs varies from two to three. The graph for 10° is almost a single straight line and that for 22° is nearly so. In seven of the series of measurements the initial weight was 20 gm., and in the three remaining, for temperatures of 4°, 22°, and 30°, it was 10 gm. The time interval between readings while the weight was acting was generally 1.5 min., increasing to 2.5 min. when the increment of stress was increased to 20 gm. The corresponding values in Table VII show again a maximum extension of the muscles at 8°, a second maximum at 17°, and a third at 26°.

TABLE VII

ELASTICITY OF MUSCLES. *Homarus americanus* (LOBSTER)

Weight, gm.	log *W*	Extension mm. 4° C.	Extension mm. 8° C.	Extension mm. 10° C.	Extension mm. 12° C.	Extension min. 17° C.	Extension mm. 22° C.	Extension mm. 26° C.	Extension mm. 27° C.	Extension mm. 30° C.	Extension mm. 35° C.
20	1.30	0.42	—	—	—	—	0.41	—	—	0.61	—
30	1.48	0.93	0.52	0.35	0.40	0.18	0.84	0.37	0.35	1.07	0.18
40	1.60	1.30	0.98	0.74	0.65	0.34	1.28	0.82	0.75	1.56	0.34
50	1.70	1.60	1.37	1.10	0.97	0.75	1.60	1.20	1.12	1.87	0.44
60	1.78	1.81	1.70	1.40	1.45	1.13	1.81	1.52	1.35	2.05	0.60
70	1.85	2.19	2.05	1.56	1.73	1.65	2.08	1.86	1.65	2.21	0.75
80	1.90	2.41	2.30	1.82	1.95	1.85	2.23	2.09	1.82	2.42	1.04
90	1.95	2.67	2.50	2.00	2.10	2.12	2.42	2.39	2.09	2.67	1.45
100	2	2.80	2.74	2.17	2.37	2.48	2.60	2.61	2.37	2.86	1.62
110	2.04	2.93	2.98	2.27	2.55	2.70	2.79	2.87	2.61	3.02	1.81
120	2.08	—	3.07	2.43	2.72	2.98	—	3.09	2.78	—	1.96
130	2.11	3.20	—	—	—	—	2.95	—	—	3.28	—
140	2.15	—	3.30	2.65	2.90	3.30	—	3.35	3.10	—	2.24
150	2.18	3.37	—	—	—	—	3.13	—	—	3.59	—
160	2.20	—	3.42	2.80	3.10	3.52	—	3.62	3.36	—	2.47
170	2.23	3.61	—	—	—	—	3.37	—	—	3.77	—
180	2.26		3.59	3.01	3.37	3.78	—	3.91	3.71	—	2.80
190	2.28		—	—	—	—	3.51			3.95	—
200	2.30		3.72	3.22	3.42	3.98				—	3.02
210	2.32			—	—	—				4.11	
220	2.34			3.37	3.66	4.32					

Without exception the 35 graphs, for three different kinds of tissues, in this communication, as well as a number not herein contained, conform to the logarithmic law of physiological elasticity. Whatever may be the factors in the complex constitution of muscles that combine to give them their elasticity, it invariably follows a definite mathematical law. When it is remembered that an error in the measurement of the extension of a muscle of 0.1 mm. throws a point perceptibly off from the straight line in the graph, and that no point has a greater variation than 0.2 mm., it will be realized how precise is the conformity to the law. The presence of several linear parts in each graph shows also that muscular elasticity has not the same constants at all extensions or stresses, and that temperature modifies the elastic properties and constants without, however, destroying or changing the law. In its elastic properties muscular tissue clearly behaves much differently from inorganic materials which follow Hooke's simple law. It is quite possible that

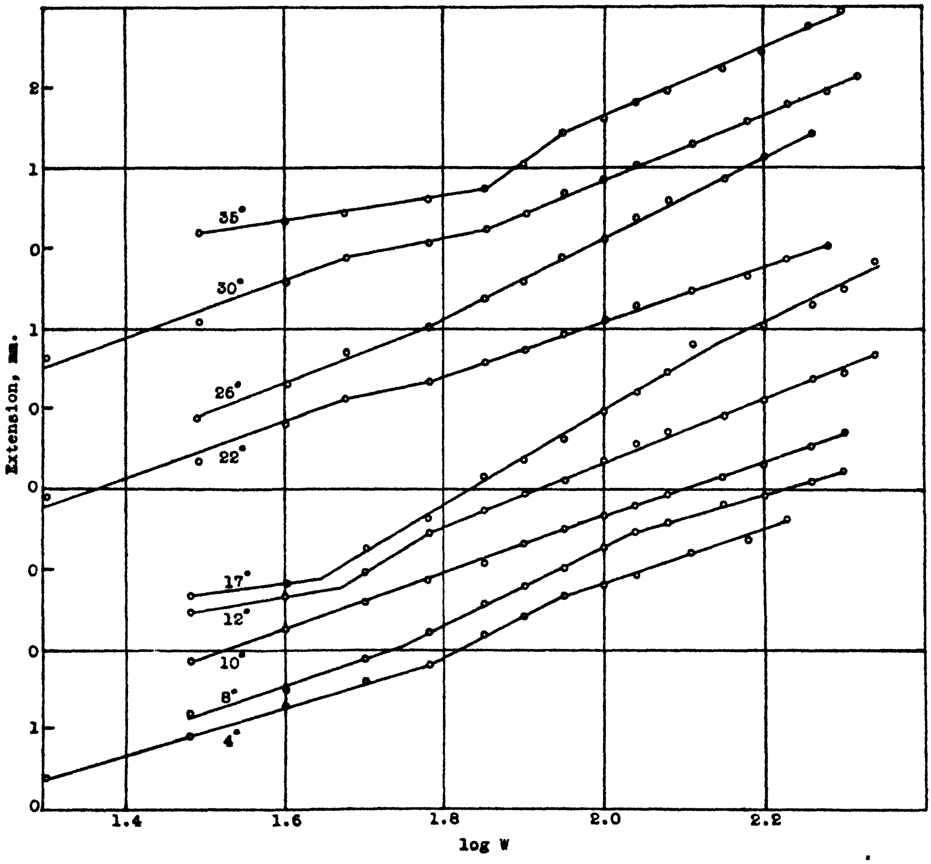

FIG. 7. *Elasticity of pereiopodal muscles of lobster.*

the logarithmic function enters the law of physiological elasticity because of the fact that a muscle is neither homogeneous nor isotropic in structure like a wire, but is composed of large numbers of fibres, each of which has contractility as well as elasticity. It is probable that each muscle fibre also obeys the same law of physiological elasticity since it likewise has a very complex structure. The logarithmic law of elasticity of muscles has the same form as the law of response to stimulation which has been found by Ferry (7) and by Porter (13) in vision, by Allen and O'Donoghue (5) in the post-contraction of muscles, by Allen (2) and his associates in the secretion of saliva, in the responses of the senses of hearing (1), taste (6) and touch (4), and in the processes of learning and relearning (3). Fundamentally it is similar to

Fechner's law connecting sensation and intensity of stimulation. It seems to be the characteristic mode of response for all activities of the organism where reactions to stimulation are involved.

It has generally been found that the elongations of a muscle under a stretching force gradually diminish in magnitude as the stress increases. This behaviour, indeed, is necessary for the effective working of muscles. It will be noticed in Tables V, VI, and VII that the elongations somewhat rapidly diminish towards fairly constant values, though in only two specimens of muscles (Table V) was the stress carried to the point of rupture of the muscles. In these cases the initial elongations for a stress of 10 gm. were 0.15 mm. and 0.45 mm.; with the former the elongation for an increase from 140 to 150 gm. fell to only 0.04 mm., and with the latter it was 0.02 mm. This is in accordance with other findings. In Table VI the measurements are shown for stresses up to 370 gm. In one case, at 7° C., the initial elongation for 10 gm. was 0.74 mm.; while for the last increment of 50 gm. it was 0.28 mm., which represents a lengthening of about 0.06 mm. for 10 gm. At 22° C. the corresponding elongations were 0.57 mm. and about 0.09 mm., and at 30° C. they were 0.94 mm. and 0.07 mm.

It may be concluded, therefore, that if the stresses had been sufficiently increased in all the experiments, there would have been found the conformity with the elastic behaviour of muscles which has been generally observed.

Acknowledgment

The authors desire to express their grateful appreciation of the generosity of Mr. James Richardson and Mr. H. E. Sellers of Winnipeg, who very kindly supplied the funds whereby the cost of the investigations at Wood's Hole was defrayed.

References

1. ALLEN, F. Phil. Mag. 47 : 941-944. 1924.
2. ALLEN, F. Quart. J. Exptl. Physiol. 19 : 337-362. 1929.
3. ALLEN, F. Brit. J. Psychol. 26 : 217-232. 1936.
4. ALLEN, F. and HOLLENBERG, A. J. Exptl. Physiol. 14 : 351-378. 1924.
5. ALLEN, F. and O'DONOGHUE, C. H. J. Exptl. Physiol. 18 : 199-242. 1927.
6. ALLEN, F. and WEINBERG, M. J. Exptl. Physiol. 15 : 385-420. 1925.
7. FERRY, E. S. Am. J. Sci. 44 : 192-207. 1892.
8. GASSER, H. S. and HILL, A. V. Proc. Roy. Soc. B, 96 : 398-437. 1924.
9. HILL, A. V. Proc. Roy. Soc. B, 126 : 136-195. 1938.
10. HOWELL, W. H. Textbook of physiology. 12th ed. W. B. Saunders and Company. Philadelphia. 1934.
11. LEVIN, A. and WYMAN, J. Proc. Roy. Soc. B, 101 : 218-243. 1927.
12. MAREY, E. J. Du mouvement dans les fonctions de la vie. 1868.
13. PORTER, T. C. Proc. Roy. Soc. 63 : 347-356. 1898.
14. SAUNDERSON, J. B. Textbook of physiology, Vol. 2, 363-364. Schaefer. 1900.
15. WERTHEIM, M. G. Ann. chim. phys. 21 : 385-414. 1847.

Canadian Journal of Research

Issued by The National Research Council of Canada

VOL. 17, SEC. A. APRIL, 1939 NUMBER 4

3 - 7 - 3

THE CONSTRUCTION OF A MAGNETIC ELECTRON MICROSCOPE OF HIGH RESOLVING POWER[1]

By Albert Prebus[2] and James Hillier[3]

Abstract

A brief historical review of the development of the electron supermicroscope is given. This is followed by a theoretical discussion of the resolving power attainable with the instrument and a summary of the important results which have been obtained by other workers. A description is given of the supermicroscope which has been recently constructed in Toronto. A number of photographs taken with the instrument demonstrate its high resolving power and its applicability as a tool in the sciences.

Introduction

(a) Historical

Modern atomic physics has shown that with a particle of mass m travelling at a velocity v there is associated a probability function which ascribes characteristics of a wave-train to the moving particle. The wave-length associated with an electron which has been accelerated by a potential difference of E volts is given by the de Broglie expression

$$\lambda = \frac{h}{mv} = \sqrt{\frac{150}{E}} \times 10^{-8}\ \text{cm.}$$

where h is Planck's constant. As the resolving power of present day microscopes is limited by the wave-length of the radiation used to illuminate the specimen under observation, the possibility of utilizing a high velocity electron beam for microscopic observation suggested itself. As shown by H. Busch (12) and C. J. Davisson and C. J. Calbick (14, 15), any axially symmetric magnetic or electrostatic field can be used for focusing an electron beam. We consequently speak of magnetic or electrostatic electron lenses. It was realized quite early that the simple magnetic lens consisting of the magnetic field of a solenoid was the most promising for the attainment of high resolving power and correspondingly high magnifications in the examination of microscopic specimens which do not themselves emit electrons.

Beginning their work in 1931, M. Knoll and E. Ruska (17, 18) devised the first magnetic electron microscope which consisted of two lenses, an objective and a projector. This work culminated in the construction of a two stage

---

[1] *Manuscript received January 19, 1939.*
Contribution from the McLennan Laboratory, Department of Physics, University of Toronto, Toronto, Canada.

[2] *Holder of a Bursary and Studentship under the National Research Council of Canada.*

[3] *Demonstrator in the Department of Physics, University of Toronto.*

microscope by E. Ruska (34, 35) in 1934, the resolving power of which definitely surpassed that of a light microscope. Except for the new "Rastermikroskop" of von Ardenne (2), the above-mentioned instrument is the prototype of all the microscopes which have since been constructed for a similar purpose. A beam of fast electrons (10 to 100 kv.) is incident normally upon an object which is in the form of a thin film. The transmitted beam is focused by means of a magnetic objective lens to form a real image of the object upon a fluorescent screen. Any part of this image may be remagnified by means of a magnetic projection lens to form a final highly magnified image upon a fluorescent screen or photographic plate. Focal lengths of the order of 5 mm. are attainable in each of the lenses. With an image distance of 50 cm. in each stage, a total magnification of 10,000 and greater is possible. Contemporary with this work of Ruska's, a similar microscope was constructed by L. Marton (26–32) in Belgium; the latter made the first attempt to examine biological specimens with such an instrument. A third microscope of this kind was constructed by L. C. Martin, R. V. Whelpton, and D. H. Parnum (24) in England. Owing to technical difficulties encountered, which have been described by L. C. Martin (23), the results obtained with this instrument have been seriously limited. More recently, the Siemens and Halske Allgemeine Gesellschaft, with the assistance of B. von Borries and E. Ruska (8), have constructed a new instrument based on Ruska's design of 1934. This instrument is especially designed for speed and convenience of manipulation and it is capable of a magnification of 56,000 diameters.

(b) Resolving Limit of a Magnetic Lens

It is of interest to review briefly the main factors which determine the limit of the resolving power, or more concisely, the resolving limit of a magnetic microscope objective lens. The term "resolving limit" may be defined on the basis of one of the factors to be considered, namely diffraction. Of course the actual resolving power of a magnetic lens is limited essentially by other factors to be considered later.

Two neighbouring points in an object which are either self luminous or which scatter incoherently the radiation incident on them from an extraneous source give rise to two independent diffraction patterns of the lens aperture in the plane of the image. The resolving limit R of the lens is defined as the distance between two such neighbouring points when the central maximum of one of their diffraction patterns falls upon the first minimum of the other. The numerical value of R is obtained from the well known formula of Abbé for a light lens with a circular aperture

$$R = \frac{1 \cdot 22\lambda}{2\mu \sin \alpha} \tag{1}$$

where λ is the wave-length of the radiation used;

μ is the refractive index of the medium in which the object is immersed;

and α is the semi-angle of the cone subtended by the aperture of the lens at the object.

In the case of the magnetic lens, the object is situated in a field-free region, so that μ may be set equal to unity; $\sin \alpha$ may be replaced by $\frac{D}{2f}$, where D is the aperture diameter of the lens and f is its focal length. This results in the approximate formula

$$R = \frac{1 \cdot 22\lambda}{2 \cdot \frac{D}{2f}} \tag{2}$$

In the above formula, it is to be observed that by increasing D the value of R can be made as small as desired.

The first factors which prohibit an unlimited increase in D are the third order lens errors. These have been studied by a number of investigators whose results are summarized by Busch and Brueche (13, p. 24 *et seq.*). Of the eight third order errors classified, spherical aberration is of the greatest importance since it affects the quality of the centre of an image as well as its eccentric regions. On the basis of Ruska's experimental work, von Ardenne (1) set up an empirical formula for the transverse spherical aberration which contains the results for one particular set of lens pole pieces of Ruska's microscope objective. This formula is

$$R' = \frac{D}{2} \cdot K \cdot \left(\frac{D}{D_p}\right)^2 \tag{3}$$

where R' is the radius of the circle of least confusion in the image plane divided by the magnification;

K is an empirical factor with the value 0.7;

D is the diameter of the aperture of the magnetic lens which is given approximately by the diameter of the circular opening in the diaphragm which is placed in the gap midway between the pole pieces P (see Fig. 1);

and D_p is the diameter of the narrowest part of the channel which is drilled through the pole pieces and through which the electrons pass.

In this relation, R' increases with D in contrast to the diffraction formula in which R decreases with increasing D.

On the assumptions *(a)* that when the diffraction pattern of a point is very small compared to the transverse spherical aberration, two points are resolved when the distance between them is equal to or greater than R', and *(b)* that when the radius of the circle of least confusion is equal to the radius of the first minimum of the diffraction pattern, two points are resolved for the same values of the radii as if either spherical aberration or diffraction alone were present, Equations (2) and (3) may be solved for $R'(= R)$ and D. With the numerical values

$f = 2.8$ mm.
$E = 75$ kv,

which are attainable with the new microscope of the Siemens and Halske Allgemeine Gesellschaft (8), and a value of D_p assumed by the authors

$$D_p = 3 \text{ mm.}$$

substituted into the equations, the values

$$R = 11 \times 10^{-8} \text{ cm.}$$
$$D = 1.4 \times 10^{-2} \text{ mm.}$$

are obtained. This resolving limit of 11 Å is two orders of magnitude greater than the resolving limit of a highly corrected oil immersion light microscope objective (4, p. 74). To realize this resolving power in practice, however, there are a number of other sources of error to be overcome.

The first of these is the analogue of chromatic aberration. In the first approximation, the focal length of a magnetic lens varies directly as the accelerating potential E of the electron beam. If the beam contains electrons which are accelerated within the range E to $E + \Delta E$, which may be due either to a constant velocity distribution or to a fluctuation in the accelerating potential, then a point image on the optic axis of the lens becomes a disc the radius d of which is given by a formula of von Ardenne (1)'

$$d = \frac{D}{2} \cdot \frac{\Delta E}{E}$$

Hence, to attain the limit of the resolving power of the lens under discussion, the constant velocity distribution and voltage fluctuation of the electron beam must have ranges which together amount to less than 2 volts.

The voltage fluctuation can be reduced to this low value only by the use of large condensers and special filtering devices in the high tension system. Any existent steady velocity distribution in the electron beam is enhanced by the passage of the beam through the specimen to be examined. Direct experimental data concerning this velocity distribution is scarce. The best estimate of its magnitude can be made from the older experiments which determine the most probable velocity loss and assuming that the half-width of the velocity distribution curve is equal to the most probable velocity loss. The results of these determinations in the range of velocities of interest in this connection may be represented by a formula given by W. Bothe (11), *viz.*,

$$v_0^4 - v^4 = ax \tag{4}$$

where v_0 and v are the incident and most probable velocities, respectively, of an electron which has traversed normally a metallic film of thickness x cm. The constant a depends upon the material of the film and is related to the atomic number Z, density ρ and atomic weight A of the element composing the film by the formula given by H. Bethe (7)

$$a = k \cdot \frac{\rho}{A} \cdot Z \tag{5}$$

where k is a constant. If the velocities v_0, v are converted into the correspending accelerating potentials $E + \Delta E$, E and the value of a for aluminium *viz.*, $a = 5.5 \times 10^{42}$, is substituted into the equations, Formulae (4) and (5) reduce to the convenient form

$$E \, . \, \Delta E = 22.1 \times 10^{9}\left(\rho \frac{Z}{A}\right)x \tag{6}$$

Predictions made with this formula may be expected to hold with reasonable accuracy for values of x greater than 10^{-4} cm., for it was with films of this thickness that the underlying data of the formula were obtained. Thus it is possible to predict the magnitude of the smallest observable details in the examination of specimens which consist of sections cut by a microtome. In the present state of development of these instruments, the practical lower limit of the thickness of a cut section is about 1×10^{-4} cm. If for example, such a cut section is composed of materials the atomic properties of which are similar to those of aluminium, then by Equation (6), a velocity distribution of 580 volts is to be expected. With the use of the objective lens which possesses a resolving power of 11 Å in the examination of a specimen which introduces no chromatic aberration, such a specimen may be examined with a resolving power of only 540 Å. This does not greatly exceed the resolution attainable with a good light microscope. However, a recent publication of von Ardenne's (3), in which he claims to have developed a new microtome capable of cutting sections much thinner than the above-mentioned limit, indicates that a considerably higher resolving power will be attained in the examination of this type of specimen.

Added to chromatic aberration there is another effect arising in the object which reduces the resolving power. This is the phenomenon of angular scattering. The quantitative calculations of von Ardenne (1) concerning this effect are applicable to film thicknesses greater than 10^{-4} cm., for his calculations are based on the assumption that multiple scattering obtains in the film. However, for film thicknesses less than this by several orders of magnitude, multiple scattering does not obtain and only qualitative conclusions can be drawn. It is evident that a section of film between the object element under examination and the objective lens causes a diffusion of the electrons which is analogous to the effect of inserting a ground glass screen between an object and lens when a light microscope is employed. Since the scattering becomes more diffuse with increasing film thickness, this must be kept low on account of angular scattering as well as for the effects of chromatic aberration. Because of these two phenomena, the type of specimen which is most ideally suited to observation with the electron microscope consists of small particles that are supported on a film which can be made arbitrarily thin. In this way the form and size of a great variety of particles which are otherwise too small to be visible may be determined. It is essentially in this domain that the electron microscope will have its most useful application, for it is just the instrument required to bridge the gap between X-ray and light microscope observations.

The sources of error discussed above are of fundamental importance. There are a number of others which reduce the resolving power, but these will not be discussed further here. They are mostly of an experimental nature and their effects more amenable to control.

(c) Image Formation

It is of interest to review briefly the factors which give rise to contrast in an electron optical image, for the intensity modulation of the electron beam is caused by phenomena which differ from those causing light intensity modulation. The intensity of a point in the image is governed by the electron absorption and scattering by the material at the corresponding point in the object. The quantitative discussions of von Ardenne (1) and Marton (25) of the magnitudes of these two effects are sufficiently accurate for film thicknesses greater than 10^{-4} cm. For thinner films, scattering is the essential cause of contrast, but a quantitative discussion is impossible for the same reason mentioned in the previous paragraph. If we consider two neighbouring object elements which are of the same density but of different thickness, or of the same thickness and of different densities, the number of electrons scattered by them into a cone of given angle will differ. Since the numerical aperture of a magnetic objective is very small (10^{-2} to 10^{-3}), a slight difference in thickness or density of the two object elements produces a large difference in the number of electrons which pass through the lens to reach the corresponding image points. It has been clearly demonstrated by previous workers that specimens which must be dyed in order to be seen by means of a light microscope can be photographed with ample contrast in the image by means of an electron microscope without the use of dyes, the contrast being produced by the scattering phenomenon.

(d) Applications of the Electron Microscope

The electron microscopes of E. Ruska and L. Marton have been used to examine a large variety of specimens. Marton (26) was the first to photograph prepared biological sections. His procedure consisted in impregnating the cell structures with an osmium salt. Thereupon he photographed an osmium skeleton of the cell after the natural structure had been charred by the electron bombardment. The first unprepared biological specimens to be photographed were sections of a fly's wing. This was accomplished by H. O. Müller (16) who used Ruska's microscope. However, it was F. Krause (20, 21, p. 59) who succeeded in obtaining photographs of delicate cell structures without the use of dyeing or fixing agents.

During the summer of 1936 Krause made a thorough investigation into the sources of experimental errors of Ruska's microscope, and then made a more exact determination of the resolving power of the instrument by examining diatom structures (19, 20). He was unable to find a sufficiently fine diatom structure to determine the resolving limit, and for this reason he investigated, with the co-operation of D. Beischer (5), primary crystallites of iron and nickel aerosols in which the particle sizes had been determined independently by an X-ray method. By this means he was able to obtain evidence which led him to conclude that a resolving power of 50 Å had been reached. This investigation together with further work with D. Beischer (6) has demonstrated the usefulness of the electron microscope in colloid chemistry. The size and form of the particles of a variety of colloid systems have been determined; whereas the particle size alone could be inferred by the older established indirect methods.

One of the most interesting applications of the electron microscope up to the present has been in the examination of bacteria and viruses. Reproductions, with a previously unattained magnification of 20,400, are shown of bacteria in a publication by B. von Borries, E. Ruska and H. Ruska (10). These permitted identification of structures and particles which were unknown before. It was F. Krause (22) who first photographed viruses, the greatest dimensions of which are less than 200 Å, particles which are nearly ten times smaller than those which can be observed in a light microscope. Viruses which had been previously increased in volume by artificial means and then just detected as points in a light microscope have been photographed in their natural state at a magnification of 21,900 and seen in their true form by means of the new microscope of the Siemens and Halske Allgemeine Gesellschaft (33). In this publication, as well as in a more recent one by B. von Borries and E. Ruska (9), further excellent examples of viruses and colloidal particles at very high magnifications are shown.

Description of Apparatus

In Fig. 1 is shown schematically a cross section of the magnetic electron microscope which was constructed in this laboratory in the spring of 1938.

Electrons leaving the cathode *F* are accelerated vertically downwards and pass through the anode *A*, deflection plates *D*, and condensing lens *Co*. This lens converges the beam of electrons to a small cross section at the position of the object *O*. The object elements scatter and absorb the electrons striking them, in proportion to their relative thickness and atomic properties. The scattered electrons, which on leaving the object elements pass through the aperture of the objective lens *Obj*, are focused by the strong axially symmetrical magnetic field of this lens to conjugate image points upon the first image screen I_1. The electrons from any desired part of this image are directed through an opening in the screen into the second or projection lens *Pro*. They are focused by the magnetic field of this lens to form a magnified image of this selected part of the first image on the second screen I_2. The image at this point may be viewed with the aid of the fluorescent screen or recorded photographically by replacing the screen with a photographic plate. A high magnification is obtained in each lens by the choice of a large ratio image distance to object distance. The total magnification is of course the product of the magnifications produced by each lens.

Before various parts of this apparatus are described in more detail, some fundamental factors which were considered in its design will be discussed.

An examination of the data on the phenomena which cause aberrations in image formation shows that all of them are reduced as the accelerating potential of the electron beam is increased. Hence it is desirable to use the highest possible accelerating voltage consistent with other considerations. Ruska's

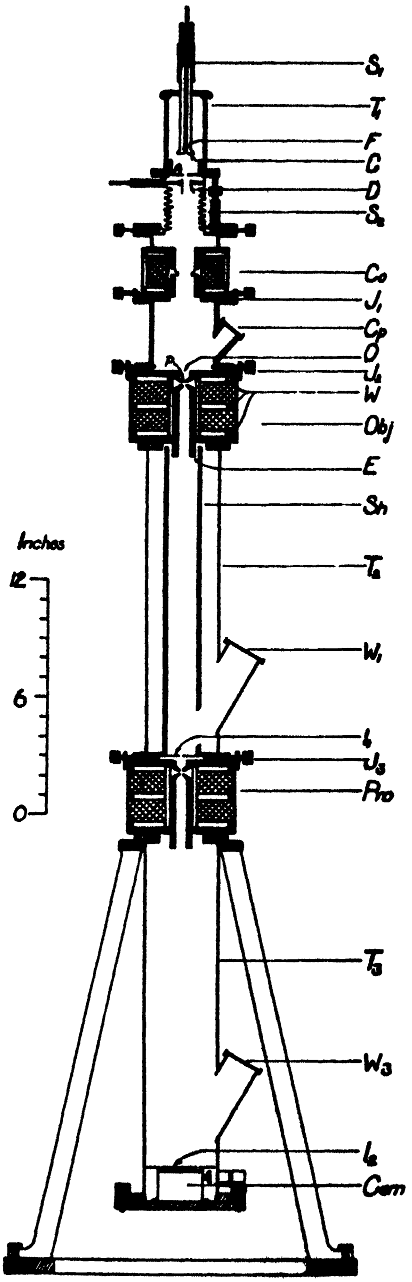

FIG. 1

experimental results (34, 35) and von Ardenne's considerations reviewed in the "Introduction" indicate that a resolving power of the order of 10 Å might be attainable with an uncorrected simple lens. With the use of fine grained photographic plates of resolving power 1×10^{-2} mm. the minimum magnification required to record the smallest details in the image produced by such a lens is 10,000. An image distance of 50 cm. in each stage was chosen as convenient from the point of view of construction and operation. If the magnifications obtained in each stage are equal, a focal length of less than 5 mm. is required in each lens. The lenses were designed and constructed to fulfil these requirements, and later tests showed that for an accelerating potential of 45,000 volts a focal length of less than 2 mm. is attainable. Since the focal length is directly proportional to the accelerating potential of the electron beam, it appears that focal lengths of less than 5 mm. will be easily attainable at the highest potential deemed practical, *viz.*, 100,000 volts. The remainder of the instrument and the auxiliary apparatus were designed accordingly.

(a) Electron Source and High Tension System

After gas discharge tubes of various designs were tried as a source of electrons, a choice was made in favour of a hard vacuum thermionic tube because of its ease of control and constancy of operation. As shown in Fig. 1, the source of electrons is a tungsten filament F in the shape of a hairpin which is mounted at the lower end of a rod. This may be raised or lowered with respect to the remainder of the cathode assembly while the apparatus is in operation by means of a screw and bellows arrangement S_1. The lower tip of the filament is situated on the axis of the tube just above the centre of a circular opening in the concave cathode shield C. The whole cathode assembly is sealed with wax to the upper end of the glass tube T_1 which serves as an insulator. The adjustment of the filament position with respect to the cathode shield overcomes two difficulties found in the use of a hot cathode as an electron source. First, it is possible to draw the filament far enough into the cathode shield so that only the electrons emitted from the very tip of the hairpin filament can escape. Thus the advantage of point emission of the gas-discharge tube is retained. Second, the efficiency of the thermionic cathode is greatly increased, and it is possible to keep the total emission current well below the limit set by the permissible chromatic error with ample intensity of the image for observation. In the high tension system used, the voltage ripple and consequent chromatic error increases directly with the total emission current.

The high tension system consists of a step-up transformer with one terminal earthed, hard vacuum half-wave rectifier, and a filter system. This consists of a condenser the negative terminal of which is connected to the anode of the rectifier and the cathode of a saturation diode, the anode of which is connected to the negative terminal of a second condenser. The cathode of the microscope discharge tube is connected through a stabilizing resistance to the negative terminal of this second condenser. All of the high tension apparatus and connecting leads are carefully shielded against the effects of corona. Calculation shows that if the total current drawn is below 0.1 ma. the fluctuation in the accelerating potential is less than 1 volt in 50,000. The actual control of the ripple is highly sensitive to the adjustment of the saturation diode.

(b) Beam Trap and Condenser Lens

The beam trap consists of a pair of deflection plates D, Fig. 1, so arranged that the beam is deflected away from the object when one plate is raised to a potential of 2,000 volts with respect to the other. It is used as a shutter when a photographic exposure is made and in general to limit the time of exposure of the object to the electron beam to the minimum which is required for focusing and photographing.

The electron source and the beam trap are attached to the upper end of the condenser by means of a bellows adjustment arrangement S_2 which allows the source to be displaced horizontally or tilted in any direction in order to bring the electron beam into coincidence with the axis of the condenser coil. The condenser Co is an iron encased coil with a central circular gap which concentrates the magnetic field to a small region along its axis. The coil consists of 2700 turns of No. 24 B & S enamelled wire and it is provided with a disc shaped water cooling jacket on each side. The lower face of the iron casing is ground plane and sealed with vacuum grease to a corresponding ground surface J_1 on the upper side of the object chamber. By means of this sliding joint and adjustment screws it is possible to move the electron source, beam trap, and condenser as a unit in any direction perpendicular to the axis of the microscope. In this way the illuminating pencil of electrons can be brought into coincidence with the axis of the objective lens, and the image of the emitting area of the cathode can be focused upon the centre of the object.

(c) Object Chamber and Specimen Holders

Specimen holders are inserted into the apparatus through the opening Cp of the object chamber. This opening is a simple conical grease joint. Two types of specimen holders have been used. One of these is in the form of a hollow cartridge which fits snugly into a collar over the objective lens. The lower end of the cartridge is about 5 mm. above the centre of the gap between the pole pieces of the lens. This simple arrangement makes it easy to replace the specimen holder into exactly the same position after it has been removed and reloaded. The other type of specimen holder is a similar cartridge mounted on the end of a hollow screw. With this it has been possible to vary the object distance during operation by turning the plug of a grease joint to which the screw is geared. This joint is fixed in the wall of the object chamber. The actual specimens are suspended across a small hole (0.05 to 0.3 mm.) in the centre of a circular platinum diaphragm which is held at the lower end of the specimen holder by a cap. During operation the holders are held in position by a support fixed in the object chamber. Since this is sealed to the objective lens by means of a flat grease joint J_2, the object is readily displaced in any horizontal direction. Hence any part of it may be selected for examination.

(d) Lenses

In the design of the lenses, the foremost consideration was given to ease of adaptability or alteration, for it was expected that their optical properties would vary widely with the configuration and strength of their fields. Since, with the exception of the pole pieces, the projection coil is identical with the objective, a description of only one of them will be given.

Two coils, each of 2700 turns of No. 22 B & S enamelled wire are wound upon a brass cylinder. To the ends of this cylinder are soldered two iron discs with their outer faces ground plane. Similar ground plates forming the bases of the image tubes and object chamber may be sealed to the coil with vacuum grease. The outer iron cylinder which slides snugly over the coil, and the inner sleeve E, which is threaded into the base plate and central brass cylinder, complete the magnetic circuit. Into the upper end plate and upper end of the central sleeve, interchangeable pole pieces P are threaded. The distance between these may be altered at will by turning the sleeve E. Three disc shaped water jackets W are provided for cooling the coils and the grease joints

The pole pieces in use are conical with flattened ends. An accurately machined brass spacer arrangement placed between the pole pieces permits them to be aligned with precision and fixed rigidly. The diaphragm which is used to limit the spherical aberration of the lens is a piece of platinum foil through which a small hole (0.1 to 0 05 mm. in diameter) is punched. This is soldered to the end of a brass tube which fits tightly inside the spacer.

(e) Miscellaneous Parts

At the lower end of the brass tube T_2, which separates the objective and projection lenses, a fluorescent screen is mounted upon which the first image may be viewed through the window W_1. Inside this first tube and concentric with it there is a soft iron pipe Sh which is used to shield the electron beam from stray varying magnetic fields. The third grease joint J_3 allows the second image to be displaced relative to the projection coil. The second tube in the microscope T_3 is fastened to the support of the instrument. This consists of four bronze legs. The lower end of the tube carries the camera Cam and the second image screen I_2 which are fastened to the upper side of the plate that seals the end of the tube. This also is a flat grease joint. The camera consists of a platform which bears the photographic plate and a hinged fluorescent screen I_2 which covers it. When a photographic record of the image is desired, the screen may be lifted out of the way by means of a conical grease joint fixed in the wall of the tube

Experimental Results

The work carried out with the apparatus since its construction was completed has been restricted to the identification and elimination of the perturbing effects which cause undesired movements of the image. These effects are numerous and have not yet been overcome completely.

As mentioned under a previous heading, a cold cathode gas discharge tube was used initially as the source of the electron beam. This was chosen because of two advantages which it possesses over a hard vacuum thermionic cathode tube. Emission of the electrons from a small spot of the cathode allows a beam of small cross section to be focussed upon the object without the necessity of a specially constructed electron converging lens. Secondly, the impedance of a gas discharge tube to a voltage ripple in the high tension system is an order of magnitude lower than that of a thermionic cathode tube. This property of the tube was considered as a necessary complement to the filter system initially employed. However, all the various gas discharge tubes which were tried were found defective in one respect. Subsequent to the letting of air into the apparatus, they required several hours of operation before they reached a steady state. The delays occasioned by this troublesome outgassing process prevented a systematic study of other perturbing effects. An efficient thermionic cathode tube and magnetic condensing lens were finally constructed, and with these it is possible to obtain steady operating conditions immediately after the apparatus has been sufficiently well exhausted. Furthermore, the intensity of the electron beam can be varied within wide limits, and it is now possible to observe with ease images magnified 20,000 diameters and to photograph them in exposure times of the order of one second.

Another of the major difficulties encountered is the effect of electric charges which are built up on the surfaces of the specimen holders and lens diaphragms owing to oxidation brought about by electron bombardment and subsequent exposure to air. It was found necessary to shield all parts of the specimen holders, lens diaphragms, and spacers from exposure to the electron beam by means of platinum diaphragms which can readily be removed and cleaned.

Destruction of the collodion membranes which are used to support the specimens by the heating effect of the electron beam was also a cause of trouble. A thin film suspended across the opening of a diaphragm should be heated in proportion to its absorption coefficient for the electron beam. However it was found that quite transparent membranes ruptured and disintegrated rapidly when under observation, apparently because of excessive heating. The cause of this was traced to the absorption of electrons by the metal diaphragm over which the membrane was suspended. By placing a

---

CAPTIONS FOR PLATE I, FACING THIS PAGE.

FIG. 2-A. *Light microscope photograph of Pleurosigma angulatum; magnification, 480; 4 mm. water immersion achromatic objective of N. A. 1.00; blue filter.*

FIG. 2-B. *Light microscope photograph of Pleurosigma angulatum; magnification, 1070; 1/12 in. oil immersion achromatic objective of N. A. 1.30; blue filter.*

FIG. 2-C. *Electron microscope photograph of Pleurosigma angulatum; magnification, 1700; enlarged to 2500. Accelerating potential, 16 kv.*

FIG. 2-D. *Electron microscope photograph of Pleurosigma angulatum; magnification, 6250; enlarged to 25,000. Accelerating potential, 45 kv.*

FIG. 2-E. *Electron microscope photograph of Pleurosigma angulatum; magnification, 9000; enlarged to 36,000. Accelerating potential, 45 kv.*

FIG. 2-F. *Electron microscope photograph of edge of melted section of Pleurosigma angulatum; magnification, 20,000; enlarged to 80,000. Accelerating potential, 45 kv.*

PLATE I

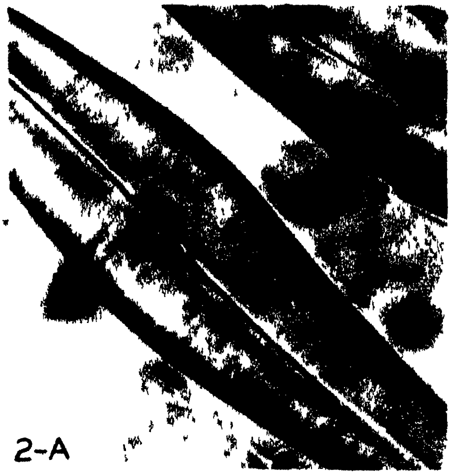
2-A

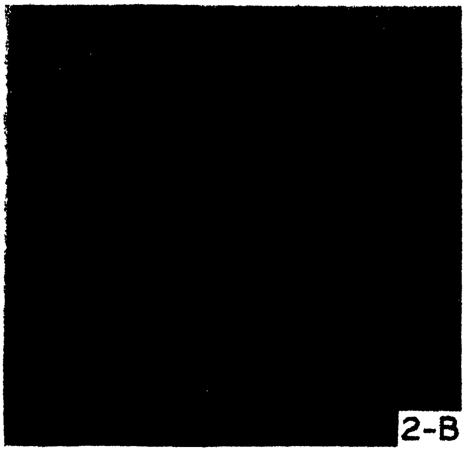
2-B

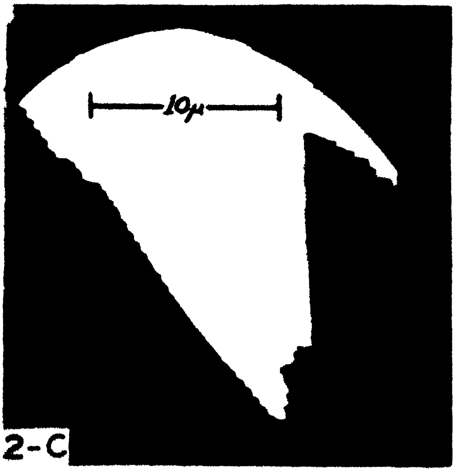

2-C

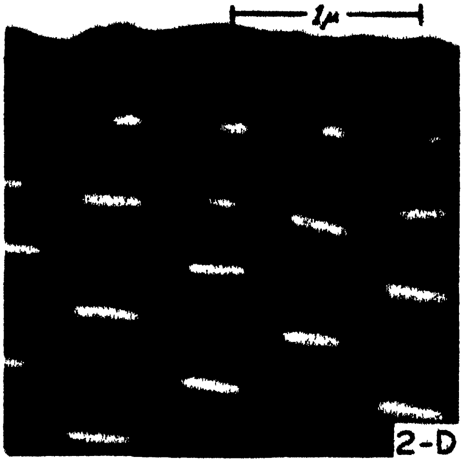

2-D

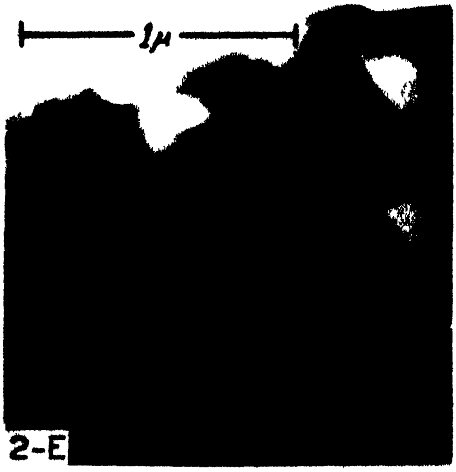

2-E

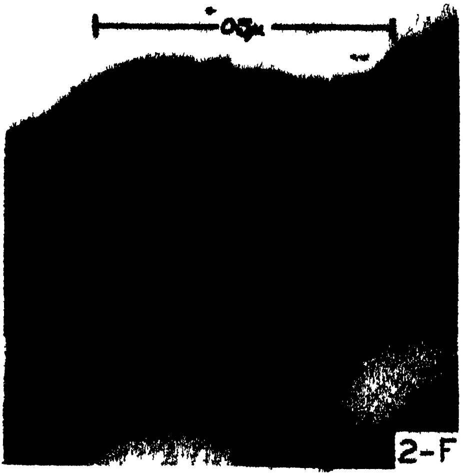

2-F

diaphragm a considerable distance above the specimen to limit the cross section of the electron beam so that it struck the membrane alone, the heat generated by the absorption of electrons by the metal was dissipated by conduction away from the specimen.

The photographs shown in Figs. 2 and 3 are selected from those which have been taken in the course of the investigation of the effects which impair the quality of the photographic records of the observed images.

Figs. 2-A and 2-B are light microscope photographs of sections of a diatom *(Pleurosigma angulatum)* magnified 480 and 1070 diameters respectively. These are representative of the resolving power attainable with a good microscope. Fig. 2-A was taken with the use of a water immersion achromatic objective lens of focal length 4 mm. and numerical aperture 1.00 with blue light illumination; Fig. 2-B with an achromatic 1/12 in. oil immersion objective of numerical aperture 1.30. Fig. 2-C is a reproduction of a section of the same diatom magnified 2500 diameters; this was obtained at a magnification of 1700 diameters with the electron microscope shortly after its completion. The accelerating potential of the electron beam was 16 kv. Although a shift of the image caused by an unavoidable change of pressure in the discharge tube then used is evident, the sharpest bounding edge of the diatom in the photograph allows a resolving power of 600 Å to be inferred. This is considerably better than the resolving power shown in the light microscope photographs. Figs. 2-D, 2-E, and 2-F are reproductions, enlarged four diameters, of electron microscope images of the same type of diatom which have been obtained recently. These are magnified 6,250, 9,000, and 20,000 diameters respectively by the electron microscope. Although the photographs demonstrate the high resolving power attained with the apparatus, an exact evaluation of its magnitude cannot be made from them owing to the fact that the bounding edges of the structures are not sharply defined for a high velocity electron beam. In Fig. 2-E the effect of an image shift is again evident. Fig. 2-F demonstrates the sharpness of image definition attainable even at the high magnification of 20,000 diameters. It shows a small section of the silica shell of a diatom after it has been partially melted by the heat of the electron beam.

Fig. 3-A is an enlarged reproduction (four diameters) of the image of the cutting edge of an unused razor blade magnified 8,000 diameters by means of the electron microscope; double the width of the best defined regions of the bounding edge, as measured in the original of the reproduction, divided by the corresponding magnification, leads to a value of 140 Å for the resolving power shown in this photograph. Figs. 3-B and 3-C are similarly enlarged reproductions of images, magnified 9,000 diameters by the electron microscope, of particles of two specimens of clay supported on a collodion membrane approximately 150 Å thick. These specimens are of a fresh and burned clay, respectively, which is used in refining gasoline. The photographs are also of interest because of the large number of small particles visible, whose origin is in the supporting membrane. A number of pairs of these particles may be

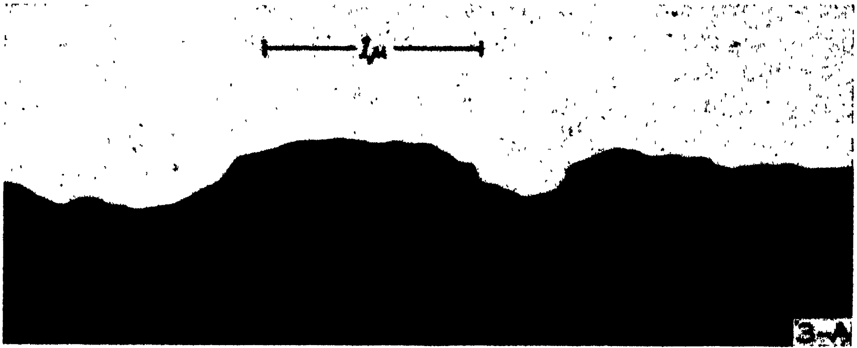

3-A

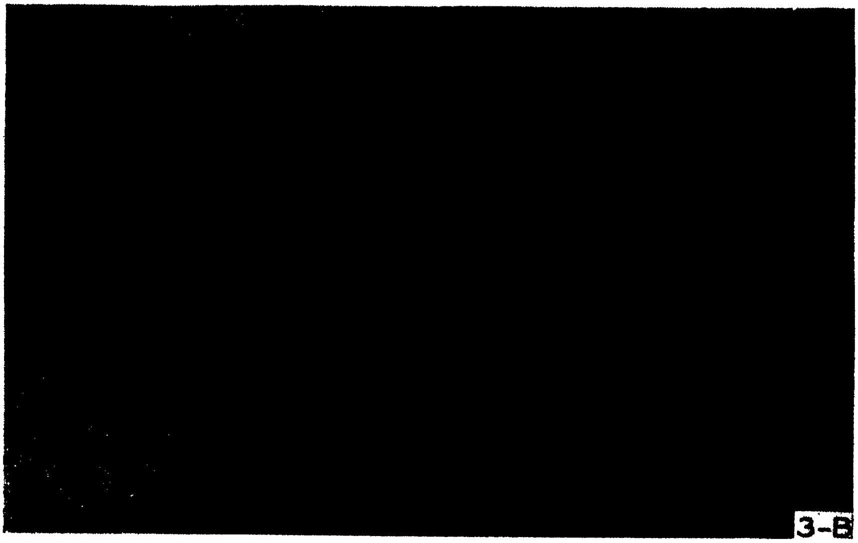

3-B

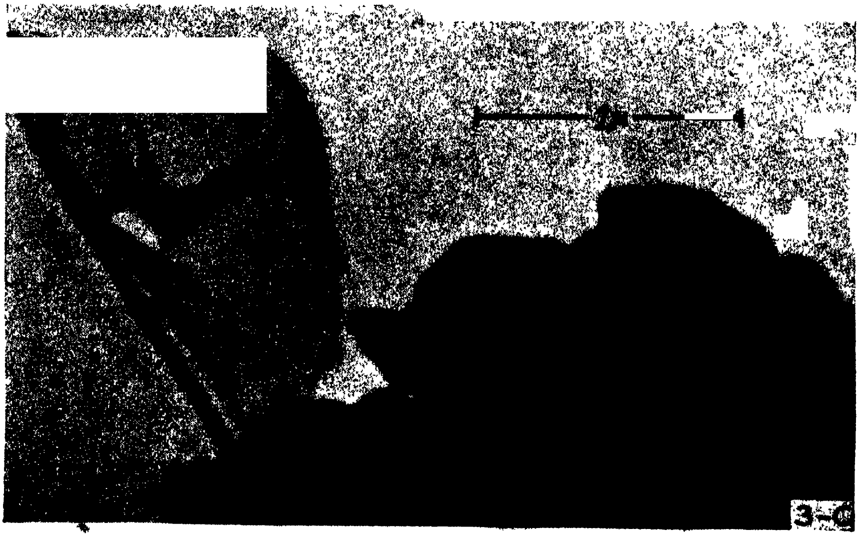

3-C

found which are just separated. The smallest distances of separation, measured in the original, show that the resolving power is better than 200 Å.

Acknowledgments

The authors take this opportunity to express their appreciation to Dr. E. F. Burton, Director of the McLennan Laboratory, University of Toronto, for the interest he has shown in the progress of this work and for the laboratory facilities which he has placed at their disposal.

To Prof. Stanley Smith, Department of Physics, University of Alberta, they wish to express their gratitude for the loan of two high tension condensers which are the property of the University of Alberta.

References

1. Ardenne, M. von. Z. Physik, 108 : 338-352. 1938.
2. Ardenne, M. von. Z. Physik, 109 : 553-572. 1938.
3. Ardenne, M. von. Z. Physik, 111 : 152-157. 1938.
4. Beck, C. The microscope. R. and J. Beck, London. 1937.
5. Beischer, D. and Krause, F. Naturwissenschaften, 25 : 825-829. 1937.
6. Beischer, D. and Krause, F. Angew. Chem. 51 : 331-335. 1938.
7. Bethe, H. Ann. Physik, 5 : 325-400. 1930.
8. Borries, B. von and Ruska, E. Wiss. Veröffent. Siemens-Werken, 17 : 99-106. 1938.
9. Borries, B. von and Ruska, E. Z. tech. Physik, 19 : 402-407. 1938.
10. Borries, B. von, Ruska, E., and Ruska, H. Wiss. Veröffent. Siemens-Werken, 17 : 107-111. 1938.
11. Bothe, W. Handbuch der Physik, 25 : 26. Julius Springer, Berlin. 1927.
12. Busch, H. Ann. Physik, 81 : 974-993. 1926.
13. Busch, H. and Brueche, E. Beitr. zur Elektronenoptik. J. Barth. Leipzig. 1937.
14. Davisson, C. J. and Calbick, C. J. Phys. Rev. 38 : 585. 1931.
15. Davisson, C. J. and Calbick, C. J. Phys. Rev. 42 : 580. 1932.
16. Driest, E. and Müller, H. O. Z. wiss. Mikroskop. 52 : 53-55. 1935.
17. Knoll, M. and Ruska, E. Ann. Physik, 12 : 607-640. 1932.
18. Knoll, M. and Ruska, E. Z. Physik, 78 : 318-339. 1932.
19. Krause, F. Z. Physik, 102 : 417-422. 1936.
20. Krause, F. Naturwissenschaften, 25 : 817-825. 1937.
21. Krause, F. Beitr. zur Elektronenoptik. J. Barth. Leipzig. 1937.
22. Krause, F. Naturwissenschaften, 26 : 122. 1938.
23. Martin, L. C. Nature, 142 : 1062-1065. 1938.
24. Martin, L. C., Whelpton, R. V., and Parnum, D. H. J. Sci. Instruments, 14 : 14-24. 1937.
25. Marton, L. Physica, 3 : 959-967. 1934.
26. Marton, L. Nature, 133 : 911. 1934.
27. Marton, L. Bull. acad. roy. Belg. 20 : 92. 1934.
28. Marton, L. Bull acad. roy. Belg. 20 . 439-446. 1934.
29. Marton, L. Phys. Rev. 46 : 527-528. 1934.
30. Marton, L. Rev. optique, 14 : 129-145. 1935.
31. Marton, L. Bull acad. roy. Belg. 21 : 553-564. 1935.
32. Marton, L. Bull. acad. roy. Belg. 21 : 606-617. 1935.
33. Müller, H. O. Elektrotech. Z. 59 : 1189-1194. 1938.
34. Ruska, E. Z. Physik, 87 : 580-602. 1934.
35. Ruska, E. Z. Physik, 89 : 90-128. 1934.

Captions for Figs. 3-A, 3-B, and 3-C, facing this page.

(Reproductions slightly reduced in printing)

Fig. 3-A. *Electron microscope photograph of the cutting edge of a razor blade; magnification, 8000; enlarged to 32,000. Accelerating potential, 45 kv.*

Fig. 3-B. *Electron microscope photograph of a particle of fresh clay. Blackened area is a section of the particle; background is the supporting collodion membrane; magnification, 9000; enlarged to 36,000; Accelerating potential, 45 kv.*

Fig. 3-C. *Electron microscope photograph of a particle of burned clay. Blackened area is a section of the particle. The ruptured supporting membrane is shown at the left; magnification, 9000; enlarged to 36,000. Accelerating potential, 45 kv.*

THE EFFECT OF CHROMATIC ERROR ON ELECTRON MICROSCOPE IMAGES[1]

By James Hillier[2]

Abstract

The effect on the intensity distribution of point to point variation of the chromatic error in electron microscope images is investigated qualitatively. The intensity distribution in the image is found to possess a maximum value just outside, and a minimum value just inside, the image of the edge of the object. The deductions are verified by microphotometer traces taken across the photographic record of the image of a diatom edge. It is suggested that the intensity distribution curve may be used in the physical analysis of the object.

Owing to the close analogy between geometrical electron optics and geometrical light optics it is possible to apply the methods of the latter to the investigation of the errors present in the images produced by electron lenses. The large amount of theoretical and experimental work which has been done on this subject during the past few years has justified the use of these methods. However, the *variation* in the chromatic error from point to point in the image of an inhomogeneous object (of varying thickness and density) has no counterpart in light optical phenomena. In the following work, the effect of this variation on the intensity distribution in the image is considered from a purely qualitative point of view.

The electron intensity distribution in the image of an ideal test object, which consists of a film of some organic material in the position of the focal plane of the electron microscope objective, will be considered. In order to introduce a variation in the chromatic error present in the image of this film it will be assumed that the film in half of the field of view of the objective is uniform and extremely thin, while that in the other half is also uniform but thicker and of denser material. This object is an ideal representation of the usual type of biological specimen viewed by the electron microscope, *viz.*, one in which the organisms under investigation are supported on an extremely thin carrier film of collodion. Furthermore, it is assumed that the incident electrons are travelling parallel to the axis of the objective and with equal velocities. Fig. 1 is a diagrammatic representation of the cross section of such an arrangement.

In passing through an element of area of a thin film, electrons may suffer a number of elastic and inelastic collisions with the atoms composing the film, so that, on emergence, their direction of motion may be altered. Those

---

Author's Note:

This paper is the result of a discussion with Prof. C. D. Ellis during his recent stay in Toronto. Professor Ellis suggested that the chromatic error may be used in the physical interpretation of the images obtained with the electron microscope.

[1] *Manuscript received February 13, 1939.*

Contribution from the McLennan Laboratory, Department of Physics, University of Toronto, Toronto, Canada.

[2] *Demonstrator, Department of Physics, University of Toronto.*

electrons with directions outside the cone subtended at the point of emergence by the aperture of the objective do not pass through the aperture and thus are prevented from reaching the image. The probability of an incident electron being deflected from its path by the effect of the relatively high charge on the atomic nuclei is small but, nevertheless, appreciable for the thin part of the film and very large for the thick part. As a result, a larger number of the electrons leaving the thick part of the film are scattered outside the aperture of the objective. Furthermore, the emergent electrons may possess different velocities which are, in general, less than the homogeneous velocity of the incident beam. In the case of a film which is only a few atoms thick the probability of the occurrence of a sufficient number of inelastic collisions between a high speed incident electron and the atomic electrons to cause an appreciable lowering of the velocity of the electron is extremely small. However, as this probability increases rapidly with thickness and density, the electrons emerging from the thicker film possess a wide range of velocities.

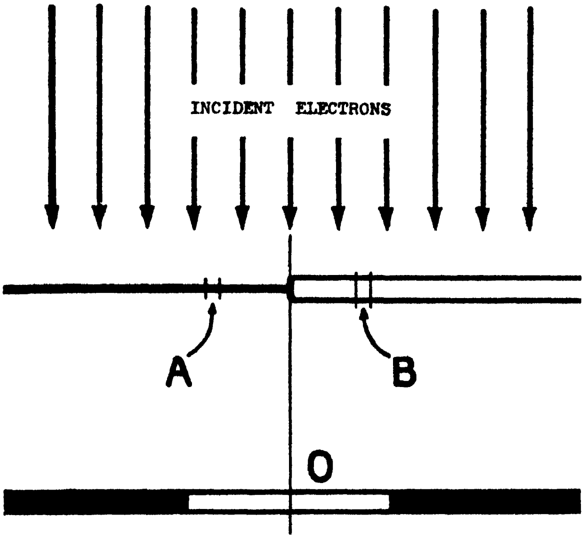

FIG. 1

If the objective lens were perfect the intensity distribution in the image of a small element of area at *A* (Fig. 1) in the thin part of the film would be represented by the curve shown in Fig. 2*a*. The area under the curve is a representation of the number of electrons which reach the image after passing through the element of area at *A* and the aperture of the objective *O*. As shown above, the chromatic aberration is negligible in the case of the thin film; however, owing to spherical aberration, there is a small image error present which modifies this curve so that it has a shape similar to that of a narrow error function curve as shown in Fig. 2*b*. As the spherical aberration has no effect on the number of electrons reaching the image, the area under the curve in Fig. 2*b* is the same as that under the curve in Fig. 2*a*. Once again, if the objective lens were perfect the intensity distribution in the image of an element of area at *B* (Fig. 1) in the thick film would be represented by the curve shown in Fig. 2*c*. The difference in the intensities of the images of elements of area at *A* and *B* (*i.e.*, the contrast) introduced by the spatial scattering is represented by the relative areas under the curves in Figs. 2*a* and 2*c*. However, owing to the effect of chromatic as well as spherical aberrations in the image of an element of area at *B*, the intensity distribution curve obtained in practice has a shape very similar to that of a very broad error function as shown in Fig. 2*d*. The area under the curve in Fig. 2*d* is equal to that under the curve in Fig. 2*c*.

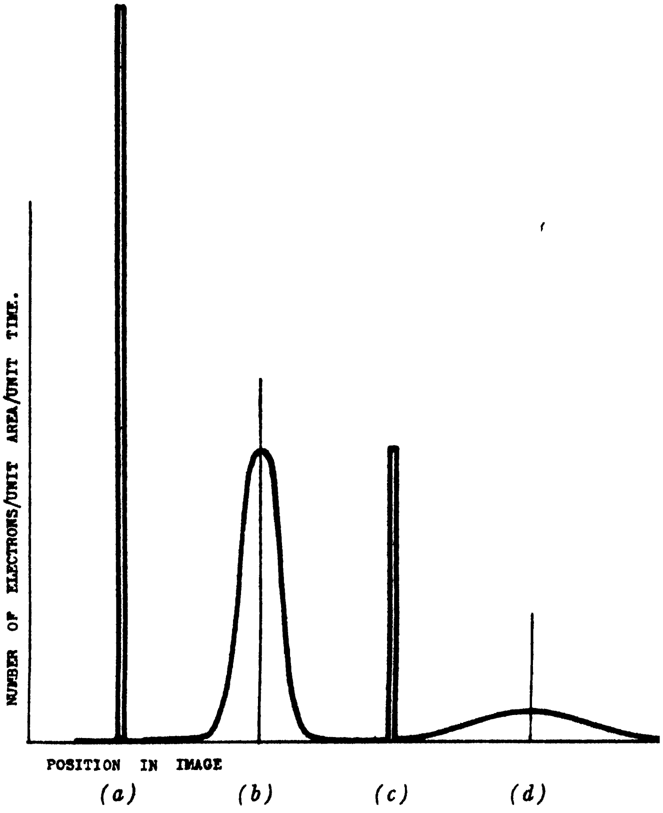

FIG. 2

The intensity distribution in the entire image will now be determined by superposing the images of all the elements of area of the object shown in Fig. 1. Since, in the image of any object element, there is a measurable intensity over a considerably larger area than that of the geometrical image, the intensity at any one point of the image will depend not only on the number of electrons reaching it from the corresponding object point but also on the number reaching it from all other points of the object. This is represented graphically in Fig. 3, where the curve of the intensity distribution in the image

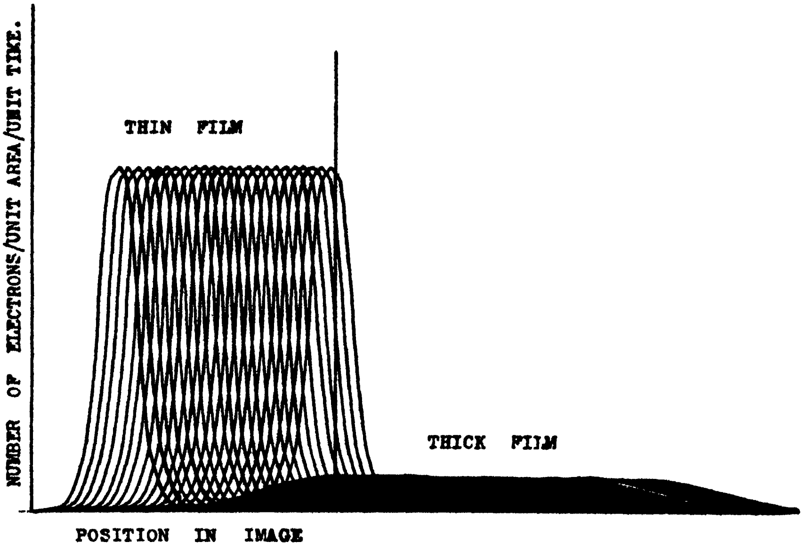
NUMBER OF ELECTRONS/UNIT AREA/UNIT TIME.
THIN FILM
THICK FILM
POSITION IN IMAGE

FIG. 3

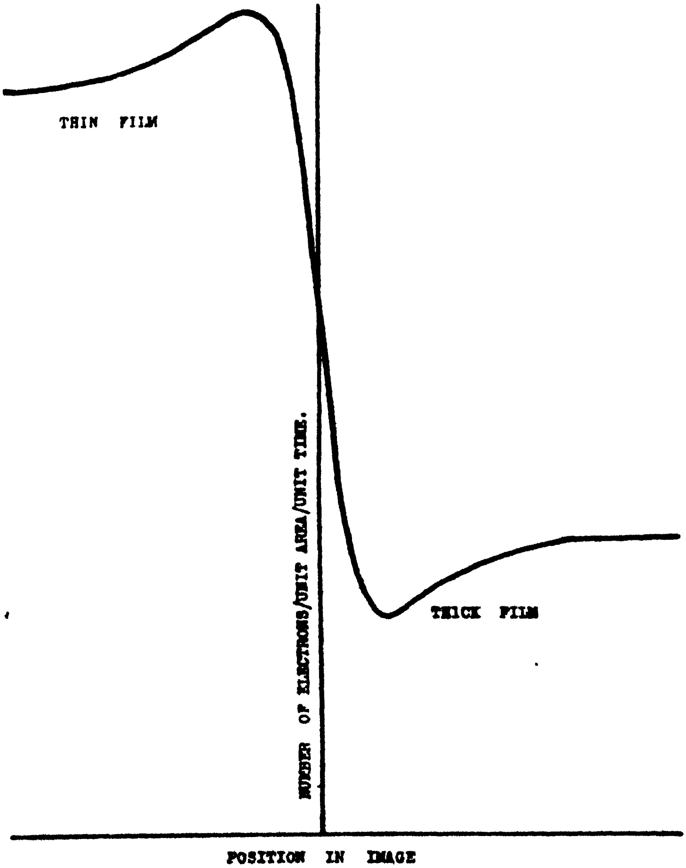
THIN FILM
THICK FILM
NUMBER OF ELECTRONS/UNIT AREA/UNIT TIME.
POSITION IN IMAGE

FIG. 4

of each element of area is drawn in its proper position. The intensity at any point in the image is determined by the sum of the ordinates (taken at the point in question) of all the curves which have a measurable value at the point. The actual intensity distribution in the complete image may then be plotted. This has been done in Fig. 4, and gives a rather unexpected result that has no analogue in the light optical theory of images. Just outside the geometrical image of the edge of the thick film there is a maximum in which the intensity is greater than in the image of the thin film, while just inside this edge there is a minimum in which the intensity is less than in the image of the thick film. Moreover, the shape of this intensity distribution depends on the difference in the magnitude and nature of the angular and velocity distributions of electrons leaving the two parts of the object.

In practice, this means that a band of greater intensity than that in the image of the supporting film should appear just outside the geometrical image of the edge of the organism under investigation, while a band of lower intensity than that in the image of the organism should appear just inside this edge. A number of photographs which have been taken with the electron microscope described in the preceding paper show this effect very clearly. Fig. 5 is a reproduction of a microphotometer trace taken across the photographic record of the image of a diatom edge. This organism has a maximum thickness of about 0.5 μ which decreases considerably towards the edge and is, therefore, sufficiently transparent to electrons for this test. In Fig. 6 the photographic blackening has been plotted from the curve in Fig. 5. As the blackening is approximately proportional to the electron intensity, this curve represents the actual intensity in the electron microscope image. The fact that the minimum intensity is not as clearly defined as in the hypothetical case may be due to the fact that thickness of the diatom is increasing at a short distance from the edge. This is indicated by the decrease in intensity as one proceeds farther into the image of the diatom.

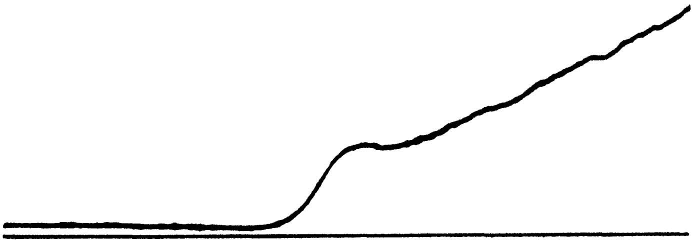
FIG. 5

From the above considerations, it is apparent that the contrast in electron microscope images is due to the differences in spatial scattering of the electrons by the object elements, while the unusual intensity distribution in the images of boundary edges is entirely due to the electron velocity distribution which has been introduced by the material of the object. In other words, the physical interaction between a beam of electrons and the object produces two measurable, independent image effects which have no counterpart in light optics. A complete quantitative study of these effects, which the author hopes to make the subject of a future paper, should lead to a more precise physical interpretation of electron microscope images.

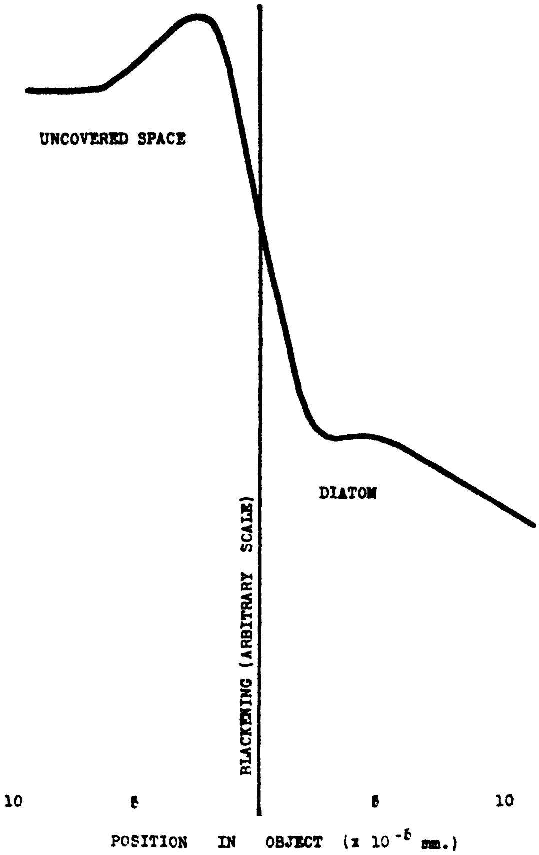

Fig. 6

Acknowledgments

The author wishes to thank Prof. C. D. Ellis for his suggestions, and to express his appreciation of the interest in this work shown by Prof. E. F. Burton. The photographs used were obtained by Mr. A. Prebus.

Canadian Journal of Research

Issued by The National Research Council of Canada

VOL. 17, SEC. A. MAY, 1939 NUMBER 5

24-7-37
LIBRARY

NOTE ON THE PERMANENCE OF STANDARDS OF LENGTH[1]

By R. H. Field[2]

Abstract

A few reasons are presented for believing that the fundamental standards for the Metre and the Yard, and also the legal Dominion Standards of length, are not changing appreciably. On the other hand, measurements of a number of laboratory nickel-iron rules show progressive shortening which is still taking place, through periods up to 20 years.

Definition of a Permanent Length

The distance between two points of a bar will here be considered as permanent if, when the bar is subjected to a given set of conditions (temperature, pressure, method of support, etc.), measurements of any lengths in nature made with reference to the bar, at different times, do not result in variations which cannot be explained as due to some known property peculiar to the medium extending through the length measured, or to the method of measurement.

Permanence of the International Metre

No satisfactory evidence has been produced to throw doubt on the stability of the platinum-iridium alloy from which the international prototype metres are constructed. To ascertain whether relative changes had occurred, a special re-comparison between the International Standard itself (No. 6) and most of the copies was made in the period 1920–32 at le Bureau International des Poids et Mesures, Sèvres (5). For the 25 rules concerned, the mean difference between the two values (1890 minus 1920) was $+0.08\mu$. The maximum differences were -0.88μ and $+0\ 66\mu$, and 15 of the rules showed agreement between the two values to 0.2μ. Plausible explanations could be advanced for several of the larger discrepancies—known accidents to the rules, poor fiducial marks, excessive use and cleaning, etc.—and, when due allowance had been made for these, only in one or two cases was the difference greater than the conceded experimental errors.

It is interesting to observe that the re-comparisons just mentioned were made as a result of the insistence of the late Mr. Louis A. Fischer, Chief of the Metrology Division, National Bureau of Standards, Washington. In 1904

---

[1] *Manuscript received February 1, 1939.*
Contribution from the Division of Physics, National Research Laboratories, Ottawa, Canada. Issued as N.R.C. No. 810.

[2] *Physicist, National Research Laboratories, Ottawa.*

Mr. Fischer took to Sèvres the legal standard of length for the United States (prototype No. 27) and a comparison with the International Bureau working standards, No. 26, and Type 3, indicated a shortening of 0.4μ from the original length of 27 (4). The subsequent investigations confirmed Mr. Fischer's suspicion that the Sèvres rules, and not the United States standard, had changed (5).

The change had not been detected previously, as both International Bureau prototypes were affected in the same way, and hence yielded consistent results in observations where they were employed as standards. The explanation given was that the necessary frequent wiping of the speculum "mouches", bearing the graduation lines, had changed the positions of the edges of these lines as seen through the comparator microscopes. Such an occurrence, however, in an institution like the Bureau, renowned for patient investigation and the search for "one more decimal place", illustrates the pitfalls which consistent results prepare even for experienced observers, and emphasizes the necessity for proper checks in absolute measurements, no matter how good the observations appear.

There still remains the possibility of a progressive change affecting all the prototypes alike, which is quite feasible owing to the common origin of the bars. Since Michelson's original determination of the wave-length of the red cadmium radiation at Sèvres in 1893, the experiment has been repeated from time to time by other observers, but no differences have been found which can be ascribed as due solely to changes in the standard metre.

Such experiments have, however, given one more instance of the difficulty in obtaining accuracy in absolute measurements. Within the last few years a carefully designed and constructed apparatus was built at the National Physical Laboratory, for determining wave-lengths in terms of metre or yard standards (8). It was designed for a precision of $1 : 4 \times 10^8$ in the verification of the end standards (étalons) in terms of wave-lengths, and hence the over-all accuracy should be limited only by the transfer of length between these end standards and the fundamental line standard. With the method adopted, a precision approaching 0.1 micron ($1 : 10^7$) should be possible for this operation.

Concurrently (2) equally precise determinations, for the metre, were in progress at the Physikalisch-Technische Reichsanstalt. Yet the values found at these two laboratories differed to the order of 0.5μ ($5 : 10^7$), and, so far as known, have not been reduced, even though careful checks were made, including the exchange of the experienced observers—the latest report available (2) indicating that the discrepancy continues. Incidentally, this result shows that metrologists should not be too hasty in displacing the platinum-iridium metre standard by a reference to light.

Permanence of the Imperial Standard Yard

The Imperial Standard Yard is a bronze bar, cast about 1845. Unfortunately thermometry was not then in such an advanced state as it was some forty-five years later when the metre prototypes were intercompared, and the

Committee responsible for replacing the Yard (1) did not refer their thermometers to the gas scale. Consequently the yard standard cannot be brought to its reference temperature of 62° F. with a certainty of two or three tenths of a degree (corresponding to practically as many whole microns in its length).

So far as relative differences are concerned, comparisons between the Imperial Standard and its copies have not shown conclusive evidence of change (7). In this connection it is interesting to observe that a duplicate of the Standard, Bronze Yard No. 16, made and compared at the same time as the Standard, and which is now preserved in the Museum of the National Research Council at Ottawa, was reverified at Ottawa in 1927. Its length was then found to be within 0.00008 inch from that given in reference 1 (3).

There is some evidence (7) that a similar bronze bar made in 1878 changed measurably during the first 10 years of its "life", but a comparison between the International Metre and the Imperial Yard made in 1893 yielded values differing only by 0.8μ from results obtained within the last few years (5).

Canadian Legal Standards of Length

The Canadian Legal Standard Yard is a bronze bar, one inch square in section and provided with two wells, drilled to the neutral surface, where the fiducial lines are ruled on gold plugs. It is similar to the Imperial standard. A reverification carried out at Ottawa in 1927 (3) indicated no change exceeding 0.00007 inch from the original value, obtained in London in 1874 (the reference standard being the Imperial Yard).

For the metre the Canadian standard is a nickel bar of H-section, with graduations on the exposed neutral surface. The lines on this bar (made in 1920) are considerably finer than those on any of the bronze bars previously mentioned, and consequently its length can be determined with greater precision.

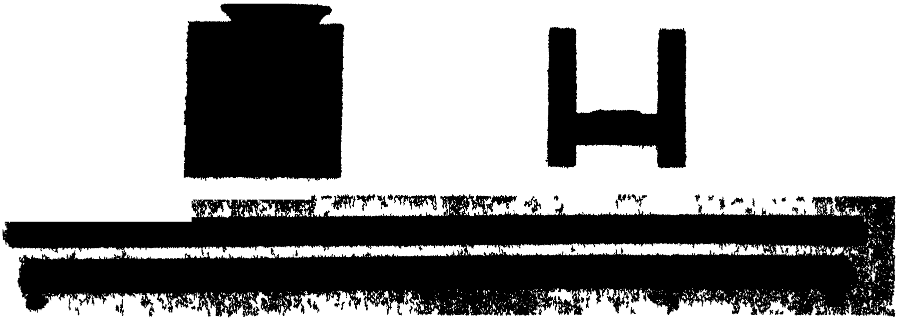

FIG. 1. *The Dominion Standard Metre (centre and right). The Dominion Standard Yard (bottom and left).*

Both legal standards are preserved in the National Research Laboratories, Ottawa, and are illustrated in Fig. 1. The upper, end photographs are reproduced to a larger scale than the lower view, but serve to show the cross sections of the two bars.

The nickel metre rule has been compared at various times directly with platinum-iridium prototypes of the International Metre, and the results are given in Table I.

TABLE I

COMPARISON OF THE NICKEL METRE RULE WITH PLATINUM-IRIDIUM PROTOTYPES

Year	Place	Prototype No.	Length of Nickel Standard Metre (at 0° C.)
1921	Sèvres	26	1 metre + 17 0* μ
1924	Sèvres	26	+ 17 5
1928	Washington	27	+ 17 3
1929	Sèvres	26	+ 16.8

* *Corrected for the change subsequently found in the length of No. 26 (mentioned previously).*

There is no evidence in these figures of any change in the Canadian Standard Metre relative to the prototypes during the period covered, and the standard is assumed to have a length of 1 metre + 17.1μ, for determining the lengths of laboratory working standards.

Experience with Some Nickel-iron Length Standards

In the National Research Laboratories, Ottawa, five nickel-iron alloy rules are in use as secondary standards in metrological activities. These all bear fine reference lines, their thermal dilation equations are accurately known, and they can be compared with one another or with suitable standards to a precision of 0.2μ, as judged by the results obtained by different observers and in different verifications. Four of the rules are of H-section, similar to the Dominion nickel standard metre, while the fifth (No. 191) is of approximately an inverted T-section, having been made for a special purpose, but it is capable of the same precision in comparisons as the other four.

An intercomparison of these rules and the nickel standard was made in December, 1938, and yields interesting information on the stability of the former, when considered together with the results of previous verifications. Fig. 2 shows the lengths of the secondary standards plotted against a time base. These rules are ordinarily kept at room temperature, and are rarely disturbed in their individual storage cases; consequently, it would appear that the changes in length shown are due to some internal process going on in the metal, rather than to the effect of external influence.

Rule No. 191 is the oldest of the series, and was first verified in 1919. It is of 36% nickel (invar) and expands about 2 parts in 10^6 per 1° C. Despite the 20 year period of observation the curve reveals little evidence that the rule

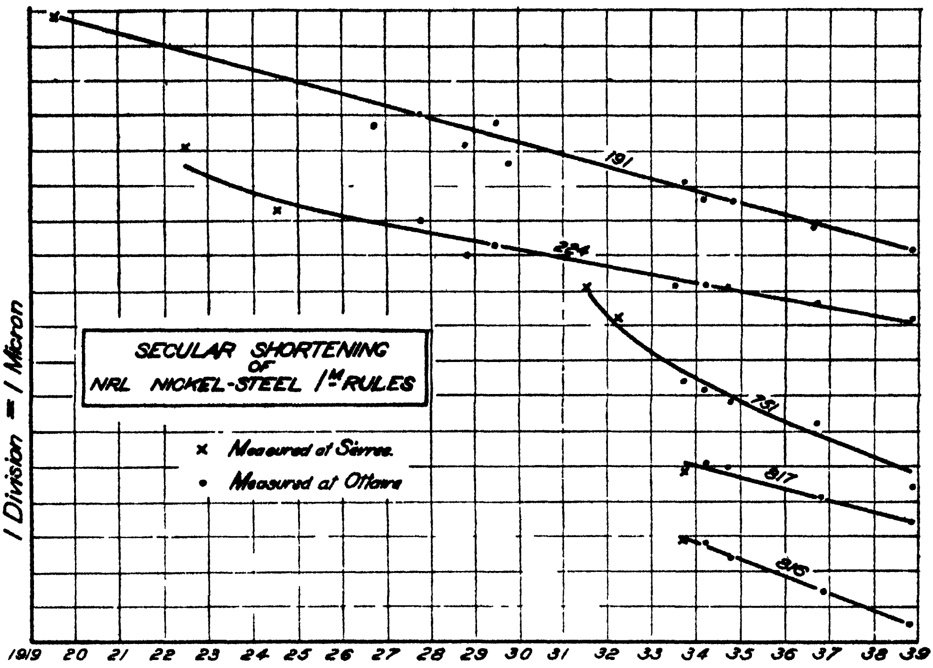

FIG 2.

is approaching a steady length. No. 224 contains 42% nickel and has about the same thermal dilation as platinum. It, too, seems to be changing at a constant rate, even after 16 years of observation. No. 751 is a 36% nickel rule, made from the alloy known as "Fixinvar", developed by Guillaume in efforts to obtain a more stable form of the famous invar, which was known to suffer from secular change, as well as from other irreversible effects to the length. So far the results with this rule throw doubt on the accomplishments, as it has changed by 6.5μ in seven years—more than 6 : 10^6. The thermal expansion of 751 is about 1 part in 10^6 per 1° C. Rules 816 and 817 are of 42% nickel, and also show an unmistakable shortening with time. While the evidence will not be conclusive until more comparisons have been made, the curves indicate a different rate of change for these two rules, although they were made together from the same melt.

It is understood that all these rules, purchased from La Société Genevoise d'Instruments de Physique, were submitted to the best-known methods of heat treatment to achieve stability. An interesting observation is that all the nickel-iron rules under discussion shorten with time, whereas published results of observations on invar show it to lengthen. Johnson (6) gives an instance of an invar rule at the National Physical Laboratory which lengthened by 21μ in 19 years, while Dr. Judson, Chief of the Length Section, National Bureau of Standards, informs the writer that an invar bar purchased in 1903 is still increasing in length, being 0.75μ longer in 1938 than in 1936. It is to be noticed that tempered steel shows anomalous behaviour of the same kind. Tempered steel gauges of the Johansson type hence require periodical checking when used as standards in precise length measurements.

References

1. Airy, G. B. Account of the construction of the new national standard of length and its principal copies. (Typed copy.) Phil. Trans. Roy. Soc. Part III. 1857.
2. Comité International des Poids et Mesures. Procès Verbaux des Séances. Vol. 17. 1935.
3. Field, R. H. A study of the Dominion standard yard and other standards of length. Dept. of the Interior, Canada, Topographical Survey, Bull. 60. 1929.
4. Fischer, L. A. Recomparison of the United States prototype meter. U.S. Bureau of Standards, Bull. No. 1 : 5-19. 1904.
5. Guillaume, C. E. Les récents progrès du système métrique, *In* Travaux et Mémoires du Bureau International des Poids et Mesures, Paris. Vol. 19. 1934.
6. Johnson, W. H. Line standards of length. *In* Dictionary of applied physics, edited by Sir R. Glazebrook. Macmillan and Company, London. Vol. 3 : 465-477. 1923.
7. Sears, J. E. Precise length measurements. Cantor Lectures. Proc. Roy. Soc. Arts, Lond. 71 : 775-841. 1923.
8. Sears, J. E. and Barrell, H. A new apparatus for determining the relationship between wave-lengths of light and fundamental standards of length. Phil. Trans. Roy. Soc. Ser. A, 231 : 75-145. 1932.

UNE ÉLECTRODE ARGENT–CARBONATE D'ARGENT OBTENUE PAR ÉLECTROLYSE[1]

PAR PIERRE DEMERS[2]

Sommaire

Par l'électrolyse, avec une anode d'argent, d'une solution diluée de bicarbonate de soude, on a obtenu un dépôt adhérent de carbonate d'argent. L'électrode ainsi obtenue, immergée dans une solution de carbonate et de bicarbonate alcalin, prend un potentiel défini, reproductible, et égal à celui de l'électrode Ag (cristallin), Ag_2CO_3 (cristallin). À 25° C., le potentiel normal a été trouvé égal à -0.4769 volt, et le produit de solubilité égal à $10^{-11}\,1.27$.

Quelques auteurs ont étudié l'électrode $Ag–Ag_2CO_3$. Spencer et Le Pla (14), Abegg et Cox (1), et Masaki (11) se sont servis d'un bâton d'argent entouré de carbonate d'argent précipité par double décomposition. Walker, Bray et Johnston (15) ont employé de l'argent cristallin obtenu par électrolyse, et du carbonate lentement précipité par un courant de dioxyde de carbone. Les International Critical Tables (6) donnent pour valeur du potentiel normal: $E_0 = -0.50$ volt.

On connaît d'ailleurs l'importance du procédé habituellement employé par Harned (électrodes du type II) (3), qui consiste à déposer le sel d'argent voulu, par l'électrolyse d'une solution appropriée, sur une anode d'argent réduit. Moyennant quelques modifications, nous avons finalement réussi à préparer des électrodes $Ag–Ag_2CO_3$ selon ce principe.

I. Préparation de l'électrode

On soude bout à bout un fil d'argent à un fil de cuivre; on introduit ce fil dans un tube de verre de telle longueur que le fil en émerge aux deux bouts. On fond une extrémité de ce tube autour du fil d'argent. Avec le bout du fil d'argent qui dépasse on forme une spirale qu'on recouvre d'une pâte d'oxyde d'argent purifié, puis on réduit cet oxyde en chauffant à 450–550° C., selon le procédé usuel (7). Après refroidissement, on assure l'étanchéité du joint verre-argent, en fondant avec précaution un peu de paraffine à l'intérieur du tube. Avec cette électrode pour anode, et un fil de platine pour cathode, on fait passer 10 milliampères par cm^3 d'électrode pendant 30 min., à travers une solution $0.02M$ de bicarbonate de soude. Il se dépose sur l'argent du carbonate d'argent jaune, qui verdit facilement à la lumière.

Plusieurs électrodes préparées de cette façon, et immergées dans une solution contenant du bicarbonate de soude et du carbonate de soude, s'accordent entre elles à un ou deux dixièmes de millivolt. Des électrodes vieilles de quelques jours s'accordent moins bien entre elles, et ont été trouvées plus négatives en moyenne que des électrodes fraîches.

---

[1] *Manuscrit reçu le 11 octobre, 1938.*
Contribution du laboratoire de Physique de l'Université de Montréal, Montréal, Québec, Canada.

[2] *Chargé de cours, département de physique, faculté des sciences, Université de Montréal, Montréal, Québec, Canada.*

Des électrodes préparées de la façon décrite ont été comparées dans une même solution de carbonates, avec l'électrode Pt, Ag (cristallin), Ag_2CO_3 (cristallin); elles s'accordent avec cette dernière à un ou deux dixièmes de millivolt. L'argent cristallin employé pour cette comparaison, a été obtenu par l'électrolyse d'une solution chaude d'azotate d'argent, sous une forte densité de courant, selon le procédé de Lewis (7), Linhart (8), et Randall et Young (13). Le carbonate d'argent cristallin a été préparé par lent barbotage d'un courant de dioxyde de carbone dans une dissolution d'azotate d'argent ammoniacal, selon Walker, Bray et Johnston (15).

La préparation du carbonate d'argent, par dépôt électrolytique ou par réaction du dioxyde de carbone, a été effectuée à la chambre noire. La comparaison des électrodes a été opérée dans des récipients noircis.

II. Détermination du potentiel normal

Nous avons mesuré la f.e.m. E, à 25° C., de la pile suivante:

$-$Ag, AgCl $\mid$ Na_2CO_3 m_1, $NaHCO_3$ m_2, NaCl m_3 $\parallel$
(compartiment et solution No. 1)

Na_2CO_3 m_1, $NaHCO_3$ m_2 $\mid$ Ag_2CO_3(électr.), Ag(réd.)$+$
(compartiment et solution No. 2)

m_1, m_2, m_3, représentent les concentrations en molécules grammes par 1000 g. d'eau.

Les électrodes Ag, Ag_2CO_3 ont été préparées par le procédé décrit dans la première partie, et employées moins de 24 h. après leur traitement électrolytique; chacune n'a servi que dans une pile Les électrodes Ag, AgCl sont du type II décrit par Harned (3). Avant de constituer la pile, nous avons lavé les électrodes pendant une heure au moins avec la solution de leur compartiment respectif. Au cours de cette opération, la solution où elles étaient immergées a été renouvelée de quatre à huit fois. Les électrodes ont été fixées dans des bouchons de liège paraffiné.

Les solutions ont été établies par pesée des produits purs et secs; les pesées ont été ramenées au vide.

Le récipient utilisé pour constituer la pile, en verre ordinaire, est divisé en deux compartiments: l'un renferme la solution 1 et l'électrode Ag, AgCl; l'autre qui est noirci extérieurement, contient la solution 2 et l'électrode Ag, Ag_2CO_3. Les compartiments sont reliés à un robinet à trois voies qui permet de les rincer et de les remplir avec la solution qu'ils doivent contenir. Ce robinet empêche le mélange des deux solutions; il n'établit la jonction entre les compartiments qu'au moment des mesures. La solution 2, plus légère, est alors au-dessus de la solution 1, ce qui empêche leur mélange par convection.

Les opérations nécessaires au lavage de l'électrode Ag, Ag_2CO_3, ainsi qu'à sa mise en place dans la pile, ont été effectuées dans une chambre noire.

Le thermostat, à eau, était réglé à 25° C. ± 0.02.

Nous nous sommes servis d'un potentiomètre de type K.

La f.e.m. atteint une valeur stable après une demi-heure, et commence à dériver après une heure et demie ou deux heures.

Nous avons tenu compte de l'hydrolyse de l'ion $CO_3^=$, selon les équations:

$$CO_3^= + H_2O \rightleftarrows HCO_3^- + OH^- \tag{1}$$

$$\frac{x(m_2 + x)}{m_1 - x} = K_{hydr} = \frac{K_w}{K_2} \tag{2}$$

x est la quantité hydrolysée, dont il faut augmenter la concentration du bicarbonate, et diminuer celle du carbonate. Pour K_{hydr}, négligeant sa variation avec la force ionique, nous avons adopté la valeur constante 0.000177, tirée des valeurs de K_2, la seconde constante d'ionisation de l'acide carbonique, de MacInnes et Belcher (10), et de K_w, la constante d'ionisation de l'eau, de Harned et Hamer (5). Nous avons négligé la solubilité du carbonate d'argent.

Nos résultats expérimentaux sont représentés dans le tableau 1 et sur la figure 1.

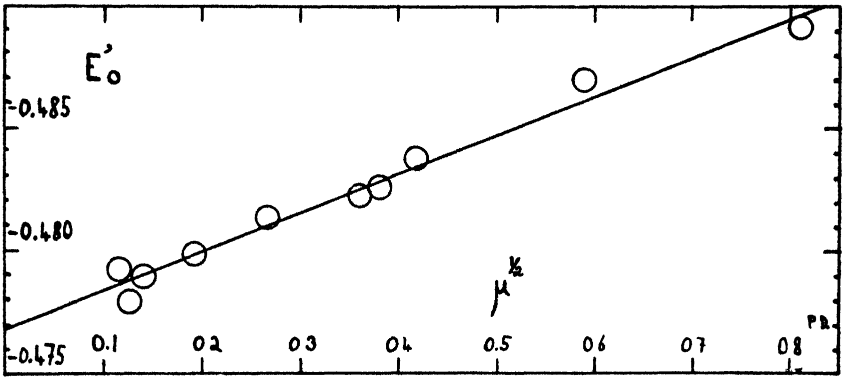

FIG. 1. *E'_0 est donné par l'équation (5); μ est la force ionique des solutions No. 2: $\mu = 3m_1 + m_2 - x$. Les résultats expérimentaux sont représentés par des cercles. La droite représente l'équation appliquée selon la règle des moindres carrés: $E'_0 = E_0 + b\mu^{½}$; pour $\mu = 0$, $E'_0 = -0\ 4769$ volt $= E_0$, le potentiel normal de l'électrode $Ag–Ag_2CO_3$.*

Si l'on néglige le potentiel de jonction entre les solutions peu différentes, 1 et 2, la f.e.m. E peut s'écrire:

$$E = E_{0\,AgCl} - E_{0\,Ag_2CO_3} - \frac{RT}{2kF} \log \frac{(CO_3^=)}{(Cl^-)^2} \tag{3}$$

d'où l'on tire:

$$E_{0\,Ag_2CO_3} + \frac{RT}{2kF} \log \frac{y_{CO_3^=}}{y^2_{Cl^-}} = \tag{4}$$

$$E_{0\,AgCl} - E - \frac{RT}{2kF}\left(\log\,[CO_3^=] - 2\log\,[Cl^-]\right)$$

$E_{0\,\mathrm{AgCl}}$ est le potentiel normal de l'électrode Ag, AgCl, qui est égal à -0.22239 volt selon Harned et Ehlers (4); $E_{0\,\mathrm{Ag_2CO_3}}$ est le potentiel normal cherché. Toutes les quantités du membre de droite de l'équation (4) sont connues pour une expérience donnée.

En remplaçant le membre de gauche de (4) par E_0', et en introduisant la valeur numérique du facteur $\frac{RT}{2kF}$, il vient:

$$(5) \qquad E_0' = -0.22239 - E - 0.02957\,(\log(m_1 - x) - 2\log m_3)$$

Mais l'on peut écrire:

$$(6) \qquad E_0' = E_{0\,\mathrm{Ag_2CO_3}} + 0.02957\,(\log y_{\mathrm{CO_3^=}} - 2\log y_{\mathrm{Cl^-}})$$

E_0' tend donc vers $E_{0\,\mathrm{Ag_2CO_3}}$ à mesure que décroît la force ionique μ: puisque, selon la théorie de Debye et Hückel (2), le dernier terme du membre de droite de (6) est proportionnel à $\mu^{1/2}$, aux faibles concentrations. Il paraît légitime, au degré d'approximation de nos résultats, d'extrapoler E_0' par une fonction linéaire de $\mu^{1/2}$:

$$(7) \qquad E_0' = E_{0\,\mathrm{Ag_2CO_3}} + b\mu^{1/2}$$

Par la méthode des moindres carrés, l'on trouve:

$$(8) \qquad E_{0\,\mathrm{Ag_2CO_3}} = -0.4769 \text{ volt}$$

$$(9) \qquad b = -0.01575$$

La loi de Debye et Hückel prévoit pour b une valeur absolue plus élevée, $b = -0.0299$; on peut déduire de (9) que les coefficients d'activité de l'ion $\mathrm{CO_3^=}$ sont notablement plus élevés que ne l'indique la loi limite de la théorie. Voir à ce sujet les conclusions de Lortie et Demers (9).

Du potentiel normal, on peut déduire le produit de solubilité thermodynamique du carbonate d'argent; pour une solution saturée de ce sel:

$$(10) \qquad K_{sol} = (\mathrm{CO_3^=})(\mathrm{Ag^+})^2$$

On obtient K_{sol} au moyen de l'équation suivante:

$$(11) \qquad \log K_{sol} = \frac{1}{0.02957}\,(E_{0\,\mathrm{Ag}} - E_{0\,\mathrm{Ag_2CO_3}})$$

$E_{0\,\mathrm{Ag}}$ est le potentiel normal de l'électrode d'argent, que nous prenons égal à -0.7991 volt selon Owen et Brinkley (12).

$$(12) \qquad K_{sol} = 1.27 \times 10^{-11}$$

Remerciements

Nous désirons remercier bien vivement l'Ecole polytechnique de Montréal qui a eu l'amabilité de nous prêter un potentiomètre de type K, dont nous nous sommes servis pour faire ces mesures.

TABLEAU I

m_1	m_2	m_3	x	μ	$\mu^{1/2}$	E	E_0'	Nombre de piles
0.1883	0.09490	0.03463	0.000345	0.6595	0.8121	0.20174	0.48914	5
0.08788	0.08687	0.01412	0.000178	0.3503	0.5919	0.18644	0.48700	3
0.04350	0.045302	0.00608	0.000169	0.1756	0.4190	0.17077	0.48381	6
0.03417	0.04368	0.01712	0.000138	0.1461	0.3822	0.19926	0.48261	3
0.03274	0.03177	0.02089	0.00020	0.1298	0.3603	0.20460	0.48226	3
0.01824	0.01596	0.003242	0.00020	0.07066	0.2658	0.16325	0.48142	3
0.008906	0.01034	0.004001	0.00015	0.03687	0.1920	0.17656	0.47992	3
0.005008	0.004676	0.001057	0.00018	0.01952	0.1398	0.14909	0.47900	3
0.003921	0.004554	0.002127	0.00014	0.01617	0.1772	0.16920	0.47799	3
0.003233	0.003755	0.001612	0.00014	0.01331	0.1154	0.16607	0.47931	3

Bibliographie

1. Abegg, R. et Cox, A. J. Z. physik. Chem. 46 : 1-12. 1903.
2. Debye, P. et Hückel, E. Physik. Z. 24 : 185-206. 1923.
3. Harned, H. S. J. Am. Chem. Soc. 51 : 416-427. 1929.
4. Harned, H. S. et Ehlers, R. W. J. Am. Chem. Soc. 55 : 2179-2193. 1933.
5. Harned, H. S. et Hamer, W. J. J. Am. Chem. Soc. 55 : 2194-2206. 1933.
6. International Critical Tables. McGraw-Hill Book Company, New York, 6 : 333. 1928.
7. Lewis, G. N. J. Am. Chem. Soc. 28 : 158-171. 1906.
8. Linhart, G. A. J. Am. Chem. Soc. 41 : 1175-1180. 1919.
9. Lortie, L. et Demers, P. A paraître.
10. MacInnes, D. A. et Belcher, D. J. Am. Chem. Soc. 55 : 2630-2646. 1933.
11. Masaki, K. Bull. Chem. Soc. Japan, 5 : 345-348. 1930.
12. Owen, B. B. et Brinkley, S. R. J. Am. Chem. Soc. 60 : 2233-2239. 1938.
13. Randall, M. et Young, L. E. J. Am. Chem. Soc. 50 : 989-1004. 1928.
14. Spencer, J. F. et LePla, M. Z. anorg. Chem. 65 : 10-15. 1910.
15. Walker, A. C., Bray, U. B. et Johnston, J. J. Am. Chem. Soc. 49 : 1235-1256. 1927.

THE β- AND γ-RAYS OF ACTINIUM B AND ACTINIUM C″[1]

By B. W. Sargent[2]

Abstract

The absorption method of finding the end-point of a β-ray spectrum has been made more precise and free of errors that are due to straggling and the γ-ray background. The absorption curves of the β-rays of radium E and uranium X_2 were taken as standard, since, from experiments with the magnetic spectrograph, their end-points are known to be 1.15 and 2.32 Mev respectively. The extrapolated ranges of these fastest β-rays are, from experiments with homogeneous beams, 0.51 and 1.12 gm. per cm.^{2} of aluminium. In general the extrapolated range R can be expressed in terms of the energy E in Mev by the equation:

$$R = 0.526\,E - 0.094,$$

for $E > 0.6$ Mev. It is shown that the final portions of the absorption curves of the β-rays from radium E and uranium X_2 have the same shape when plotted against m/R, where m is the mass in gm. per cm.^{2} of absorber and R is the range of the fastest β-rays in the spectrum. The range and end-point of another β-spectrum can be found by fitting its absorption curve to the standard one.

The absorption curve of the β-rays of actinium B was obtained separately from that of actinium C″ for the first time. Growth curves were plotted from measurements of the β-activity of the active deposit obtained by exposing aluminium foils to filtered actinon for a few minutes. The β-activity was measured through thickness of aluminium up to 0.32 gm. per cm.^{2} From the initial portions of the growth curves and from the absorption curve of the β-rays of actinium (B + C) in equilibrium, separate absorption curves were plotted which indicated ranges of 0.64 and 0.68 gm. per cm.^{2} of aluminium for the β-rays of actinium B and actinium C″ respectively. The corresponding end-points are 1.39 and 1.47 Mev.

There is some evidence that the β-spectrum of actinium B consists of two primary components, namely, a strong one having an end-point at 1.39 Mev and a weak one having an end-point at about 0.5 Mev. The difference between the two end-points is approximately equal to the energy (0.83 Mev) of a γ-ray emitted in the transformation actinium B.C. The ratio of the numbers of β-particles in the two partial spectra is approximately 1:7. This gives an excitation probability of 0.12 for the 0.83 Mev level of the actinium C nucleus, which is of the same order of magnitude as that obtained from the intensities of the γ-rays.

Introduction

In 1908 Hahn and Meitner (21) obtained absorption curves for the β-rays of actinium C″ and of actinium (B + C) in equilibrium under the same experimental conditions. After the rays had passed through a certain small thickness of absorber, both curves of the logarithm of the ionization of the β-rays against thickness of aluminium were found to have identical slopes. The curves showed further that a weak group of easily absorbed β-rays were emitted by actinium (B + C) but not by actinium C″. Lacking further evidence, Hahn and Meitner concluded that when the source was actinium (B + C) the β-rays of actinium C″ were solely responsible for the ionization after the rays had passed through an initial small thickness of absorber, and that the easily absorbed β-rays were those of actinium B. Later, the writer (37, 38) repeated and extended the absorption measurements. In many careful experiments no certain difference was found in the penetrating power of the β-rays of actinium C″ and of actinium (B + C) in equilibrium after they had passed through an initial mass of 0.08 ± 0.02 gm. per cm.^{2} of paper or of aluminium. The conclusion drawn was that the β-rays of actinium B have a range of 0.08 gm. per cm.^{2} in aluminium and a maximum energy of 300,000 volts. However, there were two disturbing points. The first was that the intensity of the easily absorbed group of β-rays was too small for a complete spectrum after liberal allowance had been made for their absorption in the window of the measuring electroscope. The second point was that actinium B did not fit into either of the two groups of β-ray bodies which showed relations between their maximum energies and transformation constants (39). The energy 300,000 volts was evidently not great enough to correspond to a half-period of 36.1 min. In the light of later experimental work the following conclusion, which was not precluded by any of the absorption measurements, is more accurate. The β-spectrum of actinium B consists of a portion of low energy β-rays and a portion that is almost identical in energy distribution with the spectrum of actinium C″.

---

[1] *Manuscript received February 20, 1939.*
Contribution from the Department of Physics, Queen's University, Kingston, Canada. This paper was read at the Ottawa meeting of the American Association for the Advancement of Science and was summarized in The Physical Review, vol. 54, p. 232, Aug. 1, 1938.

[2] *Assistant Professor of Physics.*

The first experimental evidence for the hard component of the β-spectrum of actinium B was obtained by Lecoin (26). Sources, which were almost pure actinium B at first, were obtained by activating strips of cellophane in actinon for a few seconds. The tracks of the β-rays emitted shortly afterwards were photographed in a cloud chamber situated in a magnetic field. A distribution curve of the β-rays was obtained from the number of tracks, their radii of curvature, and the strength of field. When corrected for a small number of β-rays from actinium C″, this shows a maximum number at an energy of 100,000, a minimum at 300,000, a maximum at 400,000, and an end-point at 950,000 volts. The energy at the minimum between the two peaks agrees well with that found by the absorption method. Supporting evidence for the high energy component was obtained by Sanielevici (36) from heating measurements with a micro-calorimeter. By assuming 470,000 volts for the average energy of the β-rays of actinium C″, he found that the average energy in the β-spectrum of actinium B was 370,000 volts. This agrees well with 360,000 volts obtained by Lecoin from the energy spectrum. Therefore, the β-rays of actinium B are much more penetrating than had been believed for 28 years.

In 1908 Hahn and Meitner (20) published some growth curves obtained from measurements of the β-activity of the active deposit collected during short exposure to actinon. However, since these had never been studied for various thicknesses of absorber, it was thought worth while to seek confirmation of the discovery of Lecoin and Sanielevici by the absorption method. Growth curves were obtained for masses of aluminium up to 0.32 gm. per cm.^{2} Separate absorption curves for the β-rays of actinium B and of actinium C″ were then deduced. The end-point of the β-spectrum of actinium C″ had been found previously to be 1.40 Mev from the range 0.62 gm. per cm.^{2}

of aluminium for the β-rays of actinium (B + C) in equilibrium (37). This end-point might be low on account of the weakness of activity and the admixture of β-rays from actinium B. Therefore, one of the main purposes of the present experiments was to establish with greater accuracy the end-points of the two spectra. By a comparison method these were found to be 1.39 and 1.47 Mev respectively for actinium B and actinium C''. If the β-spectrum of actinium B is assumed to consist mainly of two primary components, their intensities and difference in end-points are in fair agreement with the intensities and energies of accompanying γ-rays.

Experimental Details

(a) *Apparatus and Adjustments*

The investigation required an instrument that would measure ionization currents from 4×10^{-15} to 2×10^{-12} amp. A Compton electrometer (Cambridge Instrument Co. model) and steel ionization chambers were adopted. The electrometer was housed in a bell-jar standing on a pump plate. The connection from the insulated pair of quadrants passed downwards through the pump plate into a hollow brass block where it was joined to a horizontal brass wire, which passed axially through the two steel chambers. The first chamber was cylindrical, 12.3 cm. long and of 4 cm. inside diameter, and was fitted with brass flanges at its ends. One flange was bolted to the brass block with an insulating rubber gasket between them. The other flange was bolted to the steel end of the large steel chamber with an earthed guard-ring and rubber gaskets between the chambers. The more important insulators for the axial wire were ebonite coated with paraffin wax, as described by Bradfield (4). The large chamber was cylindrical, 15.5 cm. deep and of 13 cm. inside diameter. The β- and γ-radiations entered through a cellophane window of 0.0069 gm. per cm.^{2} in the end of the chamber. Inside the large chamber the axial electrode could be connected to earth by contact with a brass wire that could be swung through a small angle by means of its attachment to a plunger inside a small steel-clad solenoid.

The ionization chamber was maintained at a potential of 270 volts above earth with dry batteries. An atmosphere of dry carbon dioxide was maintained in this chamber by its slow continuous flow from a commercial cylinder.

The small steel chamber was originally intended to be used to balance out large γ-intensities in the large chamber. Therefore the former was made gas-tight and insulated electrically. A small mica-covered slot in its under side was provided to admit β-radiation from an old emanation tube. Alternatively this chamber might be used as the compensating condenser in the Townsend balance method. In the experiments to be described here it contained air and was earthed.

The movable quadrant and the needle of the electrometer could be raised or lowered with the aid of brass tubes inserted through the hole in the top of the bell-jar. Ordinarily, two wires from the batteries passed through the rubber stopper in this hole to the needle and case of the electrometer. The pressure in the bell-jar was kept below 2 mm. of mercury. The electrometer was used under negative electrostatic control. With positive voltages of 24, 48, and 72 on the needle, the voltage sensitivities were 1010, 2650, and 7850 mm. per volt respectively at a scale distance of 110 cm. The corresponding current sensitivities were in the ratios 100 : 170 : 200. In these experiments the needle was maintained at 48 volts above earth, which gave a satisfactory current sensitivity and a stable zero. The capacity of the electrometer and steel chambers was 32 $\mu\mu f$. Under these conditions the natural leak of the ionization chamber of 2060 cc. volume was a drift of 2 cm. per min., or 4×10^{-15} amp. Of this the cosmic-ray intensity would be about 1×10^{-15} amp. In what follows, the β- and γ-ray intensities are expressed in centimetres per minute at a scale distance of 110 cm. from the electrometer mirror. These can be converted to amperes by multiplying by 2.0×10^{-15}.

(b) Corrections to Rates of Deflection

The rate of deflection of the electrometer needle is an oscillatory function of the time measured from the instant that the ion-collecting electrode is disconnected from earth. A graph of this function is shown in the upper part of Fig. 1. The ordinates are approximations to the instantaneous rates,

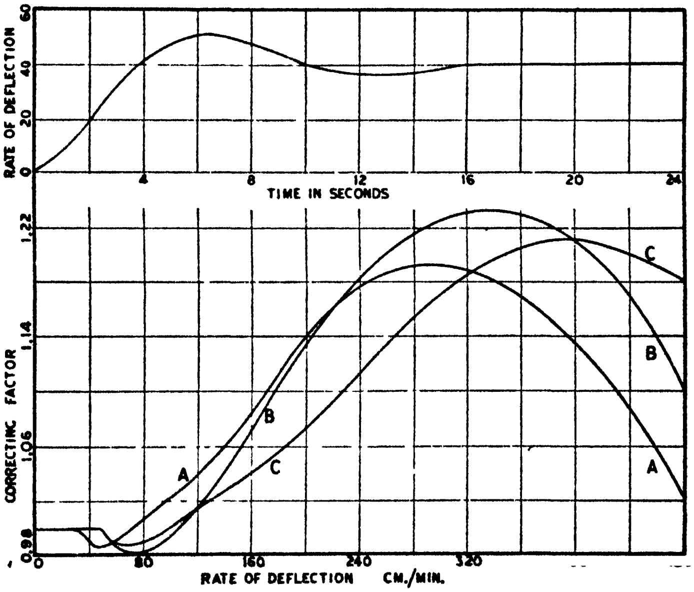

FIG. 1. *Upper graph: variation of the rate of deflection in centimetres per minute of the electrometer needle with the time. Lower graph: correcting factors for various observed rates of deflection of the needle.*

A. θ_0 = *7 cm.,* θ_1 = *30 cm.*
B. θ_0 = *10 cm.,* θ_1 = *30 cm.*
C. θ_0 = *10 cm.,* θ_1 = *40 cm.*

and were obtained by timing the spot of light reflected from the mirror over short distances along the scale. In measuring β- and γ-ray ionization currents it is usually impracticable to measure directly the steady rates of deflection after about 16 sec. (Fig. 1), when oscillations have practically ceased. Therefore, corrections were calculated, which, when applied to the observed rates of deflection, gave the steady rates. The latter are of course comparable measures of the β- and γ-ray intensities.

In practice, the spot of light is allowed to move from rest over a constant distance θ_0 on the scale and is then timed with a stop-watch over another constant distance $\theta_1 - \theta_0$. Let t_0 and t_1 be the times (seconds) required by the spot of light to reach θ_0 and θ_1 respectively from rest. Let $\dot{\theta}_s$ and $\dot{\theta}$ be the respective rates of drift at any chosen time t for the standard case shown in the upper part of Fig. 1 and for the general case, and $\dot{\theta}_{ms}$ and $\dot{\theta}_m$ the corresponding steady rates of drift. It was found experimentally that the shape of the curve for θ as a function of t does not depend on the rate of deflection. A factor k can therefore be introduced to take account of the different rates; hence,

$$\dot{\theta} = k\dot{\theta}_s \quad \text{and} \quad \dot{\theta}_m = k\dot{\theta}_{ms}.$$

For the two observable (but different) average rates the following relations may be written:

$$\bar{\theta} \text{ (if observed)} = \frac{\theta_0}{t_0} = \frac{k}{t_0}\int_0^{t_0} \dot{\theta}_s dt, \tag{1}$$

$$\text{and } \bar{\theta} \text{ (observed)} = \frac{\theta_1 - \theta_0}{t_1 - t_0} = \frac{k}{t_1 - t_0}\int_{t_0}^{t_1} \dot{\theta}_s dt. \tag{2}$$

From these equations

$$\frac{\theta_1}{k} = \int_0^{t_1} \dot{\theta}_s dt. \tag{3}$$

The integral $\int_0^t \dot{\theta}_s dt$ was calculated graphically from Fig. 1, and its value plotted against its upper limit t. From this graph t_0 and t_1 were read for values of θ_0/k and θ_1/k, that is, for chosen values of θ_0 and θ_1 and for various values of k, such as 1 0, 1 5, 2.0, ... 12. If the units of rate of drift are now changed from centimetres per second to centimetres per minute,

$$\bar{\dot{\theta}} \text{ (observed)} = \frac{\theta_1 - \theta_0}{t_1 - t_0} \cdot 60 \quad \text{and } \dot{\theta}_m = k(40).$$

The required correcting factor is.

$$\dot{\theta} \text{ (observed)} \div \dot{\theta}_m \text{ or } \frac{\theta_1 - \theta_0}{t_1 - t_0} \div \frac{60}{k(40)}$$

The calculated correcting factors plotted against observed rates of deflection are shown as Curves A, B, and C in Fig. 1. For rates smaller than 30 cm. per min. the factor is one, since the steady rates of deflection have been attained before time measurements were begun. This point was verified by measuring the intensities of the β-rays from two radium (D + E) sources separately and together. For rates smaller than 30 cm. per min. the sum of the rates of deflection for the two sources measured separately was always equal within ½% to the rate for the two sources together. Further, after the corrections shown in Fig. 1 were applied, all decay graphs of actinium B or of actinium C″ plotted semilogarithmically were found to be straight lines with the same slope.

Range Method of Determining Maximum Energies of β-Spectra

Early absorption measurements by Schmidt (40, 41, 42) and Gray (16) showed clearly that the β-rays of radium E and of actinium (B + C) have definite ranges. These could have been compared with the extrapolated ranges of homogeneous β-rays, first measured by Wilson (48) in 1909, with the purpose of finding the maximum energies or end-points of these spectra. However, the absorption method was not generally applied until a program was started in the Cavendish Laboratory in 1927 for finding the maximum energies of the β-particles from many substances. The results of these experiments were presented in papers by Chalmers (5), the writer (37, 38, 39), and Feather (11).

Recent progress on the theoretical explanation of the β-spectrum and on the interrelation of partial β-spectra and γ-rays has placed emphasis on the need for more and improved measurements of end-points. While the absorption method has been widely applied to the β-emission of the new radioactive bodies, only in certain cases have the ranges and the corresponding end-points been determined with high accuracy. This is due to the lack of an exact definition of the range of a continuous spectrum. It has been known for some time that the good agreement between the end-points of certain natural β-bodies by the range method and by magnetic analysis is partly fortuitous. Two factors oppose each other near the end of the range. While the extrapolated range of homogeneous β-rays is exactly defined, it must be remembered that β-ionization is detectable well beyond this range. This effect may be called straggling. On the other hand, the limited activity of natural sources and the finite sensitivity of the measuring instrument impose a limit on the detection of the β-rays having energies just below the maximum Further, the limit of accuracy of readings imposes a severe restriction when there is a large γ-ray background.

While the previously accepted range of the β-rays of radium E was about 0.475 gm. per cm.^{2} of aluminium, Gray and Henderson (18) found that these β-rays were detectable through aluminium of more than 0.60 gm. per cm.^{2} when a powerful preparation was placed close to an electroscope. Gray (17) suggested that the range might be defined as that thickness of aluminium which reduces the ionization of the β-rays to 1 part in 50,000 for its initial value. One should not, however, expect this definition to be applicable with equal accuracy to other spectra of β-rays. Baschwitz (2, 3) has recently studied the effect of strength of source, γ-ray background, solid angle subtended at the source by the ionization chamber or counter, and canalization of the beam of β-rays, on their range found in a special way. The main factor that modified the value obtained for the range seems to be the γ-ray background. This is shown in a striking manner in the case of thorium C″, which emits a large amount of γ-radiation. The observed range is 0.47, while the expected range is about 0.85 gm. per cm.^{2} of aluminium from the known end-point of this β-spectrum. After studying the effect of experimental conditions on the range, Widdowson and Champion (47) developed an objective method of treating absorption data based on the absorption of the β-rays of radium E and thorium C. While the present paper was being written, a paper by Feather (13) appeared which describes a method very similar to that to be outlined here.

The writer has adopted a comparison method of finding the ranges of continuous β-spectra in order to avoid errors due to unequal straggling and unequal γ-ray backgrounds for different bodies. The β-rays of radium E and uranium X_2 were chosen as standards*, since their maximum energies have been determined with precision in magnetic spectrographs. The end-point of radium E has recently been determined by several experimenters (1, 14, 25, 29, 32, 46) with concordant results. A value for $H\rho$ of 5280 gauss-cm. or 1.15 Mev is chosen. The end-point of uranium X_2 is 9300 gauss-cm. or 2.32 Mev, according to Ward and Gray (46). Further, it is necessary to know the corresponding ranges for these and other energies. The best values of the extrapolated ranges of homogeneous β-rays, measured by Varder (45), Madgwick (30), and Marshall and Ward (31), are simply represented above 0.6 Mev by the linear equation:

$$R = 0.526\,E - 0.094, \tag{4}$$

where R is the range in grams per square centimetre of aluminium for β-rays of energy E expressed in Mev.† (For the ranges at lower energies the graphs given by Marshall and Ward (31) should be consulted.)

Some of the absorption measurements, plotted semilogarithmically, are shown in Fig. 2. The sources were thin and covered an area of 3 or 4 sq. cm. of glass or of aluminium, which reflect the β-rays equally. These were placed 8 cm. from the cellophane window of 13 cm. diameter in the ionization chamber, and the aluminium absorption sheets were placed close to the window. It was necessary to use two preparations of radium (D + E) of quite different activities to obtain a complete curve. Both were covered with mica of 0.0062 gm. per cm.² Three preparations of uranium X were used, although the results for one only are shown in Fig. 2. In this case the

---

* *The first use of these bodies for comparison was probably that of J. A. Gray and W. J. Henderson (22) in their study of the β-rays of potassium about three years ago.*

† *The linear equation* $R = aE + b$ *connecting the range* R *of a* continuous *spectrum and the maximum energy* E *has been frequently used since it was proposed by Feather (11) in 1930. From time to time new values of the constants* a *and* b *have been proposed (47, 13).*

In calculating the constants in Equation 4, great weight was given to the results of Marshall and Ward. On the suggestion of Dr. J. A. Gray a correction of +1.2% was applied to their values of the magnetic field below 500 gauss. Energies were calculated using $e/m = 1.7575 \times 10^7$ *e.m.u. per gm.,* $e = 1.601 \times 10^{-20}$ *e.m.u. and* $c = 2.9978 \times 10^{10}$ *cm. per sec.*

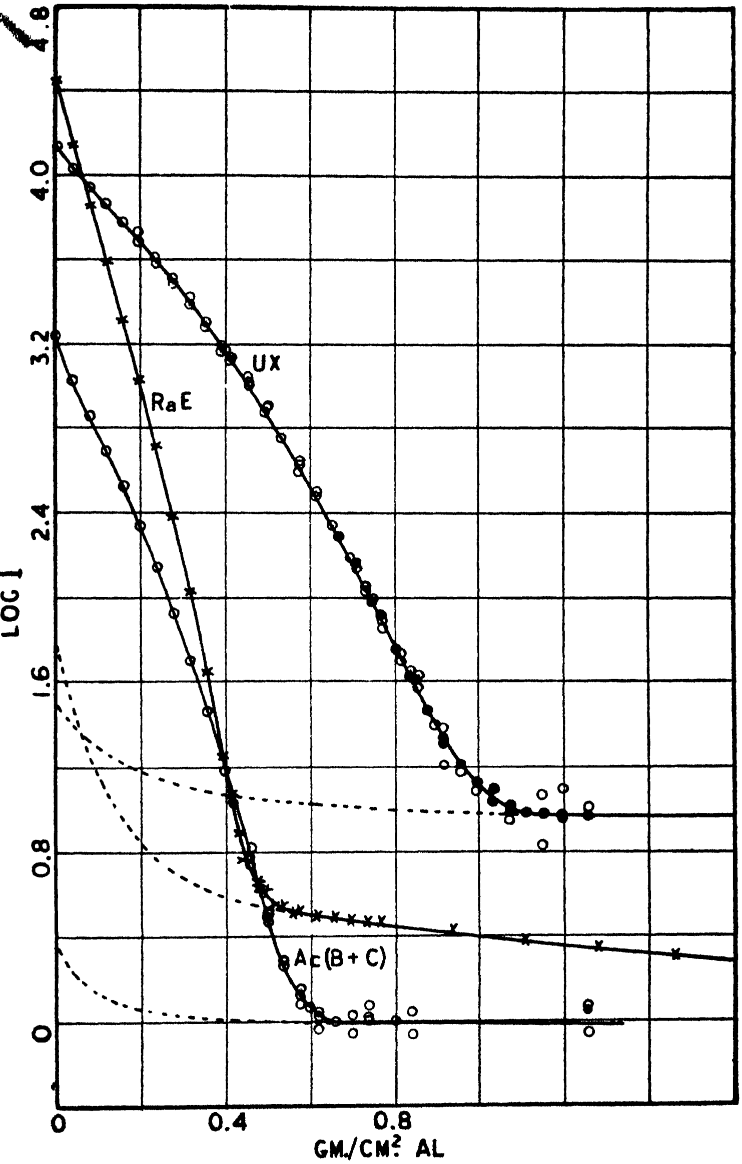

FIG. 2. *Absorption curves of the β- and γ-rays of uranium X, radium E and actinium (B + C). In order to avoid confusion the logarithms of the intensities in centimetres per minute were reduced by 0.400 in the case of radium E and by 0.300 in the case of actinium (B + C). The intensities shown are true measures of the most active source used.*

active material was placed at the end of a glass tube, 1.6 cm. in diameter and 2 cm. long. The logarithms of the intensities of the canalized beam of β-rays are indicated by filled circles when the preparation was new, and by unfilled circles when it was from three to eight months old. By this time the activity had fallen to 6% or less of the initial value. The active deposit of actinium was obtained by recoil on aluminium discs 2 cm. in diameter. These discs were coated with shellac on one side and dried before exposure to the actinon. After activation the shellac and the undesired active deposit were removed from the one side of the disc with chloroform.

The γ-intensities for absorbers having a mass per square centimetre less than the ranges of the β-rays were estimated with the aid of curves published by Rutherford and Richardson (33, 34, 35), and are shown in Fig. 2 by the broken lines. The ranges of the β-rays of radium E, uranium X_2, and actinium (B + C), by inspection of Fig. 2, are 0.56, 1.10, and 0.64 gm. per cm.^{2} respectively. When corrected for the intervening air, cellophane window, and mica these become 0.58, 1.12, and 0.67 gm. per cm.^{2} Values found in a similar way by others are 0.47–0.61 (3, 11, 16, 18, 40) for radium E; 0.95, 1.10, and 1.11 (3, 39, 12) for uranium X_2; and 0.62 and 0.60–0.65 (37, 3) for actinium (B + C). However, good agreement of the absorption limits determined by inspection with different experimental arrangements is not expected.

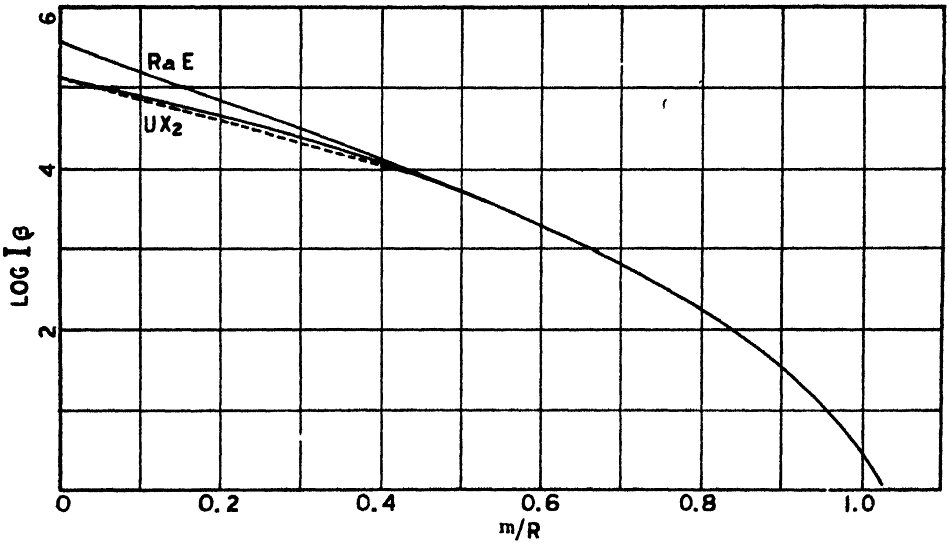

FIG. 3. *Absorption curves of the β-rays of radium E and uranium X_2.* m *is the mass in grams per square centimetre of absorber, and* R *is the extrapolated range of the fastest β-rays in the spectrum.* R = *0.51 for radium E and 1.12 gm. per cm.^{2} for uranium X_2.*

After the γ-intensities had been subtracted, the logarithms of the β-intensities were plotted against m/R (Fig. 3), where m is the mass per square centimetre of all intervening material and R is the extrapolated range corresponding to the known end-point. R was taken to be 0.51 gm. per cm.^{2} for radium E and 1.12 gm. per cm.^{2} for uranium X_2. It is seen that the curves for radium E and uranium X_2 are coincident between $m/R = 0.5$ and 1. This supports the underlying assumption that many β-spectra have the same shape between the maximum energy and one-half of it.

In order to see to what extent the standard absorption curve is influenced by the angular width of the beam and by reflected β-rays, two additional preparations of uranium X were tried. One was distributed over 8 sq. cm. of a watch-glass. The β-absorption curve for this case is shown by the broken line in Fig. 3. The third preparation had an area 7 mm. × 10 mm. and was also mounted on a watch-glass. A lead plate, containing a circular hole, 1 cm. in diameter, and placed half-way between the source and the chamber window, limited the beam. The absorption curve (not shown) in this case falls more rapidly between $m/R = 0$ and 0.1, but it is coincident with the broken curve for all larger values. Therefore, after most of the reflected β-rays have been removed by absorption, the absorption curve has a definite shape, while its slope changes progressively from point to point.

The empirical rule, $R\mu/\rho = 7.5$, connecting the range R with the mass absorption coefficient μ/ρ in aluminium, given by Chalmers (6), does not hold with accuracy for these β-spectra. If $R\mu/\rho$ were a constant then the initial parts of the curves would also be coincident. However, μ/ρ is usually determined from the initial straight portion, and this is highly susceptible to the reflected β-rays from the material behind the source and to the shape of the energy spectrum in the low energy region. The absorption coefficients from the straight portions of Fig. 3 are 16.6 and 5.80 for radium E and uranium X_2, while the products $R\mu/\rho$ are 8.5 and 6.5 respectively. It does not seem likely that two values of $R\mu/\rho$, such as 6.5 and 8.5, are sufficient to represent generally the results for the two groups of permitted and forbidden transitions. In agreement with Feather (13), it is seen that there is a greater proportion of slow β-rays in the spectrum of radium E than in that of uranium X_2. At the ranges chosen here the β-ionization has been reduced to 1 part in 125,000 and 1 part in 45,000 respectively for radium E and uranium X_2.

The range of another β-spectrum can be found, accurate to 2% under the most favourable conditions, by fitting its absorption curve onto the standard curve of Fig. 3. The source must be strong enough to allow measurements of the β-radiation penetrating aluminium of mass per unit area greater than half the range. Of course the further the measurements can be carried the more accurate will be the derived range. The agreement of the new absorption curve with that of Fig. 3 above $m/R = 0.5$ can be tested by trying a series of values of R. A number of equally spaced points are chosen on the new curve (log I_β plotted against m), and the values of log I_β are read. Using one of the chosen values of R, the ratios m/R are calculated for these points. The corresponding values of log I_β are then read from the standard curve and subtracted from those observed at the chosen points. This is repeated for other values of R until the differences in the logarithms become constant for various values of m/R. The value of R for this best fit is the desired range, and the corresponding energy is found from Equation 4.

When the absorption curve for the β-rays of the combined spectra of actinium (B + C) is compared with the standard curve, the best agreement is obtained with $R = 0.66$ gm. per cm.^{2} At low values of m/R the curve for actinium (B + C) falls below that for radium E but above that for uranium X_2. However, the ranges of the β-rays of actinium B and actinium C″ separately can be found after the composite curve has been split up with the aid of information to be given.

Theoretical Growth Curves of Actinium Active Deposit

The active deposit of actinium was obtained by exposing an aluminium foil to decaying actinon for a few minutes. For the purpose of calculation, the supply of actinon is assumed to be constant during the activation, and in practice the supply was maintained by pumping fresh actinon into the activation chamber either continuously or at frequent intervals. Further, since the next product, actinium A, has a very short half-period, it may be assumed that its successor, actinium B, is collected on the foil at a constant rate, say one atom per second. Let P, Q, and R represent the numbers of atoms of actinium B, C, and C″ respectively at any time t measured from the end of the exposure of duration T, and λ_1, λ_2, and λ_3 their respective transformation constants. From the Rutherford-Soddy theory of successive transformations it can be shown that

$$P = 3125(1 - e^{-\lambda_1 T})e^{-\lambda_1 t},$$

$$Q = 198.9(1 - e^{-\lambda_1 T})e^{-\lambda_1 t} - 11.90(1 - e^{-\lambda_2 T})e^{-\lambda_2 t},$$

$$R = 504.8(1 - e^{-\lambda_1 T})e^{-\lambda_1 t} + 21.8(1 - e^{-\lambda_2 T})e^{-\lambda_2 t} - 114.6(1 - e^{-\lambda_3 T})e^{-\lambda_3 t}.$$

The transformation constants used were $\lambda_1 = 0.000320$, $\lambda_2 = 0.005348$, and $\lambda_3 = 0.002427$ sec.$^{-1}$. The values of λ_1 and λ_3 were verified in separate experiments

The α-activity of the active deposit is proportional to $\lambda_2 Q$, graphs of which are shown in Fig. 4. The β-activity is proportional to $k\lambda_1 P + \lambda_3 R$ (when the β-activity of actinium C is neglected). The constant k is the relative activity of actinium B to actinium C″ and depends on (i) the average number per atom, (ii) the ionization per particle, and (iii) the penetrating ability of the β-particles of actinium B relative to those of actinium C″. Calculated curves of the variation of the β-activity of the active deposit, obtained during an exposure of four minutes, with the time measured from the end of the exposure, are shown in Figs. 5 and 6. For convenience later, these, for different values of k, were made coincident over the time range 50 to 60 min. If the values of k for different absorbers can be found experimentally then separate absorption curves can be deduced for the β-rays of actinium B and actinium C″ from the composite absorption curve for actinium (B + C) in equilibrium.

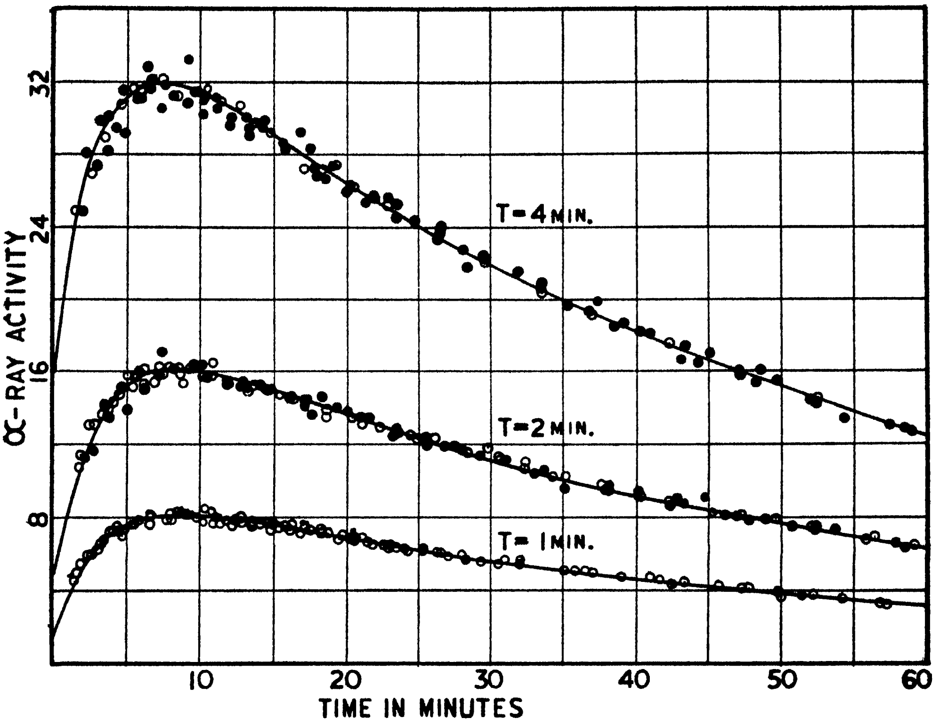

FIG. 4. *Growth curves of the α-ray activity of active deposit obtained by exposing an aluminium foil to filtered actinon for a time* T.

Experimental Growth Curves of Actinium Active Deposit

The activation chamber was a brass tube, 7.5 cm. long and 3 cm. in diameter, closed at its ends by two rubber stoppers through which passed glass tubes containing stopcocks. One was connected to the actinium container and the other to an aspirator. The aluminium foil to be activated had an area 5 cm. × 10.5 cm. and was rolled up in contact with the inner surface of the brass tube. A collecting potential difference of about 500 volts was maintained between the tube and an axial wire. Air containing actinon was drawn into the tube, usually at 15-sec. intervals.

Steps were taken to prevent any old active deposit from being carried over from the actinium container, (i) by maintaining a sweeping electric field in this container, and (ii) by the use of filtering plugs of cotton and glass wool inserted in the short connecting tube at its entrance to the activation chamber. Since old active deposit collected on the aluminium foil would change the shape of the growth curve of the β-activity at the beginning, where its accuracy is most desired, a special investigation was necessary to test the efficacy of these precautions. If any actinium C were carried over and deposited on the foil, the experimental growth curves of the α-activity would not agree with the calculated ones. Consequently α-activity-time curves were obtained with an α-ray electroscope. After small corrections were applied for the

β-activity, which varied with time in accordance with the curves in Fig. 5, the α-ray readings were multiplied by the factor that gave the best agreement with the theoretical curve between 15 and 60 min. Since the times

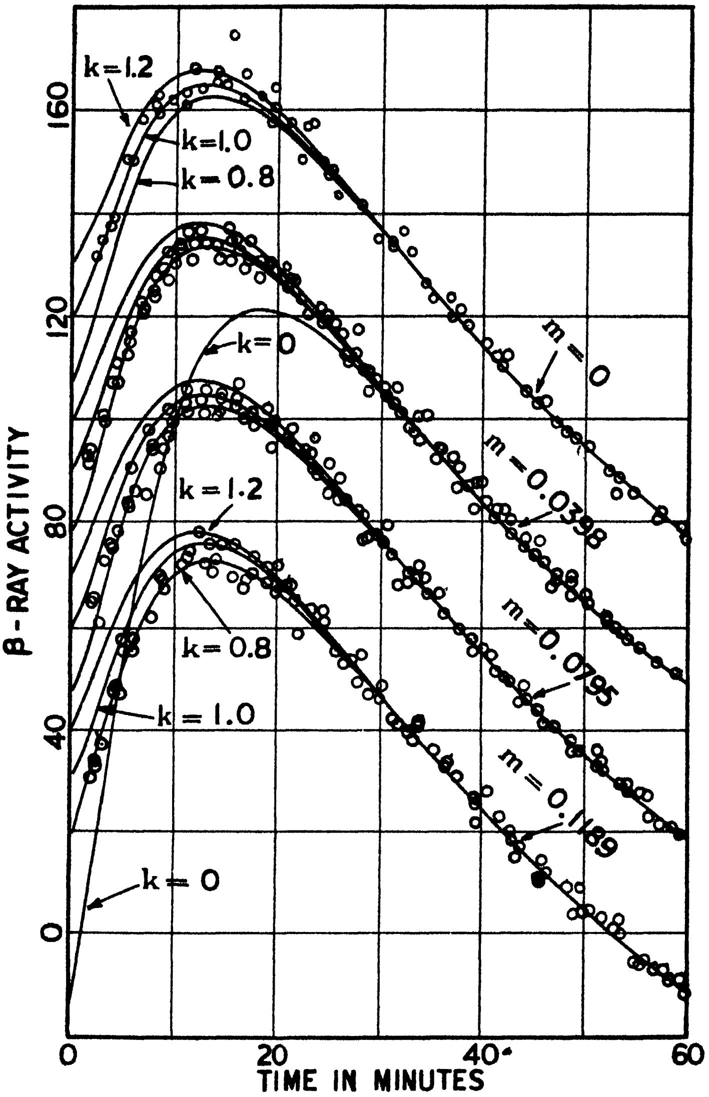

FIG. 5. *Growth curves of active deposit obtained by exposing an aluminium foil to filtered actinon for four minutes. The β-ray activity is measured through aluminium of mass* m *in grams per square centimetre. The ordinates shown apply to the uppermost set of curves* (m = *0*)*. The other curves have been displaced downwards by multiples of 30 units.*

for the α-ray readings were always short, no errors were introduced when they were plotted at their mid-points of time. The results of four runs are included on each curve in Fig. 4. Points marked by filled circles refer to experiments in which the air and actinon were drawn through a bottle of water and glass wool in addition to the usual filters. No difference was found. Since the observed values increase with time in good agreement with the calculated curves, the actinon reaching the activation chamber was free of actinium C.

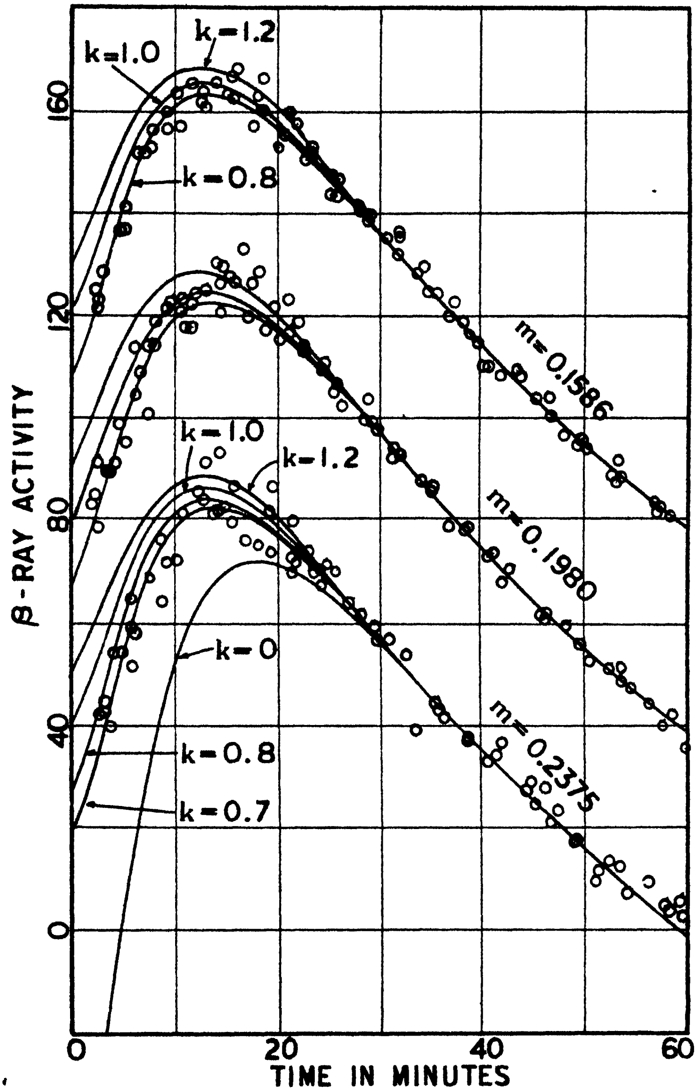

FIG. 6. *Growth curves of the active deposit obtained during a four minute exposure to filtered actinon.* m *is the mass in gm. per cm.*^{2} *of aluminium absorber. The ordinates shown apply to the uppermost set of curves (*$m = 0.1586$*). The other curves have been displaced downwards by multiples of 40 units.*

It seems likely therefore that this actinon was also free of actinium B and actinium C″.

For a study of the β-activity, the aluminium foil of 0.0032 gm. per cm.^{2}, after its exposure to actinon, was folded over once with the active deposit inside and mounted on a thick plate of aluminium. This was placed 2.5 cm. from the window of the ionization chamber, and the β-activity penetrating a given absorber was followed for one hour. The rates of deflection (after correction for natural leak) were multiplied by the factor that gave the best agreement with the theoretical curves in the region 20 to 60 min. Only in a few cases were the electrometer readings of sufficient duration (five minutes) that corrections were considered necessary when the rates of deflection were plotted at their mid-points of time. These corrections are the ratios of the time average of the activity over the interval $t_2 - t_1$ of the reading to the activity at the mid-point of the interval. The former is

$$\frac{1}{t_2 - t_1}\int_{t_1}^{t_2} (k\lambda_1 P + \lambda_3 R)\,dt.$$

Experimental results obtained with the electrometer are shown in Figs. 5 and 6 and in Table I. Four or five runs were taken for each mass m per unit area of aluminium and at each time T of activation. It is seen at once that, since k is nearly 1 initially and decreases slowly with m, the energy spectrum of actinium B is not quite as extensive as that of actinium C''.

TABLE I

Initial absorbers: aluminium, 0.0032; air, 0.0030; cellophane, 0.0069 gm. per cm.^{2}

m, gm./cm.^{2} Al	k (observed)				Limit of error	Average k
	T = 1 min.	T = 2 min.	T = 4 min.	T = 10 min.		
0	0.95	0.95	0.97	—	±0.05	0.96
0.0398	0.90	—	0.90	—	0.05	0.90
0.0795	0.85	—	0.85	—	0.05	0.85
0.1189	—	0.80	0.80	—	0.05	0.80
0.1586	—	—	0.80	—	0.05	0.80
0.1980	—	—	0.80	—	0.10	0.80
0.2375	—	—	0.72	—	0.10	0.72
0.2766	—	—	—	0.67	0.10	0.67
0.3164	—	—	—	0.65	0.15	0.65

Earlier evidence for the penetrating component of the β-spectrum of actinium B was obtained with a Geiger-Müller counter and a scale-of-two recording circuit. In this case the active deposit was collected directly on the inside of the brass cylinder forming the activation chamber. This was placed coaxially with a paper cylinder, a copper absorber, and the Dowmetal counter. The paper of 0.0057 gm. per cm.^{2} prevented contamination of the counter and absorbers. The numbers of particles per minute were recorded. After corrections for the β-particles missed owing to the finite relaxation time of the recorder, and for the natural count, had been applied, moving averages in particles per minute were taken over six-minute intervals. The values of k for best agreement with the theoretical growth curves are shown in Table II.

TABLE II

Initial absorbers: paper, 0.0057; air, 0.0007; Dowmetal F, 0.0354 gm. per cm.^{2}

m, gm. per cm.^{2} Cu	k (observed)		Relative intensity Ac (B + C) in equilibrium
	T = 1 min.	T = 1.5 min.	
0	1.0 ± 0.1	1.0 ± 0.2	100
0.104	—	0.9 ± 0.1	22.7 ± 0.9
0.168	—	0.8 ± 0.2	9.87 ± 0.54

Absorption of the β-rays of Actinium B and of Actinium C″

The absorption data of Table III were obtained for the β-rays of actinium (B + C) in equilibrium, actinium C″, and radium E, when the sources were mounted on aluminium and placed 2.5 cm. from the window of the ionization chamber. The ratio k (Table I), of the ionization produced by the β-rays of actinium B to the ionization produced by those of actinium C″ at each absorber thickness, being known, the composite data of Column 2 (Table III) for actinium (B + C) were resolved into the separate groups for the β-rays of actinium B and C″ given in Columns 3 and 4. The values in Column 4 obtained in this way are in good agreement with those in Column 5 obtained directly with pure sources of actinium C″. The estimated errors given in this column (and in Column 4 of Table II) are the averages of the differences from the average values of four independent sets.

TABLE III

Initial absorbers: aluminium, 0.0032; air, 0.0030; cellophane, 0.0069 gm. per cm.^{2}
(for RaE, mica 0.0062 instead of aluminium 0.0032 gm. per cm.^{2})

m, gm. per cm.^{2} Al	Relative intensity				
	Ac (B + C)	AcB	AcC″	AcC″	RaE
0	100	100	100	100	100
0.0398	64.0	61.8	66.1	66.1 ± 0.4	42.9
0.0795	41.1	38.6	43.5	44.0 ± 0.4	20.9
0.1189	26.8	24.3	29.2	29.4 ± 0.2	10.7
0.1586	17.4	15.8	19.0	18.9 ± 0.2	5.58
0.1980	10.8	9.80	11.8	12.0 ± 0.2	2.73
0.2375	6.60	5.63	7.53	7.54 ± 0.07	1.29
0.2766	3.90	3.18	4.59	4.54 ± 0.06	0.575
0.3164	2.24	1.80	2.67	2.67 ± 0.04	0.245

After allowance had been made for small amounts of γ-radiation, the absorption curves for actinium B and actinium C″ were fitted to the absorption curve for radium E (Table III), over the region investigated, by the method explained earlier. Best agreement was obtained when the ranges of the β-rays of actinium B and C″ were respectively 0.65 and 0.68 gm. per cm.^{2}

The composite curve for actinium (B + C), placed 8 cm. from the chamber, given in Fig. 2 was next resolved into separate curves by using the same values of k for the same total mass per unit area of absorber as in Table I. Further, it was necessary to extrapolate for k beyond the limit of direct measurement (m = 0.32 gm. per cm.^{2}). The ranges obtained with the aid of the standard curve of Fig. 3 are 0.62 and 0.68 gm. per cm.^{2} Therefore, 0.64 and 0.68 gm. per cm.^{2} may finally be taken to be the respective ranges of the β-particles of actinium B and C″. The corresponding energies from Equation 4 are 1.39 and 1.47 Mev.

From the energy spectrum of actinium B obtained with a cloud chamber, Lecoin (27) has concluded that the end-point is 1.00 Mev by inspection and 1.25 Mev from a Konopinski-Uhlenbeck plot. While the extent and accuracy of the absorption measurements of the present paper were severely restricted by the small activity available, it seems reasonably certain that this upper limit of energy is greater than 1.25 Mev. This conclusion is conditional on the assumption that this β-spectrum does not descend towards its limit more sharply than the average spectrum.

Further, Lecoin (27) has obtained two end-points, namely, 1.50 and 1.85 Mev, of the β-spectrum of actinium C″ by a K−U plot. The presence of a small fraction of the β-rays having the higher limit was taken to indicate a partial spectrum. Most of the disintegrations should therefore be accompanied by a γ-ray (or γ-rays) of 0.35 Mev energy. In the next section it will be shown that the γ-rays of actinium C″, if they exist at all, are very weak.

The γ-rays of Actinium (B + C)

The absorption of the γ-rays of actinium (B + C) has been studied by Rutherford and Richardson (35), and by Curie and Savel (8). The γ-rays of actinium X and its products were found by the former to have a mass absorption coefficient of 0.073 in aluminium of thickness between 6 and 9 cm. The latter obtained 0.076 for the mass absorption coefficient in lead of thickness between 4.6 and 10.6 cm. when the source was actinium and its products. It seems likely that both coefficients refer to the more penetrating γ-rays of actinium (B + C). The energies of these were most accurately obtained by Graf (15), Surugue (43), and Choong and Surugue (7) from the energies of the internal conversion electrons and their binding energies. The more intense γ-rays are listed in Table IV.

The origin of the 0.3497 Mev γ-ray is definitely known, since its energy is equal to the difference in energy of the two groups of α-particles from actinium C. The origin in each of the remaining cases was originally based on the best numerical agreement obtained in the γ-ray energy when the binding energies of atoms of the correct atomic number were added to the energies of the conversion electrons from the different levels. The assignments to the transition actinium B.C have been verified by an experiment by Choong and Surugue (7), in which they failed to find any strong β-ray lines from a source of pure actinium C''. In a preliminary experiment the writer found by ionization through 1 cm. of steel in a pressure chamber that the γ-rays of actinium C'' are less than one-quarter as intense as those of actinium (B + C) in equilibrium for equal β-ray activities of actinium C''.

TABLE IV

Energy, Mev	Origin	γ-Ray intensity, $p(1-\alpha)$	Nuclear excitation probability, p	γ-Ray energy per disintegration, Mev
0.4040	AcB.C	0.062	0.066	0.0250
0.4258	AcB.C	0.058	0.062	0.0247
0.8296	AcB C	0.132	0.133	0.1095
0.3497	AcC.C''	0.144	0.160	0.0504
	Total	0.396		0.2096

The intensities of the γ-rays were estimated by Li (28) from the relative photographic intensities of the secondary β-ray lines measured by Surugue (44), the absolute intensity of the K-line of the 0.3497 Mev γ-ray, and the values of the internal conversion coefficients α. Since the type of nuclear transition in which a given γ-ray is produced is not known, several choices of α should be considered. Li has used the values for electric dipole and quadripole radiation taken from the empirical curves of Hulme, Mott, Oppenheimer, and Taylor (23). While the γ-ray of 0.3497 Mev energy must be electric quadripole to agree with the relative intensities of the two groups of α-particles from actinium C, the character of the other γ-rays is not definite. Differing from Li in the cases of the 0.404 and 0.425 Mev γ-rays, all have been assigned intensities in Table IV on the assumption of electric quadripole radiation. These intensities are the smaller of the two choices being considered, by a factor lying between 3 and 3.8, and therefore are in better agreement with the ionization measurements of Kara-Michailova (24) and the writer. From the ionization measurements of Curie and Savel (8) the intensity of the hard γ-ray of 0.8296 Mev was estimated at 0.079 by Kara-Michailova. Further, the total γ-ray energy per disintegration of actinium (B + C) was found (24) to be 0.107 Mev by comparison with thorium (B + C) and radium C.

The writer has made a rough determination of the ratio of the number of γ-quanta to the number of primary β-particles from the measurements of Fig. 2. The intensity of the γ-rays was measured through 0.80 gm. per cm.^{2} of aluminium, and their mass absorption coefficient in the next 6.3 gm. per cm.^{2} of aluminium was about 0.050 when the absorber was close to the chamber. When corrections for absorption were applied the initial intensities of the β- and γ-rays were respectively 4200 and 2.12 cm. per min. The intensity of the β-rays of actinium B alone was about 2100; and this must be reduced by the factor 1.32 on account of reflection from the aluminium discs. The mass absorption coefficient of the β-rays is about 9.0 in paper. It may be assumed that 0.050 and 9.0 are the coefficients of the γ- and β-rays in the carbon dioxide filling the ionization chamber. In accordance with a method used by Gray and Hinds (19) the relative ionization currents must be divided by the respective absorption in the gas and by the average energies in order to obtain the relative numbers of β-particles and γ-quanta. The average energies of the β-particles of actinium B and of the γ-rays of actinium (B + C) are assumed to be 400,000 and 450,000 electron volts. Finally, the number of γ-quanta from actinium (B + C) is about 19 per 100 β-particles from actinium B. While this estimate may be in error by as much as 50%, it agrees with the measurements of Kara-Michailova. However both disagree with the values expected from the work of Li (28) and Surugue (44) (Table IV). While the cause of the discrepancy* is not apparent, it is perhaps worth mentioning that the γ-ray intensities of Table IV would be reduced if all or part of the γ-rays of actinium B were assumed to be magnetic dipole instead of electric quadripole radiation (23).

Partial β-Spectra and the γ-Rays of Actinium B

As mentioned in the introduction, there is some evidence both in Lecoin's energy spectrum (27) and in absorption experiments by the writer (37, 38) for a weak component and a minimum number at 300,000 volts in the β-spectrum of actinium B. The intensity of the low energy peak is of the order of magnitude of 1 in 10 for the main component. While the weak component occurs in the region of some of the β-ray lines, Li (28) has found at most 3.3 secondary β-rays per 100 disintegrations. Though the evidence for two partial spectra is admittedly weak, it is in approximate agreement with the general hypotheses of Ellis and Mott (10) and the energies and intensities of the γ-rays.

Owing to overlapping, the end-point of the soft component must be greater than the energy of 300,000 volts at the minimum in the combined energy spectrum; and, from graphical attempts at breaking up the spectrum into two reasonable components, 500,000 electron volts may be taken as its approximate value. Further, owing to overlapping, the ratio of the numbers of β-particles of the soft to hard components must be increased from 1 : 10 given above to 1 : 7, and it may be as high as 1 : 5.

The actinium B nucleus may transform into actinium C in the ground state in a number of ways, as indicated in Fig. 7. The energy levels of the excited nucleus of actinium C were taken from the paper by Choong and Surugue (7). By the less frequent mode of transformation the actinium B nucleus emits a β-particle and a neutrino of 0.50 Mev energy, and the resulting excited nucleus falls to the ground state usually with the emission of one γ-ray of 0.829 Mev or two γ-rays of 0.425 + 0.404 Mev energy. By the more frequent mode of transformation the actinium B nucleus emits a β-particle and a neutrino of 1.39 Mev energy.

---

* *If the photographic intensities of the β-ray lines, measured by Surugue, are corrected for the variation of the blackening of the plates with energy, the intensity of the 0.8296 Mev γ-ray may be increased by as much as 50% [Ellis (9)]. This would increase the discrepancy.*

From the relative β-intensities given above, the excitation probability of the 0.829 Mev level is approximately 0.12, and it may be as high as 0.17.

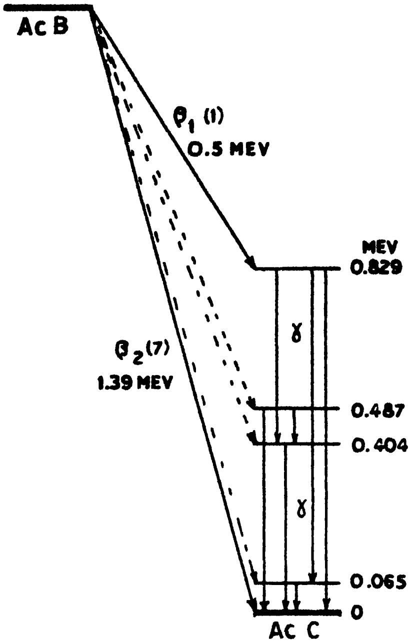

FIG. 7. *The transformation actinium B.C. The energy levels of the excited nucleus of actinium C are shown.*

From Table IV, based on Li's work, the corresponding value is 0.195. In view of the difficulties of measuring β- and γ-ray intensities the agreement is as good as can be expected.

If the tentative explanation presented here can be confirmed it provides a striking example in favour of the use of maximum energies instead of average energies of β-spectra. If the average energies of the partial spectra are assumed to be 0.15 and 0 45 Mev, the disintegration energy is 0.15 + 0.83 = 0.98 Mev by one path and 0.45 Mev by the alternative path. The discrepancy is more striking than in the well known thorium C branching, where the large α-ray energies mask the disagreement.

The difficulty, mentioned in the introduction, in connection with actinium B in the log-log plot of end-points against transformation constants (39), is now partly removed. The partial transformation constants are 0.000040 and 0.00028 sec.$^{-1}$ for the end-points of 0.50 and 1.39 Mev respectively. The soft component of the spectrum falls on the curve for permitted transitions, while the hard component falls between the two curves.

Acknowledgments

The actinium preparation used in these experiments was the gift of Dr. A. v. Grosse of the University of Chicago. The writer wishes to record his sincere thanks to Dr. v. Grosse for the actinium and his careful purification of it, and to Prof. J. A. Gray for helpful advice and the privilege of carrying out some of the experiments in his laboratory. One of the preparations of uranium X was extracted by Mr. A. G. Ward and one by Dr. H. M. Cave. The writer is indebted to them, and also to Mr. J. S. Marshall and Dr. N. Feather of the Cavendish Laboratory for the third preparation of uranium X.

References

1. ALICHANOW, A. I., ALICHANIAN, A. I., and DZELEPOW, B. S. Nature, 137 : 314-315. 1936.
2. BASCHWITZ, A. J. phys. radium, 7 : 37-39. 1936.
3. BASCHWITZ, A. J. phys. radium, 9 ; 120-122. 1938.
4. BRADFIELD, R. D. Can. J. Research, A, 16 : 76. 1938.
5. CHALMERS, J. A. Proc. Cambridge Phil. Soc. 25 : 331-339. 1929.
6. CHALMERS, J. A. Proc. Cambridge Phil. Soc. 28 : 319-327. 1932.
7. CHOONG, S. P. and SURUGUE, J. J. phys. radium, 9 : 437-439. 1938.
8. CURIE, MME. P. and SAVEL, P. J. phys. radium, 4 : 457-458. 1933.
9. ELLIS, C. D. Proc. Roy. Soc. London, A, 138 : 318-339. 1932.
10. ELLIS, C. D. and MOTT, N. F. Proc. Roy. Soc. London, A, 141 : 502-511. 1933.
11. FEATHER, N. Phys. Rev. 35 : 1559-1567. 1930.
12. FEATHER, N. Proc. Cambridge Phil. Soc. 34 : 115-119. 1938.
13. FEATHER, N. Proc. Cambridge Phil. Soc. 34 : 599-611. 1938.
14. FLAMMERSFELD, A. Physik. Z. 38 : 973-975. 1937.
15. GRAF, T. Compt. rend. 197 : 238-241. 1933.
16. GRAY, J. A. Proc. Roy. Soc. London, A, 87 : 487-489. 1912.
17. GRAY, J. A. Nature, 130 : 738. 1932.
18. GRAY, J. A. and HENDERSON, W. J. Phys. Rev. 49 : 477. 1936.
19. GRAY, J. A. and HINDS, J. F. Can. J. Research, A, 16 : 75-76. 1938.
20. HAHN, O. and MEITNER, L. Physik Z. 9 : 649-655. 1908.
21. HAHN, O. and MEITNER, L. Physik. Z. 9 : 697-702. 1908.
22. HENDERSON, W. J. Phys. Rev. 55 : 238. 1939.
23. HULME, H. R., MOTT, N. F., OPPENHEIMER, F., and TAYLOR, H. M. Proc. Roy. Soc. London, A, 155 : 315-330. 1936.
24. KARA-MICHAILOVA, E. Proc. Cambridge Phil. Soc. 34 : 429-434. 1938.
25. LANGER, L. M. and WHITAKER, M. D. Phys. Rev. 51 : 713-717. 1937.
26. LECOIN, M. Compt. rend. 202 : 1057-1059. 1936.
27. LECOIN, M. J. phys. radium, 9 : 81-95. 1938.
28. LI, K. T. Proc. Roy. Soc. London, A, 158 : 571-580. 1937.
29. LYMAN, E. M. Phys. Rev. 51 : 1-7. 1937.
30. MADGWICK, E. Proc. Cambridge Phil. Soc. 23 : 970-981. 1927.
31. MARSHALL, J. S. and WARD, A. G. Can. J. Research, A, 15 : 39-41. 1937.
32. O'CONOR, J. S. Phys. Rev. 52 : 303-314. 1937.
33. RICHARDSON, H. Phil. Mag. 27 : 252-256. 1914.
34. RUTHERFORD, E. and RICHARDSON, H. Phil. Mag. 26 : 324-332. 1913.
35. RUTHERFORD, E. and RICHARDSON, H. Phil. Mag. 26 : 937-948. 1913.
36. SANIELEVICI, A. Compt. rend. 202 : 1055-1057. 1936.
37. SARGENT, B. W. Proc. Cambridge Phil. Soc. 25 : 514-521. 1929.
38. SARGENT, B. W. Proc. Cambridge Phil. Soc. 29 : 156-160. 1933.
39. SARGENT, B. W. Proc. Roy. Soc. London, A, 139 : 659-673. 1933.
40. SCHMIDT, H. W. Physik. Z. 8 : 361-373. 1907.
41. SCHMIDT, H. W. Physik. Z. 8 : 737-743. 1907.
42. SCHMIDT, H. W. Physik. Z. 10 : 929-948. 1909.
43. SURUGUE, J. J. phys. radium, 7 : 337-346. 1936.
44. SURUGUE, J. Ann. phys. 8 : 484-554. 1937.
45. VARDER, R. W. Phil. Mag. 29 : 725-733. 1915.
46. WARD, A. G. and GRAY, J. A. Can. J. Research, A, 15 : 42-44. 1937.
47. WIDDOWSON, E. E. and CHAMPION, F. C. Proc. Phys. Soc. 50 : 185-195. 1938.
48. WILSON, W. Proc. Roy. Soc. London, A, 82 : 612-628. 1909.

Canadian Journal of Research

Issued by THE NATIONAL RESEARCH COUNCIL OF CANADA

VOL. 17, SEC. A. JUNE, 1939 NUMBER 6

LIBRARY

THE HALF-PERIODS OF ACTINIUM B, ACTINIUM C″, AND URANIUM X_1[1]

BY B. W. SARGENT[2]

Abstract

From measurements of the β-ray intensities by ionization at different times and semilogarithmic plots of these intensities against the time, the half-periods of actinium B, actinium C″, and uranium X_1 were found to be 36.1 ± 0.2 min., 4.76 ± 0.02 min., and 24.1 ± 0.2 days, respectively.

In the course of some work (5) on the end-points of β-spectra, the half-periods of actinium B, actinium C″, and uranium X_1 were determined with sufficient accuracy to be worth recording. The experimental details are given in the previous paper (5). The β-ray activity of a source was measured at different times by means of the ionization produced in a cylindrical steel chamber, 15.5 cm. long and of 13 cm. inside diameter. The gas in the chamber was carbon dioxide at a pressure of one atmosphere. A potential difference of 270 volts was maintained between the steel wall and a small axial wire, which was connected to a Compton electrometer. The ionization current is directly proportional to the observed rate of deflection of the electrometer needle when allowance is made for the effect of the initial oscillatory nature of the rate of deflection as a function of the time (5).

The logarithms of the β-ray activities were plotted against the times from the beginning of measurements to the mid-points of the readings. No error is introduced if the duration of the observation is short in comparison with the half-period. This condition was fulfilled in nearly every case. The exceptions were a few of the readings taken with sources of actinium C″. Corrections were calculated from the exponential law of decay and applied to these readings so that they also could be plotted without error at their mid-points of time. In each case the half-period was obtained from the slope of the straight line of the graph.

Actinium B

The half-period of actinium B has been determined by at least ten experimenters with concordant results. The extreme values of the last seven

---

[1] *Manuscript received March 18, 1939.*
Contribution from the Department of Physics, Queen's University, Kingston, Canada.

[2] *Assistant Professor of Physics, Queen's University.*

determinations are 35.7 and 36.4 min. and of the last four, 36.0 and 36.2 min., as seen in a list compiled by Meyer and Schweidler (4, p. 482). While the average, 36.1 min., needs no further confirmation, the writer's values are presented here to show that systematic errors were eliminated in this case and therefore likely eliminated also in the cases of actinium C″ and uranium X_1.

Actinium (B + C) was collected by recoil when aluminium discs were exposed to actinon for several hours. The sources were covered with mica to prevent loss of active deposit by α-ray recoil during the measurements. From the theory of successive transformations, the β-activity decays exponentially with the half-period of actinium B after 40 min. Measurements with each source were continued for three or four hours. In eight trials the extreme values of the half-period were 35.8 and 36.4 min., and the average value was 36.1 ± 0.2 min. The error attached is the average of the residuals obtained by subtracting the individual values from the average half-period. When the period of collection of the active deposit was limited to 10 or 15 hr., no corrections were found to be necessary for impurities of long half-period.

Actinium C″

There are only three published determinations of the half-period of actinium C″, and these are not in particularly good agreement. When Hahn and Meitner (2) discovered actinium C″ they made six measurements of its half-period. The extreme values were 5.05 and 5.4 min., and the average was 5.1 ± 0.1 min. Using 150 sources, Kovařik (3) found the half-period to lie between 4.60 and 4.85 min. and to have the average value 4.71 min. Finally, Albrecht (1) studied the decay of nine sources for about 20 min. each and obtained 4.76 ± 0.02 min.

In the present work the sources were prepared by recoil in air on to aluminium discs from the active deposit on polished nickel discs. The β-activity of each source was measured for 20 to 30 min. The half-periods obtained from the decay graphs of the first 10 trials lay between 4.63 and 4.83 min. and had an average of 4.76 ± 0.05 min. Seven more sources were used, under the best of conditions, and the half-periods were found to lie between 4.74 and 4.77 min. and to have an average of 4.76 ± 0.01 min. As a result of all the measurements, 4.76 ± 0.02 min. is adopted. No trace of any radioactive substance of long half-period was found.

Uranium X_1

The later published values of the half-period of uranium X_1 are 23.8 and 24.5 days (4, p. 377; 6), with greater emphasis on the latter.

In the present work the uranium X was so strong at first that its β-activity could be measured only after reduction by sheets of aluminium. It was an easy matter later to study the absorption of the β-rays in aluminium and to estimate the earlier intensities of the source without absorbers. Table I shows the β-ray intensities at various times.

TABLE I

β-RAY INTENSITIES

Time, days	0	97	118	141	152	174	233
β-intensity, cm./min.	13,330	769	432	220	166	87.7	15.8

Two types of corrections have been applied. In order to avoid errors due to changes in the sensitivity of the electrometer, a preparation of radium (D + E) in equilibrium was used as a standard source, and the uranium X was compared with it on each occasion. Small corrections for the decay of the radium D were applied.

The second type of corrections was necessary on account of a radioactive impurity in the preparation of uranium X. By a comparison of the penetrating power of the β-rays from the preparation when it was freshly prepared with that after 174 and 233 days, it was found that the penetrating power decreased with age. Actinium seemed to be a probable impurity on account of its well known generic relation to uranium. Moreover, the penetrating power of the β-rays from the preparation of uranium X after 233 days could be quantitatively accounted for on the assumption that 19.5% of the β-activity was due to actinium and its products, and 80.5% to uranium X. This calculation was possible since the absorption in aluminium of the β-rays of actinium and its products had been studied previously. The later β-ray activities of the preparation of uranium X have therefore been reduced by a constant amount to allow for the β-rays of actinium and its products.

From the semilogarithmic plot of the data in Table I the half-period of uranium X_1 is 24.1 ± 0.2 days.

Acknowledgments

The writer is glad to take this opportunity of thanking Dr. A. v. Grosse of the University of Chicago who kindly provided the actinium that was used in these experiments. It is a pleasure also to thank Prof. J. A. Gray and Mr. A. G. Ward for the preparation of uranium X.

References

1. Albrecht, E. Sitzber. Akad. Wis., Wien, 128, Abt. IIa : 925-944. 1919.
2. Hahn, O. and Meitner, L. Physik. Z. 9 : 649-655. 1908.
3. Kovářik, A. F. Physik. Z. 12 : 83. 1911.
4. Meyer, S. and Schweidler, E. Radioaktivität. Teubner, Leipzig. 1927.
5. Sargent, B. W. Can. J. Research, A, 17 : 82-102. 1939.
6. Walling, E. Z. Physik, 75 : 432-433. 1932.

THE EQUILIBRIUM OF A THIN COMPRESSIBLE MEMBRANE[1]

By G. E. Hay[2]

Abstract

An investigation has been made of the equilibrium of a thin incompressible elastic membrane lying between two rigid bodies, one fixed and the other mobile. The present paper concerns the corresponding problem for a compressible membrane.

Membranes are divided mathematically into four classes according as their compressibility is (i) finite, (ii) small, (iii) very small, (iv) so small that the membrane may be considered as incompressible. The movable boundary is assigned a rigid body displacement. By the introduction of approximation based on the thinness of the membrane a determination of the resulting stress, strain and displacement is made for each of the above four classes of membranes.

1. Introduction

In some previous papers J. L. Synge (6, 7, 8) considered the elastic equilibrium of thin curved membranes of incompressible material, with application to the periodontal membrane or pericementum which fills the space between the tooth and the jaw-bone and is attached to both. It was later pointed out by J. N. Goodier that a compressibility even as small as that of water introduced terms comparable with those retained in the theory as developed on the assumption of incompressibility. The elastic equilibrium of thin flat compressible membranes was then considered by J. L. Synge (9). The present work deals with the equilibrium of thin curved compressible membranes, and in a later paper (5) the theory will be applied to a compressible periodontal membrane. In view of this application the theory will be developed for membranes bounded by two rigid bodies, of which one is fixed and the other is movable. The edge of the membrane is subject to atmospheric pressure. A determination will be made of the stress in the membrane and the displacement of the movable boundary when that boundary is subjected to assigned force systems.

2. Notation and Equations of Equilibrium of a Homogeneous Isotropic Elastic Medium

The points of the elastic medium will be referred to the curvilinear co-ordinate system x^i $(i=0,1,2)$. Latin indices will stand for the range 0,1,2, Greek indices for the range 1,2, and in accordance with the usual convention summation over either of these ranges will be signified by factors with repeated indices except where such indices are enclosed in brackets.

The line-element will be of the form

$$ds^2 = a_{ij}dx^i dx^j, \tag{2.1}$$

---

[1] *Original manuscript received September 28, 1938.*

Contribution from the Department of Applied Mathematics, University of Toronto, Toronto, Canada.

[2] *Holder of a Bursary under the National Research Council of Canada.*

and A_i will denote the operation of taking the covariant derivative with respect to a_{ij}. The contravariant derivative will then be

$$A^i = a^{ij} A_j , \tag{2.2}$$

where a^{ij} is the cofactor of a_{ij} in the determinant $|a_{ij}|$ divided by that determinant. Partial differentiation will be indicated in the two ways

$$\frac{\partial U}{\partial x^i} = U_{,i} , \tag{2.3}$$

where U is any function containing x^i. Thus for an invariant V,

$$A_i V = V_{,i} , \quad A^i V = a^{ij} V_{,j} , \tag{2.4}$$

and for the vector V^j or $V_j (= a_{jk} V^k)$,

$$A_i V^j = V^j_{,i} + F^j_{ik} V^k_, \quad A_i V_j = V_{j,i} - F^k_{ij} V_k , \tag{2.5}$$

where F^i_{jk} is the Christoffel symbol of the second kind,

$$F^i_{jk} = \tfrac{1}{2} a^{il} (a_{lj,k} + a_{kl,j} - a_{jk,l}) . \tag{2.6}$$

For a mixed tensor $V_k^{\cdot j}$,

$$A_i V_k^{\cdot j} = V_{k,i}^{\cdot j} + F^j_{il} V_k^{\cdot l} - F^l_{ik} V_l^{\cdot j} . \tag{2.7}$$

The (infinitesimal) components of displacement will be denoted by u^i, and hence the covariant components of strain are*

$$e_{ij} = \tfrac{1}{2} (A_i u_j + A_j u_i) . \tag{2.8}$$

Since the medium is homogeneous and isotropic the stress-strain relations are

$$T_{ij} = \frac{E}{1+\sigma} \left(e_{ij} + \frac{\sigma}{1-2\sigma} \theta a_{ij} \right) , \tag{2.9}$$

where T_{ij} are the components of stress, E is Young's modulus, σ is Poisson's ratio and

$$\theta = e_i^{\cdot i} = A_i u^i : \tag{2.10}$$

θ is called the cubical dilatation. From (2.9),

$$\Theta = \frac{E}{1-2\sigma} \theta, \qquad \Theta = T_i^{\cdot i} . \tag{2.11}$$

In the absence of body forces the equations of equilibrium are

$$A_j T_i^{\cdot j} = 0 . \tag{2.12}$$

Since the space is Euclidean ($A_i A_j = A_j A_i$), substitution in (2.12) from (2.8), (2.9) and (2.10) leads to the following result:—

I. The equations of equilibrium of an elastically homogeneous and isotropic medium acted on by no body forces are

$$A^i \theta + (1-2\sigma) A^j A_j u^i = 0 , \qquad (i=0,1,2), \tag{2.13}$$

---

* *A more detailed application of tensor notation to elasticity is given in Reference (1, p. 91).*

where A^i and A_i denote the contravariant and covariant derivatives respectively, u^i are the components of displacement, θ is the cubical dilatation and σ is Poisson's ratio.

3. The Parameter of Approximation

To solve (2.13) approximation is introduced based on (*a*) the thinness of the membrane, (*b*) the smallness of the compressibility, in the way followed by Synge in (6) and (9) respectively. The method of introducing thinness was also used by Birkhoff (2), Garabedian (3), and Goodier (4).

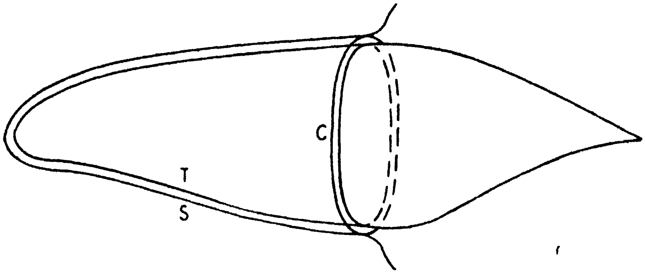

FIG. 1. *Elastic system formed by a thin membrane attached to two rigid bodies S and T.*

Fig. 1 shows the elastic system under consideration. It consists of a thin membrane bounded by and attached to two rigid bodies S and T, and having a free edge C. The membrane is thin and a dimensionless parameter ϵ is introduced, defined by

$$(3.1) \qquad \epsilon = \frac{\text{average thickness of the membrane}}{\text{average length of the membrane}}$$

whence $\epsilon << 1$. When a length is comparable with $\epsilon^r \times$ *average length of the membrane*, $(r=1,2, \ldots)$, it will be said to be of order ϵ^r and when $r=0$ it will be referred to as a "finite length". Thus the thickness of the membrane is of order ϵ.

Since σ is Poisson's ratio, $1-2\sigma$ is dimensionless, vanishes for an incompressible medium and is a measure of the compressibility: it never exceeds unity and is frequently much smaller than unity: in any case it is permissible to write

$$(3.2) \qquad 1-2\sigma = k\epsilon^n, \qquad (n=0,1,2, \ldots),$$

where n is to be so chosen that k is comparable with unity. The cases $n=0,1,2$, and $n>2$ will be considered successively: they refer respectively to finite compressibility, small compressibility, very small compressibility, and essential incompressibility, the reason for this last nomenclature being explained in §9.

4. The Normal Co-ordinate System. Transformation of the Equations of Equilibrium

Fig. 2 shows a section of the membrane: S and T are the bounding rigid bodies. The letters S and T can without ambiguity be used to denote their surfaces: S is regarded as fixed and on it are chosen curvilinear co-ordinates x^α ($\alpha=1,2$). From a general point in the membrane, QN is drawn normal to S. Then by definition $x^0=QN$, whence x^i ($i=0,1,2$) define a set of curvilinear co-ordinates which are regular (*i.e.*, there is but one set of co-ordinates for each point in the membrane) if QN is less than the smaller of the two principal radii of curvature of S at N. In view of the thinness of the membrane this inequality may be assumed to be satisfied.

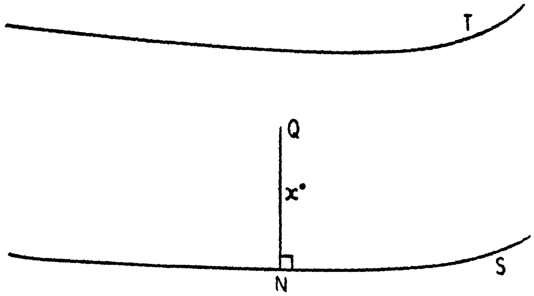

FIG. 2. *Section of the membrane and the bounding rigid bodies.*

The equation of T is

$$x^0=h(x^1,x^2)\,, \tag{4.1}$$

where $h(x^1,x^2)$ is a regular function over S: it is the thickness of the membrane. Then $0\leqslant x^0\leqslant h$ and the range of x^0 is small in comparison with the ranges of x^α ($\alpha=1,2$). Consequently ξ and τ are introduced, defined by

$$x^0=\epsilon\xi\,,\qquad h(x^1,x^2)=\epsilon\tau\,(x^1,x^2)\,, \tag{4.2}$$

where ϵ is the small parameter defined in (3.1). Then $0\leqslant\xi\leqslant\tau$ and the ranges of ξ, x^1 and x^2 are all finite lengths.

From the nature of the co-ordinate system x^i ($i=0,1,2$),

$$a_{\alpha 0}=0\,,\qquad a_{00}=1\,,\qquad a^{\alpha 0}=0\,,\qquad a^{00}=1\,. \tag{4.3}$$

Thus the Christoffel symbols are

$$F^0_{00}=F^\alpha_{00}=F^0_{0\alpha}=0\,,\qquad F^0_{\alpha\beta}=-\tfrac{1}{2}a_{\alpha\beta,0}\,,\qquad F^\alpha_{\beta 0}=\tfrac{1}{2}a^{\alpha\gamma}a_{\beta\gamma,0}\,. \tag{4.4}$$

It is noted that any Christoffel symbol with two or more zero indices vanishes. All the remaining Christoffel symbols are regular functions of x^0, x^1 and x^2; expansion in power series in x^0 gives

$$F^i_{jk}=\sum_{m=0}^{\infty}\frac{1}{m!}\,\epsilon^m\xi^m F^i_{jk(m)}\,, \tag{4.5}$$

where

$$F^i_{jk(m)}=\left(\frac{\partial^m F^i_{jk}}{(\partial x^0)^m}\right)_{x^0=0}\,,\qquad 0!=1 \text{ (by definition)}, \tag{4.6}$$

and $F^i_{jk(m)}$ are regular functions of x^1 and x^2.

Similarly

$$(4.7)\qquad a^{\alpha\beta} = \sum_{m=0}^{\infty} \frac{1}{m!}\, \epsilon^m \xi^m a^{\alpha\beta}_{(m)}, \quad a_{\alpha\beta} = \sum_{m=0}^{\infty} \frac{1}{m!}\, \epsilon^m \xi^m a_{\alpha\beta(m)},$$

where

$$(4.8)\qquad a^{\alpha\beta}_{(m)} = \left(\frac{\partial^m a^{\alpha\beta}}{(\partial x^0)^m}\right)_{x^0=0}, \qquad a_{\alpha\beta(m)} = \left(\frac{\partial^m a_{\alpha\beta}}{(\partial x^0)^m}\right)_{x^0=0}.$$

Since

$$(4.9)\qquad \frac{\partial}{\partial x^0} = \frac{1}{\epsilon}\frac{\partial}{\partial \xi},$$

then by (2.5)

$$(4.10)\qquad \left\{\begin{aligned} &A_0 u^0 = \frac{1}{\epsilon}\frac{\partial u^0}{\partial \xi}, && A_0 u^\alpha = \frac{1}{\epsilon}\frac{\partial u^\alpha}{\partial \xi} + F^\alpha_{0\beta} u^\beta, \\ &A_\alpha u^0 = u^0_{,\alpha} + F^0_{\alpha\beta} u^\beta, && A_\alpha u^\beta = u^\beta_{,\alpha} + F^\beta_{\alpha\iota} u^\iota, \end{aligned}\right.$$

and by (2.7),

$$(4.11)\qquad \left\{\begin{aligned} A^0 A_0 u^0 &= \frac{1}{\epsilon^2}\frac{\partial^2 u^0}{\partial \xi^2}, \\ A^0 A_0 u^\gamma &= \frac{1}{\epsilon^2}\frac{\partial^2 u^\gamma}{\partial \xi^2} + \frac{2}{\epsilon} F^\gamma_{\beta 0}\frac{\partial u^\beta}{\partial \xi} + F^\gamma_{\beta 0,0} u^\beta + F^\gamma_{\beta 0} F^\beta_{\alpha 0} u^\alpha, \\ A^\alpha A_\alpha u^0 &= a^{\alpha\beta}\Big[-\frac{1}{\epsilon} F^0_{\alpha\beta}\frac{\partial u^0}{\partial \xi} + u^0_{,\alpha\beta} - F^\gamma_{\alpha\beta} u^0_{,\gamma} + F^0_{\beta\gamma} F^\gamma_{\alpha 0} u^0 \\ &\qquad + 2F^0_{\alpha\gamma} u^\gamma_{,\beta} + (F^0_{\alpha\delta,\beta} + F^0_{\beta\gamma} F^\gamma_{\alpha\delta} - F^\gamma_{\alpha\beta} F^0_{\gamma\delta}) u^\delta \Big], \\ A^\alpha A_\alpha u^\gamma &= a^{\alpha\beta}\Big[-\frac{1}{\epsilon} F^0_{\alpha\beta}\frac{\partial u^\gamma}{\partial \xi} + 2F^\gamma_{\alpha 0} u^0_{,\beta} \\ &\qquad + (F^\gamma_{\alpha 0,\beta} + F^\gamma_{\beta\delta} F^\delta_{\alpha 0} - F^\delta_{\alpha\beta} F^\gamma_{\delta 0}) u^0 + u^\gamma_{,\alpha\beta} + 2F^\gamma_{\alpha\delta} u^\delta_{,\beta} \\ &\qquad - F^\delta_{\alpha\beta} u^\gamma_{,\delta} + (F^\gamma_{\alpha\delta,\beta} + F^\gamma_{\beta\iota} F^\iota_{\alpha\delta} - F^\iota_{\alpha\beta} F^\gamma_{\iota\delta}) u^\delta \Big]. \end{aligned}\right.$$

From (4.10) the cubical dilatation θ is given by

$$(4.12)\qquad \theta = \frac{1}{\epsilon}\frac{\partial u^0}{\partial \xi} + u^\alpha_{,\alpha} + F^\alpha_{\alpha\iota} u^\iota.$$

Substitution from (4.11) in (2.13) produces the following:—

II. Relative to the co-ordinate system ξ, x^1, x^2 the equations of equilibrium are

$$\begin{aligned}(4.13)\qquad &\frac{1}{\epsilon}\frac{\partial\theta}{\partial\xi}+(1-2\sigma)\left\{\frac{1}{\epsilon^2}\frac{\partial^2u^0}{\partial\xi^2}+a^{\alpha\beta}\left[-\frac{1}{\epsilon}F^0_{\alpha\beta}\frac{\partial u^0}{\partial\xi}+u^0_{,\alpha\beta}-F^\gamma_{\alpha\beta}u^0_{,\gamma}\right.\right.\\ &\qquad\left.\left.+F^0_{\beta\gamma}F^\gamma_{\alpha0}u^0+2F^0_{\alpha\gamma}u^\gamma_{,\beta}+(F^0_{\alpha\delta,\beta}+F^0_{\beta\gamma}F^\gamma_{\alpha\delta}-F^\gamma_{\alpha\beta}F^0_{\gamma\delta})u^\delta\right]\right\}=0,\end{aligned}$$

$$\begin{aligned}(4.14)\qquad &a^{\gamma\alpha}\theta_{,\alpha}+(1-2\sigma)\left\{\frac{1}{\epsilon^2}\frac{\partial^2u^\gamma}{\partial\xi^2}+\frac{2}{\epsilon}F^\gamma_{\beta0}\frac{\partial u^\beta}{\partial\xi}+[F^\gamma_{\delta0,0}+F^\gamma_{\beta0}F^\beta_{\delta0}]u^\delta\right.\\ &\qquad+a^{\alpha\beta}\left[-\frac{1}{\epsilon}F^0_{\alpha\beta}\frac{\partial u^\gamma}{\partial\xi}+2F^\gamma_{\alpha0}u^0_{,\beta}\right.\\ &\qquad\qquad+(F^\gamma_{\alpha0,\beta}+F^\gamma_{\beta\delta}F^\delta_{\alpha0}-F^\delta_{\alpha\beta}F^\gamma_{\delta0})u^0\\ &\qquad\qquad+u^\gamma_{,\alpha\beta}+2F^\gamma_{\alpha\delta}u^\delta_{,\beta}-F^\delta_{\alpha\beta}u^\gamma_{,\delta}\\ &\qquad\qquad\left.\left.+(F^\gamma_{\alpha\delta,\beta}+F^\gamma_{\beta i}F^i_{\alpha\delta}-F^i_{\alpha\beta}F^\gamma_{i\delta})u^\delta\right]\right\}=0.\end{aligned}$$

In these formulae ϵ is the dimensionless parameter defined in (3.1), u^i are the components of displacement within the membrane, a_{ij} and a^{ij} are respectively the covariant and contravariant forms of the fundamental tensor, F^i_{jk} are the Christoffel symbols defined in (2.6), θ is expressed by (4.12), a subscript preceded by a comma signifies partial differentiation as illustrated in (2.3), Greek indices have the range 1,2, and Latin indices have the range 0,1,2.

5. The Formal Process of Integration of the Equations of Equilibrium

It is required to solve (4.13) and (4.14) for the principal parts of u^i where $0\leqslant\xi\leqslant\tau(x^1,x^2)$ and the range of values of x^1 and x^2 corresponds to the part of the solid T covered by the membrane. The boundary conditions are that $u^i=0$ for $\xi=0$, that for $\xi=\tau$ the values of u^i shall be equal to the components of the rigid body displacement of the solid T, and that over the edge of the membrane the normal stress shall be a constant pressure P.

It is assumed for all small values of ϵ that (4.13) and (4.14) admit of solutions which are expressible in power-series in ϵ with coefficients which are regular functions of ξ, x^1 and x^2. The thickness of the membrane is of order ϵ and since u^i must be of higher order,

$$(5.1)\qquad u^i=\sum_{m=2}^{\infty}\epsilon^m u^i_{(m)},$$

where $u^i_{(m)}$ are finite.

The boundary conditions are as follows:—

(5.2)

for $\xi=0$, $u^i=0$,

for $\xi=\tau$, $u^i=\beta^i=\sum_{m=2}^{\infty}\epsilon^m\beta^i_{(m)}$,

the stress normal to $f(x^1, x^2)=0$ is independent of ϵ and is a pressure P,

where β^i are the components of the rigid body displacement of T, $\beta^i_{(m)}$ are functions of x^1 and x^2 only and are comparable with any finite length, and $f(x^1, x^2)=0$ is the edge of the membrane: P will be assumed to be of the form

$$P=\sum_{m=0}^{\infty}\epsilon^m P_{(m)}\,, \tag{5.3}$$

where $P_{(0)}$, $P_{(1)}$, . . . are constants independent of ϵ.

From (2.5), (2 8), (4 2) and (4 4) the strain components and the dilatation are

$$\begin{aligned}
e_{00}&=\frac{1}{\epsilon}\frac{\partial u^0}{\partial\xi}\,,\\
e_{\alpha 0}&=\tfrac{1}{2}\left\{a_{\alpha\beta}\left(\frac{1}{\epsilon}\frac{\partial u^\beta}{\partial\xi}+F^\beta_{0\gamma}u^\gamma\right)+u^0_{,\alpha}+F^0_{\alpha\beta}u^\beta\right\}\,;\\
e_{\alpha\beta}&=\tfrac{1}{2}\left\{a_{\beta\gamma}(u^\gamma_{,\alpha}+F^\gamma_{\alpha i}u^i)+a_{\alpha\gamma}(u^\gamma_{,\beta}+F^\gamma_{\beta i}u^i)\right\}\,,\\
\theta&=\frac{1}{\epsilon}\frac{\partial u^0}{\partial\xi}+u^\alpha_{,\alpha}+F^\alpha_{\alpha i}u^i\,.
\end{aligned} \tag{5.4}$$

Using (4 5), (4 7) and (5 1), these can be expressed explicitly in ϵ, whence

$$\left\{\begin{aligned}
e_{00}&=\epsilon\frac{\partial u^0_{(2)}}{\partial\xi}+\epsilon^2\frac{\partial u^0_{(3)}}{\partial\xi}+0(\epsilon^3)\,,\\
e_{\alpha 0}&=\tfrac{1}{2}\left\{\epsilon a_{\alpha\gamma(0)}\frac{\partial u^\gamma_{(2)}}{\partial\xi}+0(\epsilon^2)\right\}\,,\\
e_{\alpha\beta}&=\tfrac{1}{2}\Big\{\epsilon^2[a_{\beta\gamma(0)}(u^\gamma_{(2),\alpha}+F^\gamma_{\alpha i(0)}u^i_{(2)})\\
&\qquad+a_{\alpha\gamma(0)}(u^\gamma_{(2),\beta}+F^\gamma_{\beta i(0)}u^i_{(2)})]+0(\epsilon^3)\Big\}\,,
\end{aligned}\right. \tag{5 5}$$

$$\theta=\epsilon\theta_{(1)}+\epsilon^2\theta_{(2)}+\ -\ -\ -\,, \tag{5.6}$$

where

$$\theta_{(1)}=\frac{\partial u^0_{(2)}}{\partial\xi}\,,\qquad \theta_{(r)}=\frac{\partial u^0_{(r+1)}}{\partial\xi}+u^\alpha_{(r),\alpha}+\sum_{s=0}^{r-2}\frac{1}{s!}\,\xi^s F^\alpha_{\alpha i(s)}u^i_{(r-s)}\,, \tag{5 7}$$

$$(r=2,\ 3,\ -\ -\ -\ ).$$

The system of stresses compatible with the strain (5.5) must remain finite as $\epsilon \to 0$. Using (2.11) and (3.2), the sum of the principal stresses is given by

$$\Theta = \frac{E}{k\epsilon^n}(\epsilon\theta_{(1)} + \epsilon^2\theta_{(2)} + \cdots). \tag{5.8}$$

If $n=0$ or 1, Θ (and also the stress components T_{ij}) remain finite as $\epsilon \to 0$. If $n=2$ it is necessary that $\theta_{(1)}=0$ and by (5.7), $u^0_{(2)}$ is then a function of x^1 and x^2 only. Thus $\beta^0_{(2)}=0$ and hence since T is a rigid body $\beta^i_{(2)}=0$. This is summed up as follows:—

III. If $n=0$ or 1 the condition of finite stress is satisfied when u^i is of order ϵ^2. If $n=2$ it is necessary that

$$u^0_{(2)}=0, \qquad \theta_{(1)}=0, \qquad \beta^i_{(2)}=0. \tag{5.9}$$

If $n>2$, (5.9) must be satisfied and also

$$\theta_{(r)} = \frac{\partial u^0_{(r+1)}}{\partial \xi} + u^\alpha_{(r),\alpha} + \sum_{s=0}^{r-2} \frac{1}{s!}\, \xi^s F^\alpha_{\alpha i(s)} u^i_{(r-s)} = 0, \qquad (r=2, 3, \cdots n-1). \tag{5.10}$$

In the absence of restrictions as regards the value of n, substitution in the equations of equilibrium (4.13) and (4.14) for $1-2\sigma$, F^i_{jk}, $a^{\alpha\beta}$, $a_{\alpha\beta}$ and u^i from (3.2), (4.5), (4.7) and (5.1) gives three equations each of which is (*i*) explicit in ϵ, (*ii*) a power series in ϵ, (*iii*) true for all small values of ϵ. Hence the coefficients of all powers of ϵ must vanish identically, and by equating to zero the coefficient of the lowest power of ϵ occurring in each equation three partial differential equations for the principal parts of the displacement are obtained. This is summed up as follows:—

IV. The differential equations for the principal parts of the displacement u^i $(i=0,1,2)$ are obtained by equating to zero the coefficient of the lowest power of ϵ occurring in (4.13) and in (4.14) after substitution has been carried out for $1-2\sigma$, F^i_{jk}, $a^{\alpha\beta}$, $a_{\alpha\beta}$ and u^i from (3.2), (4.5), (4.7) and (5.1).

6. The Case $n=0$ (Finite Compressibility)

Upon taking $n=0$ in (3.2) and carrying out the substitutions indicated in IV, one finds that the lowest power of ϵ occurring both in (4.13) and in (4.14) is ϵ^0 and that the corresponding coefficients give rise to the equations

$$(1+k)\frac{\partial^2 u^0_{(2)}}{\partial \xi^2} = 0, \tag{6.1}$$

$$k\frac{\partial^2 u^\alpha_{(2)}}{\partial \xi^2} = 0. \tag{6.2}$$

The following boundary conditions are obtained from (5.2):—

(6.3) for $\xi=0, \quad u^i_{(2)}=0,$

(6.4) for $\xi=\tau, \quad u^i_{(2)}=\beta^i_{(2)},$

(6.5) the stress normal to $f(x^1, x^2)=0$ is a constant pressure P, where $f(x^1, x^2)=0$ is the edge of the membrane. Since $k \neq -1$, the solution of (6.1) and (6.2) subject to (6.3) and (6.4) is

$$u^{\iota}_{(2)}=\xi\beta^{\iota}_{(2)}/\tau. \tag{6.6}$$

The boundary condition (6.5) has yet to be satisfied.

Substitution from (6.6) in (5.5) gives for the strain components and dilatation

$$\left\{\begin{aligned} &e_{00}=\epsilon\beta^{0}_{(2)}/\tau+0(\epsilon^2),\\ &e_{\alpha 0}=\tfrac{1}{2}\epsilon a_{\alpha\gamma(0)}\beta^{\gamma}_{(2)}/\tau+0(\epsilon^2),\\ &e_{\alpha\gamma}=\tfrac{1}{2}\epsilon^2\xi\{a_{\gamma\delta(0)}(\beta^{\delta}_{(2)}/\tau)_{,\alpha}+a_{\alpha\delta(0)}(\beta^{\delta}_{(2)}/\tau)_{,\gamma}\\ &\qquad\qquad+(a_{\gamma\delta(0)}F^{\delta}_{\alpha\iota(0)}+a_{\alpha\delta}F^{\delta}_{\gamma\iota(0)})(\beta^{\iota}_{(2)}/\tau)\}+0(\epsilon^3),\\ &\theta=\epsilon\beta^{0}_{(2)}/\tau+0(\epsilon^2). \end{aligned}\right. \tag{6.7}$$

Since $1-2\sigma=k$, by (2.9) the stress components are

$$\left\{\begin{aligned} &T_{00}=\frac{E(1-\sigma)}{(1+\sigma)(1-2\sigma)}\,\frac{\beta^{0}_{(2)}}{\tau}\,\epsilon+0(\epsilon^2),\\ &T_{\alpha 0}=\frac{E}{2(1+\sigma)}\,\frac{\beta^{\gamma}_{(2)}}{\tau}\,a_{\gamma\alpha(0)}\epsilon+0(\epsilon^2),\\ &T_{\alpha\gamma}=\frac{E\sigma}{(1+\sigma)(1-2\sigma)}\,\frac{\beta^{0}_{(2)}}{\tau}\,a_{\alpha\gamma(0)}\epsilon+0(\epsilon^2). \end{aligned}\right. \tag{6.8}$$

If the outward normal to the edge of the membrane is denoted by the unit vector $(0, n^1, n^2)$, the covariant components of the stress across this edge are $T_{\iota}=T_{\iota\alpha}n^{\alpha}$, whence

$$\left\{\begin{aligned} &T_0=\frac{E}{2(1+\sigma)}\,\frac{\beta^{\alpha}_{(2)}}{\tau}\,n^{\gamma}a_{\alpha\gamma(0)}\epsilon+0(\epsilon^2),\\ &T_{\alpha}=\frac{E\sigma}{(1+\sigma)(1-2\sigma)}\,\frac{\beta^{0}_{(2)}}{\tau}\,n^{\gamma}a_{\gamma\alpha(0)}\epsilon+0(\epsilon^2). \end{aligned}\right. \tag{6.9}$$

The pressure P over the edge of the membrane is expressed by (5.3) and if the stress system (6.9) is to be such a pressure it is necessary that

$$a_{\alpha\gamma(0)}\beta^{\alpha}_{(2)}n^{\gamma}=0,\ \frac{E\sigma}{(1+\sigma)(1-2\sigma)}\,\frac{\beta^{0}_{(2)}}{\tau}=-P_{(1)},\ P_{(0)}=0. \tag{6.10}$$

It is possible to satisfy these conditions only when $P_{(0)}=P_{(1)}=\beta^{\iota}_{(2)}=0$. The method then breaks down since it is impossible to satisfy all the boundary conditions. However the strain and stress components given in (6.7) and (6.8) are valid throughout all the membrane except a narrow strip around the edge; this is taken into account by saying that in the case $n=0$ there is an edge effect.

These results are summed up as follows, expressed explicitly in the small quantities, the ϵ-method having now served its purpose:—

V. For a thin curved membrane of finite compressibility there is an edge effect in a narrow strip around the edge of the membrane. In the rest of the membrane the principal parts of the displacement are

$$u^i = \beta^i x^0/h\,, \tag{6.11}$$

the principal parts of the strain and dilatation are

$$\left\{\begin{aligned} & e_{00} = \beta^0/h\,, \qquad e_{\alpha 0} = \tfrac{1}{2} a_{\alpha\gamma}\beta^\gamma/h\,, \\ & e_{\alpha\gamma} = \tfrac{1}{2} x^0 \{ a_{\gamma\delta}(\beta^\delta/h)_{,\alpha} + a_{\alpha\delta}(\beta^\delta/h)_{,\gamma} \\ & \qquad\qquad + (a_{\gamma\delta}F^\delta_{\alpha\iota} + a_{\alpha\delta}F^\delta_{\gamma\iota})(\beta^\iota/h) \}, \\ & \theta = \beta^0/h\,, \end{aligned}\right. \tag{6.12}$$

and the principal parts of the stress are

$$\left\{\begin{aligned} & T_{00} = \frac{E(1-\sigma)}{(1+\sigma)(1-2\sigma)}\,\frac{\beta^0}{h}\,, \qquad T_{\alpha 0} = \frac{E}{2(1+\sigma)}\,\frac{\beta^\gamma}{h}\,a_{\gamma\alpha}\,, \\ & T_{\alpha\gamma} = \frac{E\sigma}{(1+\sigma)(1-2\sigma)}\,\frac{\beta^0}{h}\,a_{\alpha\gamma}\,. \end{aligned}\right. \tag{6.13}$$

In these formulae β^ι are the components of the displacement of a point (x^1, x^2) on T and are of order ϵ^2, x^0 is the length of the normal to S, h is the thickness of the membrane, a_{ij} is the fundamental tensor, E is Young's modulus, σ is Poisson's ratio and ϵ is the small parameter defined in (3.1).

7. The Case $n=1$ (Small Compressibility)

Upon taking $n=1$ in (3.2) and carrying out the substitutions indicated in IV, it is found that the lowest power of ϵ occurring in (4.13) is ϵ^0 and in (4.14) is ϵ. The corresponding coefficients give rise to the equations

$$\frac{\partial^2 u^0_{(2)}}{\partial \xi^2} = 0\,, \tag{7.1}$$

$$a^{\alpha\gamma}_{(0)}\,\frac{\partial}{\partial \xi}\,(u^0_{(2),\gamma}) + k\,\frac{\partial^2 u^\alpha_{(2)}}{\partial \xi^2} = 0\,. \tag{7.2}$$

The following boundary conditions are obtained from (5.2):—

(7.3) for $\xi = 0$, $u^\iota_{(2)} = 0$,

(7.4) for $\xi = \tau$, $u^\iota_{(2)} = \beta^\iota_{(2)}$,

(7.5) the stress normal to $f(x^1, x^2) = 0$ is a constant pressure P, where $f(x^1, x^2) = 0$ is the edge of the membrane. Using (7.3) and (7.4), integration of (7.1) gives

$$u^0_{(2)} = \xi \beta^0_{(2)}/\tau \,, \tag{7.6}$$

and upon substitution of this value of $u^0_{(2)}$ in (7.2) integration gives

$$u^\alpha_{(2)} = \frac{\xi \beta^\alpha_{(2)}}{\tau} + \frac{(\tau - \xi)\xi}{2k} a^{\alpha\gamma}_{(0)} (\beta^0_{(2)}/\tau)_{,\gamma} \tag{7.7}$$

satisfying (7.3) and (7.4). The boundary condition (7.5) has yet to be satisfied.

Substitution from (7.6) and (7.7) in (5.5) gives for the strain components and dilatation

$$\left\{ \begin{array}{ll} e_{00} = \epsilon \beta^0_{(2)}/\tau + 0(\epsilon^2) \,, & \\ e_{\alpha 0} = 0(\epsilon) \,, & e_{\alpha\gamma} = 0(\epsilon^2) \,, \\ \theta = \epsilon \beta^0_{(2)}/\tau + 0(\epsilon^2) \,. & \end{array} \right. \tag{7.8}$$

Since $1 - 2\sigma = k\epsilon$, so that $\sigma = \frac{1}{2}$ approximately, by (2.9) the stress components are

$$\left\{ \begin{array}{l} T_{00} = E\beta^0_{(2)}/(3k\tau) + 0(\epsilon) \,, \\ T_{\alpha 0} = 0(\epsilon) \,, \\ T_{\alpha\gamma} = E\beta^0_{(2)} a_{\alpha\gamma(0)}/(3k\tau) + 0(\epsilon) \,. \end{array} \right. \tag{7.9}$$

Thus the principal part of the stress is a finite pressure

$$p = -E\beta^0_{(2)}/(3k\tau) \,, \tag{7.10}$$

and to satisfy (7.5) it is necessary that

$$P_{(0)} = -E\beta^0_{(2)}/(3k\tau) \,. \tag{7.11}$$

There is obviously an edge effect as in §6.

These results are summed up as follows:—

VI. For a thin curved membrane of small compressibility, $1 - 2\sigma$ being comparable with ϵ, there is an edge effect in a narrow strip around the edge of the membrane. In the rest of the membrane the principal parts of the displacement are

$$\left\{ \begin{array}{l} u^0 = \dfrac{x^0 \beta^0}{h} \,, \\ u^\alpha = \dfrac{x^0 \beta^\alpha}{h} + \dfrac{(h - x^0)x^0}{2(1 - 2\sigma)} a^{\alpha\gamma} (\beta^0/h)_{,\gamma} \,, \end{array} \right. \tag{7.12}$$

and the principal part of the stress is a finite pressure

$$p = -E\beta^0/\{3h(1-2\sigma)\}. \tag{7.13}$$

In these formulae β^i are the components of the displacement of a point (x^1, x^2) on T and are of order ϵ^2, x^0 is the length of the normal to S, h is the thickness of the membrane, a_{ij} is the fundamental tensor, E is Young's modulus, σ is Poisson's ratio and ϵ is the small parameter defined in (3.1).

8. The Case $n=2$ (Very Small Compressibility)

This case is more interesting since, as it turns out, the membrane under consideration has the elastic properties of the periodontal membrane. The condition for finite stress (5.9) requires that

$$u^0_{(2)} = 0, \qquad \theta_{(1)} = 0, \qquad \beta^i_{(2)} = 0. \tag{8.1}$$

Upon taking $n=2$ in (3.2) and carrying out the substitutions indicated in IV, it is found that the lowest power of ϵ occurring in (4.13) is ϵ and in (4.14) is ϵ^2. The corresponding coefficients give rise to the equations

$$\frac{\partial\theta_{(2)}}{\partial\xi} = 0, \tag{8.2}$$

$$a^{\alpha\gamma}_{(0)}\theta_{(2),\gamma} + k\frac{\partial^2 u^\alpha_{(2)}}{\partial\xi^2} = 0, \tag{8.3}$$

where from (5.7),

$$\theta_{(2)} = \frac{\partial u^0_{(3)}}{\partial\xi} + u^\alpha_{(2),\alpha} + F^\alpha_{\alpha\gamma(0)}u^\gamma_{(2)}. \tag{8.4}$$

The following boundary conditions are obtained from (5.2):—

(8.5) for $\xi = 0, \quad u^0_{(3)} = u^\alpha_{(2)} = 0,$

(8.6) for $\xi = \tau, \quad u^0_{(3)} = \beta^0_{(3)}, \quad u^\alpha_{(2)} = 0,$

(8.7) the stress normal to $f(x^1, x^2) = 0$ is a constant pressure P, where $f(x^1, x^2) = 0$ is the edge of the membrane.

From (8.2) it is seen that $\theta_{(2)}$ is a function of x^1 and x^2 only, and hence (8.3) has the solution

$$ku^\alpha_{(2)} = \tfrac{1}{2}(\tau-\xi)\,\xi a^{\alpha\gamma}_{(0)}\theta_{(2),\gamma}, \tag{8.8}$$

satisfying (8.5) and (8.6). This value for $u^\alpha_{(2)}$ is substituted in (8.4), and since the resulting equation is explicit in ξ easy integration gives

$$ku^0_{(3)} = -\frac{1}{12}\xi^2(3\tau-2\xi)\{(a^{\alpha\gamma}_{(0)}\theta_{(2),\gamma})_{,\alpha} + F^\alpha_{\alpha\gamma(0)}a^{\gamma\delta}_{(0)}\theta_{(2),\delta}\} - \frac{1}{4}\xi^2 a^{\alpha\gamma}_{(0)}\theta_{(2),\gamma}\tau_{,\alpha} + k\xi\theta_{(2)}, \tag{8.9}$$

satisfying (8.5). To satisfy (8.6) it is necessary that

$$(8.10) \qquad k\beta^0_{(3)} = -\frac{\tau^3}{12}\left\{(a^{\alpha\gamma}_{(0)}\theta_{(2),\gamma})_{,\alpha} + F^{\alpha}_{\alpha\gamma(0)}a^{\gamma\delta}_{(0)}\theta_{(2),\delta}\right\} - \frac{1}{4}\tau^2 a^{\alpha\gamma}_{(0)}\theta_{(2),\gamma}\tau_{,\alpha} + k\tau\theta_{(2)}\,,$$

and upon rearranging it is seen that $\theta_{(2)}$ satisfies the partial differential equation

$$(8.11) \qquad (\tau^3 a^{\alpha\gamma}_0\theta_{(2),\gamma})_{,\alpha} + \tau^3 F^{\alpha}_{\alpha\gamma(0)}a^{\gamma\delta}_{(0)}\theta_{(2),\delta} = 12k(\tau\theta_{(2)} - \beta^0_{(3)})\,.$$

When $\theta_{(2)}$ has been found to satisfy this equation, the principal parts of the displacement follow from (8.8) and (8.9).

Thus using (5.4), the components of strain may be calculated. They are of the following orders:—

$$(8.12) \qquad e_{00} = 0(\epsilon^2)\,, \qquad e_{\alpha 0} = 0(\epsilon)\,, \qquad e_{\alpha\gamma} = 0(\epsilon^2)\,.$$

The dilatation is

$$(8.13) \qquad \theta = \epsilon^2\theta_{(2)} + 0(\epsilon^3)\,.$$

Since $1 - 2\sigma = k\epsilon^2$, by (2.9) and (4.7) the stress components are

$$(8.14) \qquad T_{ij} = \frac{E}{3k}\,\theta_{(2)}a_{ij(0)} + 0(\epsilon)\,,$$

and the principal part of the stress is a pressure

$$(8.15) \qquad p = -E\theta_{(2)}/(3k)\,.$$

Using this, (8.11) can be converted into a differential equation for the pressure: it is

$$(8.16) \qquad (\tau^3 a^{\alpha\gamma}_{(0)}p_{,\gamma})_{,\alpha} + \tau^3 F^{\alpha}_{\alpha\gamma(0)}a^{\gamma\delta}_{(0)}p_{,\delta} - 12k\tau p = 4E\beta^0_{(3)}\,.$$

If the line-element of S is given by

$$(8.17) \qquad d\eta^2 = b_{\alpha\beta}dx^{\alpha}dx^{\beta} = a_{\alpha\beta(0)}dx^{\alpha}dx^{\beta}\,,$$

then

$$(8.18) \qquad b_{\alpha\beta} = a_{\alpha\beta(0)}\,, \qquad b^{\alpha\beta} = a^{\alpha\beta}_{(0)}\,,$$

and if $G^{\alpha}_{\beta\gamma}$ are the Christoffel symbols corresponding to $b_{\alpha\beta}$ then

$$(8.19) \qquad G^{\alpha}_{\beta\gamma} = F^{\alpha}_{\beta\gamma(0)}\,.$$

The operation of taking the covariant derivative with respect to $b_{\alpha\beta}$ will be denoted by B_{α}: also

$$(8.20) \qquad B^{\alpha} = b^{\alpha\beta}B_{\beta}\,,$$

whence (8.16) can be written in the form

$$(8.21) \qquad B_{\alpha}(\tau^3 B^{\alpha}p) - 12k\tau p = 4E\beta^0_{(3)}\,.$$

These results are summed up as follows:—

VII. For a thin curved membrane of very small compressibility, $1-2\sigma$ being comparable with ϵ^2, the condition that the strain be small and the stress non-infinite requires that the displacement β^i of a point on T be of order ϵ^3 or higher. The principal part of the stress is a pressure p, a function of x^1 and x^2 satisfying the partial differential equation

$$B_\alpha(h^3B^\alpha p)-12(1-2\sigma)hp=4E\beta^0, \tag{8.22}$$

subject to the boundary condition $p=P$ on the edge of the membrane, P being atmospheric pressure. In terms of p the principal parts of the displacement are

$$\left\{\begin{aligned} u^0&=\frac{1}{4E}(x^0)^2(3h-2x^0)B_\alpha B^\alpha p+\frac{3}{4E}(x^0)^2(B^\alpha p)(B_\alpha h)-\frac{3}{E}(1-2\sigma)x^0p,\\ u^\alpha&=-\frac{3}{2E}x^0(h-x^0)B^\alpha p,\end{aligned}\right. \tag{8.23}$$

and the principal part of the dilatation is

$$\theta=-3(1-2\sigma)p/E. \tag{8.24}$$

In these formulae x^1 and x^2 are curvilinear co-ordinates on S, x^0 is the length of the normal to S, B^α and B_α are respectively the contravariant and covariant derivatives with respect to the fundamental tensor on S, h is the thickness

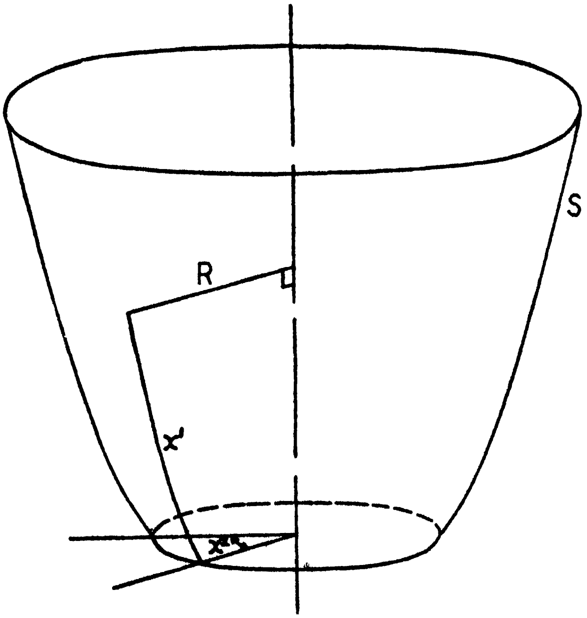

FIG. 3. *System of co-ordinates for the case in which the membrane is attached to surfaces of revolution.*

of the membrane, E is Young's modulus, σ is Poisson's ratio and ϵ is the small parameter defined in (3.1).

The equation (8.22) can also be written in the form

$$\frac{1}{\sqrt{b}}(\sqrt{b}h^3b^{\alpha\gamma}p_{,\gamma})_{,\alpha}-12(1-2\sigma)hp=4E\beta^0, \tag{8.25}$$

where b is the determinant $|b_{\alpha\beta}|$.

If the surface S is developable it is possible to find a system of surface co-ordinates x^1, x^2 such that the line-element is

$$d\eta^2=(dx^1)^2+(dx^2)^2, \tag{8.26}$$

and for such a co-ordinate system (8 25) becomes

$$(hp_{,\alpha})_\alpha-12(1-2\sigma)hp=4E\beta^0. \tag{8.27}$$

If S is a surface of revolution a co-ordinate system can be chosen in which x^1 is the meridian distance from a standard section normal to the axis of revolution and x^2 is the azimuth (Fig. 3). If R is the radius of a general section normal to the axis of revolution, the line-element will be

$$d\eta^2=(dx^1)^2+R^2(dx^2)^2, \tag{8.28}$$

where R is a function of x^1 only. Then (8 25) takes the form

$$\frac{1}{R}\frac{\partial}{\partial x^1}\left(Rh^3\frac{\partial p}{\partial x^1}\right)+\frac{1}{R^2}\frac{\partial}{\partial x^2}\left(h^3\frac{\partial p}{\partial x^2}\right)-12(1-2\sigma)hp=4E\beta^0. \tag{8.29}$$

9. The Case $n>2$ (Essential Incompressibility)

In this case the membrane under consideration is less compressible than the periodontal membrane. The condition for finite stress (III) requires that

$$u^0_{(2)}=0, \qquad \theta_{(1)}=0, \qquad \beta^{\imath}_{(2)}=0, \tag{9.1}$$

$$\theta_{(r)}=\frac{\partial u^0_{(r+1)}}{\partial\xi}+u^\alpha_{(r),\alpha}+\sum_{s=0}^{r-2}\frac{1}{s!}\xi^sF^\alpha_{\alpha\imath(s)}u^{\imath}_{(r-s)}=0, \tag{9.2}$$

$$(r=2,\ 3,\ -\ -\ -\ n-1).$$

Upon making the substitutions indicated in IV it is found that the lowest power of ϵ occurring in (4 13) is ϵ^{n-1} and in (4.14) is ϵ^n, and the corresponding coefficients give rise to the equations

$$\frac{\partial\theta_{(n)}}{\partial\xi}=0, \tag{9.3}$$

$$a^{\alpha\gamma}_{(0)}\theta_{(n),\gamma}+k\frac{\partial^2u^\alpha_{(2)}}{\partial\xi^2}=0. \tag{9.4}$$

By a procedure which parallels that in §8 it is found that the principal part of the stress in the membrane is again a pressure satisfying

$$B_\alpha(\tau^3B^\alpha p)=4E\beta^0_{(3)}. \tag{9.5}$$

Since k does not appear in (9.5) it is evident that p does not depend on the compressibility. This means that, when $n>2$, terms introduced by the assumption of compressibility are negligible in comparison with those retained on the assumption of incompressibility. Hence the term "essential incompressibility" is explained.

Expressed explicitly in the small quantities these results, which are analogous to those in VII, are as follows:—

VIII. For a thin curved membrane of compressibility so small that $1-2\sigma$ is comparable with ϵ^n, $(n>2)$, the condition that the strain be small and the stress non-infinite requires that the displacement β^i of a point on T be of order ϵ^3 or higher. The principal part of the stress is a pressure p, a function of x^1 and x^2 satisfying the partial differential equation

$$B_\alpha(h^3B^\alpha p)=4E\beta^0, \tag{9.6}$$

with the boundary condition $p=P$ on the edge of the membrane, P being atmospheric pressure. In terms of p the principal parts of the displacement are

$$\begin{cases} u^0=\dfrac{1}{4E}(x^0)^2(3h-2x^0)B_\alpha B^\alpha p+\dfrac{3(x^0)^2}{4E}(B^\alpha p)(B_\alpha h), \\ u^\alpha=-\dfrac{3}{2E}x^0(h-x^0)B^\alpha p, \end{cases} \tag{9.7}$$

and the principal part of the dilatation is

$$\theta=-3(1-2\sigma)p/E. \tag{9.8}$$

In these formulae the notation is as in VII.

It is seen that (9.6) and (9.7) can be derived by putting $1-2\sigma=0$ in (8.22) and (8.23) respectively: (9 6) and (9.7) were also developed by Synge (6, p. 450, equations (56), (57) and (58)).

Acknowledgment

The author wishes to thank Prof. J. L. Synge for much assistance, rendered personally and derived from his papers (6, 9).

References

1. **Appell, P.** Mécanique rationelle, vol. 5. Gauthier-Villars, Paris. 1926.
2. **Birkhoff, G. D.** Phil. Mag. 43 : 953-962. 1922.
3. **Garabedian, C. A.** Trans. Am. Math. Soc. 25 : 343-398. 1923.
4. **Goodier, J. N.** Trans. Roy. Soc. Can. III, 32 : 1-25. 1938.
5. **Hay, G. E.** Can. J. Research. Forthcoming publication.
6. **Synge, J. L.** Phil. Trans. Roy. Soc. London, A, 231 : 435-477. 1933.
7. **Synge, J. L.** Phil. Mag. 15 : 969-996. 1933.
8. **Synge, J. L.** Phil. Mag. 23 : 885-897. 1937.
9. **Synge, J. L.** Trans. Roy. Soc. Can. III, 31 : 57-81. 1937.

Canadian Journal of Research

Issued by The National Research Council of Canada

VOL. 17, SEC. A. JULY, 1939 NUMBER 7

THE EQUILIBRIUM OF A THIN COMPRESSIBLE MEMBRANE WITH APPLICATION TO THE PERIODONTAL MEMBRANE[1]

By G. E. Hay[2]

Abstract

The equilibrium of a thin compressible elastic membrane has been considered. In the present work the theory developed in that paper (3) is applied to the periodontal membrane which lies between the tooth and the jaw-bone.

For simplicity, a tooth is considered of which the root is a right circular cone, the thickness of the membrane being assumed constant. A load is applied to the tooth in a plane containing the axis of the root and a determination is made of the resulting stress in the membrane and displacement of the tooth.

It is also found that the periodontal membrane holds the tooth in place in a way different from that commonly accepted by dentists.

Introduction

In a preceding paper (3) the equilibrium of a thin compressible membrane has been considered. In the present paper the theory there developed is applied to the periodontal membrane which lies between the tooth and the jaw-bone and is attached to both. The theory is applicable to multiple-rooted as well as single-rooted teeth but only the latter type will be considered, in particular the upper central incisor which has the following average measurements (1, p. 19):—

Length over all	0.88 in.
Crown length	0.39 in.
Root length	0.49 in.
Mesio-distal diameter at neck (side to side)	0.24 in.
Labio-lingual diameter at neck (front to back)	0.27 in.

The average thickness of the periodontal membrane is from 0.0091 to 0.0099 in. (6, p. 123).

The equilibrium of the periodontal membrane considered as incompressible has been considered by J. L. Synge (8), and there is an interesting comparison between his results and those of this paper.

In the author's preceding paper (3, §3) there was introduced the equation

$$1-2\sigma=k\epsilon^{n}, \tag{1.1}$$

---

[1] *Original manuscript received September 28, 1938.*

Contribution from the Department of Applied Mathematics, University of Toronto, Toronto, Canada.

[2] *Holder of a Bursary under the National Research Council of Canada.*

where σ was Poisson's ratio, ϵ was a small dimensionless parameter defined by

$$\epsilon = \frac{\text{average thickness of the membrane}}{\text{average length of the membrane}}, \tag{1.2}$$

and n was an integer to be so chosen that k was comparable with unity. Owing to the method of approximation used in solving the equations of equilibrium, different results were obtained in the four cases $n=0$, 1, 2, and $n>2$. The first step is thus to determine which case applies to the periodontal membrane, for which the following average values may be taken

$$\begin{cases} \epsilon = 2\times10^{-2}, \qquad \epsilon^2 = 4\times10^{-4}, \qquad \epsilon^3 = 8\times10^{-6}, \\ \mu = \text{rigidity (2)} = 73 \text{ lb. in.}^{-2} \end{cases} \tag{1.3}$$

Since the human body is composed largely of water it seems logical to take for the bulk modulus of the membrane that of water

$$\kappa = 2.96\times10^{5} \text{ lb. in.}^{-2} \tag{1.4}$$

Hence

$$1-2\sigma = \frac{3\mu}{3\kappa+\mu} = 2.5\times10^{-4}, \tag{1.5}$$

and so if $n=1,2,3$, the respective values of k are

$$\begin{aligned} k &= (1-2\sigma)/\epsilon = 1.2\times10^{-2}, \\ k &= (1-2\sigma)/\epsilon^2 = 0.6, \\ k &= (1-2\sigma)/\epsilon^3 = 30. \end{aligned} \tag{1.6}$$

Thus it appears that the case $n=2$ applies to the periodontal membrane. This case has been investigated (3, §8): it was found that the principal part of the stress in the membrane was a hydrostatic pressure satisfying a partial differential equation (3, Equation (8.22)), subject to the boundary condition that the pressure at the free edge be atmospheric. This differential equation appears in a modified form in §2 and is solved in §3 for a restricted shape of tooth.

2. The Tooth of Revolution. The Pressure in the Membrane Expressed by the Solution of Three Ordinary Differential Equations

For a general tooth the partial differential equation satisfied by the pressure is rather complicated. The case will now be considered when the socket S and tooth T both have surfaces of revolution about a common axis. This implies that the thickness of the membrane has the same symmetry of revolution. The edge of the membrane is assumed to be a circle normal to the axis of revolution, although in practice this is not realized very closely.

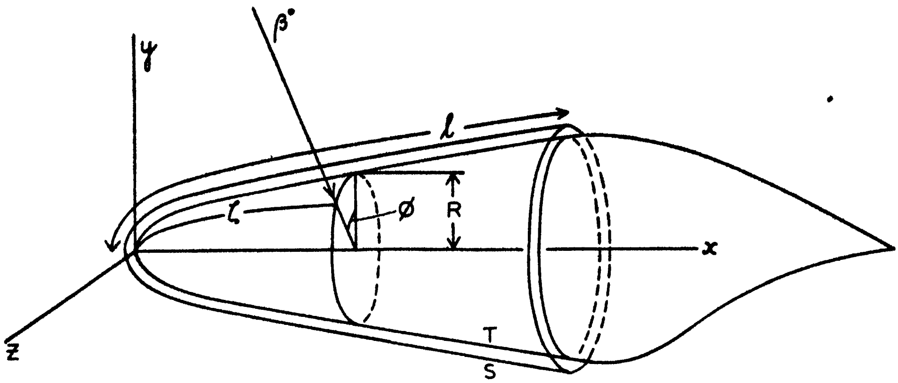

FIG. 1. *Model of a tooth and periodontal membrane.*

A set of rectangular cartesian axes are taken with the origin at the apex, the axis of x being coincident with the axis of revolution. A set of surface co-ordinates ζ and ϕ are also taken over S where ζ is the meridian distance from the apex and ϕ is the azimuth measured from the plane $z=0$. Then the partial differential equation for the pressure p in the membrane [3, Equation (8.22)] takes the form

$$\frac{1}{R}\frac{\partial}{\partial\zeta}\left(Rh^3\frac{\partial p}{\partial\zeta}\right)+\frac{h^3}{R^2}\frac{\partial^2 p}{\partial\phi^2}-12(1-2\sigma)hp=4E\beta^0; \tag{2.1}$$

the boundary conditions are the following,

$$\begin{cases}\text{for } \zeta=0,\ p \text{ must be single valued,}\\ \text{for } \zeta=l,\ p=P;\end{cases} \tag{2.2}$$

and R is the radius of a general section normal to the axis of x, h is the thickness of the membrane, E is Young's modulus, σ is Poisson's ratio, β^0 is the component normal to S of the displacement of a point on T, counted positive when in the sense from S to T, l is the meridian length of the membrane and P is atmospheric pressure.

In (2.1) β^0 is a function of ζ and ϕ and is known when the infinitesimal rigid body displacement of T is known. To find it, the displacement of T is resolved into infinitesimal translations u, v and w in the directions of the axes and infinitesimal rotations ω_1, ω_2, and ω_3 about them. Then the displacement of a point (x, y, z) on T has components

$$u-y\omega_3+z\omega_2, \qquad v-z\omega_1+x\omega_3, \qquad w-x\omega_2+y\omega_1,$$

and hence

$$\begin{aligned}\beta^0=u\frac{dR}{d\zeta}&-\cos\phi\left\{v\frac{dx}{d\zeta}+\omega_3\left(x\frac{dx}{d\zeta}+R\frac{dR}{d\zeta}\right)\right\}\\ &-\sin\phi\left\{w\frac{dx}{d\zeta}-\omega_2\left(x\frac{dx}{d\zeta}+R\frac{dR}{d\zeta}\right)\right\}.\end{aligned} \tag{2.3}$$

Thus (2.1) can be written in the form

$$(2.4)\qquad \frac{1}{R}\frac{\partial}{\partial\zeta}\left(Rh^3\frac{\partial p}{\partial\zeta}\right)+\frac{h^3}{R^2}\frac{\partial^2 p}{\partial\phi^2}-12(1-2\sigma)hp$$

$$=4Eu\frac{dR}{d\zeta}-4E\cos\phi\left\{v\frac{dx}{d\zeta}-\omega_3\left(x\frac{dx}{d\zeta}+R\frac{dR}{d\zeta}\right)\right\}$$

$$-4E\sin\phi\left\{w\frac{dx}{d\zeta}-\omega_2\left(x\frac{dx}{d\zeta}+R\frac{dR}{d\zeta}\right)\right\}.$$

It is to be noted that ω_1 does not appear in (2.4), since it contributes nothing to β^0.

Except for $\cos\phi$ and $\sin\phi$ the right-hand side of (2.4) is a known function of ζ and the solution of (2.4) must then have the form

$$(2.5)\qquad p=f(\zeta)+\cos\phi g(\zeta)+\sin\phi g'(\zeta).$$

Upon substitution of this in (2.4) a differential equation is obtained for each of f, g and g', whence follows the result:—

I. In the case of a tooth of revolution the pressure in the periodontal membrane is given by (2.5) where f, g and g' satisfy the equations

$$(2.6)\qquad \frac{1}{R}\frac{d}{d\zeta}\left(Rh^3\frac{df}{d\zeta}\right)-12(1-2\sigma)hf=4Eu\frac{dR}{d\zeta},$$

$$(2.7)\qquad \frac{1}{R}\frac{d}{d\zeta}\left(Rh^3\frac{dg}{d\zeta}\right)-\left\{\frac{h^3}{R^2}+12(1-2\sigma)h\right\}g$$

$$=-4E\left\{v\frac{dx}{d\zeta}+\omega_3\left(x\frac{dx}{d\zeta}+R\frac{dR}{d\zeta}\right)\right\},$$

$$(2.8)\qquad \frac{1}{R}\frac{d}{d\zeta}\left(Rh^3\frac{dg'}{d\zeta}\right)-\left\{\frac{h^3}{R^2}+12(1-2\sigma)h\right\}g'$$

$$=-4E\left\{w\frac{dx}{d\zeta}-\omega_2\left(x\frac{dx}{d\zeta}+R\frac{dR}{d\zeta}\right)\right\},$$

with the boundary conditions

$$(2.9)\qquad f(0)\text{ must be finite, } f(l)=P,$$

$$(2.10)\qquad g(0)=g(l)=0,$$

$$(2.11)\qquad g'(0)=g'(l)=0.$$

In these formulae R, ζ, ϕ, x and l are as shown in Fig. 1, h is the thickness of the membrane, E is Young's modulus, σ is Poisson's ratio and the infinitesimal rigid body displacement is specified by the translation (u, v, w) and the rotation $(\omega_1, \omega_2, \omega_3)$ relative to the axes of x, y and z in Fig. 1.

3. The Conical Model under Plane Displacement

A tooth of which the root is a right circular cone will now be considered. This is the simplest geometrical figure which can be chosen to represent the average shape of a single-rooted tooth. The rest of the paper is confined to membranes of uniform thickness h, although the thickness varies considerably in the human tooth.

Only plane displacements of the tooth will be considered, *i.e.*, displacements in which the axis of the tooth remains in a plane, and the axis of y will be chosen to lie in this plane. Hence in the notation of §2,

$$w=\omega_1=\omega_2=0. \tag{3.1}$$

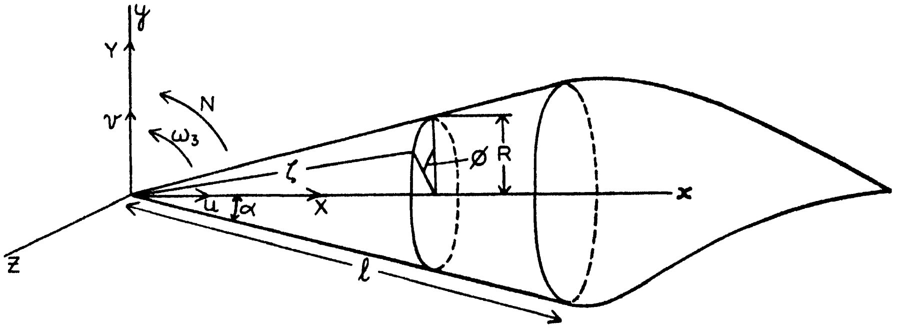

FIG. 2. *Conical model of a tooth.*

Fig. 2 shows the conical model for which

$$R=\zeta \sin \alpha, \qquad x=\zeta \cos \alpha, \tag{3 2}$$

and substitution from (3.1) and (3.2) in (2.6), (2.7) and (2.8) gives

$$h^3 \frac{d^2f}{d\zeta^2}+\frac{h^3}{\zeta}\frac{df}{d\zeta}-12(1-2\sigma)hf=4Eu\sin\alpha, \tag{3.3}$$

$$h^3 \frac{d^2g}{d\zeta^2}+\frac{h^3}{\zeta}\frac{dg}{d\zeta}-\left\{12(1-2\sigma)h+\frac{h^3}{\zeta^2\sin^2\alpha}\right\}g = -4E(v\cos\alpha+\omega_3\zeta), \tag{3.4}$$

$$h^3 \frac{d^2g'}{d\zeta^2}+\frac{h^3}{\zeta}\frac{dg'}{d\zeta}-\left\{12(1-2\sigma)h+\frac{h^3}{\zeta^2\sin^2\alpha}\right\}g'=0. \tag{3.5}$$

A variable ζ_1, a constant l_1 and the functions f_1, g_1 and g_1' are defined as follows:—

$$\zeta_1=\nu\zeta, \qquad l_1=\nu l, \tag{3.6}$$

$$f_1(\zeta_1)=f(\zeta), \qquad g_1(\zeta_1)=g(\zeta), \qquad g_1'(\zeta_1)=g'(\zeta), \tag{3.7}$$

where

$$\nu=\sqrt{12(1-2\sigma)}/h. \tag{3.8}$$

Then the differential equations (3.3), (3.4) and (3.5) take the forms

$$\zeta_1^2 \frac{d^2 f_1}{d\zeta_1^2} + \zeta_1 \frac{df_1}{d\zeta_1} - \zeta_1^2(G+f_1) = 0, \tag{3.9}$$

$$\zeta_1^2 \frac{d^2 g_1}{d\zeta_1^2} + \zeta_1 \frac{dg_1}{d\zeta_1} - (\text{cosec}^2\alpha + \zeta_1^2)g_1 = C\zeta_1^2 - D\zeta_1^3, \tag{3.10}$$

$$\zeta_1^2 \frac{d^2 g_1'}{d\zeta_1^2} + \zeta_1 \frac{dg_1'}{d\zeta_1} - (\text{cosec}^2\alpha + \zeta_1^2)g_1' = 0. \tag{3.11}$$

The boundary conditions obtained from (2.9), (2.10) and (2.11) are

$$f_1(0) \text{ must be finite, } f_1(l_1) = P, \tag{3.12}$$

$$g_1(0) = g_1(l_1) = 0, \tag{3.13}$$

$$g_1'(0) = g_1'(l_1) = 0, \tag{3.14}$$

where G, C, and D are the constants

$$G = 4Eu \sin \alpha/(h^3 v^2), \quad C = -4Ev \cos \alpha/(h^3 v^2), \quad D = -4E\omega_s/(h^3 v^3), \tag{3.15}$$

and all other quantities are defined in I.

Solutions for (3.9), (3.10) and (3.11) will be obtained in turn. Since (3.9) is Bessel's modified equation of order zero, the solution satisfying the boundary condition (3.12) is

$$f_1(\zeta_1) = -G + (P+G)I_0(\zeta_1)/I_0(l_1), \tag{3.16}$$

where

$$I_0(\zeta_1) = \sum_{m=0}^{\infty} \frac{(\frac{1}{2}\zeta_1)^{2m}}{(m!)^2}, \qquad (0! = 1). \tag{3.17}$$

In the course of solving (3.10) it is found that the form of the solution is different in the three cases (i) cosec $\alpha \neq$ integer, (ii) cosec α = odd integer, (iii) cosec α = even integer. Since α is the semi-angle of the root cone, the arithmetical values in §1 give cosec $\alpha = 4.0$. Thus a solution will be required in Case (iii) only, in which case

$$\text{cosec}\, \alpha = 2n, \qquad (n = 1, 2, \ldots). \tag{3.18}$$

The left-hand side of (3.10) is then Bessel's modified equation of order $2n$ and the complete solution of (3.10) is

$$g_1(\zeta_1) = D\psi(\zeta_1) + C\chi(\zeta_1) + AI_{2n}(\zeta_1) + BK_{2n}(\zeta_1), \tag{3.19}$$

where A and B are arbitrary constants, D and C are the known constants defined in (3.15), $I_{2n}(\zeta_1)$ and $K_{2n}(\zeta_1)$ are Bessel functions and ψ and χ are any solutions of

$$\zeta_1^2 \frac{d^2\psi}{d\zeta_1^2} + \zeta_1 \frac{d\psi}{d\zeta_1} - (4n^2 + \zeta_1^2)\psi = \zeta_1^3, \tag{3.20}$$

$$\zeta_1^2 \frac{d^2\chi}{d\zeta_1^2} + \zeta_1 \frac{d\chi}{d\zeta_1} - (4n^2 + \zeta_1^2)\chi = \zeta_1^2. \tag{3.21}$$

When n is an integer (3.20) has the solution in series*

$$\psi(\zeta_1) = \sum_{m=1}^{\infty} \frac{\zeta_1^{2m+1}}{\prod_{r=1}^{m} \{(2r+1)^2 - 4n^2\}}, \tag{3.22}$$

and (3.21) has the solution in series**

$$\begin{aligned}\chi(\zeta_1) = {} & \sum_{m=1}^{n-1} \frac{\zeta_1^{2m}}{\prod_{r=1}^{m} \{(2r)^2 - 4n^2\}} \\ & + \frac{\log_e \zeta_1}{4n \prod_{r=1}^{n-1} \{(2r)^2 - 4n^2\}} \left[\zeta_1^{2n} + \sum_{m=n+1}^{\infty} \frac{\zeta_1^{2m}}{\prod_{r=n+1}^{m} \{(2r)^2 - 4n^2\}} \right] \\ & - \sum_{m=n}^{\infty} \left[\frac{1}{4n} + {\sum_{r=1}^{m}}' \frac{4r}{(2r)^2 - 4n^2} \right] \frac{\zeta_1^{2m}}{4n {\prod_{r=1}^{m}}' \{(2r)^2 - 4n^2\}},\end{aligned} \tag{3.23}$$

where the dash on the Π and Σ signs means that the terms $r = n$ are to be omitted. Using the boundary conditions (3.13), a determination can be made of A and B, whence

$$g_1(\zeta_1) = D\psi(\zeta_1) + C\chi(\zeta_1) - \{D\psi(l_1) + C\chi(l_1)\} I_{2n}(\zeta_1)/I_{2n}(l_1). \tag{3.24}$$

It is noted that

$$I_{2n}(\zeta_1) = \sum_{m=0}^{\infty} \frac{(\frac{1}{2}\zeta_1)^{2(m+n)}}{m!(m+2n)!}, \qquad (n = 1, 2, \ldots). \tag{3.25}$$

Since (3.11) is Bessel's modified equation of order $2n$, it has the complete solution

$$g_1'(\zeta_1) = A'I_{2n}(\zeta_1) + B'K_{2n}(\zeta_1), \tag{3.26}$$

where A' and B' are arbitrary constants. Using the boundary conditions (3.14), it is found that $A' = B' = 0$, whence

$$g_1'(\zeta_1) \equiv 0. \tag{3.27}$$

These results are summed up as follows:—

II. For a conical model of a tooth subjected to the plane displacement specified by u, v, and ω_3 as shown in Fig. 2, the pressure in the periodontal membrane is given by

$$p(\zeta_1) = f_1(\zeta_1) + \cos\phi\, g_1(\zeta_1), \tag{3.28}$$

---

* *This is derived in Appendix A.*

** *This is derived in Appendix B.*

where

$$f_1(\zeta_1) = -G + (P+G) I_0(\zeta_1)/I_0(l_1) ,$$

$$g_1(\zeta_1) = D\psi(\zeta_1) + C\chi(\zeta_1) - \{D\psi(l_1) + C\chi(l_1)\} I_{2n}(\zeta_1)/I_{2n}(l_1) ,$$

$$G = 4Eu \sin\alpha/(h^3\nu^2), \quad C = -4Ev \cos\alpha/(h^3\nu^2), \quad D = -4E\omega_3/(h^3\nu^3) ,$$

$$\nu = \sqrt{12(1-2\sigma)}/h, \qquad \operatorname{cosec}\alpha = 2n, \qquad (n = \text{integer}),$$

and $\psi(\zeta_1)$, $\chi(\zeta_1)$ and $I_{2n}(\zeta_1)$ are defined in (3.22), (3.23) and (3.25) respectively.

In these formulae ϕ is the azimuth measured from the plane $z=0$ of the displacement (Fig. 2), P is atmospheric pressure, E is Young's modulus, σ is Poisson's ratio, h is the thickness of the membrane and is a constant, α is the semi-angle of the root cone and ζ_1 is a co-ordinate running along a generator of the root cone, having the value zero at the apex and at the edge of the membrane the value $l_1 = \nu l$, where l is the slant length of the root cone.

The external force system, exclusive of atmospheric pressure, acting on the tooth and producing such a pressure p in the membrane is statically equivalent to forces X and Y acting along the axes of x and y respectively and a couple N acting about the axis of z: thus

$$(3.29) \quad \left\{ \begin{aligned} X &= -\int_{\zeta=0}^{l}\int_{\phi=0}^{2\pi} (p-P)\zeta \sin^2\alpha \, d\zeta \, d\phi , \\ Y &= \int_{\zeta=0}^{l}\int_{\phi=0}^{2\pi} (p-P)\zeta \sin\alpha \cos\alpha \cos\phi \, d\zeta \, d\phi , \\ N &= \int_{\zeta=0}^{l}\int_{\phi=0}^{2\pi} (p-P)\zeta^2 \sin\alpha \cos\phi \, d\zeta \, d\phi . \end{aligned} \right.$$

Since $\zeta_1 = \nu\zeta$ substitution for p from II and easy integration gives the following result:—

III. The external force system necessary to produce the pressure distribution in II is statically equivalent to the force system (X, Y, N), (Fig. 2), and

$$(3.30) \quad X = \frac{\pi}{\nu^2} (P+G) \sin^2\alpha \{l_1^2 - 2I_{0,1}(l_1)/I_0(l_1)\},$$

$$(3.31) \quad Y = \frac{\pi}{\nu^2} \sin\alpha\cos\alpha \{D\psi_1(l_1) + C\chi_1(l_1) - [D\psi(l_1) + C\chi(l_1)] I_{2n,1}(l_1)/I_{2n}(l_1)\},$$

$$(3.32) \quad N = \frac{\pi}{\nu^3} \sin\alpha \{D\psi_2(l_1) + C\chi_2(l_1) - [D\psi(l_1) + C\chi(l_1)] I_{2n,2}(l_1)/I_{2n}(l_1)\},$$

where

$$I_{2n,t}(l_1) = \int_0^{l_1} \zeta_1{}^t I_{2n}(\zeta_1)\, d\zeta_1, \tag{3.33}$$

$$= 2^{t+1} \sum_{m=0}^{\infty} \frac{(\tfrac{1}{2}l_1)^{2m+2n+t+1}}{(2m+2n+t+1)m!(m+2n)!},$$

$$(0! = 1, \quad n = 0, 1, \ldots, \quad t = 1, 2),$$

$$\psi_t(l_1) = \int_0^{l_1} \zeta_1{}^t \psi(\zeta_1)\, d\zeta_1, \tag{3.34}$$

$$= \sum_{m=1}^{\infty} \frac{l_1{}^{2m+t+2}}{(2m+t+2) \prod_{r=1}^{m} \{(2r+1)^2 - 4n^2\}}, \qquad (t = 1, 2),$$

$$\chi_t(l_1) = \int_0^{l_1} \zeta_1{}^t \chi(\zeta_1)\, d\zeta_1, \tag{3.35}$$

$$= \sum_{m=1}^{n-1} \frac{l_1{}^{2m+t+1}}{(2m+t+1) \prod_{r=1}^{m} \{(2r)^2 - 4n^2\}}$$

$$+ \frac{\log_e l_1}{4n \prod_{r=1}^{n-1} \{(2r)^2 - 4n^2\}} \left[\frac{l_1{}^{2n+t+1}}{2n+t+1} + \sum_{m=n+1}^{\infty} \frac{l_1{}^{2m+t+1}}{(2m+t+1) \prod_{r=n+1}^{m} \{(2r)^2 - 4n^2\}} \right]$$

$$- \frac{1}{4n \prod_{r=1}^{n-1} \{(2r)^2 - 4n^2\}} \left[\frac{l_1{}^{2n+t+1}}{(2n+t+1)^2} + \sum_{m=n+1}^{\infty} \frac{l_1{}^{2m+t+1}}{(2m+t+1)^2 \prod_{r=n+1}^{m} \{(2r)^2 - 4n^2\}} \right]$$

$$- \sum_{m=n}^{\infty} \left[\frac{1}{4n} + \sideset{}{'}\sum_{r=1}^{m} \frac{4r}{(2r)^2 - 4n^2} \right] \frac{l_1{}^{2m+t+1}}{4n(2m+t+1) \sideset{}{'}\prod_{r=1}^{m} \{(2r)^2 - 4n^2\}}, \quad (t = 1, 2),$$

and the notation is as in II, the dash on the Σ and Π signs again indicating that the terms $r = n$ are to be omitted.

The following values consistent with one another and with the physical data are assumed as the basis for calculation:

$$\left\{ \begin{array}{ll} b = \text{over-all length of tooth} & = 0.88 \text{ in.} \\ l = \text{slant length of root cone} & = 0.50 \text{ in.} \\ \alpha = \text{semi-angle of root cone} & = \sin^{-1} \tfrac{1}{4}. \\ h = \text{thickness of membrane} & = 0.0098 \text{ in.} \\ \nu = \sqrt{12(1-2\sigma)}/h & = 5.6 \text{ in.}^{-1} \end{array} \right. \tag{3.36}$$

In §5, on account of the cancellation of positive and negative terms, it is found necessary to work initially with eight-figure accuracy in order to obtain three significant figures in the result.

4. The Conical Model Subjected to a Force X Acting on the Crown and Parallel to the Axis of the Root

The crown is assumed to lie on the axis of the root. The tooth then undergoes an axial displacement only, and in the notation of §3,

$$(4.1)\qquad Y = N = 0, \qquad v = \omega_3 = 0, \qquad C = D = 0.$$

Since $G = 4Eu \sin\alpha/(h^3\nu^2)$ the axial displacement is, from (3.30),

$$(4.2)\qquad u = \frac{h^3\nu^2}{4E\sin\alpha}\left[-P + \frac{X\nu^2}{\pi\sin^2\alpha}\,\{l_1^2 - 2I_{0,1}(l_1)/I_0(l_1)\}^{-1}\right],$$

and in terms of u the pressure distribution is, from II,

$$(4.3)\qquad p(\zeta_1) = -\frac{4Eu\sin\alpha}{h^3\nu^2} + \left(P + \frac{4Eu\sin\alpha}{h^3\nu^2}\right)\frac{I_0(\zeta_1)}{I_0(l_1)}\,.$$

It is to be noted that the membrane is in the unstressed state when the external load and the atmospheric pressure both vanish. When $X = 0$ the whole system (tooth, membrane and jaw) is subject to atmospheric pressure P only, and the axial displacement, which will be denoted by $\bar{u}$, is

$$(4.4)\qquad \bar{u} = -Ph^3\nu^2/(4E\sin\alpha).$$

Then from (4.3) and (4.4),

$$(4.5)\qquad p(\zeta_1) = -4E\bar{u}\sin\alpha/(h^3\nu^2) = P,$$

i.e., the pressure throughout the membrane is atmospheric.

The points of maximum pressure in the membrane will now be determined for a general axial load on the tooth. The pressure at the edge of the membrane is always atmospheric, and, since the gradient of $I_0(\zeta_1)$ is positive, from (4.3) it can be seen that

$$\frac{dp}{d\zeta_1} > 0 \text{ or } < 0 \text{ according as } P + 4Eu\sin\alpha/(h^3\nu^2) > 0 \text{ or } < 0.$$

Substitution for u from (4.2) gives

$$\frac{dp}{d\zeta_1} > 0 \text{ or } < 0 \text{ according as } X\{l_1^2 - 2I_{0,1}(l_1)/I_0(l_1)\}^{-1} > 0 \text{ or } < 0.$$

Using the values in (3.36), it is found that $l_1 = 2.80$, $I_0(l_1) = 4.16$ and $I_{0,1}(l_1) = 9.24$, whence $l_1^2 - 2I_{0,1}(l_1)/I_0(l_1) = 3.40$. Thus

$$\frac{dp}{d\zeta_1} > 0 \text{ or } < 0 \text{ according as } X > 0 \text{ or } < 0.$$

These results are summed up as follows:—

IV. When the external load acts from apex to crown the minimum pressure occurs at the apex and the maximum at the edge of the membrane. When the external load acts from crown to apex the minimum pressure occurs at the edge of the membrane and the maximum at the apex. In each case the pressure at the edge of the membrane is atmospheric and the pressure at the apex is

$$p(0) = P - \frac{X\nu^2}{\pi \sin^2 \alpha} \{1 - 1/I_0(l_1)\}\{l_1^2 - 2I_{0,1}(l_1)/I_0(l_1)\}^{-1}, \tag{4.6}$$

where P is atmospheric pressure, $\nu = 5.6$ in.$^{-1}$, $l_1 = 2.8$, $I_0(l_1) = 4.16$, $I_{0,1}(l_1) = 9.24$ and $\sin \alpha = \frac{1}{2}$.

A diagram will now be constructed illustrating the pressure variation along a generator of the root cone when X is such that, (*i*) $p(0) = 2P$, (*ii*) $p(0) = 0$.

When $p(0) = 2P$, the external load will be denoted by X', the corresponding displacement by u' and the corresponding pressure by $p'(\zeta_1)$. From (4.6) it is found that

$$X' = -\frac{\pi}{\nu^2} P \sin^2\alpha \{l_1^2 - 2I_{0,1}(l_1)/I_0(l_1)\}\{1 - 1/I_0(l_1)\}^{-1}, \tag{4.7}$$

and hence by (4.2),

$$u' = -\frac{Ph^2\nu^2}{4E \sin \alpha} \frac{2I_0(l_1) - 1}{I_0(l_1) - 1}. \tag{4.8}$$

Finally from (4.3),

$$p'(\zeta_1) = P\{2I_0(l_1) - 1 - I_0(\zeta_1)\}\{I_0(l_1) - 1\}^{-1}. \tag{4.9}$$

When $p(0) = 0$, the external load will be denoted by X'', the corresponding displacement by u'' and the corresponding pressure by $p''(\zeta_1)$. It is found that

$$X'' = -X', \qquad u'' = -u', \qquad p''(\zeta_1) = 2P - p'(\zeta_1). \tag{4.10}$$

To compute u' and u'' requires Young's modulus for the membrane. Since $\sigma = \frac{1}{2}$, approximately, then $E = 3\mu$:
since μ is known (2)

$$E = 219 \text{ lb. in.}^{-2} \tag{4.11}$$

When $P = 15$ lb. in.$^{-2}$ the values in (3.36) give

$$\left\{\begin{aligned} X' &= -X'' = -0.42 \text{ lb.}, \\ u' &= -u'' = -2.65 \times 10^{-6} \text{ in.}, \\ \bar{u} &= -1.99 \times 10^{-6} \text{ in.} \end{aligned}\right. \tag{4.12}$$

The graphs of $p'(\zeta_1)$ and $p''(\zeta_1)$ are shown in Fig. 3.

When the membrane is incompressible the corresponding values derived by Synge (8) are

$$(4.13)\quad \begin{cases} X' = -X'' = -0.38 \text{ lb.}, \\ u' = -u'' = -8.8\times 10^{-7} \text{ in.}, \end{cases}$$

and the graphs corresponding to $p'(\zeta_1)$ and $p''(\zeta_1)$ are shown in Fig. 3.

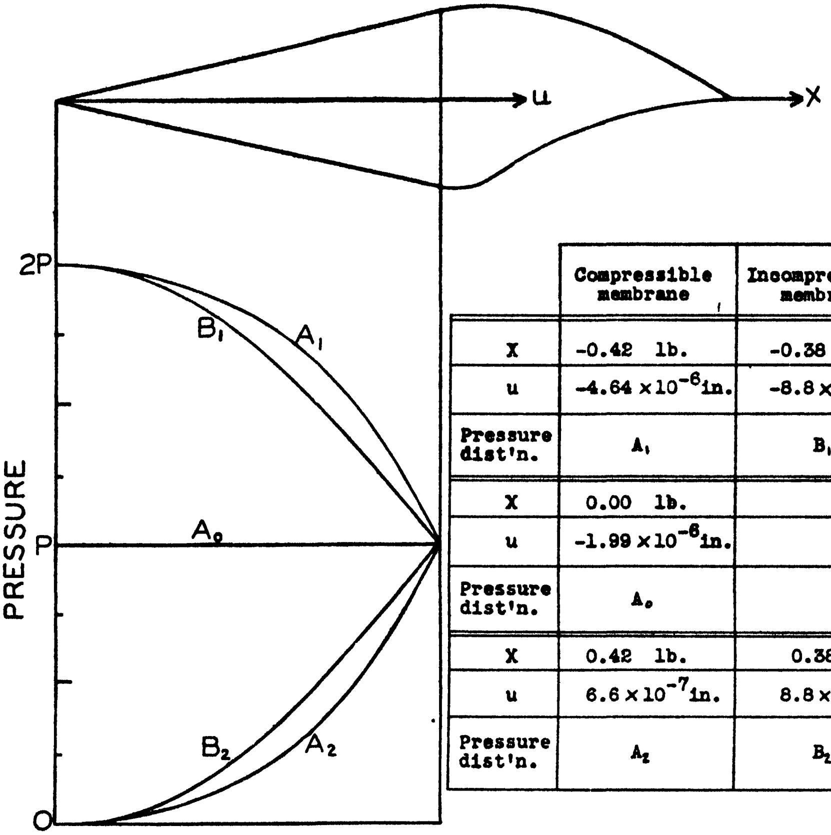

	Compressible membrane	Incompressible membrane
X	-0.42 lb.	-0.38 lb.
u	-4.64×10^{-6} in.	-8.8×10^{-7} in.
Pressure dist'n.	A_1	B_1
X	0.00 lb.	
u	-1.99×10^{-6} in.	
Pressure dist'n.	A_0	
X	0.42 lb.	0.38 lb.
u	6.6×10^{-7} in.	8.8×10^{-7} in.
Pressure dist'n.	A_2	B_2

P = atmospheric pressure (= 15 lb. in.$^{-2}$),
X = external load,
u = displacement due to X and atmospheric pressure.

In the case of the compressible membrane the total displacement u is made up of a part due to atmospheric pressure and a part due to the load X. When $X = -0$ 42 lb., the part due to atmospheric pressure is -1.99×10^{-6} in. and the part due to X is -2.65×10^{-6} in.

FIG. 3. *Conical model under axial load.*

5. The Conical Model Subjected to a Force Y Acting on the Crown and Perpendicular to the Axis of the Root

The calculations in this section must be carried out initially to eight figures, as explained at the end of §3. The crown is again assumed to lie on the axis of the tooth. Then, in the notation of §3, $X=0$ and $N=bY$, where b is the over-all length of the tooth. Hence from (3.30), (3.31) and (3.32),

$$P+G=0, \tag{5.1}$$

$$C\alpha_1+D\beta_1=Yv^2/(\pi \sin\alpha\cos\alpha), \tag{5.2}$$

$$C\alpha_2+D\beta_2=bYv^3/(\pi\sin\alpha), \tag{5.3}$$

where

$$\left\{\begin{aligned} &\alpha_1=\chi_1(l_1)-\chi(l_1)I_{2n,1}(l_1)/I_{2n}(l_1), \quad \beta_1=\psi_1(l_1)-\psi(l_1)I_{2n,1}(l_1)/I_{2n}(l_1),\\ &\alpha_2=\chi_2(l_1)-\chi(l_1)I_{2n,2}(l_1)/I_{2n}(l_1), \quad \beta_2=\psi_2(l_1)-\psi(l_1)I_{2n,2}(l_1)/I_{2n}(l_1), \end{aligned}\right. \tag{5.4}$$

and the remaining notation is defined in II and (3.33), (3.34) and (3.35).

Numerical values are now introduced from (3.36). Then $n=2$ and the following values can be computed:—

$$\left\{\begin{aligned} &I_4(l_1)=0.234\ 079\ 08, && \psi(l_1)=-\ 6.601\ 251\ 5,\\ & && \quad\chi(l_1)=-1.618\ 780\ 30,\\ &I_{4,1}(l_1)=0\ 279\ 338\ 86, && \psi_1(l_1)=-\ 8.601\ 708\ 7,\\ & && \quad\chi_1(l_1)=-2.309\ 403\ 8,\\ &I_{4,2}(l_1)=0\ 677\ 170\ 52, && \psi_2(l_1)=-20.547\ 149,\\ & && \quad\chi_2(l_1)=-5.407\ 079\ 8, \end{aligned}\right. \tag{5.5}$$

whence

$$\left\{\begin{aligned} &\alpha_1=-0.377\ 628\ 3, \quad &&\beta_1=-0.724\ 088\ 6,\\ &\alpha_2=-0.724\ 088\ 5, \quad &&\beta_2=-1.450\ 300. \end{aligned}\right. \tag{5.6}$$

The solution of (5.2) and (5.3) is thus

$$C/Y=3\ 537.441, \qquad D/Y=-1\ 901.81, \tag{5.7}$$

and using (5.1), the pressure distribution is, from II,

$$p(\zeta_1)-P=Y\cos\phi[-1901.81\psi(\zeta_1)+3537.44\chi(\zeta_1)-29170I_4(\zeta_1)], \tag{5.8}$$

where ζ_1 runs from zero at the apex to 2.8 at the free edge, ϕ is the azimuth as shown in Fig. 2 and $\psi(\zeta_1),\chi(\zeta_1)$ and $I_4(\zeta_1)$ are defined in (3.22), (3.23) and (3.25) respectively. The graph of $p(\zeta_1)$ is shown in Fig. 4. The maximum pressure occurs at M and N, and it is found that the external load necessary to produce a maximum pressure of two atmospheres (30 lb. in.$^{-2}$) is

$$Y=0.188 \text{ lb.} \tag{5.9}$$

From Synge (8) the corresponding load for the incompressible membrane is $Y=0.190$ lb.

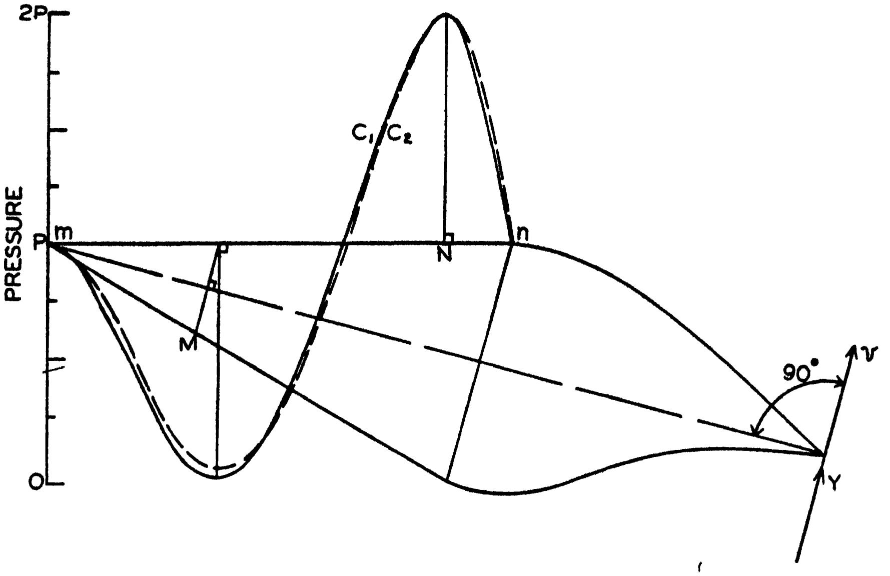

P = atmospheric pressure (= 15 lb. in.$^{-2}$),
Y = external load,
v = displacement produced by Y.

	Compressible membrane	Incompressible membrane
Apex to centre of rotation	0.29 in.	0.31 in.
Y	0.188 lb.	0.190 lb.
v	3.62×10^{-5} in.	2.8×10^{-5} in.
Pressure distribution on mn	C_1	C_2

FIG. 4. *Conical model under transverse load.*

The definitions of C and D are given in II, whence from (5.7),

$$v = -35.4 \times 10^2 \frac{Yh^3\nu^2}{4E \cos \alpha}, \qquad \omega_3 = 19.0 \times 10^2 \frac{Yh^3\nu^3}{4E}, \tag{5.10}$$

where the units of measurement are the pound and inch.

Now $E = 219$ lb. in.$^{-2}$, and when the biting edge is acted upon by the critical transverse load (0.188 lb.) it undergoes a displacement δ and

$$\begin{aligned} \delta &= v + b\omega_3, \\ &= 3.62 \times 10^{-5} \text{ in.} \end{aligned} \tag{5.11}$$

The corresponding displacement in the case of the incompressible membrane is $\delta = 2.80 \times 10^{-5}$ in.

The centre of rotation of the tooth is at a distance x' from the apex where $v+x'\omega_3=0$, whence $x'=-v/\omega_3$ and from (3.36) and (5.10) it is found that $x'=0.29$ in. Since the axial length of the root is 0.48 in. the following result is obtained.

V. When the conical model is subjected to a transverse load applied at the biting edge, the centre of rotation divides the root approximately in the ratio of two to three and is farthest from the apex.

This result agrees roughly with that of R. Kronfeld (5, p. 1270).

6. Discussion

There are blood capillaries in the periodontal membrane. The blood is squeezed out of those parts of the membrane where the blood pressure is exceeded by the pressure due to the external load on the tooth. There is said to be strangulation of the membrane in such regions. From Fig. 3 it is seen that, if axial load is steadily increased from zero, strangulation will first appear at the apex of the root. From Fig. 4 it is seen that, if transverse load is steadily increased from zero, strangulation will first appear at M and N. Computation shows that strangulation will be produced in small regions surrounding these points by a transverse load of 3 gm. Schwarz (7) conducted experiments on the teeth of dogs and found that the symptoms of strangulation appeared for a transverse load of 5 gm. This agreement is quite good, as the teeth of dogs differ in shape from those of humans.

The periodontal membrane contains a large number of small fibres running from the tooth to the jaw-bone. It is commonly believed among dentists that the resistance against displacement of a loaded tooth is supplied by tension in these fibres (4, pp. 336–337). In this paper it is found that the resistance is attributed to the pressure in the membrane, and the agreement in the previous paragraph between calculated and empirical results substantiates this claim.

Acknowledgments

The author wishes to thank Prof. J. L. Synge for much assistance, rendered personally and derived from his paper (8). Thanks are also due to Prof. W. J. Webber for the contents of Appendix B.

Appendix A

To obtain a solution in series of the equation

$$\zeta_1^2\frac{d^2\psi}{d\zeta_1^2}+\zeta_1\frac{d\psi}{d\zeta_1}-(4n^2+\zeta_1^2)\psi=\zeta_1^3, \tag{A.1}$$

where n is an integer.

This equation has a solution of the form

$$\psi=\sum_{s=3}^{\infty} b_s\zeta_1^s, \tag{A.2}$$

if b_s satisfy the equations

$$\left\{\begin{aligned} &b_3(3^2-4n^2)=1, \\ &b_4(4^2-4n^2)=0, \\ &b_s(s^2-4n^2)-b_{s-2}=0, \qquad (s=5,6,\ldots). \end{aligned}\right. \tag{A.3}$$

If

$$b_s=0, \qquad (s=4,6,\ldots), \tag{A.4}$$

then a solution of (A.1) is

$$\psi=\sum_{m=1}^{\infty}\frac{\zeta_1^{2m+1}}{\prod_{r=1}^{m}\{(2r+1)^2-4n^2\}}. \tag{A.5}$$

Appendix B

To obtain a solution in series of the equation

$$\zeta_1^2\frac{d^2\chi}{d\zeta_1^2}+\zeta_1\frac{d\chi}{d\zeta_1}-(4n^2+\zeta_1^2)\chi=\zeta_1^2, \tag{B.1}$$

where n is an integer.

If an attempt is made as in Appendix A to obtain a solution of the form

$$\chi=\sum_{s=2}^{\infty}a_s\zeta_1^s, \tag{B.2}$$

it is found that

$$a_{2(n+t)}=\infty, \qquad (t=0,1,2,\ldots), \tag{B.3}$$

and so some modification is necessary.

The equation

$$\zeta_1^2\frac{d^2\chi_{+\epsilon}}{d\zeta_1^2}+\zeta_1\frac{d\chi_{+\epsilon}}{d\zeta_1}-(4n^2+\zeta_1^2)\chi_{+\epsilon}=\zeta_1^{2+\epsilon}, \quad \epsilon<<1, \tag{B.4}$$

has a solution of the form

$$\chi_{+\epsilon}=\sum_{s=2}^{\infty}c_s\zeta_1^{s+\epsilon} \tag{B.5}$$

if

$$\begin{aligned} &c_2\{(2+\epsilon)^2-4n^2\}=1, \\ &c_3\{(3+\epsilon)^2-4n^2\}=0, \\ &c_s\{(s+\epsilon)^2-4n^2\}-c_{s-2}=0, \qquad (s=4,5,\ldots). \end{aligned} \tag{B.6}$$

Thus

$$c_s=0, \qquad (s=3,5,7,\ldots), \tag{B.7}$$

and so

$$\chi_{+\epsilon}=\sum_{m=1}^{\infty}\frac{\zeta_1^{2m+\epsilon}}{\prod_{r=1}^{m}\{(2r+\epsilon)^2-4n^2\}}. \tag{B.8}$$

Since $(2n+\epsilon)^2-4n^2=\epsilon(4n+\epsilon)$, then

$$\chi_{+\epsilon}=\sum_{m=1}^{n-1}\frac{\zeta_1^{2m+\epsilon}}{\prod_{r=1}^{m}\{(2r+\epsilon)^2-4n^2\}}+\frac{\zeta_1^{\epsilon}}{\epsilon}\phi(\epsilon), \tag{B.9}$$

where

(B.10)

$$\phi(\epsilon)=\frac{1}{(4n+\epsilon)\prod_{r=1}^{n-1}\{(2r+\epsilon)^2-4n^2\}}\left[\zeta_1^{2n}+\sum_{m=n+1}^{\infty}\frac{\zeta_1^{2m}}{\prod_{r=n+1}^{m}\{(2r+\epsilon)^2-4n^2\}}\right].$$

Now

$$\zeta_1^{\epsilon}=1+\epsilon\log_e\zeta_1+\frac{\epsilon^2(\log_e\zeta_1)^2}{2!}+\;.\;.\;.\;., \tag{B.11}$$

whence

(B.12)

$$\chi_{+\epsilon}=\sum_{m=1}^{n-1}\frac{\zeta_1^{2m+\epsilon}}{\prod_{r=1}^{m}\{(2r+\epsilon)^2-4n^2\}}+\left\{\frac{1}{\epsilon}+\log_e\zeta_1+\;.\;.\right\}\left\{\phi(0)+\epsilon\left(\frac{\partial\phi}{\partial\epsilon}\right)_{\epsilon=0}+\;.\;.\;\right\}.$$

Similarly by changing the sign of ϵ a function $\chi_{-\epsilon}$ can be obtained. Hence a solution of

$$\zeta_1^2\frac{d^2\chi_\epsilon}{d\zeta_1^2}+\zeta_1\frac{d\chi_\epsilon}{d\zeta_1}-(4n^2+\zeta_1^2)\chi_\epsilon=\tfrac{1}{2}(\zeta_1^{2+\epsilon}+\zeta_1^{2-\epsilon}) \tag{B.13}$$

is

(B.14)

$$\begin{aligned}\chi_\epsilon&=\tfrac{1}{2}(\chi_{+\epsilon}+\chi_{-\epsilon}),\\&=\tfrac{1}{2}\sum_{m=1}^{n-1}\left[\frac{\zeta_1^{2m+\epsilon}}{\prod_{r=1}^{m}\{(2r+\epsilon)^2-4n^2\}}+\frac{\zeta_1^{2m-\epsilon}}{\prod_{r=1}^{m}\{(2r-\epsilon)-4n^2\}}\right]\\&\quad+\phi(0)\log_e\zeta_1+\left(\frac{\partial\phi}{\partial\epsilon}\right)_{\epsilon=0}+\epsilon^2[\;.\;.\;.\;.\;.\;]+\;.\;.\;.\;.\end{aligned}$$

By letting $\epsilon\to 0$ simultaneously in (B.13) and (B.14) it is found that a solution of (B.1) is

$$\begin{aligned}\chi&=\lim_{\epsilon\to 0}.\;\chi_\epsilon,\\&=\sum_{m=1}^{n-1}\frac{\zeta_1^{2m}}{\prod_{r=1}^{m}\{(2r)^2-4n^2\}}+\phi(0)\log_e\zeta_1+\left(\frac{\partial\phi}{\partial\epsilon}\right)_{\epsilon=0},\end{aligned}$$

or

$$(B.15) \qquad \chi = \sum_{m=1}^{n-1} \frac{\zeta_1^{2m}}{\prod_{r=1}^{m} \{(2r)^2-4n^2\}}$$

$$+ \frac{\log_e \zeta_1}{4n \prod_{r=1}^{n-1} \{(2r)^2-4n^2\}} \left[\zeta_1^{2n} + \sum_{m=n+1}^{\infty} \frac{\zeta_1^{2m}}{\prod_{r=n+1}^{m} \{(2r)^2-4n^2\}} \right]$$

$$- \sum_{m=n}^{\infty} \left[\frac{1}{4n} + \sum_{r=1}^{m}{}' \frac{4r}{(2r)^2-4n^2} \right] \frac{\zeta_1^{2m}}{4n \prod_{r=1}^{m}{}' \{(2r)^2-4n^2\}} ,$$

where the dash on the Σ and Π signs means that the terms $r = n$ are to be omitted.

References

1. Black, G. V. Dental anatomy. S. S. White Dental Manufacturing Co., Philadelphia. 1902.
2. Dyment, M. L. and Synge, J. L. Oral Health, 25:105-109. 1935.
3. Hay, G. E. Can. J. Research, A, 17 : 106-121. 1939.
4. Kronfeld, R. Histopathology of the teeth and their surrounding structures. Lea and Febigen, Philadelphia. 1933.
5. Kronfeld, R. J. Am. Dental Assoc. 18 : 1242-1274. 1931.
6. Orban, B. Dental histology and embryology. P. Blakiston's and Co., Philadelphia. 1929.
7. Schwarz, A. M. Intern. J. Orthodontia, Oral Surgery and Radiography, 18 : 331-352. 1932.
8. Synge, J. L. Phil. Trans. Roy. Soc. Lond. A, 231 : 435-477. 1933.

THE RESONANT RADIAL FREQUENCIES OF A CYLINDER OF ANY WALL THICKNESS[1]

By G. S. Field[2]

Abstract

Equations have been derived for the resonance radial frequencies of a cylinder of any wall thickness. For the degenerate case of the internal radius equal to zero, the equations are shown to reduce to those previously given for a solid rod. For a cylinder with a very thin wall, the frequency equation becomes very simple, but contains an additional factor compared with the equation usually given for a thin-walled cylinder. It is suggested that the two cases correspond to slightly different types of vibration, and that the one considered in this paper is physically more likely.

Radial Particle Velocity

In a previous paper (1) it was shown that for an element of a solid cylindrical rod, the expression for the radial particle velocity is,

$$\zeta = BJ_1(kr)e^{i\omega(t-z/c_1)},$$

where, ζ = radial particle velocity at a distance r from the centre of the rod;
B = constant of integration;
ω = $2\pi \times$ frequency;
t = time;
z = distance along the length of the rod;
c_1 = phase velocity of longitudinal wave in the rod;
$J_1(kr)$ = Bessel function of the first kind, and is a solution of the following equation:

$$r^2\frac{\partial^2 f_2}{\partial r^2} + r\frac{\partial f_2}{\partial r} + (k^2r^2 - 1)f_2 = 0\,,$$

in which k is a function of c_1, ω, Young's modulus (q), the density (ρ), and Poisson's ratio (σ), but is independent of r.

The complete solution of Bessel's equation, above, includes Bessel's function of the second kind, *i.e.*, $Y_1(kr)$*, but for the solid rod this solution is not admissible, as $Y_1(kr)$ becomes infinite at $r = 0$.

For a hollow cylinder, however, $Y_1(kr)$ must be included, and the expression for the radial particle velocity becomes,

$$\zeta = [AJ_1(kr) + BY_1(kr)]e^{i\omega(t-z/c_1)}\,. \tag{1}$$

Axial Force on an Element

The equation for the axial force, p_z, along a radius vector, on an element in the wall of the cylinder, may be put in the following form (1, p. 257),

$$p_z = \frac{q}{(1+\sigma)(1-2\sigma)}\left[\frac{\partial\zeta}{\partial r}(1-\sigma) + \sigma\left(\frac{\partial\xi}{\partial z} + \frac{\partial\eta}{\partial\theta} + \frac{\zeta}{r}\right)\right], \tag{2}$$

---

[1] *Manuscript received March 28, 1939.*

Contribution from the Division of Physics, National Research Laboratories, Ottawa, Canada. Issued as N.R.C. No. 821.

[2] *Physicist, National Research Laboratories, Ottawa.*

* *$Y_n(x)$ was adopted as the canonical function of the second kind by Weber (3, p. 64) and is the most useful in the present case.*

where,

ξ = longitudinal particle velocity at a distance z along the axis;

η = tangential particle velocity corresponding to the cylindrical co-ordinate θ.

If only radial vibrations are considered, $\dfrac{\partial \xi}{\partial z} = \dfrac{\partial \eta}{\partial \theta} = 0$, and,

$$p_2 = \frac{q}{(1+\sigma)(1-2\sigma)}\left[\frac{\partial \zeta}{\partial r}(1-\sigma) + \sigma\frac{\zeta}{r}\right]. \tag{3}$$

Boundary Conditions

Let the external radius of the hollow cylinder be a_1 and the internal radius be a_2. Then,

At $r = a_1$, $p_2 = 0$;

At $r = a_2$, $p_2 = 0$.

Substitute in Equation (3) for ζ and r. Then,

$$\left[\begin{array}{l} A[kr(1-\sigma)J_0(kr) - (1-2\sigma)J_1(kr)] \\ \qquad\qquad + B[kr(1-\sigma)Y_0(kr) - (1-2\sigma)Y_1(kr)] \end{array}\right]_{\substack{r=a_1\\ r=a_2}} = 0. \tag{4}$$

Let $ka_1 = x$,

Then $ka_2 = (a_2/a_1)x$.

Divide each equation by $B(1-\sigma)$.

Write, $m = \dfrac{1-2\sigma}{1-\sigma}$ and $F = A/B$.

Finally,

$$F[xJ_0(x) - mJ_1(x)] + xY_0(x) - mY_1(x) = 0, \tag{5}$$

and

$$F[(a_2/a_1)xJ_0(a_2x/a_1) - mJ_1(a_2x/a_1)] + (a_2/a_1)xY_0(a_2x/a_1) - mY_1(a_2x/a_1) = 0. \tag{6}$$

From these equations it is possible to determine F and x.

Frequency Equation

The expression determining the resonant radial frequencies is (1, p. 259),

$$f = k\alpha/2\pi, \tag{7}$$

where, f = frequency of resonant radial vibration;

$$\alpha = \sqrt{\frac{\text{extensional modulus of elasticity}}{\text{density}}}$$

$$= \sqrt{\frac{q(1-\sigma)}{(1+\sigma)(1-2\sigma)\rho}}.$$

Since $ka_1 = x$,

$$f = \frac{xa}{2\pi a_1} \tag{8}$$

Solution of Equations in x and F

In Equations (5) and (6), F may readily be eliminated; this leaves an equation containing only x and functions thereof. It is possible to solve this equation for any ratio of a_2/a_1 by substituting for different values of x the values of the Bessel functions as given in the published tables.

A simpler method of solution is a graphical one. In Equation (5) denote F by F_5, and in Equation (6) write F as F_6.

$$F_5 = -\frac{xY_0(x) - mY_1(x)}{xJ_0(x) - mJ_1(x)} = -\frac{N}{D}, \tag{9}$$

$$F_6 = -\frac{(a_2/a_1)xY_0(a_2x/a_1) - mY_1(a_2x/a_1)}{(a_2/a_1)xJ_0(a_2x/a_1) - mJ_1(a_2x/a_1)} = -\frac{H}{G}. \tag{10}$$

From these equations, values of x may be determined from the intersections of F_5 and F_6. By a consideration of the change-over points, where either the numerator or denominator of each equation equals zero, that is, where F_5 or F_6 changes sign, the ranges of x where solutions are possible may be very greatly reduced. As an illustration of the method, definite values of m and of the ratio a_2/a_1 may be taken.

Consider the values of x for which solutions are possible.

Assume $\sigma = 0.226$, from which $m = 0.709$, and assume $a_2/a_1 = 0.8$. Table I may then be set up.

TABLE I

x	N	D	H	G	F_5	F_6	Possible solution ($F_5 = F_6$) marked +
0 - 2.04	+	+	+	+	−	−	+
2 04	+	0	+	+	$-\infty$	−	
2.04 - 2 55	+	−	+	+	+	−	
2 55	+	−	+	0	+	$-\infty$	
2.55 - 3.76	+	−	+	−	+	+	+
3.76	0	−	+	−	0	+	
3.76 - 4.70	−	−	+	−	−	+	
4.70	−	−	0	−	−	0	
4.70 - 5.39	−	−	−	−	−	−	+
5.39	−	0	−	−	$-\infty$	−	
etc.	etc.		etc.		etc.		

From this table it will be observed that there are only a few ranges of x where solutions are possible. It would be expected that in the first range would be found the solution giving the fundamental resonance frequency;

in the second, the solution for the first overtone; in the third, the second overtone; and so on.

By plotting a few points for F_5 and F_6 in each range, the form of each curve may be readily obtained. From the intersection of the curves, the desired solution of x is determined and hence the resonant frequency. In Fig. 1 the curves for a particular case are given.

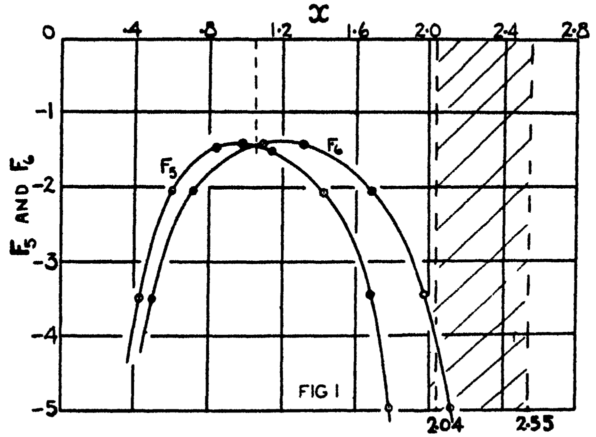

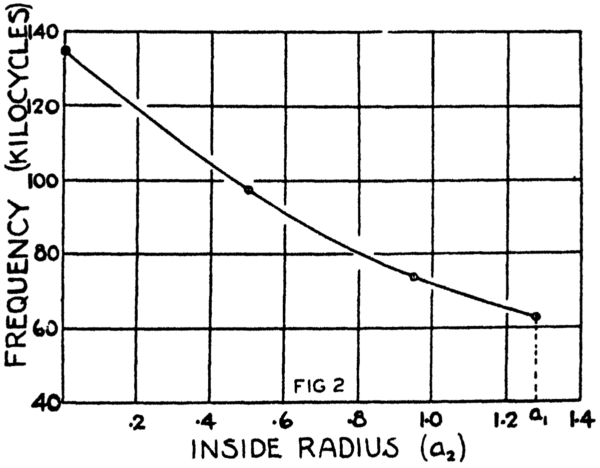

FIG. 1. *Curves of F_5 and F_6, illustrating graphical solution for x. $m = 0.709$, $a_2/a_1 = 0.8$.*

FIG. 2. *Curve showing changes in the resonant radial frequency of a cylinder with changes in the internal radius. Cylinder made of glass, external radius, 1.28 cm. Constants of glass as follows: $q = 6.4 \times 10^{11}$, $\rho = 2.6$, $\sigma = 0.226$.*

A number of resonant radial frequencies were calculated for values of x determined as above, to show the variation in frequency with variations in the ratio a_2/a_1. In Fig. 2 these are plotted against a_2.

Limiting Case of the Solid Rod ($a_2 \to 0$)

In F_6 write $(a_2/a_1)x = y$.

When $a_2 \to 0$, $y \to 0$, $J_0(y) \to 1$, $J_1(y) \to 0$ and $G \to 0$.

Hence $F_6 \to \infty$, unless $H \to 0$, in which case F_6 becomes indeterminate. Suppose $H \to 0$ as $y \to 0$. Then,

$$\lim_{y \to 0}\left(yY_0(y)\right) = \lim_{y \to 0}\left(mY_1(y)\right).$$

When $y \to 0$, $Y_0(y) \to -\infty$. Hence, for $y \to 0$, $yY_0(y)$ can be put in the form ∞/∞. Remembering that for this indeterminate form the limit of the quotient is equal to the limit of the quotient of the derivative of the numerator and the derivative of the denominator, the following may be obtained.

$$\lim_{y \to 0}\left(yY_0(y)\right) = \lim_{y \to 0}\left(\frac{Y_0(y)}{1/y}\right) = \lim_{y \to 0}\left(\frac{-Y_1(y)}{-1/y^2}\right) = \lim_{y \to 0}\left(y^2Y_1(y)\right).$$

Then,

$$\lim_{y \to 0}\left(y^2Y_1(y)\right) = \lim_{y \to 0}\left(mY_1(y)\right).$$

But, since the limit of the product of a finite number of quantities is equal to the product of their limits,

$$\begin{aligned}\lim_{y \to 0}\left(y^2Y_1(y)\right) &= \left[\lim_{y \to 0}(y^2)\right] \times \left[\lim_{y \to 0}\left(Y_1(y)\right)\right]\\ &= \left[\lim_{y \to 0}(m)\right] \times \left[\lim_{y \to 0}\left(Y_1(y)\right)\right].\end{aligned}$$

Hence,

$$\lim_{y \to 0}(m) = \lim_{y \to 0}(y^2),$$

which is obviously untrue.

Therefore, as $a_2 \to 0$, H does not $\to 0$, and $F_6 \to \infty$.

Since $F_5 = F_6$, as $a_2 \to 0$, $F_5 \to \infty$.

Hence, for $a_2 \to 0$,

$$xJ_0(x) - mJ_1(x) \to 0,$$

or,

$$xY_0(x) - mY_1(x) \to \infty.$$

Since $xY_0(x) - mY_1(x)$ can approach infinity only for $x \to 0$, the only useful solution for x is contained in the expression,

$$xJ_0(x) \to mJ_1(x).$$

It has previously been shown (1, p.259) that the frequencies of radial resonance of a solid rod are given by the equation,

$$xJ_0(x) = mJ_1(x),$$

so that for the limiting case ($a_2 \to 0$) the equations developed in this paper are seen to degenerate to the correct form.

Limiting Case of the Cylinder with Infinitely Thin Walls ($a_2 \to a_1$)

Write $(a_2/a_1)x = x - h$.

Then, $h = (1 - a_2/a_1)x$,

and, as $a_2 \to a_1$, $h \to 0$.

From Taylor's theorem,

$$f(x - h) = f(x) - hf'(x) + \frac{h^2}{2!}f''(x) - \dots .$$

By means of this equation, F_6 becomes,

$$\frac{(x - h)[Y_0(x) - hY_0'(x)] - m[Y_1(x) - hY_1'(x)]}{(x - h)[J_0(x) - hJ_0'(x)] - m[J_1(x) - hJ_1'(x)]},$$

in which expression h^2 and higher powers of h have been neglected, since only those values of h that approach zero are considered.

To obtain the desired solution for x, F_6 is to be equated to F_5, as follows. To simplify writing the equations, J_0 is written for $J_0(x)$, Y_0 is written for $Y_0(x)$, and so on.

$$\frac{(x - h)[Y_0 - hY_0'] - m[Y_1 - hY_1']}{(x - h)[J_0 - hJ_0'] - m[J_1 - hJ_1']} = \frac{xY_0 - mY_1}{xJ_0 - mJ_1}. \tag{11}$$

In the preceding equation, if the various derivatives are written in and the terms in J_0, J_1, Y_0, and Y_1, are collected, the following is obtained.

$$\frac{(x - h + mh)Y_0 + \left(hx - h^2 - m - \frac{mh}{x}\right)Y_1}{(x - h + mh)J_0 + \left(hx - h^2 - m - \frac{mh}{x}\right)J_1} \quad \frac{xY_0 - mY_1}{xJ_0 - mJ_1}. \tag{12}$$

This equation reduces to,

$$Y_0J_1\left\{x\left(hx - h^2 - m - \frac{mh}{x}\right) + m(x - h + mh)\right\}$$

$$= J_0Y_1\left\{x\left(hx - h^2 - m - \frac{mh}{x}\right) + m(x - h + mh)\right\}. \tag{13}$$

Hence,

$$Y_0J_1 = J_0Y_1, \tag{14}$$

or,

$$x\left(hx - h^2 - m - \frac{mh}{x}\right) + m(x - h + mh) = 0. \tag{15}$$

The only solution of Equation (14) is $x = \infty$, because,

$$J_{n-1}(x)Y_n(x) - J_n(x)Y_{n-1}(x) = \frac{2}{\pi x}.$$

Hence only Equation (15) need be considered.

Equation (15) reduces to,

$$x^2 = m(2 - m), \tag{16}$$

if h^2 is neglected.

The radial frequency is,

$$f = \frac{x\alpha}{2\pi a_1} = \frac{1}{2\pi a_1}\sqrt{\frac{q(1-\sigma)}{\rho(1+\sigma)(1-2\sigma)} \times \frac{1-2\sigma}{1-\sigma}\left(2 - \frac{1-2\sigma}{1-\sigma}\right)}, \tag{17}$$

since,

$$m = \frac{1-2\sigma}{1-\sigma}.$$

Equation (17) reduces to,

$$f = \frac{1}{2\pi a_1}\sqrt{\frac{q}{\rho}} \cdot \sqrt{\frac{1}{1-\sigma^2}}. \tag{18}$$

This is not quite the equation ordinarily given (2, p. 138; for the case $s = 0$) for the frequency of free radial vibration of a thin-walled cylinder, as it contains the additional factor, $\sqrt{\frac{1}{1-\sigma^2}}$. As the value of Poisson's ratio usually varies between $\frac{1}{4}$ and $\frac{1}{3}$, the extra factor leads to an increased frequency of the order of about 3 to 6%. Practically this is of no very great significance, but the theoretical reason for the difference is interesting.

In the derivation of the above equations, a wave going from the inside of the cylinder wall to the outside of the wall, thence being reflected back towards the inside, and then being further reflected, was considered. In the derivation of the equation for the thin-walled cylinder, a simple extensional vibration of the tube wall is assumed; the phase of any element in the wall along the same radius vector is the same.

From what has just been said it will be realized that the type of vibration is essentially different in the two cases. Physically, the radial vibration of a cylinder must always be excited by an alternating pressure on the inside or on the outside of the wall, so that it is the type of vibration discussed in this paper that must occur. The frequency given by the simple theory is thus only an approximation to the correct value.

References

1. FIELD, G. S. Can. J. Research, 11 : 254-263. 1934.
2. LAMB, H. The dynamical theory of sound. 2nd ed. E. Arnold. London. 1925.
3. WATSON, G. N. A treatise on the theory of Bessel functions. Cambridge University Press. 1922.

Canadian Journal of Research

Issued by THE NATIONAL RESEARCH COUNCIL OF CANADA

9. OCT.

VOL. 17, SEC. A. AUGUST, 1939 NUMBER 8

THE FLOW AND VISCOSITY OF LIQUID HELIUM[1]

BY H. E. JOHNS[2], J. O. WILHELM[3], and H. GRAYSON SMITH[4]

Abstract

Experiments on the flow of liquid helium through glass capillaries ranging in diameter from 0 025 cm. to 0.0036 cm., and with lengths varying from 2 cm. to 26 cm. were carried out. Normal laminar flow was obtained for He I with a viscosity of the order of 10^{-5} c.g.s. units. For He II it was found that the flow could be expressed as the sum of a laminar flow plus an additional pressure-independent flow. The laminar portion, which obeyed Poiseuille's law, gave a viscosity of the order of 10^{-5} c.g.s. units. The pressure-independent portion appears to be partially due to "creep" over the top of the reservoir, but there still remains an additional pressure-independent flow through the capillaries. This additional flow depends among other things on the intensity of illumination and is evidently connected with the "fountain" effect.

Introduction

During the last four years a considerable controversy has arisen concerning the viscosity, and other curious transport phenomena, of He II, the low temperature modification of liquid helium. Values of the viscosity of liquid helium which have been reported by different experimenters are collected for comparison in Table I. The first experiments were carried out in 1935 by Wilhelm, Misener and Clark (18), by means of a cylinder oscillating under the liquid helium. According to these observations He I behaved as a normal liquid, its viscosity increasing with decreasing temperature. At the λ-point the viscosity suddenly decreased by a factor of about 10 with the transformation to He II. The measured values, which were admittedly approximate, are given in Table I.

Early in 1938, Allen and Misener (2), and Kapitza (9), independently described experiments on the flow of He II through long fine capillaries, and between very close parallel plates, respectively. In both cases it was reported that laminar flow could not be obtained, that the viscosity must be of the order of 10^{-9} c.g.s. units or less, and that the measurements of Wilhelm and others were invalidated because of the large value of the Reynolds number. Allen and Misener found further that the velocity varied with the pressure much more slowly than would be expected even for extreme turbulence. This fact, considered along with the condition that the flow is very rapid, suggested some kind of "superfluidity". On account of the large discrepancy between the results of these experiments, measurements of the flow were undertaken at Toronto by the authors. Preliminary results (4), using short capillaries, indicated laminar flow for small pressure heads, and normal turbulence for larger ones, with a viscosity of the order of 10^{-5} c.g.s. units.

---

[1] *Manuscript received April 1, 1939.*
Contribution from the McLennan Laboratory, Department of Physics, University of Toronto, Toronto, Canada.

[2] *Holder of a Studentship under the National Research Council of Canada.*

[3] *Assistant Professor, Department of Physics, University of Toronto.*

[4] *Associate Professor, Department of Physics, University of Toronto.*

TABLE I

COMPARISON OF RESULTS OF EXPERIMENTS ON THE VISCOSITY OF LIQUID HELIUM

Authors	Reference	Method	Viscosity			
			He I		He II	
			Temp. °K	$\eta \times 10^6$	Temp. °K	$\eta \times 10^6$
Wilhelm, Misener and Clark	18	Oscillating cylinder	4.2	110	2.2	33
			2.3	270		
Allen and Misener	2	Long capillary			2.17 1.07	<0.004 non-laminar
Kapitza	9	Flow between parallel plates				<0.001 non-laminar
Burton	4	Short capillary			2.16	50 to 80
Keesom and Macwood	10	Oscillating disc	4.0	29	2.16	16
			3.0	25	1.72	3.8
			2.3	19	1.32	1.9
Giauque, Stout and Barieau	7, 8	Flow through very small channel			2.2	15
					1.8	0.35
					1.4	0.07
Allen and Misener	3	Long capillary			2.18 1.15	Confirm (2)
		Short capillary	2.2	140	2.16	78

Two further direct measurements of the viscosity and flow have been made, and are included in Table I. Keesom and Macwood (10) have measured the viscosity from 1.3° K to 4° K by means of an oscillating disc. The results obtained for He II just below the λ-point agreed in order of magnitude with those of Wilhelm, Misener and Clark, with a rapid decrease of viscosity at lower temperatures. However, Keesom and Macwood found the viscosity of He I to be of the same order of magnitude as that of He II; they also found that the viscosity decreased as the temperature was lowered. Giauque, Stout and Barieau (7, 8) measured the flow through a channel of the order of 10^{-4} cm. in thickness. This channel was obtained between concentric cylinders by casting solder in a glass tube, and taking advantage of the differential contraction. The creep over the surface was eliminated (see below), and at very low temperatures the calculated viscosities were lower than those of Keesom and Macwood by a factor of about 10.

There is evidently a real discrepancy, connected in some way with the peculiar properties of liquid helium II, between the flow through channels of different diameters and the viscous drag on a moving body. In further experiments Allen and Misener (3) have confirmed their earlier results with long capillaries, but have found approximate laminar flow with short tubes, in agreement with the preliminary results of the authors (4). They found further that the velocity decreased quite slowly with increasing lengths of the tubes. It is evident that the flow of He II through tubes cannot be calculated from the pressure difference and dimensions by means of Poiseuille's law using any definite value for the viscosity. The question then arises of finding the factors on which flow does depend, and whether the measurements actually give the quantity of liquid passing through the tube.

That, in some cases, the measured flow may be apparent only, follows from the recent discovery that He II can "creep" over any surface with which it is in contact. Experiments of Rollin and Simon (14) led to the suggestion that a surface dipping into He II becomes covered with a thin film of the liquid. Then Daunt and Mendelssohn (5, 6) discovered that this film could cause an appreciable transfer of the liquid by a kind of syphon action. If a reservoir such as that shown in Fig 1 were sealed off at *B*, liquid would still pass into it, apparently by creeping over the top at *A*. This surface transport was found to be proportional to the circumference of the tube where it cut the helium surface and practically independent of the difference in level. It was not observed in the case of He I, but the rate of transport of He II increased very rapidly as the temperature was lowered below the λ-point. The existence of this film has been confirmed by Kikoin and Lasarew (11), who estimated the thickness to be of the order of 10^{-5} cm.

Another phenomenon which may enter into experiments on the flow of He II is the peculiar ponderomotive effect associated with the extremely high thermal conductivity. This was first observed in the fountain experiment of Allen and Jones (1). When the lower end of a tube such as that shown in Fig. 1 was partially plugged with fine emery powder, and the plug was illuminated so as to cause a rise of temperature at that point, liquid He II was forced through the plug, and ejected from the top of the tube with a velocity sufficient to produce a jet some 10 cm. in height. When a tube with a capillary attached was heated locally at the point *B*, so that heat would be conducted down the capillary, the liquid came to equilibrium in the tube at a level higher than that of the surrounding bath. These experiments indicate that when a temperature gradient is set up in He II, a pressure gradient in the opposite direction is produced. However, definite measurements on this phenomenon have not yet been made.

The principal object of the present experiments was to find how the apparent flow of liquid helium II depends on the length and diameter of the tube, and on the pressure difference. In this way the authors hoped to account for the discrepancies among the different experiments. For this purpose the flow has been measured through capillaries of a wide variety of sizes and for a wide range of pressure differences. It has been found that, under most conditions, the measured apparent flow can be expressed as the sum of a laminar flow, which satisfies Poiseuille's law with a viscosity of the order of 10^{-6} c.g.s. units, plus an additional flow which is independent of the pressure difference. This additional flow appears to be due partially to "creep" over the top of the reservoir, but there still remains an additional pressure-independent flow through the capillaries. Amongst other things, this additional flow depends on the intensity of illumination, and it is evidently connected with the fountain effect.

Experimental

Soft glass capillaries were sealed to reservoirs of approximately 0.13 cm. in diameter, as shown in Fig. 1, and the rate of flow was determined by measuring the level of the helium in the reservoirs at frequent time intervals. To do this a camera was used for the more rapid rates of flow, and a telescope with a calibrated eye-piece for the slower ones. Since the main object of the experiments was to study the apparent flow under various conditions, no

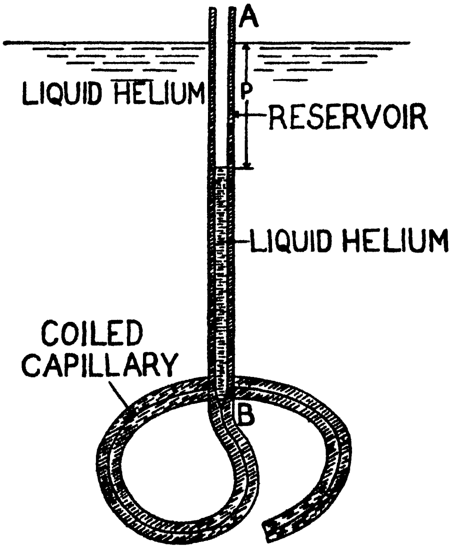

FIG. 1. *A typical coiled capillary, with its reservoir.*

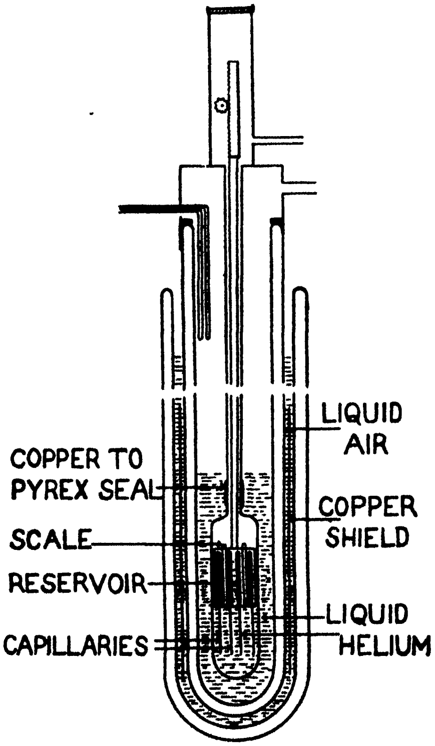

FIG. 2. *Vertical section of the flasks and capillaries. Four straight capillaries, four reservoirs, and two scales are shown in this diagram. The level of the liquid helium in the inner flask lies just below the upper end of the reservoirs.*

attempt was made to prevent the surface creep. On the other hand, the reservoirs were made as uniform as possible and left open at the top, and held in place at the bottom only, so that the surface exposed to creep would be known.

In most of the experiments the empty reservoirs were lowered into the helium, and measurements were made as the liquid ran in, because better thermal equilibrium could be obtained in this way than when the reservoirs were raised out of the helium and allowed to empty.

Fig. 2 shows a front view of the flasks, capillaries, and reservoirs as arranged for photographing a number of tubes simultaneously. Fig. 3 gives a schematic plan of the flasks, stop-watch, and camera. The reservoirs were arranged side by side with two glass scales and were held in a framework so that they could be raised or lowered by a pinion and ratchet. In preliminary experiments, difficulty was experienced owing to the changing level of the helium in the flask and reservoirs as evaporation took place. To overcome this the tubes were placed in a cylindrical glass vessel, which was joined to a piece of German silver by means of a copper-to-Pyrex seal as shown in Fig. 2. The cryostat was filled with liquid helium and then a quantity was liquefied in

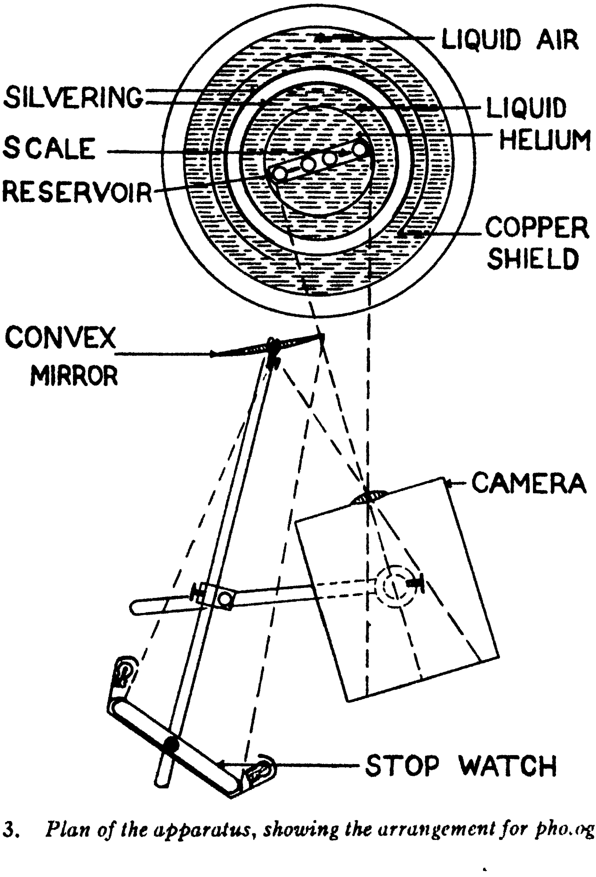

FIG. 3. *Plan of the apparatus, showing the arrangement for photographing.*

the inner vessel by allowing helium gas to flow in at a pressure slightly greater than the vapour pressure in the cryostat. This inner system was then shut off in order to prevent any evaporation from it during the experiment. Separate manometers were used to measure the vapour pressure in the cryostat and in the inner vessel. These showed that fair temperature equilibrium was obtained except when intense lighting was used. The recorded temperatures were derived from the pressure in the inner vessel.

To photograph the helium as it flowed through the capillaries an "Agfa Memo Camera" with a Bausch and Lomb anastigmat lens was used. By using an auxillary meniscus lens the camera could be brought within 5 cm. of the liquid-air flask. It was arranged as shown in Fig. 3 so that the reservoirs and scales filled half the field of view. To obtain a time record a stop-watch was photographed simultaneously on the other half of the film. The watch, with its focusing mirror, was supported by means of an adjustable clamp attached to the camera stand, so that once this was in focus the camera and watch could be moved together. With this arrangement very satisfactory pictures could be taken, and the scales and reservoirs were surprisingly clear, despite the fact that the light had passed through five concentric glass flasks and three layers of liquid. The camera used 35 mm. film and took pictures 2.5 by 2 cm. It could be loaded very rapidly to take as many as 70 pictures in succession. To advance the film it was necessary only to move a lever on the back of the camera, and this could be done fast enough to take one picture every second. The shutter could be set to give exposures of $\frac{1}{2}$, $\frac{1}{5}$, $\frac{1}{10}$, $\frac{1}{25}$ sec. with apertures *f*-3.5 to *f*-16. "Agfa Panatomic", a fast type of fine grain film, was used throughout.

To illuminate the liquid surfaces satisfactorily a light was placed about 5 cm. below them, in front of the liquid-air flask. In some cases a flash-light bulb was used, in others a 60 watt lamp. To keep the amount of light entering the flask during an experiment as small as possible a contact was arranged on the side of the camera which automatically turned on the lights when a picture was being taken. Even with this precaution it was found necessary to reduce the radiation entering the flask by means of a copper shield in the liquid-air flask and by partially silvering the helium flask. It was also found advisable to place a water cell in front of the light to cut down heat radiation. When these precautions were taken, the effect of illumination on the flow was reduced to a minimum.

To interpret the results the photographs were examined under a microscope, and a reading on the scale corresponding to the time on the stop-watch was obtained for each reservoir. By placing the scale in the helium beside the reservoirs all distortion arising from the concentric flasks was removed.

For the slower rates of flow, and with very small pressure heads, measurements were made with a travelling microscope equipped with a calibrated eye-piece. By the combined use of photographic and visual methods it was possible to study rates of flow ranging from 5×10^{-5} to 3×10^{-2} cm.^{3} per second, and to measure pressure heads from 0.02 to 4 cm. This range sufficed to study the flow through capillaries of diameters from 0.0036 to 0.025 cm., and lengths 2 to 26 cm.

Results

I. THE VISCOSITY OF HELIUM I

The results for He I at four different temperatures are given in Table II and illustrated graphically in Figs. 4 and 8. Fig. 4 shows that the relation between the logarithm of the pressure head and the time is strictly linear for pressure heads ranging from 0.2 to 2 cm. This indicates that the volume per second flowing through the capillary is strictly proportional to the pressure head, so that the viscosity may be calculated using Poiseuille's formula.

TABLE II

THE VISCOSITY OF HE I AS DETERMINED BY THE USE OF TUBE XI
(Length, 4.14 cm.; diameter, 0.00610 cm.; and reservoir diameter, 0.108 cm.)

Temperature °K.	Density, gm./cm.^{3}	Slope, $dt/d(\log_{10} P)$	Viscosity, 10^{-6} c.g.s. units	Conditions
4.25	0.1245	975	46.5	*e, c, j*
3.40	0.1372	875	45.7	*e, c, j*
2.24	0.1458	608	33.8	*e, c, j*
2.22	0.1459	616	34.2	*d, g, j*

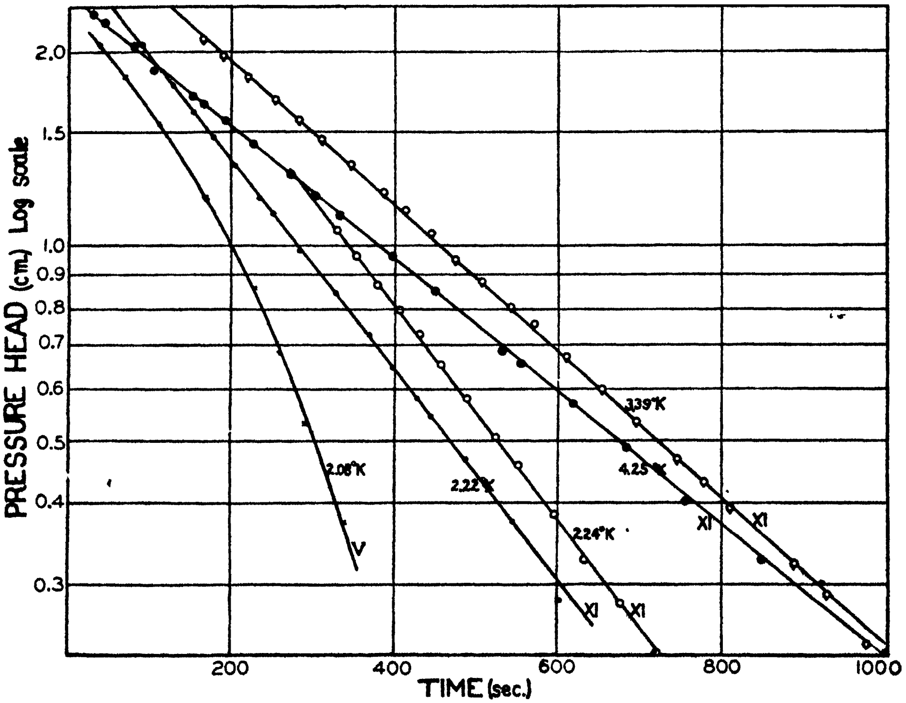

FIG. 4. *Relation between the logarithm of the pressure head and the time for He I and He II.*

For convenience the values of the slope ($dt/d(\log_{10}P)$), the density, the temperature, and the viscosity have been given in Table II. The letters in the column headed "Conditions" refer to the subscripts following Table III. They describe the way in which the experiment was carried out and the type of illumination used in photographing.

The correction to the pressure head for the kinetic energy of efflux was negligible in the experiments, amounting to ½ of 1% for a pressure head of 2 cm. at 2.22° K. The maximum Reynolds number obtained was 125, which is well within the theoretical limit for laminar flow. The variation of viscosity with temperature is shown in Fig. 8. The results show that the viscosity decreases with decrease in temperature, in agreement with the previous work of Keesom and Macwood (10), and in contradiction with the work of Wilhelm, Misener and Clark (18). The values of η, however, are considerably higher than those obtained by Keesom and Macwood.

II. Flow Experiments on Helium II

In experiments carried out with He II, straight lines are not obtained if the pressure head is plotted against the time on semilogarithmic paper; this is shown by the graph for Tube V at 2.08° K. (Fig. 4). Very long fine capillaries gave graphs which were quite curved, while shorter ones yielded curves which were nearly straight, in agreement with the previous work of the authors (4). For He II, therefore, the pressure heads, P cm. of liquid, were first plotted directly against the time, for which examples are shown in Fig. 5. It is obvious that these graphs deviate considerably from the expon-

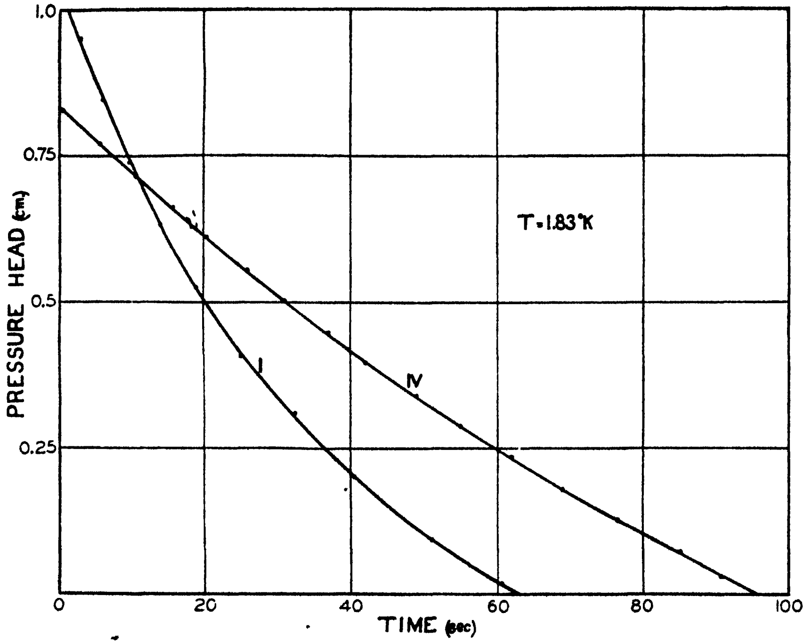

FIG. 5. *Relation between the pressure head and time for flow experiments with He II.*

ential form, especially in the case of the longer tube, No. IV. To obtain the volume flowing per second, Q cm.^{3}/sec., the slopes of these curves were measured, and from these the graphs of Q against P were obtained, as shown in Fig. 6 and 7. In general, these are straight lines satisfying a relation

$$Q = bP + Q_0$$

The two contributions to the flow, the portion bP which depends on pressure, and the pressure-independent residual flow, Q_0, will be discussed separately in the following sections.

It is evident that quite erroneous values for the viscosity of He II might be estimated from graphs similar to the graph for Tube V in Fig. 4. which somewhat resembles the curve for turbulent flow. Especially for small pressure heads and for very fine capillaries where the residual flow Q_0 is relatively important, very small apparent values for the viscosity would be obtained.

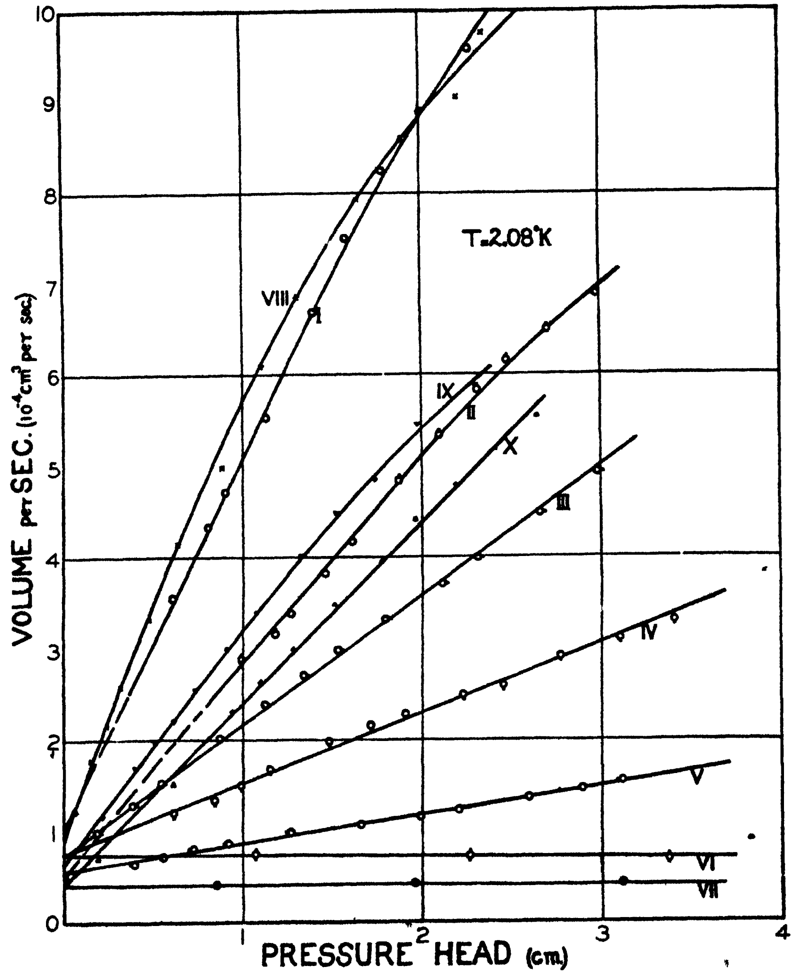

FIG. 6. *Relation between the volume per second and the pressure head for a selection of capillaries, for experiments carried out at one temperature with He II.*

II. (a) The Viscosity of Helium II

Fig. 6 and 7 indicate that except for Tubes I, VIII and IX, linear relations exist between the pressure head and the volume per second, for a large range of pressure heads. These graphs have been corrected for the kinetic energy of efflux. For Tube I the correction to the pressure head at 3 cm. amounted to 7%; for Tube II, 4%; and for Tube III, 1%, with negligible corrections for the rest of the capillaries. The Reynolds number for Tube I at a pressure head of 3 cm. was approximately 400, while this quantity for the other tubes was correspondingly smaller.

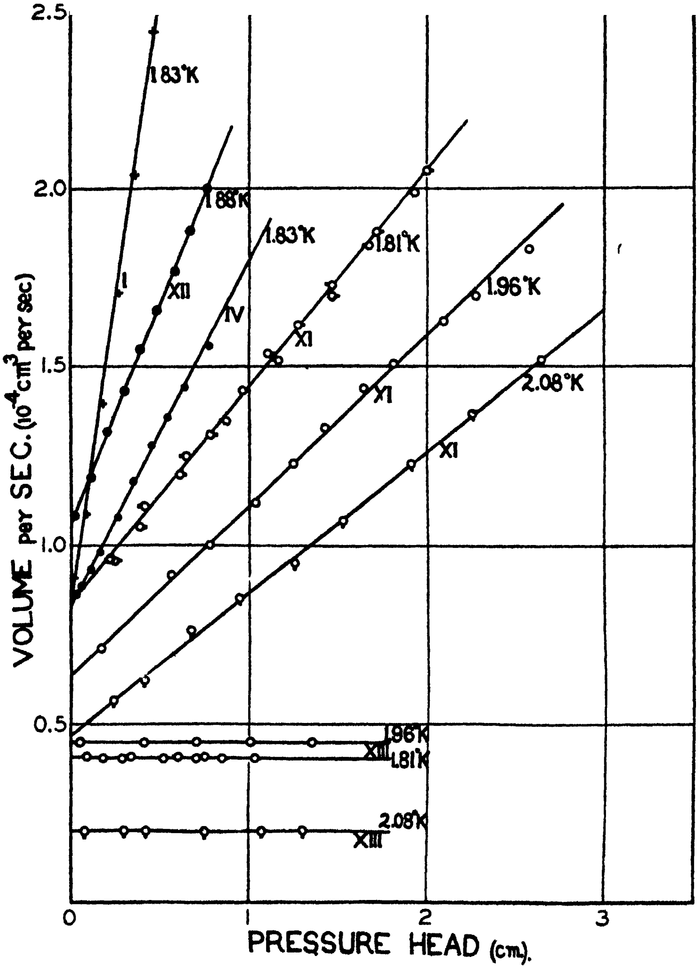

FIG. 7. *Relation between the volume per second and the pressure head for a selection of capillaries and temperatures with He II.*

The dimensions of the tubes are given in Table III where the length and the diameter of the capillaries and the inner and outer diameter of the reservoir are given. At any one temperature the values of *b* for different capillaries were proportional to a^4/l (a is the radius of the capillary and l the length); this indicates that Poiseuille's law is obeyed for this contribution to the flow. The values of the viscosity deduced from measured values of b are given in Table III. The last column of this table gives the conditions under which

TABLE III
RESULTS FOR THE FLOW EXPERIMENTS WITH He II

Tube	Length, cm.	Diameter, 10^{-4} cm.	Diameter of reservoir, mm.		Temperature, °K.	Viscosity, 10^{-6} c.g.s. units	Residual flow, 10^{-4} cm.^{3} per sec.	Transport, 10^{-4} cm.^{3} per sec.	Conditions*
			Inner	Outer					
I	2.05	90.8	1.34	2.80	2.08	28.4	1.0		*a, e*
II	3.65	91.6	1.36	2.85	2.08	28.8	0.5		*a. e*
III	5.10	87.6	1.36	2.84	2.08	28.5	0.75		*a, e*
IV	8.30	87.1	1.39	2.84	2.08	31.3	0.75		*a, e*
V	25.8	89.9	1.38	2.88	2.08	28.4	0.58		*a, e*
VI	2.2	36.0	1.18	2.07	2.08		0.74		*a, e, h*
VII	6.2	36.0	1.25	2.25	2.08		0.42		*a, e, h*
VIII	4.6	132	1.42		2.08	44.0	0.90		*a, e, i*
IX	12.2	137	1.47		2.08	39.4	0.64		*a, e, i*
X	23.9	139	1.46		2.08	27.4	0.40		*a, e, i*
I					1.83	33.5	0.83		*b, f, k*
IV					1.83	25.4	0.85		*b, f, k*
XII	8.19	86.9	1.12	1.58	1.88	19.9	1.06		*d, f*
XI	4.14	61.0	1.08	2.08	2.08	29.3	0.47		*c, e, j*
XIII	Closed off		1.13	2.14	2.08			0.20	*c, e*
XI					1.96	24.4	0.63		*c, e, j*
XIII					1.96			0.45	*c, e, j*
XI					1.81	19.2	0.83		*c, e, j*
XIII					1.81			0.41	*c, e*

* (*a*) *Strong intermittent light (one 60-watt lamp 5 cm. from the flask).*
(*b*) *Strong continuous light.*
(*c*) *Weak intermittent light (one 2-watt bulb plus a water cell 5 cm. from the flask).*
(*d*) *Weak continuous light.*
(*e*) *Measurements made with the camera.*
(*f*) *Measurements made with the microscope.*
(*g*) *Measurements made with the eye alone.*
(*h*) *Pressure-independent flow, therefore impossible to calculate the viscosity.*
(*i*) *Owing to distortion in the coiled capillary a^4/l could not be measured accurately.*
(*j*) *Reservoir was extended to a height of 24 cm. above the bath, but it was all at liquid helium temperatures owing to the protection of the outer bath.*
(*k*) *Temperature doubtful owing to the fact that the inner system was not completely covered by helium in the outer cryostat.*

the experiment was carried out. Tubes VIII and IX did not give straight lines for the higher pressure heads because of constrictions in the coiled capillaries. For this reason accurate average values of a^4/l could not be obtained, and the viscosity values given by these tubes are not reliable. At large pressure heads, Tube I (Fig. 6) shows normal turbulence as would be expected for a capillary of its dimensions. For the longer tubes the diameters were measured at many places by cutting them into centimetre

lengths and examining them under a microscope. It was found that the diameters were not very constant, owing to distortion in coiling, so that the values of the viscosity as obtained by their use were not very accurate. Tube XI however was straight and extremely uniform, the diameter varying by less than 0.3% over its length, so that the results obtained with it (Fig. 7) are considered to be more accurate than the rest.

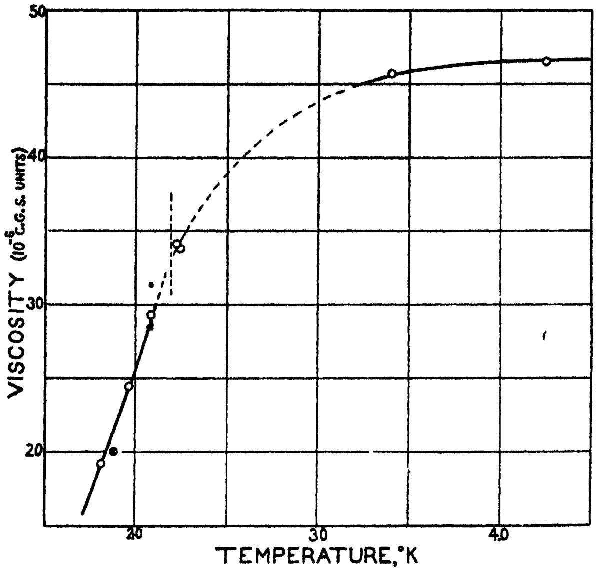

FIG. 8. *Relation between the viscosity of liquid helium and the temperature.*

The variation of viscosity with temperature is shown in Fig. 8. The results for Tube XI are shown by plain circles, while measurements made with the other tubes are shown by black dots and filled circles. The viscosity of He II was found to decrease rapidly with decrease in temperature in agreement with Keesom and Macwood (10). However, as with He I, the values obtained in this experiment were considerably larger than theirs. From Fig. 8 it appears as though the viscosity might be continuous through the λ-point, but as no measurements were made at 2 18° K this part of the curve has only been dotted.

II (b) The Residual Flow

With the experimental arrangement used, the pressure-independent residual flow, Q_0, includes the surface transport over the top of the reservoir, as pointed out in the introduction. However, a comparison of the measurements made with Tubes XI and XIII shows that only a part of Q_0 can be explained in this way, and that a part must represent actual pressure-independent flow through the capillary. Tube XIII consisted only of a reservoir sealed at the bottom, and so gave surface transport only. Tube XI had a reservoir of nearly the same diameter, but extended to a height of 24 cm.

above the helium level. The figures in Table III show that at all temperatures the residual flow of He II in Tube XI was considerably greater than the transport into Tube XIII. The effect cannot be accounted for by distillation in or out of the reservoirs, for this would take place with He I as well, and at temperatures above the λ-point the level in Tube XIII remained constant throughout the time of the experiment.

At present only qualitative statements can be made concerning the dependence of the surface transport and the residual flow on the dimensions and experimental conditions.

It was found that the surface transport into a tube which was closed at the bottom was decreased when the intensity of the illumination was increased. With strong illumination, and a thick walled reservoir, there was an apparent transport out of the tube, against the pressure head. This can be readily explained by evaporation of the film as it crept up the walls. With a sufficient heat input the film could be completely evaporated before reaching the top of the barrier, and then evaporation of the inner film would cause a loss of liquid from the reservoir.

It has been stated (14) that the surface transport is practically independent of either the pressure head or the height of the barrier. It was found in the present experiments that the effect was greatly increased when the height of the barrier was 1 mm. or less.

The true residual flow through the capillaries also depended on the illumination, in general increasing with increasing light intensity. In general also, the liquid helium continued to flow into the reservoir for some time after the pressure head was reduced to zero, and finally rose to a height of about 0.5 mm. above the level in the outer vessel. This excess pressure head also increased with increasing illumination. These observations indicate that the absorption of light energy was producing a flow and a back pressure similar to the effects observed by Allen and Jones (1). However, residual flow still took place when the capillaries were completely shielded from the light and the reservoirs alone were illuminated intermittently by a 2-watt bulb through a water cell.

For very fine capillaries (Tubes VI and VII) the observed total flow was independent of the pressure head, as reported by other authors. In these tubes the flow was practically all residual flow, and it was impossible to deduce values for the viscosity. Comparison of the results with these two tubes indicates a decrease of the residual flow with increase in length. At the same time, comparison of all the results shows that the residual flow did not vary greatly for tubes of different diameters.

Discussion

These results of experiments on the flow of He II are consistent with the view advanced by F. London (13), and also discussed by Tisza (15, 16, 17), that the peculiar properties of the liquid are due to the degeneracy of Bose-Einstein statistics. This means that a finite fraction of the atoms, the degenerate fraction, are in the lowest quantum state of translational energy, with negligibly small velocities. Both authors concluded that the degenerate atoms would contribute nothing to the viscous forces, so that a completely degenerate fluid would behave in general as a non-viscous fluid. It seems evident that the pressure-dependent flow observed in the present experiments is the ordinary viscous flow of He II, and that the residual flow is connected with the superfluid properties of the degenerate fraction. The deduced values of η are therefore believed to be real viscosities, representing the frictional forces on the walls. The viscosity obtained in this way decreases rapidly with decreasing temperature below the λ-point, in agreement with the predictions of London and Tisza. It does not, however, satisfy the theoretical viscosity-temperature formula given by Tisza. For the small temperature range covered in the present experiments, η is very closely proportional to T^3.

The mechanism which causes the residual flow is not yet clear, but it is evidently closely connected with the ponderomotive effect which accompanies a temperature gradient in He II, for it was increased by increasing the intensity of illumination. It is to be expected that absorption of light by the walls of the reservoir would cause slight differences of temperature between the reservoir and the surrounding vessel. But the experimental indications are that the residual flow can also be caused by a very small pressure difference without any input of thermal energy. This is supported by the experiments of Giauque, Stout and Barieau (7, 8), in which an external pressure was applied to a very fine capillary, and the flow also measured externally instead of by watching a reservoir. In their experiments the variation of the flow with pressure was not studied, and in view of the size of the capillary and the very small values deduced for the viscosity, it is probable that the flow was mainly of the residual pressure-independent type.

It is interesting to note the order of magnitude of the velocity and energy in the residual flow in the present experiments. The average linear velocity varied from something of the order of 0.1 cm per sec. for the largest tube (VIII) to about 5 cm. per sec. for the short fine tube (VI). The latter value is of the same order as the linear velocity in the surface transport (Tube XIII), if the estimate of Kikoin and Lasarew (11) for the thickness of the film is accepted (10^{-5} cm.). The pressure head required to maintain a velocity of 1 cm. per sec. in a non-viscous fluid is of the order of 5×10^{-4} cm , and the work done, with a flow of about 5×10^{-5} cc. per sec. in liquid helium, is of the order of 4×10^{-6} ergs per sec.

The views expressed by F. London and H. London (12), and by Tisza, concerning the mechanism by which the degenerate atoms give rise to the very high heat conductivity and the thermo-mechanical flow are quite different, but both treatments lead to the conclusion that the effects should be reversible, and that under adiabatic conditions the pressure-independent flow should cause a temperature gradient. It is therefore reasonable to conclude that the residual flow in the present experiments, the fountain effect of Allen and Jones, and the high heat conductivity of He II, are all manifestations of the same property, and are essentially thermo-mechanical phenomena, involving a selective non-viscous flow of the degenerate atoms. In the case of the flow of He II under a pressure gradient, an ordinaty flow of the whole fluid is superposed on the super-flow, and this ordinary flow is purely mechanical, obeying the laws of viscous fluids. It is this combination of the two effects which has given rise to the tremendous discrepancies in different experiments on the flow and viscosity of He II. Further experiments are still required, however, using fine capillaries, before the super-flow can be properly understood.

Acknowledgments

The authors wish to thank Prof. E. F. Burton, Director of the McLennan Laboratory, for the interest which he has shown throughout the research.

References

1. ALLEN, J. F. and JONES, H. Nature, 141 : 243-244. 1938.
2. ALLEN, J. F. and MISENER, A. D. Nature, 141 : 75. 1938.
3. ALLEN, J. F. and MISENER, A. D. Nature, 142 : 643-644. 1938.
4. BURTON, E. F. Nature, 142 : 72. 1938.
5. DAUNT, J. G. and MENDELSSOHN, K. Nature, 141 : 911-912. 1938.
6. DAUNT, J. G. and MENDELSSOHN, K. Nature, 142 : 475. 1938.
7. GIAUQUE, W. F., STOUT, J. W., and BARIEAU, R. E. Phys. Rev. 54 : 147. 1938.
8. GIAUQUE, W. F., STOUT, J. W., and BARIEAU, R. E. J. Am. Chem. Soc. 61 : 654-661. 1939.
9. KAPITZA, P. Nature, 141 : 74. 1938.
10. KEESOM, W. H. and MACWOOD, G. E. Physica, 5 : 737-744. 1938.
11. KIKOIN, A. K. and LASAREW, B. G. Nature, 142 : 289-290. 1938.
12. LONDON, H. Nature, 142 : 612-613. 1938.
13. LONDON, F. J. Phys. Chem. 43 : 49-69. 1939.
14. ROLLIN, B. V. and SIMON, F. Physica, 6 : 219-230. 1939.
15. TISZA, L. Compt. rend. 207 : 1035-1037. 1938.
16. TISZA, L. Compt. rend. 207 : 1186-1189. 1938.
17. TISZA, L. Nature, 141 : 913. 1938.
18. WILHELM, J. O., MISENER, A. D., and CLARK, A. R. Proc. Roy. Soc. London, A, 151 : 342-347. 1935.

A LARGE-SCALE THERMAL CONDUCTANCE APPARATUS USED FOR THE TESTING OF BUILDING MATERIALS[1]

By J. D. Babbitt[2]

Abstract

A short description and discussion are given of a thermal conductance apparatus of the guarded hot-box type used by the National Research Laboratories, Ottawa, for the measurement of the thermal conductivity of building materials. Results obtained with this apparatus are compared with hot-plate measurements on the same materials and indicate good agreement between the two methods.

Introduction

The Hot-box Apparatus of the National Research Laboratories, Ottawa

For several years the heat conductivity of various kinds of building materials has been measured at the National Research Laboratories by means of a hot-plate apparatus. A description of this apparatus and of the various investigations undertaken are given in several papers by C. D. Niven (2, 3, 4). During the past few years the increase in the attention paid to insulation in building construction in Canada has led to a demand for tests on those types of construction for which the hot-plate is unsuited, because this apparatus, although admittedly the ultimate authority on conductivity coefficients, has the following limitations from a practical point of view:—

1. Only the surface-to-surface conductance of a specimen can be obtained by means of the hot-plate, and there is no method by which the air-to-air transmission can be deduced from such a measurement unless the air-surface coefficients have been obtained in a separate investigation. In building construction the concern is ultimately with air-to-air transmission, as the important figure is the heat loss from the air on one side of the wall to the air on the other. It should be pointed out, however, that the air-surface coefficients have been determined for various types of surfaces at different wind velocities, and, since the coefficients do not vary greatly from surface to surface, this is not such a serious limitation to the use of hot-plate results as is often believed.

2. The hot-plate is designed for the measurement of homogeneous samples, in which, during the period of the test, the temperature gradient is the same throughout the sample. It is unsatisfactory for built-up wall sections, where the conductivities of the various constituents are different.

3. The hot-plate is suitable only for samples having smooth surfaces, which make good contact with the hot and cold plates. Walls constructed of masonry or brickwork do not lend themselves to this type of test.

---

[1] *Manuscript received May 3, 1939.*

Contribution from the Division of Physics, National Research Laboratories, Ottawa, Canada. Issued as N.R.C. No. 823.

[2] *Physicist, National Research Laboratories, Ottawa.*

4. The size of the ordinary hot-plate is such that thick wall-sections and heavy materials such as concrete or cinder blocks cannot be tested.

In order to fill this gap in testing equipment, the National Research Laboratories, Ottawa, decided to construct a heat transmission apparatus capable of comparing the conductivities of built-up wall sections and of giving directly the over-all transmission of the test samples. The apparatus most suitable for this purpose is of the Guarded Hot-box type, developed by F. B. Rowley and his collaborators at the Engineering Experiment Station of the University of Minnesota (5, 6, 7), so an apparatus was constructed which followed very closely the methods developed in Minnesota and differed only in minor details.

The guarded hot-box apparatus makes use of an elaboration of the principle employed in the hot-plate apparatus, where the heat loss in lateral directions is completely eliminated by maintaining the temperature in the outer portions of the plate (the guard-ring) at a temperature exactly equal to that of the centre portion, the heat input of which is accurately metered. In a hot-box apparatus, where in order to obtain the air-to-air coefficient, three dimensions must be considered, the heat loss from the hot-box must be eliminated on every side except that on which the sample wall is placed. This is done by means of the arrangement shown schematically in Fig. 1. The hot-box is enclosed on five sides by a guard-ring box, and the sixth side of the two boxes coincide. The sample wall is so placed as to cover this face completely, and it separates the hot-box and guard-ring box from the cold chamber. With this arrangement, when the hot-box and guard-ring are maintained at the same temperature all the heat put into the hot-box passes through the specimen wall to the cold chamber. Since this heat can be measured electrically and since the temperature of the air on the two sides of the wall can be easily determined, this apparatus furnishes a simple method of determining the air-to-air heat transmission of walls.

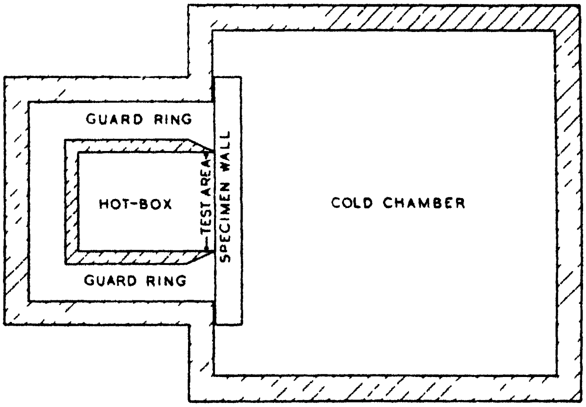

FIG. 1. *Schematic diagram of hot-box arrangement.*

Experimental

Construction and Operation of the Apparatus

The cold chamber, which is 10 by 10 by 8½ ft., can be cooled to a temperature as low as −10° F. by means of a York ammonia compressor refrigerating machine. The temperature is maintained within 0.5° F. of that desired by means of a mercury thermoregulator that controls the compressor through a relay. This method of controlling the temperature in the cold chamber proved sufficiently sensitive without the introduction of heating coils such as were found necessary by Rowley and his co-workers.

The guard-ring space has been divided into two sections by means of a sheet of galvanized iron extending at an angle from the front point of the hot-box to a point 1 ft. back on the wall of the guard-ring. Without this separation into two compartments it was impossible to maintain all parts of the guard-ring at the same temperature. The front section, being nearer to the cold sample, tended to become cooler than the back, and, since the samples differed greatly in conductivity, it required an excessive amount of adjustment to maintain even approximately a uniform temperature throughout. The separation of the guard-ring into a front and a back portion greatly facilitates the maintenance of an equal temperature distribution, since the temperature of the front section can be adjusted independently of the rest of the guard-ring.

The heat is supplied to the guard-ring through seven coils of chromel A wire attached to the outer wall and running completely around the four walls in planes parallel to the front opening. Three of these coils are in the front section and four in the back. Their position is shown in Fig. 2. The current in each coil can be regulated separately by means of a rheostat placed outside the apparatus and by these adjustments an equal temperature can be established throughout the guard-ring. The temperature is determined by means of thermocouples placed at eight different points, four of which are in the front section and four in the back. They are indicated in the diagram. A circulation of air to prevent the occurrence of temperature gradients is maintained by means of four 8-in. fans in the back section and two 6-in. fans in the front. These fans are placed, some on top of the hot-box and some below, in such a manner as to maintain a steady flow around the hot-box. They run at a speed of approximately 1000 r.p.m. and are driven by an electric motor placed outside the apparatus. This circulation system is more elaborate than that used at Minnesota but the difficulties experienced in obtaining an equal temperature throughout the guard-ring led by degrees to its development.

The heat is introduced into the hot-box proper by means of a chromel A wire which runs zigzag around four sides of the box. It is not placed on the top surface, because, owing to natural convection, the upper part of the box would then tend to become too warm. The current through this wire is carefully regulated and the power is measured by means of a recording wattmeter. To maintain an equal temperature throughout the box and to eliminate all temperature gradients, the air is stirred by four large paddle-shaped fans. These fans are attached to one horizontal shaft which is placed across the centre of the box and which turns at a speed of about 100 r.p.m.

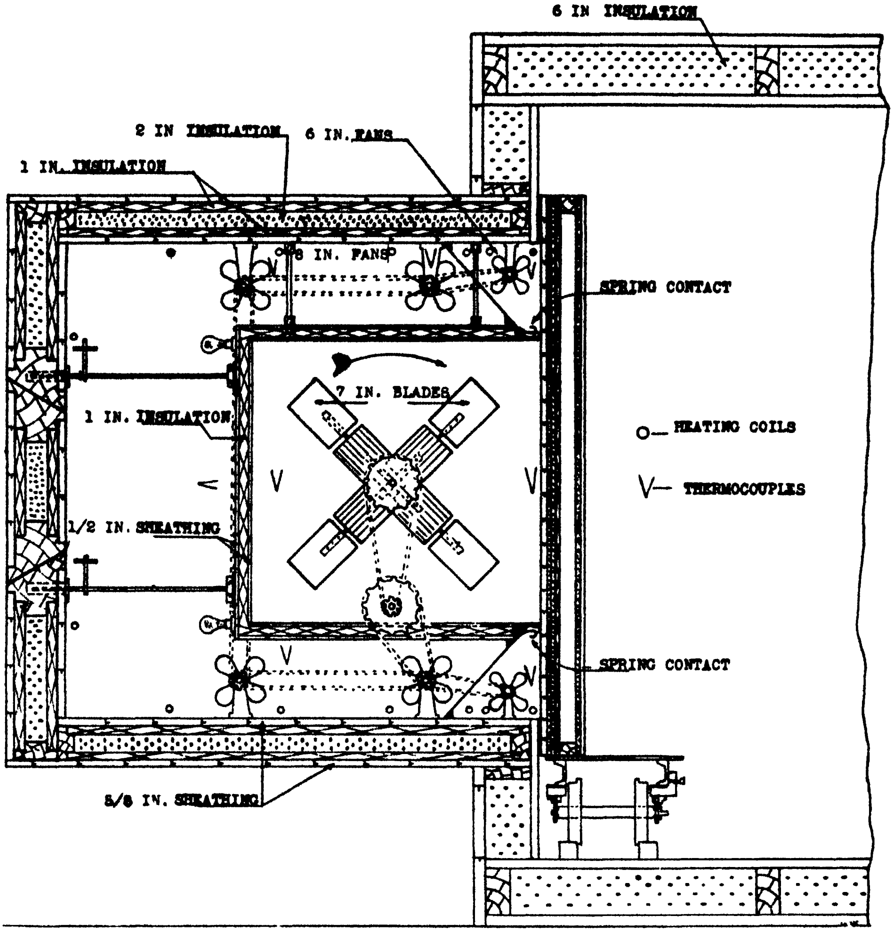

FIG. 2. *Showing construction and position of test box and test wall.*

The two centre blades are short, whereas the two outer ones are as long as the dimensions of the apparatus will conveniently allow. The blades are set at angles to the shaft in such a manner that the outer and inner blades drive the air in opposite directions and maintain a continuous circulation, the air flowing across the surface of the sample and back along the axis of the fans. With this arrangement all temperature gradients are eliminated from the box, although a difference of as much as 4° F. was detected between the bottom and top when the air was not stirred. Hot-box tests should, theoretically, be made with still air on both sides of the sample, but it is impossible to reconcile this condition with an equal temperature distribution throughout the apparatus. Therefore, since it is more important to maintain an equal temperature in all parts of the box than to have absolutely still air conditions, every effort has been made to attain the former, while, at the same time, keeping the air velocity at the surface of the sample as small as is consistent with this condition.

It was necessary to ascertain what heat, if any, was added to the hot-box by these fans. In order to do this the number of watts required by the motor was determined with the fans running at various speeds. In a second series of readings the system was run with the blades removed from the fans and the number of watts supplied to the motor again determined. Since the bearings of the shaft were outside the hot-box, the difference between the two sets of readings should indicate the heat supplied to the hot-box proper by the circulation system. Actually no appreciable difference in the power consumption was found with and without the blades, so that in computing the heat input to the hot-box the energy introduced by stirring the air could be neglected.

In order to eliminate the temperature gradients in the cold chamber, an ordinary electric house fan with 12-in. blades was placed on the floor about three feet in front of, and facing away from, the sample, and directed at an angle of about 30° to the floor. This maintains a circulatory motion of the air in the cold chamber without introducing too great a wind velocity at the surface of the samples. The air current at this point could not be detected with a vane anemometer, and various considerations (measurement of surface coefficient, etc.) lead to the conclusion that the air movement at the surface of the sample is so small that its effect on the thermal transmission can be neglected. The temperature of the air in the cold chamber is measured by means of a thermocouple placed about two feet in front of the centre of the sample.

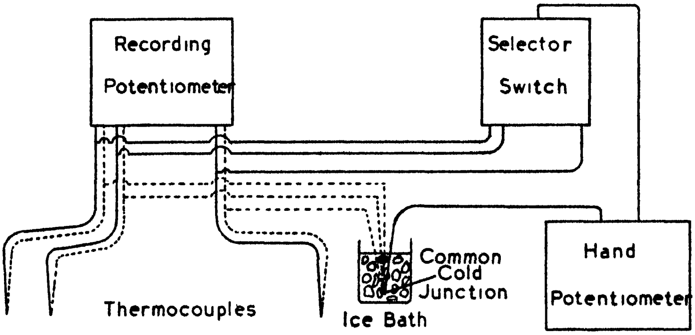

FIG. 3. *Diagram of thermocouple circuit.*

The wiring arrangement of the thermocouples is shown in Fig. 3. They may be connected either to a Leeds and Northrup Micromax recorder or to a Type K potentiometer. The recording instrument is used for preliminary measurements before the apparatus has reached equilibrium and serves also as a rough measurement once the steady state has been attained.

Method of Test

The section of wall of which the heat transmission is to be measured must be at least 6 ft. square so as to allow a 6 in. overlap when in position. The six inches of wall immediately surrounding the opening between cold chamber and hot-box guard-ring combination is covered with felt, so that this overlap is sufficient to prevent air infiltration into the guard-ring space, especially since the test sample is always pressed firmly against the felt. In order to facilitate the testing of heavy wall sections it was necessary to make some arrangement whereby the wall could easily be placed in position. This was accomplished by means of a specially constructed truck which runs on two rails laid in front of the opening to the hot-box, so that the wall when placed on the truck is exactly in position to be pressed home against the opening. Two movable rails outside the chamber are arranged to join the permanent rails through a door in the side of the chamber, and, when the wall has been placed on the truck by means of the laboratory crane, it can easily be pushed into position.

When the wall is in position it is essential that it be pressed firmly against not only the wall of the cold chamber but also the edge of the hot-box proper so as to prevent all possibility of air filtration between hot-box and guard-ring. The hot-box is suspended from the roof of the guard-ring by means of four iron rods, and it may be moved slightly in a horizontal plane. It was, therefore, a simple matter to arrange that there was no leakage between the edge of the hot-box and the wall. Four threaded iron rods were placed at the back of the box so that by turning them the hot-box was forced forward against the wall. In order to be certain that all parts of the edge of the hot-box are pressing firmly against the sample, spring contacts are arranged at the four corners in such a manner that when the box is in position electrical contact is made and a pilot lamp is lighted. These lamps and the spring contacts are shown in Fig. 2. A ¼-in. rubber tube is attached to the front edge of the hot-box to seal more tightly the contact with the sample.

From five to seven days are required for the measurement of the heat transmission of a sample. Three or four days are needed for the apparatus to reach equilibrium and to make the adjustments in the guard-ring current necessary to equalize the temperature in guard-ring and hot-box. During this period the temperatures are read on the recording potentiometer and the rheostats adjusted so as to equalize the temperatures. The final readings are taken by means of the hand potentiometer and these measurements are never made until the apparatus has been in equilibrium for at least 24 hr. In the case of thick heavy walls with a low conductance a longer time is necessary because the high heat capacity and low conductance result in a much slower approach to equilibrium, and therefore more time is required before it can be certain that the conditions are perfectly steady.

Once the temperature on the two sides of the wall and the power input to the hot-box are known, the heat transmission can be calculated from the following equation:—

$$U = \frac{Q}{A} \frac{1}{T_2 - T_1} ,$$

where U is the thermal transmission, Q the heat passing through an area A of the wall in one hour, and T_2 and T_1 are the temperatures of the air on the hot and cold side respectively. If Q is expressed in B.t.u's, A in sq. ft., and the temperatures in °F., then U is the number of B.t.u's passing through 1 sq. ft. of the wall in one hour, when the temperature difference between the air on the two sides of the wall is 1° F.

The quantity Q in this formula is given by the reading of the wattmeter measuring the electrical input to the hot-box proper.

The area A represents the area of the wall that faces the hot-box proper. There is some slight uncertainty in this quantity owing to the fact that the partition separating the hot-box and guard-ring is not infinitely thin. It tapers to a narrow edge where it touches the wall but this still has a width of approximately 0.25 in. The area of the hot-box used in computing the transmission is 9 12 sq. ft. This is the area delineated by the mid-section of the partition between hot-box and guard-ring. For T_2, the temperature of the air on the hot side of the wall, the mean of the four thermocouples in the hot-box is used. T_1 is given by the thermocouple in the cold chamber. There is a variation of about 0.5° F. in the temperature of the chamber during each cooling cycle owing to the lag of the thermostat. The thermocouple is read at the beginning and end of the run of the compressor, and the mean of these two readings is taken as the temperature of the cold chamber.

Comparison of Hot-box and Hot-plate

In order to check the performance of the hot-box, it was decided to measure the conductance of the same material in both the hot-box and the hot-plate apparatus. Since the results obtained with the hot-plate have proved satisfactory over several years, it follows that if the results obtained with the hot-box agree with those with the hot-plate then full reliance can be placed on measurements made in the hot-box. It is necessary to use some material that may be tested in both apparatus. The choice is rather limited since this material must be homogeneous and capable of being constructed into a sample 6 ft. square. In the end, two types of samples were used, the first being of fibreboard and the second of rock cork, a material manufactured from "loose rock wool combined in production with a waterproof binder, moulded into sheet form and baked". It was impossible to obtain these materials in single sheets of sufficient size, and thus the samples had to be built up from smaller sections. In the case of the fibreboard, the hot-box samples were manufactured from three pieces, the centre piece being 4 ft. wide so as to cover completely the hot-box proper. Three separate fibreboard samples were used: *A*, ordinary fibreboard 1 in. thick; *B*, similar to *A* but completely sealed with aluminum foil; *C*, fibreboard 2 in. thick, completely sealed with aluminum foil. The joints in the samples were staggered and cemented together to eliminate all possibility of air infiltration. The rock cork sample was constructed out of slabs of material 18 by 36 by 1½ in. The sample was made of double thickness, the slabs being cemented together with asphalt and all joints broken.

In order to compare the hot-box and hot-plate results it is necessary to measure in the hot-box, not the over-all transmission of the sample but the actual surface-to-surface conductance similar to that given by the hot-plate. To obtain this the surface temperatures of the hot-box samples must be known. This was determined by attaching thermocouples to the surfaces of the samples. There is always considerable doubt whether such thermocouples actually give the temperature of the free surface of the sample, as the mere fact of attaching the couple changes the nature of the surface in a slight degree. There are several methods of attaching such thermocouples. In some preliminary measurements the thermocouples were pasted on with gummed paper but subsequently a method of cementing them with Sherwin Williams Lacquer Cement was used. This cement was found to hold the couples—which could be flattened if necessary—firmly to the surface, and the difference between their temperature and the actual temperature of the surface is negligible. There is in this method a possibility that a closer approach to the surface temperature may be obtained than in the hot-plate, for in the latter the thermocouples are attached to the plates and not to the samples. It has long been known [cf. Van Dusen (8)] that there is a layer of air between the plates and the samples, and that there is a small temperature drop across this air space. In the hot-plate used for the present experiments this drop is practically negligible, as shown by some previous measurements (1). Nonetheless, as a check, the 1-in. fibreboard, hot-plate samples were tested with a ½-in. air space on each side, and the conductance was computed using temperatures obtained with thermocouples cemented on to the surfaces. The value of the conductance measured in this manner did not differ appreciably from that obtained under the usual conditions of test. This indicates that one is justified in comparing the surface-to-surface conductance as obtained in a hot-box by means of thermocouples attached to the surface with the ordinary hot-plate conductivities.

Results

The results for fibreboard sample *A* (1 in.) are given in Table I and shown graphically in Fig. 4. With the exception of three or four points, the hot-box results lie quite nicely on a straight line. The anomalous readings are scattered at considerable distances from the curve and the values are too much in error to be neglected. A possible cause of this discrepancy will be investigated later. The hot-plate measurements are shown as crosses on the same figure and the curve has been drawn to represent these results. This curve has been given a temperature coefficient of 0.0012, which is an average value for fibreboards [cf. C. D. Niven (2)]. The mass of the hot-box results agree nicely with this curve and are well within the variations shown in the hot-plate results.

TABLE I

SAMPLE A: 1 IN. FIBREBOARD

Temperature of cold surface, °F.	Temperature of warm surface, °F.	Mean temperature, °F.	Conductance, C. B.t u. per hr. per sq ft. per °F.
Hot-box tests			
10 0	76 0	43 0	0 341
14 0	73 5	43 7	0 372
16 2	72 8	44 5	0 390
15 8	79 3	47 5	0 373
17 1	78 1	47 6	0 360
25 8	85 4	55 6	0 388
20 9	90 9	55 9	0 384
21 0	90 9	56 0	0 389
20 6	92 2	56 4	0 411
22 7	94 7	58 7	0 385
29 7	98 6	64 1	0 394
31 4	101 2	66 3	0 393
22 2	115 4	68 8	0 396
44 7	98 6	71 7	0 404
49 4	118 4	83 9	0 423
Hot-plate tests			
27 0	79 4	53 2	0 388
30 5	87 2	58 9	0 383
30 5	87 9	59 2	0 385
*51 0	108 5	79 8	0 406
†27 5	85 5	56 5	0 420

**Tested with ¼ in air space on both sides of sample*

†Sample had been conditioned in cold chamber of hot-box and contained about 10% of moisture.

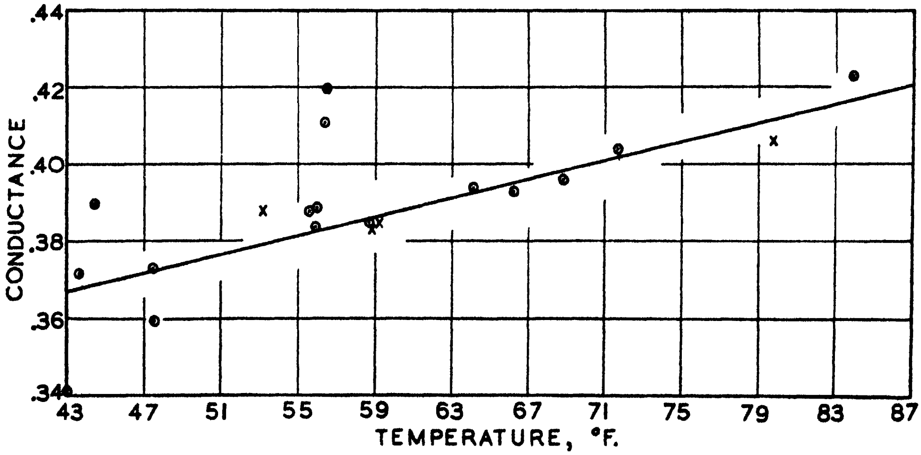

FIG. 4. *One-inch fibreboard.* O, *hot box;* X, *hot plate;* ⊗, *conditioned hot-plate.*

In searching for an explanation of the four points that are not within these limits, the influence of the moisture content of the samples immediately suggested itself. Fibreboard is, from its cellulosic nature, hygroscopic and adsorbs varying amounts of moisture depending on the relative humidity of the atmosphere with which it is in contact. Now it is a well known fact (2) that the thermal conductivity of fibreboard varies with the moisture content of the board. Thus the conductivity of certain samples has been found to increase from 0.34 in the dry condition to 0.36 when they contain 10% adsorbed moisture. Fibreboards will adsorb 10% of moisture by weight when exposed to a relative humidity of 70%. This then would be sufficient to explain the range of variation in the present results if the humidity conditions were not the same for the different tests.

During these tests no special provision was made to control the relative humidity or to condition the samples. It was originally felt that if both hot-plate and hot-box samples were allowed to come into equilibrium with the laboratory atmosphere, the conditions would be approximately equivalent. In this, however, the fact that changes in moisture content can occur during the course of a hot-box measurement was not taken into consideration. For although in the hot-plate the samples are practically enclosed and the test is of short duration (about one day), in the hot-box the conditions are quite otherwise. Here the surfaces of the sample are in contact with the atmosphere—on one side a warm atmosphere corresponding to room temperature and on the other a cold atmosphere corresponding to external winter conditions. The moisture content of the fibreboard will, during the test, assume a value and distribution so as to be in equilibrium with the relative humidities existing on both sides of it. These humidities will vary according to the conditions of the individual tests and might be widely different at different periods. The relative humidity in the cold chamber will, in general, tend to be high, depending as it does on the difference between the air temperature and the temperature of the cooling coils. The temperature in the hot-box will vary according to the temperature maintained therein and the temperature and relative humidity of the atmosphere in the laboratory. Under these conditions it is rather astonishing that the results have been as consistent as they are. As a partial test of the effect of the relative humidity on the measurements, the hot-plate samples were left standing in the cold chamber of the hot-box for two weeks. The temperature in the chamber during this time was 0° F. and at the end of this period the boards contained 10% of moisture. They were then immediately placed in the hot-plate and the thermal conductivity was measured. The value obtained was 0.420 at a mean temperature of 56.5° F. This result is shown as a cross in a circle in Fig. 4. At the end of the test the cold surfaces of the samples were quite wet and were frozen to the cold plates. The result must not be considered as an accurate figure for the conductivity, since some of the heat transfer must have been due to the migration of moisture. It does indicate, however, that changes in moisture content are quite sufficient to account for the scatter in the hot-box measurements.

If these considerations are correct and the changes in moisture content lead to variations in the results obtained with the hot-box, then to obtain a reliable check it is necessary to eliminate changes in the moisture content of the samples. There are two possible methods by which this can be done; either the fibreboard samples can be enclosed in some vapour proof material, so that there can be no gain or loss of moisture during the test; or some

TABLE II

SAMPLE B: 1 IN. FIBREBOARD, ALUMINIUM COVERED

Temperature of cold surface, °F.	Temperature of warm surface, °F.	Mean temperature, °F.	Conductance, *C*. B.t.u. per hr. per sq. ft. per °F.
Hot-box tests			
24.2	71.2	47.7	0.392
29.4	81.0	55.2	0.389
33.7	79.1	56.4	0.399
32.9	92.1	62.5	0.415
34.7	80.3	62.5	0.404
38.2	91.7	65.0	0.416
43.7	89.2	66.4	0.404
45.0	90.1	67.5	0.409
48.7	91.8	70.2	0.428
50.7	94.1	72.4	0.424
51.4	99.1	75.2	0.443
Hot-plate tests			
34.0	87.7	60.9	0.399
*29.1	85.9	57.5	0 379

**Samples cut from actual hot-box sample.*

TABLE III

SAMPLE C: 2 IN. FIBREBOARD, ALUMINIUM COVERED

Temperature of cold surface, °F.	Temperature of warm surface, °F.	Mean temperature, °F.	Conductance, *C*. B.t.u. per hr. per sq. ft. per °F.
Hot-box tests			
20.3	86.0	53.1	0.177
20.4	89.9	55.1	0.170
21.2	94.0	57.6	0.176
29.7	89.7	59.7	0.178
26.4	93.2	59.8	0.189
28.6	93.5	61.0	0.179
40.3	89.1	64.7	0.183
33.0	97.3	65.1	0.181
40.7	89.9	65.3	0.184
31.7	100.8	70.0	0 192
Hot-plate tests			
29.8	88.7	59.2	0.180

non-hygroscopic material can be used. These alternatives were tried. Fibreboard samples *B* and *C* were constructed and completely covered with aluminium foil, and, in addition, a conductimeter was constructed from rock cork, a material that is practically non-hygroscopic. The results from these tests are given in Tables II, III, and IV and depicted graphically in Figs. 5, 6, and 7.

TABLE IV

THREE-INCH ROCK CORK

Temperature of cold surface, °F.	Temperature of warm surface, °F.	Mean temperature, °F.	Conductance, *C*. B.t.u. per hr. per sq. ft. per °F.
Hot-box tests			
10.2	91.9	51.0	0.110
10.6	93.4	52.0	0.107
9.9	94.2	52.0	0.116
20.9	99.8	60.3	0.124
28.0	99.6	63.8	0.115
22.2	115.3	68.7	0.125
35.4	112.7	74.0	0.139
Hot-plate tests			
29.6	82.8	56.2	0 114

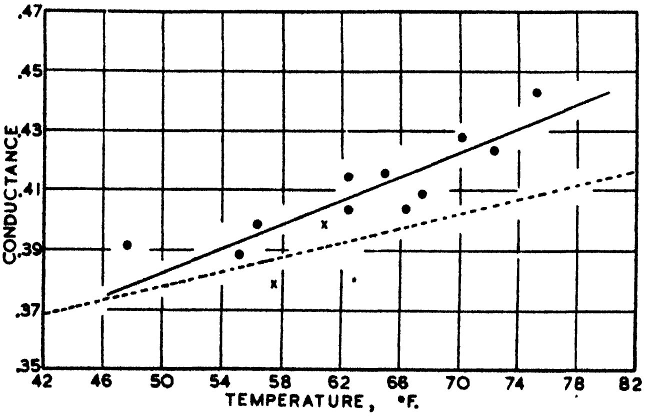

FIG. 5. *One-inch fibreboard, aluminium covered.* ⊙; *hot-box;* X, *hot-plate.*

The results obtained with the 1-in. fibreboard are unsatisfactory, since in this case the hot-box results are higher than those obtained with the hot-plate, and also show a greater temperature coefficient. The dotted line represents the results to be expected from hot-plate measurements. The aluminium foil was attached to these samples with a cold water paste and this, no doubt, accounts for the discrepancy. The samples were well sized but moisture from the plate must have entered them and caused the anomalous behaviour. It is interesting to note the increase in the temperature coefficient under these conditions, caused, most probably, by different moisture distributions resulting from different external temperatures. There is also considerable difference in the two hot-plate measurements; one of these (the smaller) was actually made on samples cut from the hot-box sample at the conclusion of the test in order to eliminate any local difference in the material comprising hot-box and hot-plate sample. The moisture content may also have something to do with this difference in hot-plate readings.

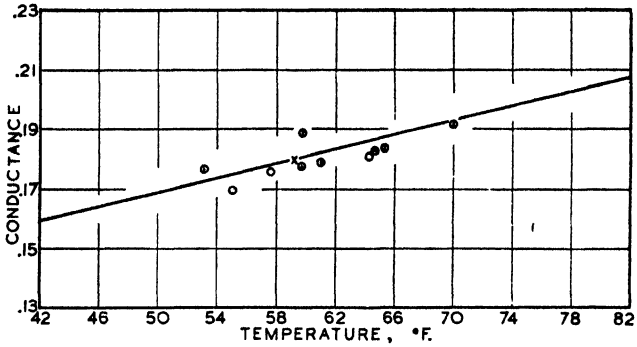

FIG. 6. *Two-inch fibreboard, aluminium covered.* ⊙, *hot-box;* X, *hot-plate.*

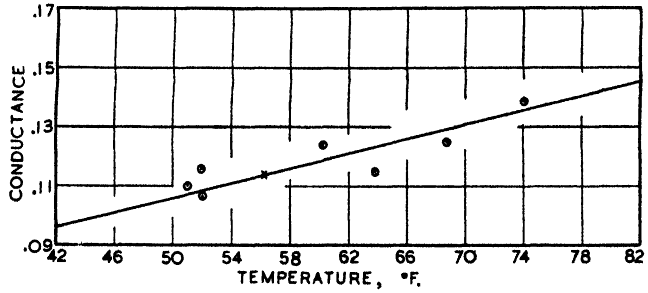

FIG. 7. *Rock cork.* ⊙, *hot-box;* X, *hot-plate.*

The results with both the 2-in. fibreboard and the rock cork are very satisfactory and the agreement between hot-box and hot-plate is as good as can be expected. The aluminium foil in the case of the 2-in. fibreboard was attached with asphalt and every precaution was taken to maintain the board in as dry a state as possible. The agreement shown by these results is such that, on the assumption that hot-plate measurements are accurate (and this has never been questioned), the worth of the hot-box as a test apparatus is completely established. The author feels, therefore, that the National Research Laboratories is entitled to proceed with the testing of walls in this apparatus and that full reliance can be placed in the results.

Acknowledgments

The author wishes to acknowledge his indebtedness to Dr. C. D. Niven of the National Research Laboratories, Ottawa, who designed the hot-box apparatus, superintended its construction, and furnished many valuable suggestions during these tests. He also would like to express his thanks for the work of C. St. Jacques, laboratory assistant, who carried out the manual work involved in the construction of the apparatus.

References

1. BABBITT, J. D. Can. J. Research, A, 16 : 82-87. 1938.
2. NIVEN, C. D. Can. J. Research, 7 : 115-130. 1932.
3. NIVEN, C. D. Can. J. Research, 9 : 146-152. 1933.
4. NIVEN, C. D. Can. J. Research, A, 13 : 16-18. 1935.
5. ROWLEY, F. B. Univ. Minn. Eng. Expt. Sta. Bull. 3. 1923.
6. ROWLEY, F. B. and ALGREN, A. B. Univ. Minn. Eng. Expt. Sta. Bull. 8. 1932.
7. ROWLEY, F. B. and ALGREN, A. B. Univ. Minn. Eng. Expt. Sta. Bull. 12. 1937.
8. VAN DUSEN, M. S. J. Am. Soc. Heating Ventilating Engrs. 26 : 625-656. 1920.

20 NOV. 19
LIBRAR

Canadian Journal of Research

Issued by The National Research Council of Canada

VOL. 17, SEC. A. SEPTEMBER, 1939 NUMBER 9

TRANSMISSION OF SOUND THROUGH THIN PLATES[1]

By F. H. Sanders[2]

Abstract

The transmission of high frequency sound through plates of brass and nickel has been studied for angles of incidence ranging from 0 to 70 degrees, using effective plate thicknesses varying from one-twentieth of a wave-length to one wave-length. In addition to strong transmissions in the region below the normal critical angle, very sharp and intense transmission maxima are observed at angles of incidence greatly in excess of the critical angle. These transmission maxima fall within three clearly defined angular regions: (i) angles between zero and the critical angle for longitudinal waves; (ii) angles between the critical angle for longitudinal waves and the critical angle for transverse waves; and (iii) angles above the critical angle for transverse waves. In Regions (i) and (ii) the observed data are in satisfactory agreement with a recent theory advanced bv Reissner, and good values of the elastic constants are obtained. By an extension of Lamb's theory for flexural vibrations in bars the results in Region (iii) can be interpreted.

Introduction

During the period 1921 to 1929, R. W. Boyle and his co-workers at the University of Alberta carried on an extensive series of experiments on the various aspects of the propagation of sound. In these experiments use was made of the relatively short sound waves obtainable at frequencies ranging from the audible region to some hundreds of kilocycles. In most cases excellent agreement between observed phenomena and classical sound theory was noted. This agreement was particularly marked in the case of the transmission and reflection of sound at normal incidence by plates of solid material immersed in a liquid. In accordance with Rayleigh's theory, it was found that, for normal incidence, maximum reflection occurred when the thickness of the plate was an odd number of quarter wave-lengths, whereas maximum transmission took place through plates an even number of quarter wave-lengths in thickness. When, however, observations were made with plates set at oblique incidence, a number of points were noted that could not be explained in terms of Rayleigh's theory for the general case of transmission of a plane longitudinal wave through a partition of finite thickness. With plates of thickness less than a wave-length, very large transmission ratios were noted at angles of incidence greatly in excess of the critical angle. A large number of observations were made and reported to the National Research Council, Canada, but never published.

---

[1] *Manuscript received June 3, 1939.*
Contribution from the Division of Physics, National Research Laboratories, Ottawa, Canada. Issued as N.R.C. No. 833.

[2] *Physicist, National Research Laboratories, Ottawa.*

In view of these interesting observations, to which the writer's attention was drawn by Dr. R. W. Boyle, it appeared that an investigation of the transmission of sound through thin plates, using modern equipment, would prove of considerable value. The earlier experiments referred to above were carried out by Boyle and Sproule (9) using a tank some fifteen feet in length and wave-lengths of a few centimetres. Measurements of the incident, transmitted, and reflected energies were made by the use of torsion balances. In the experiments to be described, wave-lengths of the order of one millimetre were used and the sound energies measured by means of the light-scattering properties of the sound field.

Since the beginning of this work the results of a study of the elastic properties of solids have been reported by A. Walti (10). He measured the sound energy transmitted through small sections of wedge-shaped plates of glass at frequencies of a few megacycles, using the scattering of light to determine the transmission ratios at various angles of incidence. By the application of a theory proposed by H. Reissner (6) he obtained excellent values for the elastic constants of glass. Walti's experiments were performed at effective plate thicknesses ranging from one-half to three wave-lengths, and all observed effects appear to be substantially in agreement with Reissner's theory. In the present investigation, plate thicknesses ranged from one-twentieth wave-length to one wave-length and strong transmissions similar to those noted by Boyle and Sproule were observed for angles of incidence much in excess of those studied by Walti.

Experimental

The experiments were carried out in a metal tank of dimensions 40 by 24 by 5 in., shown schematically in Fig. 1 (a). These relatively large dimensions were employed in order that reflections from the walls of the tank would be eliminated by absorption in the liquid medium. The source of ultrasonic vibrations was a circular X-cut quartz crystal, 38 mm. in diameter, excited by a push-pull oscillator at frequencies of 1.90, 3 18, 4.43 and 5.65 megacycles. The theoretical angle of divergence of the sound beam was very small, amounting to less than one degree at the lowest frequency employed. Bär (2) and others have pointed out that, because of transverse vibrations in the quartz, a circular or square crystal does not oscillate entirely as a simple piston-membrane, and, accordingly, the field near the crystal does not consist entirely of plane waves propagated in a direction normal to the face of the crystal. At a small distance from the source, however, it can be shown by means of the Hiedemann (1) method that the nature of the sound field approaches very closely to a simple plane wave. In the present work the plate whose transmissions were being studied was located at a distance of 15 cm. from the crystal, well beyond the doubtful region.

The plates studied were of nickel and brass, 2 in. wide by 4 in. long, and ranged in thickness from 0.004 to 0.025 in. for brass and from 0.001 to 0.025 in. for nickel. These plates, specially supplied through the kindness of Anaconda American Brass Limited, New Toronto, and Messrs. Peckovers

Limited, Toronto, were of uniform composition and had been similarly treated for the full range of thicknesses. In the experiments the plate being studied was rigidly held in a brass frame that could be set at any desired angle with respect to the direction of incidence of the sound beam. Angles of incidence could be read directly on an external scale to one-quarter of a degree.

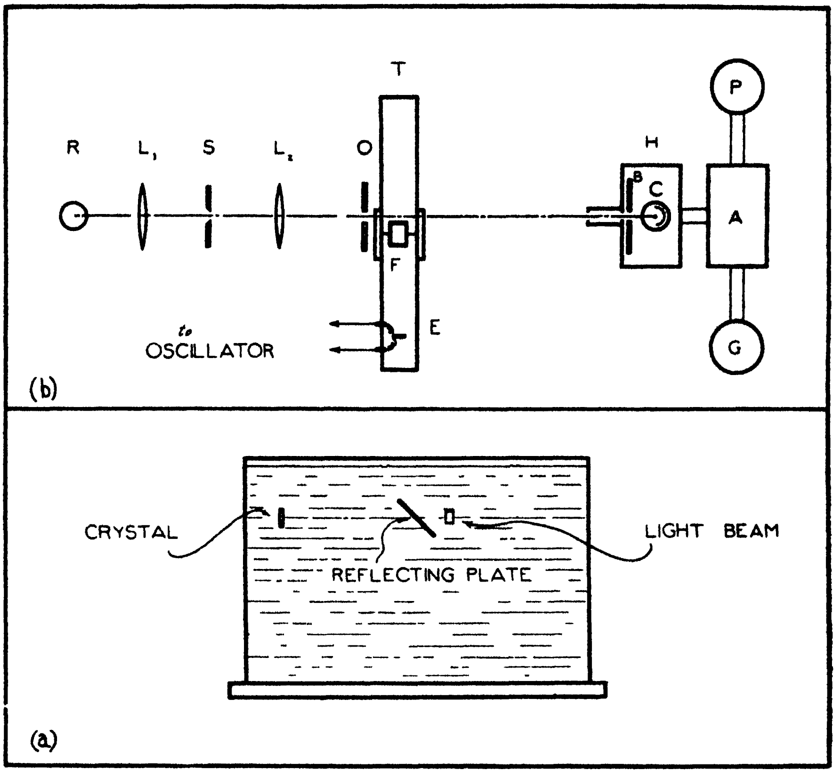

FIG. 1. *(a) Schematic diagram of tank showing relative positions of crystal, plate, a*

The intensities of the incident and transmitted sound energies were measured by the scattering of a beam of light that passed normally through the centre of the sound field at a distance of about five centimetres from the axis of the plate holder. Fig. 1 (b) shows the optical and electrical arrangements. Light from the ribbon-filament lamp, *R*, is focused by the lens L_1 on the spectrograph slit, *S*, and the image of this slit is in turn brought to a focus by the lens L_2 on the screen, *B*, some twelve feet distant. As the ratio of the distances BL_2 to L_2S was about 12 to 1, the deviation from parallelism of the light beam passing through the windows of the tank, *T*, was negligible. When the crystal, *E*, was excited by the oscillator, any sound energy passing through the plate at *F* produced scattering of the light beam, and the usual diffraction pattern appeared on the screen, *B*. This screen was provided with a slit of such dimensions that light from the central diffraction order only could fall on a photoelectric cell at *C*. A system of baffles in the box, *H*, housing the photocell shielded the latter so well that observations could be taken with moderate illumination in the room. The output of the photocell was amplified at *A* and carried to the galvanometer *G*. By the use of a potentiometric device, *P*, connected to the grid of the amplifier tube, the galvanometer could be used as a null instrument; this eliminated errors due to non-linearity of the amplifier characteristic. The photocell was a vacuum type having an excellent linear characteristic for the light intensities used.

The procedure in making the measurements was as follows:

With the frame, *F*, empty, so that the sound travelled unimpeded from the crystal to the detecting light beam, the potential exciting the crystal was varied in steps from zero to a value producing four or five diffraction orders. For each value of the applied voltage, measured as in earlier experiments (8), the intensity of the central light image was determined by means of the potentiometer, *P*. Since the intensity of the sound emitted by the crystal is directly proportional to the square of the applied voltage, this provided a calibration curve giving sound intensities in terms of potentiometer readings. The plate to be studied was next inserted in the frame and the incident sound intensity set at a convenient value. The intensity of the transmitted sound was then measured by means of the potentiometer for angles of incidence from zero to about 70 degrees. Since both incident and transmitted intensities were measured at the same point, it was unnecessary to make any correction for absorption in the liquid.

In order to guard against any change in the output of the oscillator, and thus in incident energy, the potentiometer reading was noted from time to time with the plate set parallel to the direction of incidence. As the ratio of potentiometer readings for this position, and for the case where the plate was removed, had previously been measured, any change in the output of the crystal could readily be observed and corrected.

It was found that, at most angles of incidence, practically no sound was transmitted by even the thinnest plates. At certain discrete angles, however, very intense transmissions were noted. By visual observation of the degree of light scattering it was possible to set the angle of incidence at the exact centre of a transmission peak so that maximum values of transmission could be observed. A complete study of both the intensity and location of the transmission peaks was made, at a frequency of 4.43 megacycles, using the brass plates. For brass at the other three frequencies and for nickel at all four frequencies only the location of the peaks, *i.e.*, the angle of incidence for maximum transmission, was measured, using the visual method. Because of the sensitivity of the optical method it was possible to reproduce all settings to one-half degree or better. As a further check on the locations of the transmission maxima, all measurements were carried out in four quadrants. This eliminated any error due to lack of parallelism of the plate and the external pointer indicating the angle of incidence.

The dimensions of the plates were such that, at the lowest frequency employed, the length was of the order of 50 wave-lengths, and the width, 25 wave-lengths. It thus appeared justifiable to regard all plates as effectively infinite in extent and to assume that only the thickness would have any effect on the location and intensity of the transmission maxima. As a further precaution however the frame, *F*, was replaced by one 4 by 6 in. in extent, and the locations of the transmission maxima were determined for a number of plate thicknesses. In all cases these maxima occurred at angles of incidence identical with those observed for the smaller plates.

The wavemeter used to measure the frequency was checked against equipment of the standard frequency laboratory of the National Research Laboratories, Ottawa, and found to be accurate to better than 0.1%.

Results and Discussion

Six typical curves *A*, *B*, *C*, *D*, *E* and *F*, indicating the results of the intensity measurements on brass plates at a frequency of 4.43 megacycles are shown in Fig. 2. The ratios of transmitted to incident energy are plotted as ordinates, and angles of incidence as abscissae. For a plate thickness of 0.102 mm.

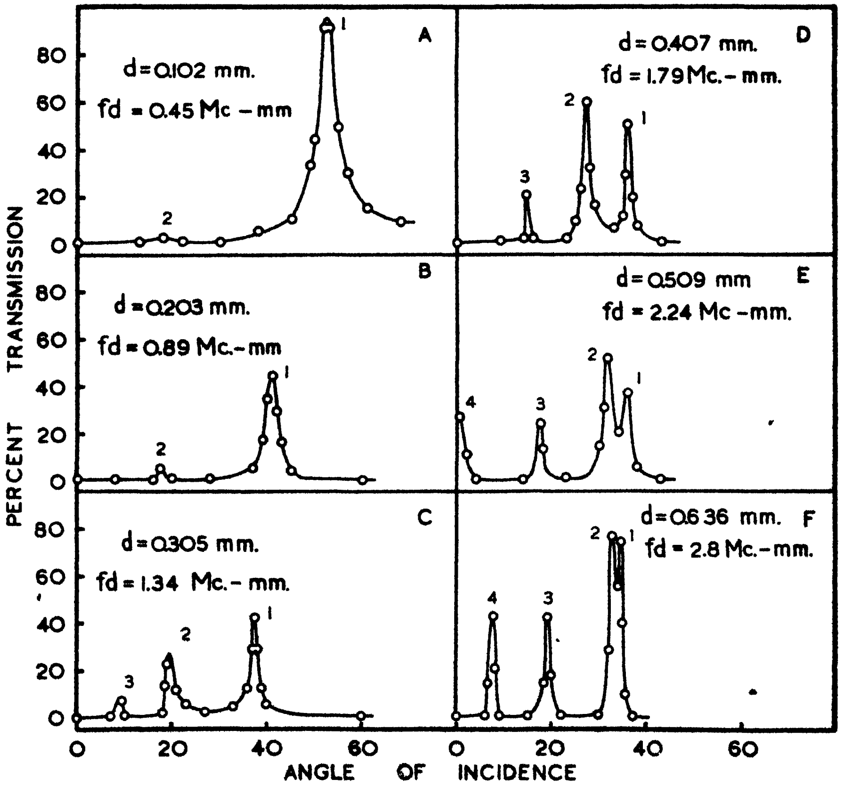

FIG. 2. *Six characteristic curves showing intensities of transmission maxima as a function of angle of incidence for brass plates at a frequency of 4.43 megacycles.*

(0.004 in.) a transmission ratio of 95% is observed at an angle of incidence of 52 degrees (peak 1), while a very faint transmission is observable at 18 degrees (peak 2). At a thickness of 0.203 mm. the position of peak 1 has moved to 41 degrees, while its intensity has dropped to about 45%. The location of peak 2 has not changed perceptibly but its intensity has increased. For a thickness of 0.305 mm. peak 1 has moved still farther to the left, its intensity changing only slightly, whereas peak 2 has moved slightly to the right with a marked increase in intensity. A new peak (3) has also appeared at an angle of incidence of 9 degrees. In the succeeding curves, *D*, *E* and *F*, peak 1 continues to move to smaller angles of incidence while peaks 2 and 3, and finally peak 4, move to larger values. In curve *F*, peaks 1 and 2 have approached each other so closely as to be barely resolvable.

Similar quantitative measurements of both location and intensity of the transmission maxima were carried out for the full range of brass plates, 0.004 to 0.025 in. in thickness. The change in location of the transmission maxima with varying thickness appeared to be of greater immediate interest and more readily adaptable to analysis than the actual magnitudes of the peaks. Measurements of location only were therefore continued on the same set of plates at frequencies of 1.90, 3.18, and 5.65 megacycles using the visual method of observation mentioned earlier.

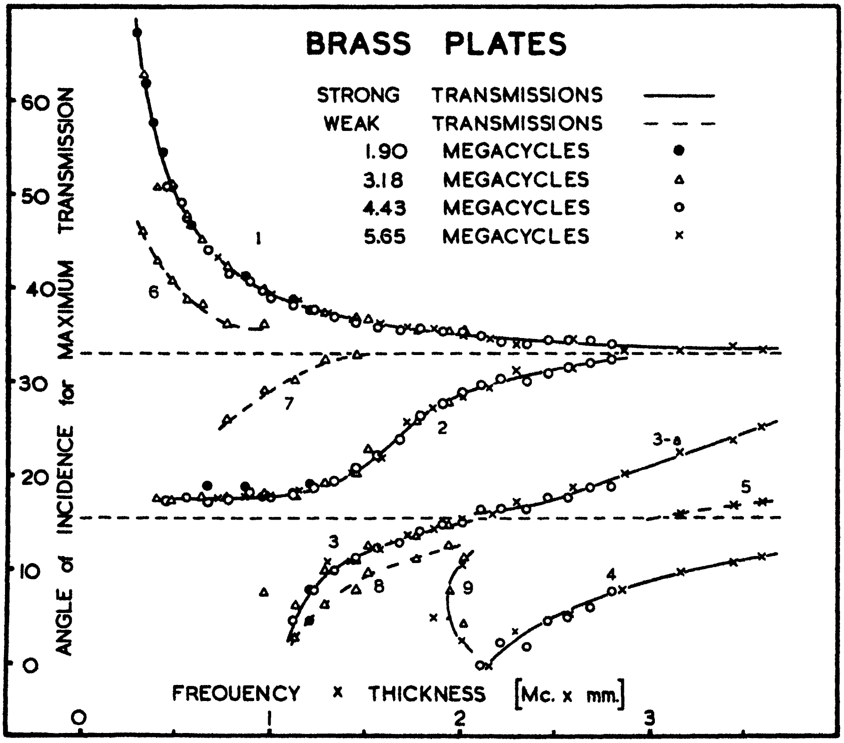

FIG. 3. *Angle of incidence at which maximum transmission occurs, as a function of the product frequency times thickness, for brass plates at four frequencies.*

Fig. 3 shows the results of the measurements on brass plates at all four frequencies. The angle of incidence at which maximum transmission occurs is plotted as a function of the product *fd*, frequency times thickness. From the excellent agreement among the data for different frequencies it is evident that the location of a given transmission maximum is determined by the product of these two quantities. The ratio of thickness to wave-length might have been used equally well for the abscissae, but, since this would have involved the velocity of sound in the metal, it appeared advisable to use the two directly measured quantities. The curves marked 1, 2, 3, 3*a*, and 4 give the locations of the peaks similarly numbered in Fig. 2. The remaining curves, 5, 6, 7, 8, and 9, correspond to maxima of very low intensity. While too weak to be measured accurately by the quantitative method, these peaks were readily detectable by the visual method and could be reproduced to the same accuracy as the stronger peaks. It is to be remarked that the major curves of Fig. 3 are identical in form with those obtained by Boyle and Sproule (9) with glass plates immersed in water.

Examination of these curves shows that they appear to fall into three angular regions. Curves 3, 4, 8, and 9 lie between 0 and about 16 degrees, Curves 2, 3*a*, 5, and 7 between 16 and about 34 degrees, and Curves 1 and 6 above 34 degrees. Now the velocity of longitudinal waves in an infinite medium is given by the expression

$$w_0\sqrt{\frac{1-\sigma}{(1+\sigma)(1-2\sigma)}}\,,$$

while the velocity of distortional or transverse waves is

$$w_0\sqrt{\frac{1}{2(1+\sigma)}}\,.$$

In these expressions σ is Poisson's ratio and w_0 is the velocity of longitudinal waves in a long rod. This velocity is a readily measurable quantity and is the value usually quoted in tables. While the values of σ and w_0 vary somewhat with the type of brass, the generally quoted values are 0.35 for σ and 3.4×10^5 cm. per sec. for w_0. The velocity of sound in the ethyl acetate used as the liquid medium in these investigations was measured experimentally by the Hiedemann (1) method and was found to be 1.15×10^5 cm. per sec. From the above figures the velocity of longitudinal waves in brass should be 4.3×10^5 cm. per sec., and that of transverse waves, 2.1×10^5 cm. per sec. These velocities correspond to critical angles of 15.5 and 33.2 degrees respectively. It is thus apparent that the three regions in Fig. 3 correspond to *(a)* angles between zero and the critical angle for longitudinal waves, *(b)* angles between the critical angle for longitudinal waves and that for transverse or distortional waves, and *(c)* angles greater than the critical angle for transverse waves. In the case of the nickel plates, the results for which are shown in Fig. 4, these three regions are again evident, the critical angles in this case being 11.5 and 23.3 degrees. In the next section the two lower regions will be considered together and the upper region separately. The regions *(a)*, *(b)*, and *(c)* will be referred to as B_I, B_{II}, and B_{III} respectively, in accordance with a theory proposed by Reissner (6), to be discussed shortly.

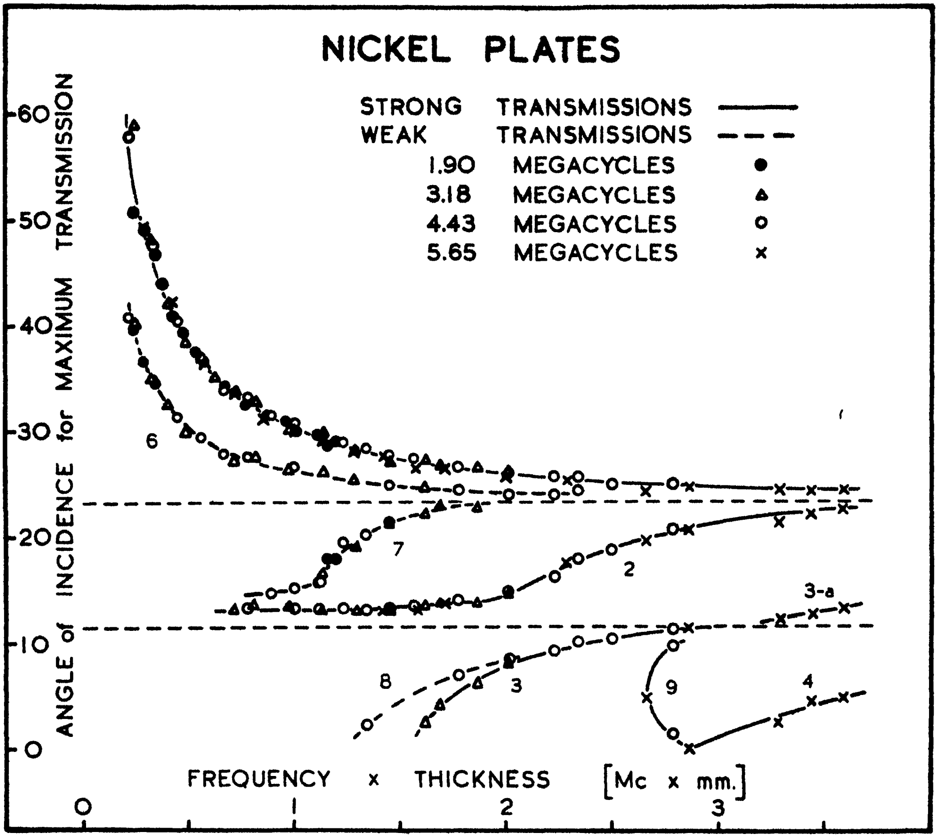

FIG. 4. *Angle of incidence at which maximum transmission occurs, as a function of the product frequency times thickness, for nickel plates at four frequencies.*

Results in Regions B_I and B_{II} below the Critical Angle for Transverse Waves

It will be noted that Curve 4 of Fig. 3 is the only one showing a definite transmission at normal incidence. Actually, an intense maximum of transmission was observed for $fd = 2.15 \times 10^6$ mm. cycles per sec. Rayleigh's theory for the transmission of a longitudinal wave through a plane partition of finite thickness gives the relation:

$$d \cos \theta_1 = \frac{m\lambda}{2}, \tag{1}$$

where d is plate thickness, θ_1 the angle of refraction, λ the wave-length of the disturbance in the plate, and m an integer. It has been shown by Boyle and Froman (3) that Equation (1) is quite valid for normal incidence. Placing m equal to unity and θ_1 equal to zero, results in a value for the velocity of the longitudinal waves of 4.30×10^5 cm. per sec., in good agreement with tabulated values. When applied to the case of oblique incidence, however, Equation (1) gives a curve which, although it begins at the point $fd = 2.15 \times 10^6$ and becomes asymptotic to the critical angle for longitudinal waves at large values of fd, deviates widely from Curve 4 of Fig. 3. Furthermore it does not account for the other maxima observed in region B_I.

H. Reissner (6) has quite recently developed a more complete theory for the transmission of sound through partitions of finite thickness at oblique incidence. He considers the case of a plane wave of sound incident on a solid partition with plane parallel walls, and assumes that internal friction may be neglected. The disturbance in the solid medium is regarded as consisting of two pairs of waves, one pair being longitudinal and the other transverse. Each pair is made up of the waves corresponding to the refracted ray and the ray reflected from the internal opposite wall. The system is regarded as a pair of waves because of the change in direction and phase at reflection. Developing this theory, Reissner obtains an expression for the transmission ratio, D, involving the angle of incidence, frequency, plate thickness, and the densities and sound velocities in both media. He shows that while, under appropriate conditions, total reflection of a sound wave entering an infinite medium may occur, this is not necessarily true for a wave entering a body of finite thickness.

In region B_I the application of Reissner's theory is extremely difficult when only the velocity of the longitudinal waves is known. The evaluation of the transverse velocity is much more readily performed in Region B_{II}. Walti (10) has described in detail two methods of determining the latter velocity in Region B_{II} from Reissner's theory. The first of these involves the determination of a certain value θ^* of the angle of incidence such that

$$\sin^2 \theta^* = \frac{w_1^2}{2w_r^2}, \tag{2}$$

where w_1 is the sound velocity in the liquid and w_r is the velocity of transverse waves in the solid. The assignment of this particular value to θ simplifies the computations very materially, so that w_r can readily be evaluated. In the second method described by Walti, w_r is evaluated from the angle of incidence to which the curves in Region B_{II} become asymptotic for large values of the product fd. For further details of these methods the reader is referred to Walti's paper.

The application of the above methods gave the value 2.12×10^5 cm. per sec. for the velocity of transverse waves in brass. With this value of w_r and the value 4.30×10^5 cm. per second for w_d, the velocity of longitudinal waves, obtained from the observations at normal incidence, Reissner's theory can be applied to the observations at any chosen angle of incidence. Actually the computation of the value of fd giving maximum transmission at any given angle of incidence is extremely laborious, even in Region B_{II}. Consequently, the theory was worked out completely for only a limited number of points. Table I lists a few angles of incidence with the corresponding values of *fd*, both observed and computed, for which maximum transmission should occur. It is seen that, in Region B_I below the critical angle for longitudinal waves, the agreement between theory and observation is extremely good. Theoretical points exist corresponding to Curves 3, 4, and 9. In Region B_{II} the agreement is good for points on Curves 2 and 3*a* not too near the critical angles, but a noticeable deviation occurs near each of these angles. This same deviation was observed by Walti. It is considerably beyond the limits of experimental error and would appear to indicate certain limitations to the theory. In general, however, the agreement is extremely satisfactory.

TABLE I

Angle of incidence for maximum transmission	Frequency × thickness					
	First maximum		Second maximum		Third maximum	
	Observed	Reissner	Observed	Reissner	Observed	Reissner
0°	1.05	1.03	2.14	2.15	2.14	2 15
5°	1.14	1.13	1.90	2.07	2 50	2 47
10°	1.32	1.32	1.96	1.96	3.16	3.09
—	—	—	—	—	—	—
18°	1.02	1.31	2.55	2.62		
20°	1.39	1.39	2.86	2.78		
22°	1.55	1.50	3.14	3.00		
24°	1.63	1.63	3.40	3 26		
26°	1.72	1.85	—	3.70		
28°	1.87	2.19	—	4.38		

TABLE II

ELASTIC CONSTANTS—OBSERVED AND TABULATED VALUES

—	Nickel		Brass	
	Observed	Tabulated	Observed	Tabulated
Velocity of longitudinal waves in an infinite medium	5.74×10^5		4.30×10^5	
Velocity of longitudinal waves in a rod	4.72×10^5	4.9×10^5	3.47×10^5	3.40×10^5
Velocity of transverse waves	2.90×10^5		2.12×10^5	
Density	8.80	8.8	8 62	8.4 to 8.7
Young's modulus	19.8×10^{11}	21.0×10^{11}	10.4×10^{11}	9.0×10^{11}
Modulus of rigidity	7.4×10^{11}	7.8×10^{11}	3.68×10^{11}	3.5×10^{11}
Poisson's ratio	0.328	0.30	0.339	0 35

The velocities of the longitudinal and transverse waves for nickel were determined in a similar manner and show satisfactory agreement with quoted values. Table II lists the various constants for both brass and nickel as obtained from the observed data, with the corresponding quoted values.

While the elastic constants naturally vary considerably for any given metal, depending on its past history, crystalline structure, etc., the tabulated values are given to indicate the general applicability of the method to the determination of elastic constants. The horizontal dotted lines in Figs. 3 and 4 indicate the critical angles corresponding to the observed velocities. It is clear that the curves fall naturally within the three regions defined by these critical angles.

Results in the Region above the Critical Angle for Transverse Waves.

As mentioned in the previous section, Reissner's theory does not require that total reflection should occur for any particular type of wave at the so-called critical angle. It was shown that in Region B_{II}, above the critical angle for longitudinal waves, the theory explained the observations in a quite satisfactory manner. When applied to Region B_{III}, however, Reissner's theory does not indicate the presence of transmission maxima at the large angles of incidence actually observed. Computations of the values of fd for which maximum transmission should occur at angles of 45 and 60 degrees gave no solutions beyond $fd = 0$, although quite intense transmissions were observed at these angles for values of fd near 0.50×10^6 mm. cycles per sec. It would thus appear probable that these transmissions are due to some type of vibration not considered in Reissner's analysis. The following explanation of the mechanism is proposed.

In Fig. 5 is shown a schematic representation of a plane longitudinal wave in a liquid, incident on a thin plate of solid material at an angle θ. This longitudinal wave will give rise to a mass flexural vibration of the plate, shown in a greatly exaggerated fashion by the dotted curve. Now, Lamb (5) has shown that flexural vibrations of this type move with a velocity that is not a constant for the material but varies with the frequency and the plate thickness. Accordingly, certain angles of incidence will exist for which a plate of thickness d, excited by a longitudinal wave of frequency f in a liquid, will vibrate flexurally with maximum amplitude and will re-transmit a longitudinal disturbance to the fluid. The wave-lengths of the disturbances in the two media will be related by the equation

$$\lambda_f = \lambda_1 \csc \theta \tag{3}$$

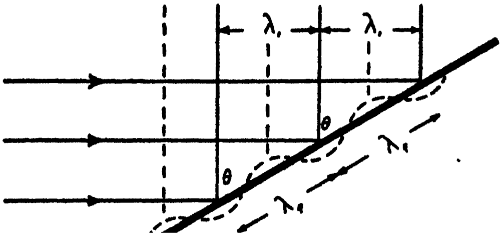

FIG. 5. *Schematic diagram of a plane longitudinal wave in a liquid, incident on a solid partition at an angle θ.*

and the velocities by

$$w_f = w_l \csc \theta \tag{4}$$

where w_l and λ_l refer to the liquid and w_f and λ_f to the solid. Lamb's theory for flexural vibrations, while developed for the case of a bar, can quite legitimately be applied† under the present experimental conditions, since the velocity of such a flexural vibration is not dependent on the width of the bar. The plate may be regarded as consisting of a series of strips, all vibrating with the same amplitude and phase, and each behaving as a bar of infinite length. For a bar of thickness d, Lamb gives the relation

$$w_f^2 = \frac{k^2\kappa^2}{1 + k^2\kappa^2} \frac{w_l^2}{w_0^2} \tag{5}$$

where κ is the radius of gyration of a section of the bar, equal to $d/\sqrt{12}$ for a rectangular bar of thickness d, k is $2\pi/\lambda_f$ and w_0 is a constant. Combining Equations (4) and (5) gives the relation:

$$\csc^2 \theta = \frac{\pi f d}{6 w_l^2} \left\{ \sqrt{\pi^2 f^2 d^2 + 12 w_0^2} - \pi f d \right\} \tag{6}$$

The only unknown quantity in Equation (6) is the constant w_0, and this, according to Lamb, should be the velocity of longitudinal waves in a thin rod. Equation (6) can be shown to give a curve similar to Curve 1 of Fig. 3. For relatively small values of fd the angle θ approaches 90 degrees, while, as fd increases indefinitely, θ approaches asymptotically to the value $\sin^{-1} w_l/w_0$. Equation (6) was applied to the observed data in Region B_{III} and the value of w_0 determined for a number of values of fd. If the theory outlined above were completely valid, w_0 should prove constant. Actually it was found that w_0 decreased consistently with increasing values of fd as shown in Fig. 6 which gives the values for w_0 obtained with brass plates. For small values of fd, w_0 approaches the velocity, $\sqrt{E/\rho}$, of longitudinal waves in a rod, while for large values of fd it approaches the velocity, $\sqrt{\mu/\rho}$, of transverse waves. E is Young's modulus, μ the modulus of rigidity, and ρ the density. This variation appears quite significant. In Lamb's derivation of Equation (5), it is shown that the stress on a section of a bent bar can be regarded as consisting of a transverse shearing force F and a bending moment M. Lamb considers only the case of a bar uniformly bent so that its axis becomes an arc of a circle. Under these conditions the shearing force F vanishes, and it is shown that the bending moment, M, is related to the curvature, R, by the expression:

$$M = \frac{E\omega\kappa^2}{R}, \tag{7}$$

ω being the area of an element of cross section and κ the radius of gyration of a section of the bar. It thus develops that the quantity w_0 in Equation (5) is determined by Young's modulus. When the product *fd* is small, the wave-length of the flexural disturbance is large compared with the thickness, and the experimental conditions should approach very closely to those imposed by Lamb's theory. That this is so is borne out by the manner in which the experimental values of w_0 approach $\sqrt{E/\rho}$ for small values of *fd* in Fig. 6. As *fd* increases, however, there is a considerable deviation from Lamb's conditions owing to the fact that the wave-length becomes comparable with the thickness. The shear forces, previously ignorable, now become very important and eventually become predominant, with the result that w_0 is determined by the modulus of rigidity rather than by Young's modulus. This is strongly supported by the definite manner in which the observed values of w_0 approach the value $\sqrt{\mu/\rho}$ for large values of *fd*.

---

† *This point has since been checked by observing the locations of transmission maxima for narrow strips ½ in. wide by 4 in. long. In all cases, for a given value of fd, transmission maxima occurred at angles identical with those observed with the original plates 2 in. wide by 4 in. long.*

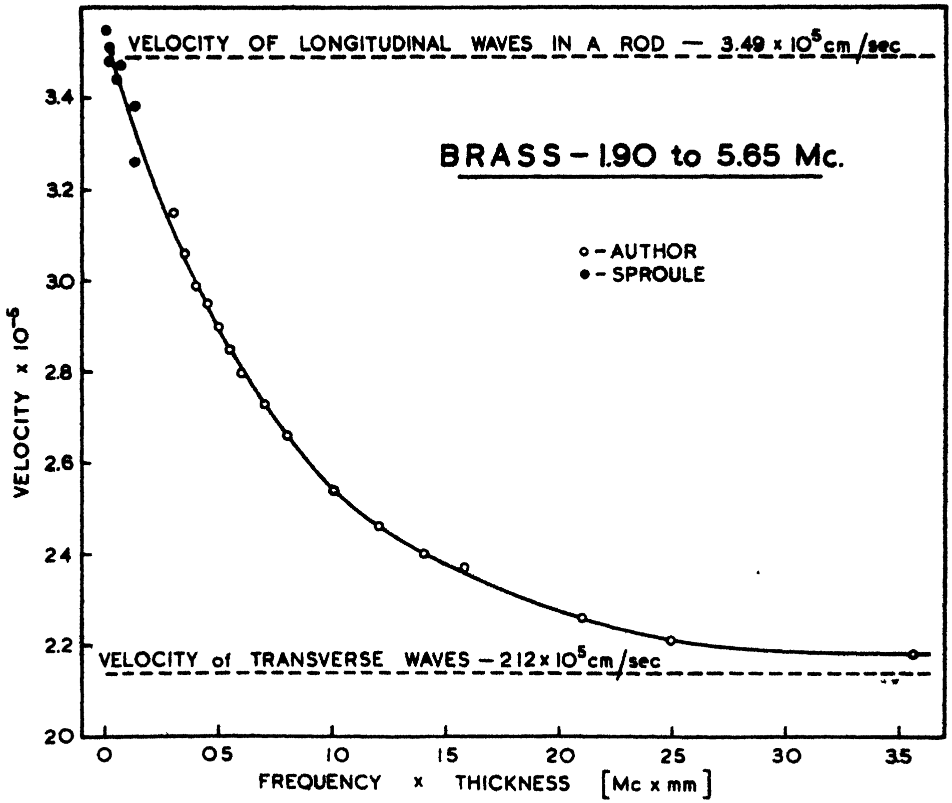

FIG. 6. *Observed values of the quantity w_0 in Equation (6) as a function of frequency times thickness for brass plates.*

The solid points in Fig. 6 at very small values of *fd* were obtained from some unpublished work performed by D. O. Sproule and kindly supplied by Dr. R. W. Boyle. In Sproule's experiments, the velocity of flexural waves in brass bars was measured at frequencies ranging from 12 to 70 kilocycles by the use of sand figures. The decrease in w_0 with increasing *fd* is quite evident and serves to corroborate the writer's observations.

The importance of shear forces at high frequencies has been pointed out by Field (4) in relation to the change in velocity of longitudinal waves in solid rods near the fundamental frequency of radial vibration. It was observed by Röhrich (7) that, near the frequency of radial resonance, the longitudinal velocity decreases rapidly, finally approaching and maintaining the velocity of the shear waves. Field has indicated how this phenomenon may be explained by proper consideration of the shear forces.

The theory outlined above was applied to the data obtained with nickel plates in Region B_{III}, and a similar variation in w_0 with fd was noted. In the case of nickel, w_0 varied from the value 4.7×10^5 cm. per sec. for fd small to 2.9×10^5 for fd very large. Comparison with Table II indicates that this variation is from the longitudinal to the transverse velocity, as in the case of brass.

Intensity Measurements

In Fig. 7 are shown the measured intensities of the transmission peaks corresponding to Curves 1, 2, 3, *3a*, and 4 of Fig. 3. All peaks should theoretically attain intensities of 100%. Actually it is seen that their intensities vary markedly with thickness. While the values appear rather scattered, particularly in the case of Curve 1, the observations were in most cases reproducible to within a few per cent, and it appears probable that the intensities fluctuate with plate thickness much more than the smooth curves would indicate. In view of the fact that present theoretical analyses are not sufficiently complete to account for deviations from total transmission, it did not

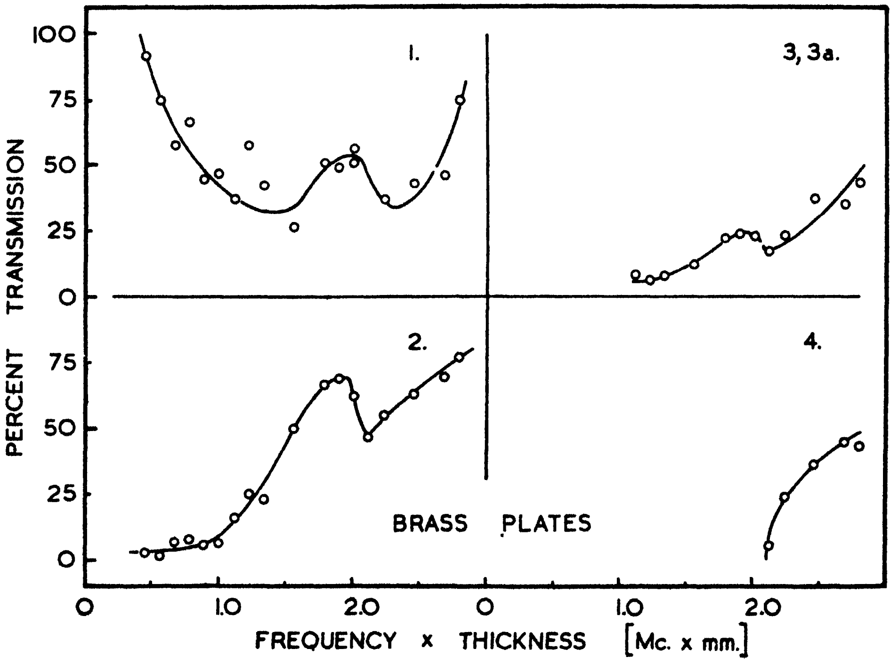

FIG. 7. *Intensities of the transmission maxima corresponding to Curves 1, 2, 3, 3a, and 4 of Fig. 3, as a function of the product frequency times thickness.*

appear necessary to pursue the intensity measurements beyond the one frequency of 4.43 megacycles.

Other Transmission Maxima

It will be noted that in Figs. 3 and 4 a number of dotted curves (5, 6, 7, and 8) appear. These curves corresponded to very weak transmissions of the order of a few per cent. In spite of their weakness, they were quite definite and consistent in their variation with frequency and thickness and were undoubtedly not due to reflections from the tank walls or to other extraneous effects. In the present state of the theory no explanation for their appearance can be given.

Summary and Conclusions

From the foregoing discussion it would appear that the transmission of sound through partitions of finite thickness can be explained in terms of three different types of vibration occurring in the solid medium. The first is the normal longitudinal or dilatational type of vibration; the second, the transverse or distortional type naturally accompanying the former in an infinite medium; and the third, a mass flexural vibration moving in a direction parallel to the boundaries of the partition. This third type is detectable only for effective plate thicknesses of one wave-length or less. At greater thicknesses the angle at which maximum transmission occurs approaches so closely to the critical angle for the transverse waves that the transmission maxima merge with those due to this type of vibration. Reissner's excellent theoretical analysis describes the phenomena due to the longitudinal and transverse vibrations in a very satisfactory manner, while the indicated extension of Lamb's theory for flexural vibrations appears to account for the transmissions at angles in excess of the critical angle for transverse waves.

Acknowledgments

The writer wishes to acknowledge his indebtedness to Dr. R. W. Boyle, Director of the Division of Physics and Electrical Engineering of the National Research Laboratories, Ottawa, who drew his attention to the earlier work at the University of Alberta and kindly supplied the information relating to it; and to Dr. D. O. Sproule for permission to use some of the results of his work. Thanks are also due to Dr. G. S. Field for many helpful suggestions and discussions, and to Mr. R. J. Smith who undertook most of the measurements.

References

1. Bachem, Ch., Hiedmann, E., and Asbach, H. R. Z. Physik, 87 : 734-737. 1934.
2. Bär, R. Helv. Phys. Acta, 10 : 311-322. 1937.
3. Boyle, R. W. and Froman, D. K. Can. J. Research, 1 : 405-424. 1929.
4. Field, G. S. Can. J. Research, 11 : 254-263. 1934.
5. Lamb, H. Dynamical theory of sound. 2nd ed. pp. 122-125. Edward Arnold & Co., London. 1925.
6. Reissner, H. Helv. Phys. Acta, 11 : 140-145. 1935.
7. Röhrich, K. Z. Physik, 73 : 813-832. 1932.
8. Sanders, F. H. Can. J. Research, A, 14 : 158-171. 1936.
9. Sproule, D. O. Acoustic reflections and transmissions by the ultrasonic method. Report to the National Research Council of Canada. April, 1929.
10. Walti, A. Helv. Phys. Acta, 11 : 113-139. 1938.

AN APPARATUS FOR THE DETECTION OF MAGNETIC MATERIALS[1]

By J. S. Johnson[2] and G. S. Field[2]

Abstract

An apparatus for the detection of magnetic materials is described which operates on continuous direct current instead of alternating current or interrupted direct current, as has been the case with previous detectors. This apparatus is highly sensitive and requires very little adjustment. Once installed it can be operated by a non-technician.

Introduction

Various types of metal detectors have been devised using either alternating current or interrupted direct current. They have the inherent difficulty of combining sensitivity with ease of adjustment. Most of these detectors are essentially balanced inductance bridges, and depend for their operation on the disturbance of the balance when a magnetic material is brought into the field of one of the inductance arms of the bridge.

The following is a description of a detector of magnetic materials which works on continuous direct current, and which, having once been set up properly, needs no further electrical adjustments. It was designed to be operated without the assistance of a technician, and to be sensitive enough to detect small objects such as a piece of hacksaw blade or small file.

Description

In Fig. 1, C_1, C_2, and C_3 are coaxial coils large enough to permit a man to walk through them; in the experimental model, 2 ft. 6 in. by 6 ft. 10 in. and spaced 9 in. apart.

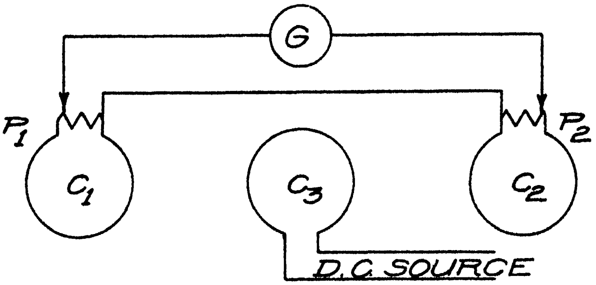

FIG 1. *Schematic diagram showing coil and galvanometer connections.*

Coil C_3 is energized by a direct current source and serves to produce a relatively high flux density through the pick-up coils, C_1 and C_2, which are connected in series opposition to a medium-sensitivity galvanometer. The potentiometers, P_1 and P_2, are necessary in order to balance out fluctuating magnetic fields, embracing both coils, which are present in most locations in ordinary buildings. Once adjusted, these potentiometers do not need to be touched unless other sources of magnetic disturbance are introduced into the vicinity of the coils.

---

[1] *Manuscript received May 16, 1939.*
Contribution from the Division of Physics and Electrical Engineering, National Research Laboratories, Ottawa, Canada. Issued as N.R.C. No 834.

[2] *Physicist, National Research Laboratories, Ottawa, Canada.*

In Fig. 2 is shown an arrangement that was used to translate the motion of the light beam from the galvanometer mirror to a relay-actuated detector service.

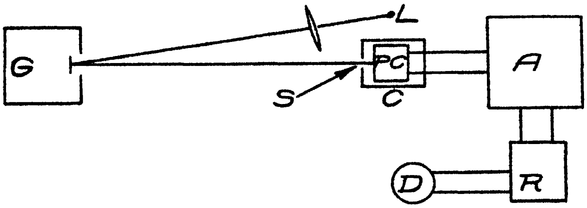

FIG. 2. *Schematic diagram showing optical system and connections to relay-actuated alarm device.*

Light from the source *L* passes through a long focus convex lens on to the mirror of the galvanometer, *G*. It is reflected from the mirror and brought to a focus on a slit, *S*, in a container, *C*, surrounding a photocell *P.C.* This cell is connected to an amplifier, *A*, whose output is used to operate a relay, *R*, and hence the alarm device, *D*.

Operation of Apparatus

When a piece of magnetic material is moved near one of the coils, C_1 or C_2, a change of the flux through the coil occurs. This causes a current to flow through the galvanometer. The resulting motion of the galvanometer mirror shifts the light beam from the slit, *S*, so that the light no longer falls on the photocell. The drop in current through the cell is amplified by *A*, and this causes the relay and hence the alarm device to operate.

In an actual installation the photocell and container should be mounted on a rack, so that a drift of the galvanometer mirror can be compensated for by moving the slit. In general this is the only adjustment of the apparatus required while it is in operation.

The metal in an ordinary shoe caused a large deflection of the galvanometer in the experimental model, and the apparatus was sufficiently sensitive to signal the passage of an ordinary hair pin through the coils.

Canadian Journal of Research

Issued by The National Research Council of Canada

VOL. 17, SEC. A. OCTOBER, 1939 NUMBER 10

LIBRARY

DISPERSION AND SELECTIVE ABSORPTION IN THE PROPAGATION OF ULTRASOUND IN FLUIDS CONTAINED IN TUBES[1]

By George S. Field[2]

Abstract

A consideration of the transmission of longitudinal sound waves down a fluid-filled tube indicates that anomalous dispersion of the wave may or may not occur at the frequency of radial resonance of the liquid column. In this paper it is shown that the criterion is the rigidity of the tube wall, as radial vibrations will ordinarily appear under the influence of a longitudinal sound wave only when the wall is able to respond appreciably to the alternating pressure occurring in the fluid.

Introduction

A few years ago a series of papers (1, 2, 3) was published dealing with the above subject, with particular reference to a number of experiments that had been carried out with various liquids, in containing tubes with walls both thick and thin in comparison with the radius of the tube. For thin-walled tubes a discontinuity in the curve of phase velocity plotted against frequency was always encountered, in the neighbourhood of the resonant radial frequency of the liquid column. For thick-walled tubes, however, there was no discontinuity, the phase velocity remaining substantially constant with frequency. At the time no explanation for the difference in behaviour of the two types of tubes was advanced. Recently, however, in a comparison of the above results with some data accumulated in connection with other work on air in a glass tube, the real importance of the containing tube has occurred to the author, and is set forth in what follows.

Experimental

In Fig. 1 are reprinted some curves and plotted data from one of the papers (1) in the series mentioned above. It will be observed that the discontinuity in phase velocity which occurs for thin-walled tubes (points plotted as circles) does not exist for the phase velocity of sound in thick-walled tubes (points plotted as crosses).

---

[1] *Manuscript received June 20, 1939.*
Contribution from the Division of Physics and Electrical Engineering, National Research Laboratories, Ottawa, Canada. Issued as N.R.C. No. 841.

[2] *Physicist, National Research Laboratories, Ottawa.*

In Fig. 2 are plotted experimental and calculated data for sound in air in a glass tube. In this case the sound was produced at one end of the tube by a high-frequency loud-speaker. Ammonium chloride fume was introduced into the tube and allowed to flocculate. It then collected at the nodal points and made phase velocity measurements possible. Unfortunately, at the time the sound intensity was not sufficiently great to produce useful flocculation at frequencies higher than about 7300 cycles per sec., so that phase velocity measurements were not made after that frequency had been reached.

The vertical broken line in Fig. 2 has been drawn at the frequency corresponding to that of radial resonance of the column of air in the tube. The curve of calculated phase velocities for higher frequencies becomes asymptotic to this line as shown. The curve of phase velocities for frequencies from zero to 24,700 cycles is almost a straight line for most of its length. It drops to the frequency axis at 24,700 cycles, which is the frequency of radial resonance in the wall of the containing tube. .

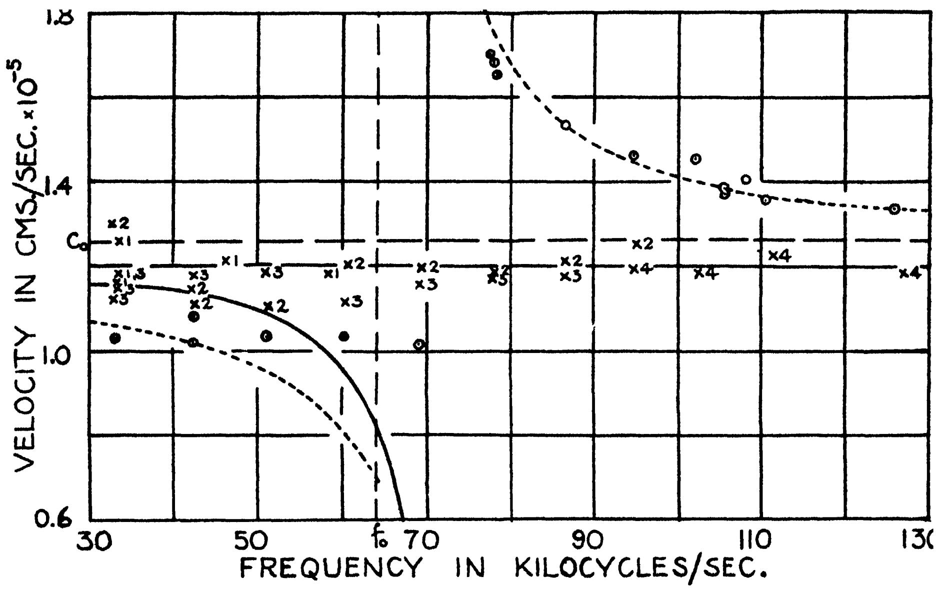

FIG. 1. *Curves showing influence of wall thickness on phase velocity. Naphtha in glass tubes of internal diameter 1.9 cm.: wall thickness, 1.2 mm.; points plotted as circles; wall thickness, 3.3 mm.; points plotted as crosses. The readings were taken on different days, as indicated by the numerals alongside the crosses. The dotted lines represent calculated phase velocities for the thin-walled tube. The solid line is for the thick-walled tube for frequencies below the resonant radial frequency (f_0) in the column of liquid. c_0 is the velocity of sound in an unconfined volume of naphtha.*

Discussion

At low frequencies the phase velocity of the longitudinal wave in a tube of liquid or gas depends to a very great extent on the rigidity or stiffness of the tube wall. When the acoustic resistance (ρc) of the wall material is not too great compared with the acoustic resistance of the fluid in the tube, or when the wall is very thin, the wall will vibrate with a fairly high amplitude as the result of the alternating pressure in the fluid within. There is a correspondingly great radial vibration of the fluid, and a diminution of the phase velocity of the longitudinal wave progressing down the tube. The theoretical phase velocity drops more and more as the frequency of radial vibration of the tube wall is approached, and eventually goes to zero as this frequency is finally reached. When the tube wall is very rigid, either through its material having comparatively high acoustic resistance or because it is quite thick, its radial motion is very slight; there is only a feeble radial vibration in the fluid column, and the phase velocity of the longitudinal wave is very little different from that of the ordinary plane wave. In fact, in this case the quantity α [see Ref. (2), page 140] is practically equal to zero, and the vibration described by the velocity potential,

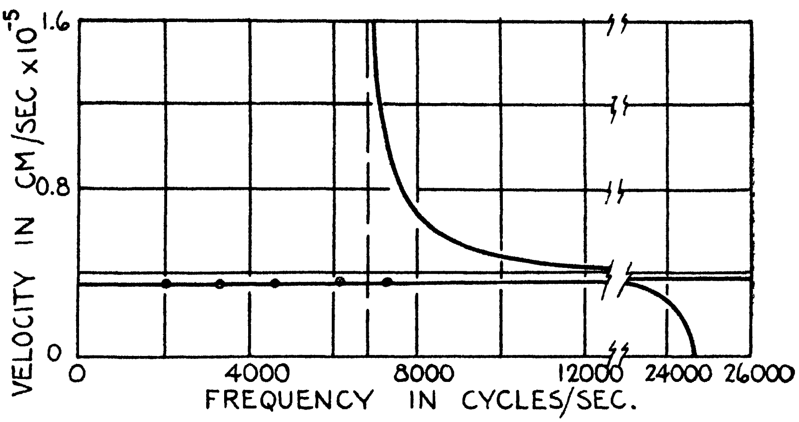

FIG. 2. *Curves showing calculated phase velocities of sound in air in a glass tube of internal diameter 6.2 cm. and wall thickness 1.7 mm. The circles are experimental points.*

$$\phi = AI_0(\alpha r)e^{i\omega(t-z/c_1)*}$$

degenerates to a plane wave, since $I_0(0) = 1$. The longitudinal vibration in the fluid has then a wave velocity independent of frequency.

In Fig. 1 is plotted as a solid line the calculated phase velocity at low frequencies for naphtha in the thick-walled glass tube mentioned under the figure. At 30 kilocycles the calculated velocity of 1.16×10^5 cm. per sec. is slightly lower than the plane wave value of 1.26×10^5 cm. per sec. It will be observed that instead of dropping as the frequency increased, the experimental values remained approximately the same. The theoretical curve, however, is based on equations that neglect the internal friction of the tube wall, and which lead to a very high amplitude of motion at the resonance frequency of the wall. The writer's previous experiments [see Ref. (3) Figs. 1 and 2, and Fig. 1, this paper] have shown that even when a diminution in phase velocity at low frequencies does occur and there is apparently a fairly strong radial vibration in the liquid [see also Ref. (3) Fig. 5 *(a)*], there is no very great drop in phase velocity near the resonant radial frequency of the wall. This indicates that the internal friction in the wall is sufficient to inhibit any large increase in radial amplitude of the wall vibration at or near this resonance frequency. Therefore, for the case of the thick-walled tube, it is not surprising that the phase velocity did not change with frequency. In fact, the wave probably remained essentially plane.

---

* *Ref. (2), Equation 37.*

There is still to be considered, however, the reason for the apparently complete absence of the type of vibration expected to occur just above the absorption band and given by the velocity potential,

$$\phi = AJ_0(kr)e^{i\omega(t-z/c_1)}*.$$

That this vibration was absent for the tube with thick walls is assumed by the lack of high phase velocities at frequencies above that of the calculated radial resonant frequency for the column of liquid.

Here again, the lack of a strong radial motion of the tube wall is probably the explanation. For a tube wall that is relatively thin, it is impossible to propagate a longitudinal wave without the wall "giving" and leading to a radial motion of the particles of fluid. This means that the wave is no longer plane and is given by one or the other of the velocity potentials quoted in this paper, the one which is favoured depending on whether the frequency is above or below the resonant radial frequency of the liquid column. When the fluid is contained in a tube with a thick wall or one having a high acoustic resistance compared with that of the fluid, however, the radial motion of the wall is very slight, and a plane wave is the most easily produced. There is then no variation in phase velocity with frequency for the longitudinal wave in the tube.

The wave given by the velocity potential,

$$\phi = AJ_0(kr)e^{i\omega(t-z/c_1)},$$

may, of course, still be set up in the tube, as such a wave does not definitely require a motion of the tube wall. In other words, this type of wave can exist either with or without a radial motion of the wall, although a plane wave requires that the wall must not move. With a rigid wall, however, this vibration requires to be excited by a special apparatus at the end of the tube, as has been pointed out in a recent paper (4). With ordinary driving apparatus, therefore, such as was used in the previous experiments, this vibration occurred only when the experimental tube had a thin wall.

---

* *Ref. (2), Equation 31.*

Conclusions

For a fluid contained in a tube having a wall either thick or of a material having a high acoustic resistance compared with that of the fluid, the longitudinal wave that will be produced in the fluid by an ordinary driving apparatus at one end of the tube will be plane. If, however, the wall is essentially nonrigid, the longitudinal wave will not be plane, strong radial vibrations will occur, and as a result the longitudinal wave will progress only with difficulty when its frequency is near to that of the resonant radial vibration of the column of fluid.

References

1. BOYLE, R. W., FROMAN, D. K., and FIELD, G. S. Can. J. Research, 6 : 102-118. 1932.
2. FIELD, G. S. Can. J. Research, 5 : 131-148. 1931.
3. FIELD, G. S. and BOYLE, R. W. Can. J. Research, 6 : 192-202. 1932.
4. HARTIG, HENRY E. and SWANSON, CARL E. Phys. Rev. 54 : 618-626. 1938.

MEASUREMENT OF SMALL OPTICAL ACTIVITIES WITH THE QUARTZ CRYSTAL LIGHT MODULATOR[1]

By D. W. R. McKinley[2]

Abstract

An experimental procedure is described for using the quartz crystal light modulator as an instrument for measuring very small optical rotations of the plane of polarization. The accuracy of the measurement is of the order of 10 sec. of arc, and the method is capable of still greater precision.

An elementary analysis of the crystal behaviour explains the fundamental and second harmonic components of light intensity present in the modulated beam of light.

In a previous paper (2) it was pointed out that optimum light modulation effects occur when light is passed through a vibrating quartz crystal in the direction of the optical axis. A special 49°-cut* crystal was adopted, because it satisfied this requirement in addition to possessing several other advantageous features. In this report some further experiments are described, an attempt is made to explain the results by an elementary analysis of the crystal action, and the technique is applied to the measurement of small optical activities.

The experiment may be arranged as shown in Fig. 1. Light from a pointolite source is polarized by the Nicol prism, N_1, (in most of this work Polaroids have been substituted for the Nicols with equal success) and is then focused on the crystal aperture by means of the lens, L_1. The crystal is set at the focus of a second lens, L_2, and is so inclined that the beam of light passes through nearly parallel to the optic axis. The light emerging from L_2 will traverse any intervening medium, X, in an approximately parallel beam. After passage through a second Nicol, N_2, the light is finally focused on a high vacuum photocell, P.

The photocell circuit, C, may be tuned either to the fundamental frequency of the crystal or to twice that frequency. The fundamental frequencies of the crystals used in these experiments were in the neighbourhood of 4 megacycles per second, and the crystals were excited at their fundamental frequencies only. The amplifier-detector system following the photocell comprises, in effect, the radio-frequency, intermediate frequency, and second detector

[1] *Manuscript received June 30, 1939.*

Contribution from the McLennan Laboratory, Department of Physics, University of Toronto, Toronto, Canada. Part of this work was undertaken at the University of Toronto as an assisted research under the National Research Council of Canada.

[2] *Physicist, National Research Laboratories, Ottawa, Canada.*

---

* *W. G. Cady has suggested that the convention regarding the orientation of the crystallographic axes in quartz be given, since the system used by Lack in his work on these crystals differs from that employed by Voigt. Lack et al. (1) state that for a rotation about the electric axis a positive angle is that formed by a clockwise rotation of the optic axis of the crystal when the electrically positive face (determined by a squeeze) is up. For a left-handed crystal a positive angle is in a counterclockwise direction. The inclination of the optic axis to the face of the crystals used in these experiments is minus 49° by this convention.*

sections of a standard high-frequency superheterodyne radio receiver. The milliammeter and galvanometer are placed in the plate circuit of a vacuum tube voltmeter connected across the resistor of the diode detector.

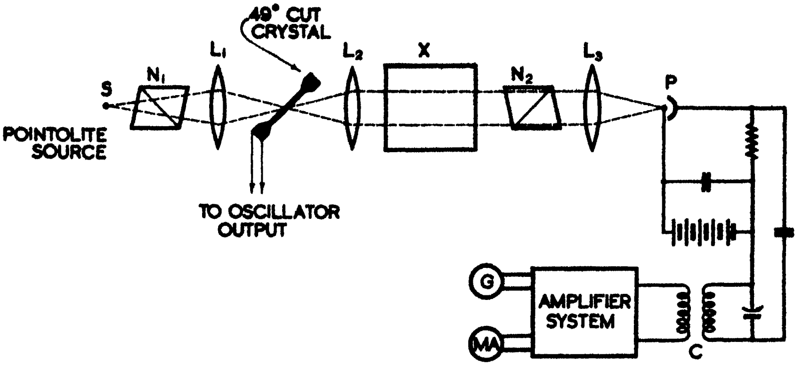

FIG. 1 *Schematic diagram.*

Let us first consider the arrangement of Fig. 1 but with no optically active medium at X. The principal plane of the first Nicol should always be set so that the light vibrations are executed in the plane of incidence, referred to the crystal faces. Then N_2 is rotated until the light intensity becomes a minimum, which will occur when the Nicols are nearly perpendicular. If the crystal is now excited at its fundamental frequency, light passes through N_2 in flashes. These light flashes falling on the photocell cause an alternating voltage to be developed across the circuit C. The galvanometer readings are proportional to this voltage.

In the preliminary experiments the second Nicol was rotated and the galvanometer readings were taken for the various settings of N_2. One set of observations was obtained in this manner with the photocell tuned to the crystal frequency, and another set with the photocell tuned to twice the crystal frequency. No galvanometer indications could be observed with the photocell circuit tuned to any other frequency, including higher harmonics of the crystal frequency. In all cases, of course, the crystal was driven at its fundamental frequency only.

In Fig. 2 the dotted curve represents the first case when the photocell was tuned to the fundamental, and the solid curve shows the results obtained with the photocell tuned to the second harmonic. There was not inconsiderable difficulty encountered in adequately shielding the receiving apparatus from direct electromagnetic pick-up from the crystal oscillator when the receiver was tuned to the crystal frequency. As a consequence the dotted curve shown does not give a reliable indication of the amplitudes, but it is useful in determining positions of zero response. However, it was possible to shield the equipment sufficiently well to eliminate all trace of stray pick-up when the receiver was tuned to the second harmonic. As will be shown, the theoretical considerations indicate that either fundamental or second harmonic operation should be equally useful, but in practice the latter is greatly to be preferred.

From a consideration of the solid curve, it is seen that, if the vacuum tube voltmeter reading observed when the Nicols are crossed is represented by V, then that obtained with the Nicols parallel is slightly higher, or about $1.25\ V$. Consequently, for certain applications in which maximum intensity of the modulated light is important, the crystal system should be operated with the Nicols in the parallel position. This practice was followed in an experiment on the velocity of light carried out at the McLennan Laboratory, University of Toronto.

If N_2 is removed entirely, the voltage across the photocell drops to about $0.8\ V$, and if both Nicols are removed the resultant response drops to about $0.1 V$, as might be expected since the crystal is now behaving merely as a diffracting body, with additional polarizing effects produced at the inclined faces.

As N_2 is rotated, the phase of the modulated light beam suddenly changes by 180° at each null point. This was easily demonstrated by connecting one pair of plates of a cathode ray oscillograph across the second detector input, and applying some voltage directly from the crystal oscillator to the other pair of plates. The resultant pattern showed that the phase reversed at each null point of the curves of Fig. 2.

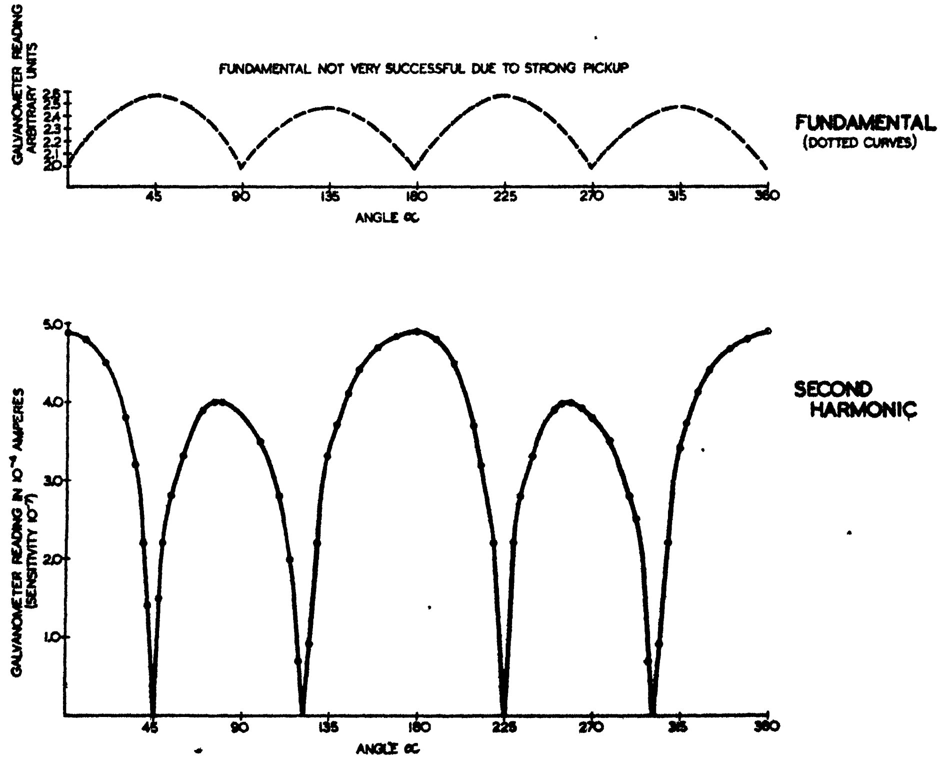

FIG. 2. *Curves showing galvanometer readings plotted against the angle α between the principal planes of the polarising and analysing Nicols.*

The action of a vibrating medium on a beam of light passing through it may be adequately explained in the general case by the theory of diffraction. However, it seems that in the particular case where light is passing along the optic axis, the optical activity of the quartz masks the diffraction patterns normally predicted. In fact, the optical activity here appears to play the more important part in the modulation of light, and the analysis of the experimental results is simplified accordingly.

Suppose the assumption is made that the plane of polarization of the light beam as it emerges from the crystal is dynamically rotated about its initial position, and that the light remains plane polarized to a large extent. Then the periodic angular change of the effective plane of polarization may be represented by $\theta_0 \sin \omega t$, where $\omega = 2\pi f$ and $f =$ the crystal frequency. The intensity of light transmitted through N_2 will be,

$$I = I_0 \cos^2(\alpha - \theta_0 \sin \omega t) \tag{1}$$

where α is the angle between N_2 and N_1, N_1 remaining fixed. That is,

$$\begin{aligned} I &= \frac{I_0}{2}\Big[1 + \cos 2(\alpha - \theta_0 \sin \omega t)\Big] \\ &= \frac{I_0}{2}\Big[1 + \cos 2\alpha \cos (2\theta_0 \sin \omega t) + \sin 2\alpha \sin (2\theta_0 \sin \omega t)\Big] \end{aligned} \tag{2}$$

When the crystal is being operated within safe limits the amplitude of the dynamic rotation may be assumed to be small. Then, for $2\theta_0 < \frac{\pi}{2}$ the term, $\sin 2\alpha \sin (2\theta_0 \sin \omega t)$, represents an alternating light intensity of amplitude $\sin 2\alpha$ and effective frequency $\frac{\omega}{2\pi}$. The term $\cos 2\alpha \cos (2\theta_0 \sin \omega t)$ represents an alternating component of amplitude $\cos 2\alpha$ and effective frequency $\frac{\omega}{\pi}$. This follows by considering that the cosine of a negative angle between 0 and $\frac{\pi}{2}$ remains positive, so that the cosine term has two maxima and two minima per period of the crystal, $T = \frac{2\pi}{\omega}$, whereas the sine term has but one maximum and one minimum in the same time interval.

For a given value of α the receiving system averages the oscillating value of the light intensity. With the photocell tuned to frequency $\frac{\omega}{2\pi}$ the component $\sin (2\theta_0 \sin \omega t)$ alone will affect the detector. Let its average value be A_1. With the system tuned to the second harmonic the term $\cos(2\theta_0 \sin \omega t)$ alone will be averaged, with value A_2, say. The amplitude of these average values is determined by the factor containing α, so the two cases may be written,

$$I_1 = A_1 |\sin 2\alpha| \tag{3}$$

for the fundamental frequency, and,

$$I_2 = A_2 |\cos 2\alpha| \tag{4}$$

for the second harmonic frequency, and in each case the absolute value is written because of the phase change of π at the null points; the light intensity never becomes negative.

Equation (3) corresponds to the dotted curve of Fig. 2, and Equation (4) to the solid curve. It will be noticed that the zeros of modulated light intensity on the solid curve vary slightly from the 135° and 315° positions of N_2. This is due to the statical rotation of the plane of polarization in the quartz slab, which has an effective optical thickness of 0.8 mm., so that the average statical rotation for white light is around 12° to 15°. The deeper modulation obtainable for the values of 0° and 180° might possibly be explained by the lessened colour absorption of the Polaroids in the parallel position, though the exact reason is not immediately apparent.

Applications

In some investigations it is desirable to have two beams of modulated light of the same frequency but with a phase difference of π. This has usually been accomplished by dividing the beam after it has passed through N_2 and permitting one of the resultant beams to traverse a path which is one-half wave-length longer than the other (at the modulation frequency, not the actual frequency, of the light). Equation (3), or Equation (4), suggests that two such beams may be obtained by dividing the beam immediately after it emerges from the crystal and then placing an analyzing Polaroid in each of the beams, one Polaroid being parallel to the polarizer and the other perpendicular to it.

Another and more interesting application is suggested by Equation (3) in the neighbourhood of 0°, 90°, 180°, and 270°; or by Equation (4) near 45°, 135°, 225°, or 315°. In the latter case the empirical values are 45.0°, 122.5°, 225.0°, and 302.5°. Near these points the curves drop very steeply, and a small angular rotation of N_2 produces a large change in the photocell response. With the radio receiver available in this research a change in the galvanometer reading of 1×10^{-7} amp. could be easily detected. As the maxima are of the order of 5×10^{-4} amp., this corresponds to an accuracy of 1 part in 5000 over a range of 45°. If the total angular variation is small one can work on the steep portion of the curve where the accuracy is much greater; for example, the error is 1 part in 2500 for a range of 5°, if the 5° are covered near one of the null points, and this corresponds to an angular error of only 8 to 10 sec. of arc. Thus the arrangement provides a sensitive device for measuring small optical rotations in any other medium which may be placed at X in Fig. 1.

Sugar solutions were made up to test the accuracy of the apparatus. The experimental results agreed within 20 sec. of the calculated values for solutions whose average rotatory power for white light ranged from 1.5 min. to 2°. Two methods of obtaining the experimental values were followed. In the first, the galvanometer curve was calibrated in terms of the angle change of the second Polaroid, which was mounted on a micrometer goniometer table, and the galvanometer readings were observed before and after addition of sugar to the water cell. In the second method, the position of N_2 for zero response was noted, then the sugar solution cell was inserted and the new position of N_2 for zero response was observed.

The first method incurs the smaller error because the instrument is operating entirely on the steep portion of the curve, and this procedure is to be preferred in investigations of the Faraday effect, for example, in which the medium is always present at X and no change occurs in the absorption of light. If the medium under test is strongly absorbing and if a correction for the absorption cannot be readily determined, then the second method should be employed, though it is somewhat less accurate because the actual minimum is not a perfect cusp, but is slightly rounded.

Acknowledgments

This work was carried out under the direction of Dr. E. F. Burton. The author also wishes to acknowledge the advice and assistance of Dr. H. A. McTaggart, Dr. M. F. Crawford, and Mr. A. Pitt.

References

1. Lack, F. R., Willard, G. W., and Fair, I. E. Bell System Tech. J. 13 : 453-463. 1934.
2. McKinley, D. W. R. Can. J. Research, A, 16 : 77-81. 1938.

4. JAN. 1940
LIBRARY

Canadian Journal of Research

Issued by THE NATIONAL RESEARCH COUNCIL OF CANADA

VOL. 17, SEC. A. NOVEMBER, 1939 NUMBER 11

THERMAL CONDUCTIVITY OF INSULATING MATERIALS[1]

BY E. A. ALLCUT[2] AND F. G. EWENS[3]

Abstract

The physical significance of "thermal conductivity" is well known, but this term has been applied commercially to a combination of conduction, convection, and radiation, which combination may vary considerably in a single material. Experimental evidence is advanced to indicate the undesirability of using this method of comparing the relative usefulness of different insulating materials.

Most of the thermal insulating materials sold in Canada and in other countries are compared on the basis of their thermal conductivities or k factors. Fourier's law is usually expressed in the form:

$$Q = kA \frac{dt}{dx},$$

where Q is the heat transmitted per hour,

A is the area perpendicular to the heat path,
$\frac{dt}{dx}$ is the temperature gradient,
k is the coefficient of conductivity.

If this basis of comparison is to be valid, the value of k must be constant for a definite material at a specified density. This then, is the physical concept of "conductivity", but the results obtained in practice, using the hot plate method of testing, are also affected by the following factors, which themselves are liable to vary:

(a) Surface resistances to the transfer of heat,

(b) The effects of convection currents (and in some cases also radiation effects).

The authors have found, in a large number of tests, that size, thickness, and density all have an influence on the "conductivity" which is obtained by calculation from the "conductance" or "resistance" measured by means of hot plate tests (1). In such instances, the "conductivity" of commerce is very different from the conductivity of Fourier's law, and the former term should be either dropped entirely or replaced by another. The authors do not see any reason why the word "conductivity" should be retained for the property (conductance × thickness), as all calculations of heat losses from buildings, etc., must be made by using the "conductance" or "resistance". Why interpose an additional property which is unnecessary and may be very misleading?

---

[1] *Manuscript received July 3, 1939.*
Contribution from the Department of Mechanical Engineering, University of Toronto, Toronto, Canada.

[2] *Professor, Department of Mechanical Engineering, University of Toronto.*

[3] *Instructor, Department of Mechanical Engineering, University of Toronto.*

Surface Resistance

Some years ago (1) the authors investigated the effects of varying thicknesses of material on the "conductivities" of various materials and suggested that the rising values of *k* with increasing thickness were probably due to increased resistance to the transmission of heat through the surface layers, particularly in the case of fibreboards and other similar materials. This question was further investigated by Babbitt (3) who found that the surface resistance of fibreboards was negligible when the outer layers were removed by sanding for the purpose of varying the thickness. One of the specimens, however, gave a value of *k* that increased from 0.409 to 0.429 when the thickness of the board was reduced from 2.081 to 1.495 in., by removing the surface layer. This difference is probably due, as he suggests, to the fact that the surface layers are arranged differently from those in the interior of the board. This matter has been studied recently at the University of Toronto, where

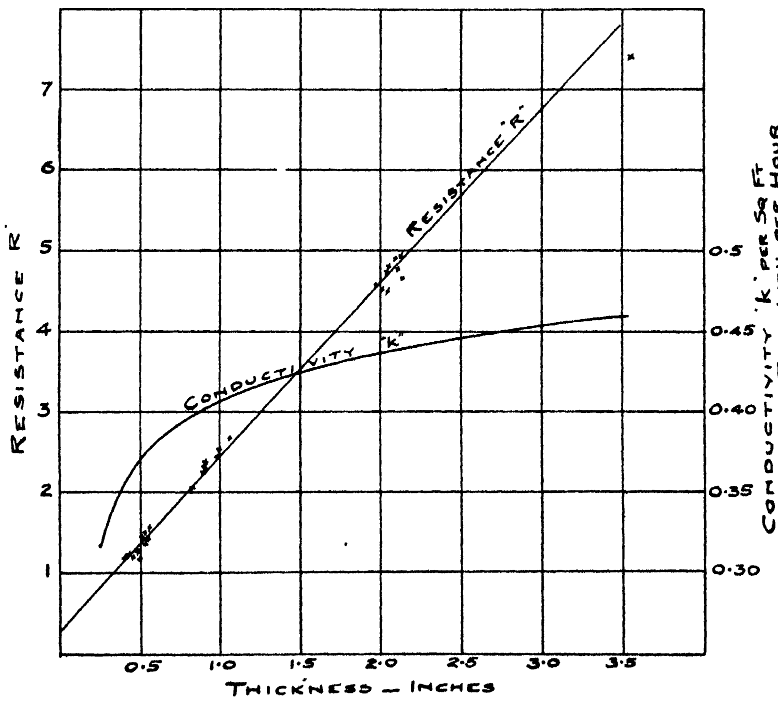

FIG. 1. *Conductivity, resistance, and thickness of fibreboards.*

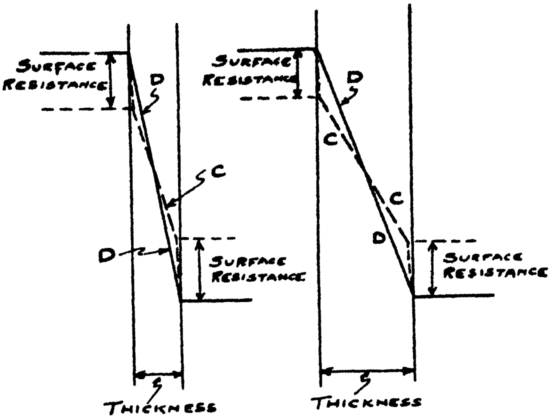

FIG. 2. *Influence of thickness on apparent temperature gradient.*

structures were examined microscopically by Dr. D. H. Hamly (Fig. 8) and where air infiltration tests (2) revealed the fact that the ease with which air passes through fibreboards is practically independent of their thickness, being a function of the density. This indicates the predominant influence of the surface layers on porosity, and by inference, their probable importance also in heat transfer. Fig. 1 shows a mean curve drawn through a number of test points obtained with fibreboards of different makes and thicknesses. On the assumption that the curve of resistance against thickness is a straight line (3), the residual resistance at zero thickness is an indication of the amount of superficial resistance, and the influence of this on the calculated value of *k* is indicated in Fig. 1. The true conductivity of the material is indicated by the slope of Curve *C*, Fig. 2, while that obtained by the hot plate test is given by Curve *D*. The former probably remains constant, while the slope of the latter varies with different thicknesses, so that in Fig. 1 the value of *k* rises from 0.37 for a 0.5 in. thickness to 0 44 for 2 in.

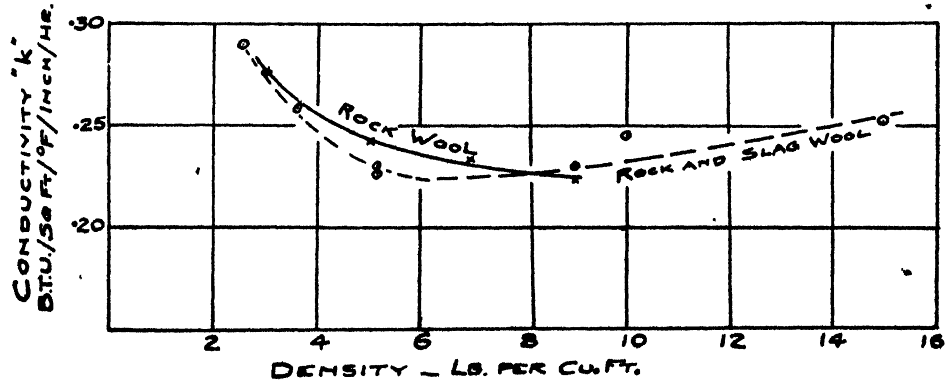

FIG. 3. *Values of k for fibrous materials at various densities.*

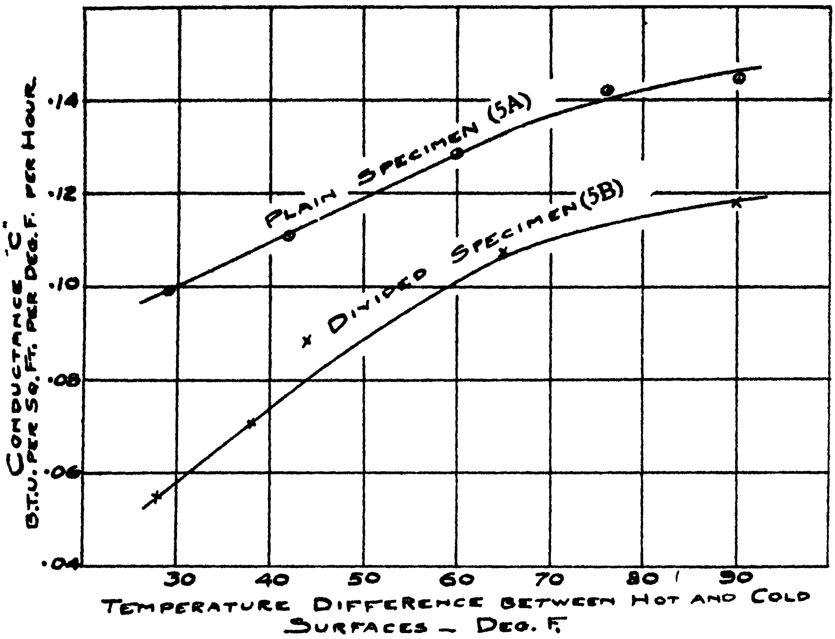

FIG. 4. *Conductances of plain and divided specimens.*

Convection Effects

Characteristic curves showing the effects of density on the "conductivity" of packed fibrous materials are shown on Fig. 3* and these indicate that some factor other than conduction is affecting the heat transfer even when packing densities as high as 9 lb. per cu. ft. are used. The smaller air spaces and the greater number of contacts between fibres at high densities tend to increase the heat transmitted by conduction, and yet the experimental curves show decreases in heat transmission up to certain optimum densities. It is probable, therefore, that even at these high densities, some of the heat is transmitted by convection. Similar indications are also obtained when tests are made on

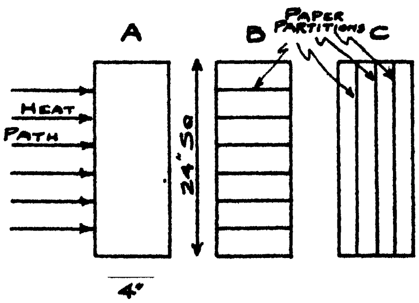

FIG. 5. *Form of specimens referred to in Figs. 4 and 6.*

---

* *See also curves in "Mechanism of Heat Flow in Fibrous Materials" (4).*

subdivided specimens. Fig. 4 gives results obtained in tests made on rock wool packed to a density of 10 lb. per cu. ft., using alternately a plain specimen (Fig. 5, *A*) and one divided into a number of horizontal layers (Fig. 5, *B*). Further tests have recently been made with a different material (density, 8 lb. per cu. ft.) tested as in Fig. 5, *A*, and also with vertical paper partitions as shown in Fig. 5, *C*.

The first tests were made on the specimen shown in Fig. 5, *C*, with thermocouples placed against the surfaces of the paper partitions, and the value of *k* calculated from the readings taken on a guarded hot plate was 0.342 B.t.u. per sq. ft. per in. thickness per degree (F) temperature difference per hr. The temperature gradient obtained from the readings after steady conditions were obtained is given in Fig. 6. The paper partitions were then removed and the test was repeated with the same specimen and with the thermocouples similarly spaced, the value of *k* for the same heat input being 0.385. As the mean temperature and temperature difference were both lower than those in the previous test, the heat input was increased to give a greater temperature gradient, as indicated by the curve for "plain specimen" in Fig. 6, whereupon the calculated value of *k* increased to 0.390.

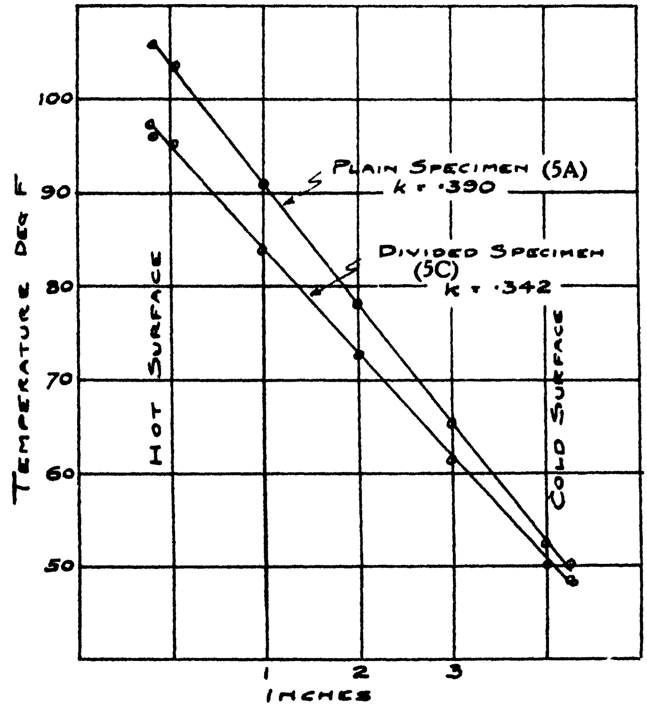

FIG. 6. *Temperature gradients through slag wool.*

Previous tests (1) had shown that the temperature difference employed between the hot and cold sides of the specimen had an influence on the cal-

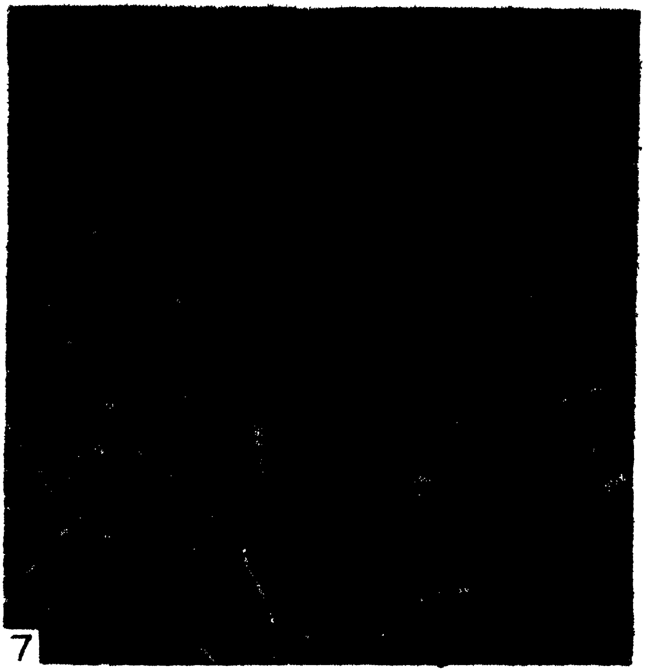
7

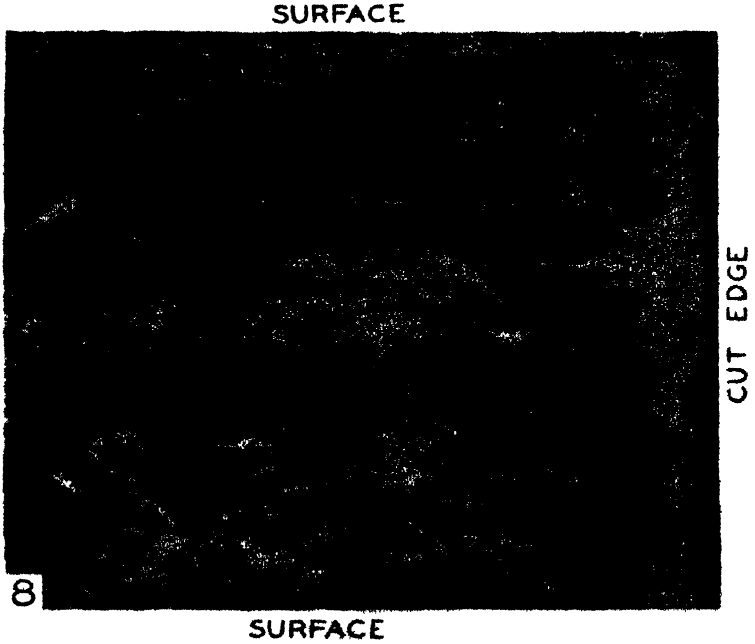

8

Fig 7. *Enlarged photograph of Shredded Redwood Bark*

Fig. 8 *Structure of fibreboard.*

culated values of *k* for thick specimens, but that this effect was small with thin specimens.

A number of tests were made on Shredded Redwood Bark (a commercial insulating product), packed to a density of 5 lb. per cu. ft., the same temperature difference and mean temperature being maintained in each case. The values of *k* for thicknesses of 1, 2, 3, 4 in. are given in Table I.

TABLE I

CONDUCTIVITIES (*k*) OF SHREDDED REDWOOD BARK AT VARIOUS TEMPERATURE DIFFERENCES AND THICKNESSES, AS OBTAINED ON HOT PLATE APPARATUS, 24 IN. SQUARE

DENSITY OF MATERIAL, 5 LB. PER CU. FT.; MEAN TEMPERATURE, 90° F.

Temperature difference across specimen, °F.	10	20	40	60	80	100
k for 1 in. thickness	0.300	0 330	0 370	0.390	0.395	0.400
k for 2 in. thickness	.300	.340	.395	.425	.450	.460
k for 3 in. thickness	.300	.345	.410	.455	.490	.510
k for 4 in. thickness	.300	.350	.420	480	.525	.550

The above values of k are in B.t.u. per square foot per inch thickness per degree F. temperature difference per hour.

These differences are difficult to account for unless it is assumed that convection currents exist in the packed material, and that they may be reduced either by increasing the density of the material, or by dividing the specimen into smaller cells.

Conclusion

The evidence given above indicates that, in the case of fibrous insulating materials, the property calculated from the "conductance" obtained by hot plate tests is not conductivity, but is a combination of various properties depending largely on the size, structure, and density of the specimen tested, and therefore its continued use in practice is undesirable.

An enlarged photograph of the structure of Shredded Redwood Bark is shown in Fig. 7. It seems unreasonable to apply the term "conductivity" to the transmission of heat through structures of this kind.

References

1. ALLCUT, F. A. and EWENS, F. G. School of Engineering Research, University of Toronto, Bull. 149. 1937.
2. ALLCUT, E. A. School of Engineering Research, University of Toronto, Bull. 158. 1939.
3. BABBITT, J. D. Can. J. Research, A, 16 : 82-87. 1938.
4. FINCK, J. L. Bureau of Standards, Research Paper No. 243. 1930.

DESCRIPTION OF A PRESSURE CELL FOR THE MEASUREMENT OF EARTH PRESSURE[1]

By I. F. Morrison[2] and W. E. Cornish[3]

Abstract

The vibrating wire method for measuring strains is used to determine the pressure applied to an earth pressure cell. The construction of the cell, the principle on which it acts, and electrical circuits are described.

Introduction

Although much has been written on the theory of earth pressures on retaining walls and below foundations, the present need is of measurements to confirm the theory and to establish such basic principles as may lead to a practical method for the computation of such earth pressures. A number of earth pressure measuring cells have been developed, but they fall short, somewhat, of what is hoped will be the ultimate development of such apparatus. It is not the purpose of this paper to give a critique of previous attempts but rather to describe still another attempt to develop a suitable earth pressure cell.

The requirement of a suitable earth pressure cell is that it shall be capable of measuring with requisite accuracy the active earth pressure that comes upon it. Some pressure cells already in use do not meet this requirement. In addition, the cell must be "hard", *i.e.*, it must measure the pressure with as little movement of the surface, to which the external pressure is applied, as possible. Moreover, the measurements must be recorded on instruments at some distance from the cell itself and, therefore, by indirect observation. In addition, it must be reliable over a considerable time interval.

To meet these requirements, it was decided to use the vibrating wire method, and to this end preliminary studies were made of the electrical arrangement to determine the most suitable size and limitations of length of wire and the best position of the electromagnets for driving the wire and picking up its vibration. This successfully accomplished, the cell was designed with due regard to the hardness requirement and its practical and rugged construction. Its range was planned to extend to an equivalent soil pressure of 7500 lb. per sq. ft., which required a load of slightly over 1000 lb. on the cell.

Description of Cell

The working part of the cell consists of a stiff, T-shaped beam which rests on a properly located knife-edge fulcrum. At the free ends of the beam, short arms project downwards. The wire is securely held at its ends by these

---

[1] *Manuscript received June 20, 1939.*
Contribution from the Departments of Civil and Electrical Engineering, University of Alberta, Edmonton, Alberta.

[2] *Professor of Applied Mechanics, University of Alberta.*

[3] *Assistant Professor of Electrical Engineering, University of Alberta.*

arms. It passes, below the beam, through a slot in the fulcrum. The T-shape was adopted in order to secure a three-point support for the cover plate through which the soil pressure is transmitted to the beam and thereby to eliminate the effect of flexural strain of the cover plate on the readings given by the electrical equipment.

In addition, since any cell for such purpose must be capable of continued operation over a long period, it was decided to lessen the possibility of creep in the wire tension by working from a higher tension to a lower, and for that purpose the single fulcrum was adopted. Besides, the single fulcrum fairly well eliminates the effect of distortion of the base of the cell. Fig. 1 shows the arrangement as described above and also the arrangement of the magnets in the vicinity of the tight wire.

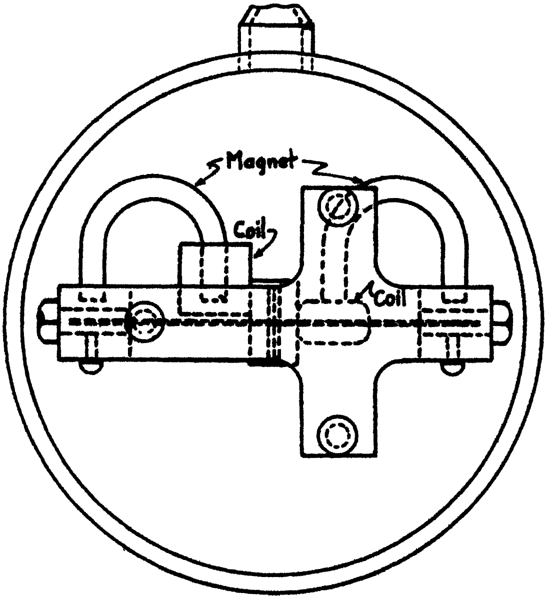

PLAN, COVER PLATE REMOVED

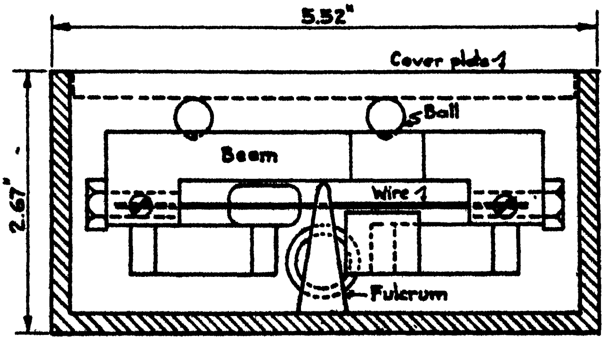

SECTION

FIG. 1

The T-beam was cut from a steel plate ½ in. thick and, as the point of application of one-third of the total pressure on the cover plate is but 1¼ in. from the fulcrum, the beam is quite stiff. For full load the computed movement of the cover plate amounted to about 0.001 in., so that the cell may be considered fairly "hard".

From previous experimental work, the most suitable size of wire was found to be 0.020 in. diameter and a piece of steel piano wire, as near this size as practical, was used. The clear length of the wire is about 2¾ in. and the ends are securely fastened into steel sockets which pass through the arms at the ends of the beam. The sockets are threaded and provided with nuts for tightening the wire to its initial tension. Also set screws are provided to keep the sockets from turning.

Electrical Set-up

As previously mentioned, the vibrating wire method is used to measure the pressure on the cell. This method consists of causing the wire to vibrate and measuring the frequency of vibration of the wire. As load is applied, the tension in the wire decreases; this decreases the frequency and thus gives a measure of the pressure on the cell.

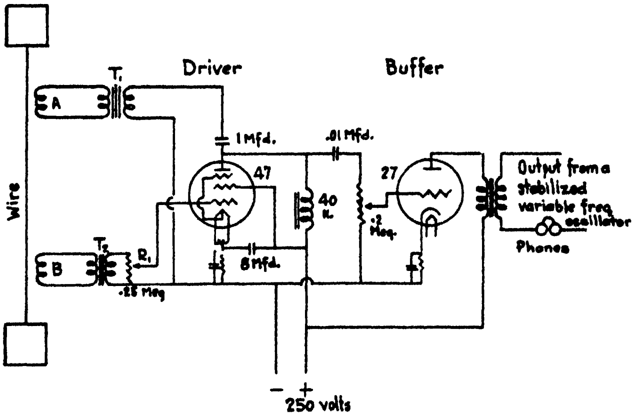

FIG. 2

In Fig. 2, *A* and *B* are the coils from a telephone headset. As shown in Fig. 1, these coils are mounted on the magnets from the headset and these magnets are fixed to the arms which hold the ends of the wire. Thus, there is a magnetic flux passing through each coil, across the gap between the coil and the wire, and along the wire back to the arm. Coils *A* and *B* are mounted at right angles so as to prevent mutual coupling between them. The impedances of the coils are matched to the impedances of the driver tube by using suitable transformers T_1 and T_2. A variable resistance R_1 is used to control the amplitude of vibration of the wire. The driver tube is a power amplifier pentode, No. 47. The reason for using this tube is its high amplification factor.

The operation of the driver is as follows: Coil A, the driving coil, causes the wire to vibrate. The wire vibrating in front of Coil B varies the magnetic flux through the coil thus inducing a voltage in it the frequency of which is the same as that of the vibrating wire. This voltage is applied to the grid of the tube, which in turn controls the current in the driving Coil A. Therefore the wire vibrates at its natural frequency, which depends entirely on the tension, which in turn depends on the pressure on the cell.

The buffer tube, a No. 27, is coupled to the driving tube by a 0 01 mfd. condenser and a 200,000 ohm potentiometer, R_2. The purpose of the buffer tube is to prevent any possibility of the oscillator pulling the wire into synchronism when the frequencies of the oscillator and of the wire are nearly the same.

The output of the buffer tube is connected in series with the output of a variable frequency oscillator and a pair of phones. The note heard in the phones, when the wire is vibrating and the oscillator operating, is the "beat-note" between the two frequencies. When the frequency of this "beat-note" is zero, then the frequency of the oscillator is the same as the frequency of vibration of the wire. The oscillator used in the preliminary tests was a simple Hartley Oscillator, the frequency of which is varied by means of a decade condenser and a continuously variable condenser.

The cell is calibrated as follows: First the frequency of the oscillator is set at some value near that of the wire by means of a tuning fork. This is done with the condenser readings set at some selected value, and the correct frequency is obtained by varying the coupling between the coils in the oscillator. Periodically this setting should be checked to make sure that the frequency of the oscillator is correct for a particular setting of the condensers. After this check is made, the output of the buffer and the phones are connected in series with the output of the oscillator. With no load on the cell, the frequency of the oscillator is varied until it is the same as the frequency of the wire, and the condenser readings are taken. Now a load is applied to the cell and the operation repeated.

The load on the cell is plotted against the condenser readings; this gives a calibration curve.

Since the frequency of the oscillator may vary with any voltage variation, a stabilized oscillator, similar to that shown on page 285 in "Measurements in Radio Engineering" by Terman, would be more satisfactory.

All the equipment shown in Fig. 2, except the wire and Coils A and B, which are in the cell, are contained in a steel cabinet, together with a power supply. The four wires from the cell are connected to a four prong plug which is plugged into a four prong socket mounted on the cabinet.

The oscillator and its power supply are contained in another cabinet equipped with suitable jacks for connecting the two outputs and phones in series.

The same equipment is used to operate any number of cells, merely by plugging in each one separately. The mechanical set-up, capable of giving the required load range which was used for calibration, is shown in Fig. 3.

This simple arrangement is sufficiently indicated to require no written description. In this work care was taken to approach the beat-note always from the same side of the cell note.

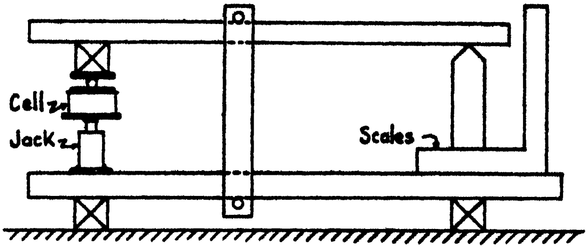

Fig. 3

Fig. 4 shows a typical calibration curve. For similar initial conditions the curve repeats fairly well. From it, when an unknown load is applied to the cell (the capacity of the condensers having been determined from the readings on the dials) the magnitude of the applied load is at once determined.

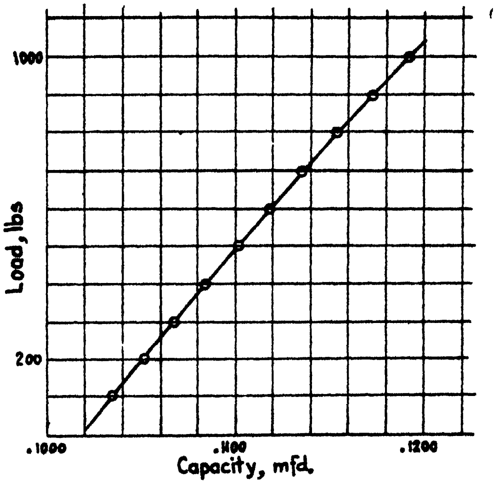

Fig. 4

The condenser set used in the tests can be improved considerably and will lead to greater accuracy of readings. The cell exhibits remarkable sensitivity, for a change in beat-note due to application of the fingers to the cell can be heard. There is every indication that the accuracy of this cell will be quite satisfactory for the purpose of the measurement of earth pressure and that its rugged construction, as well as its capacity for remaining in working condition over long periods, will make it pre-eminently suitable for that purpose.

Acknowledgment

The writers wish to acknowledge the kind assistance of Prof. R. M. Hardy in connection with the development and testing of the cell and in the preparation of this paper.

Canadian Journal of Research

Issued by The National Research Council of

VOL. 17, SEC. A. DECEMBER, 1939 NUMBER 12

LIBRARY

THE VISCOSITY OF LIQUID HYDROGEN[1]

By H. E. Johns[2]

Abstract

The viscosity of liquid hydrogen has been measured by observing its flow through a variety of capillary tubes. The resulting viscosities are about 10% higher than those obtained by Keesom and Macwood using an oscillating disc.

Introduction

The viscosity of liquid helium has recently been measured at Toronto (1) by observing its flow through fine glass capillaries. The values were about 50% higher than those obtained by Keesom and Macwood, using an oscillating disc (2). The author therefore decided to measure the viscosity of liquid hydrogen by the flow method in order to compare the results for this liquid with those of Keesom and Macwood (3). For liquid hydrogen the values obtained by the flow method are approximately 10% higher than those obtained by the oscillating disc method.

Apparatus

The apparatus employed was essentially the same as that used in the determination of the viscosity of helium (1). Several capillaries were attached to tubular reservoirs, and were mounted on a frame parallel to a scale, as shown in Fig. 1. The whole was arranged so that it could be raised or lowered in a closed vessel of liquid hydrogen to allow the liquid to flow through the capillaries in or out of the reservoirs. The vessel containing the liquid hydrogen used for the experiment was completely surrounded by a bath of liquid hydrogen in the cryostat, and during the experiment the inner vessel was closed off so that no evaporation could take place. The temperature was controlled by pumping on the liquid hydrogen in the outer vessel.

The surface tension of the liquid hydrogen caused the liquid in the reservoirs to come to an equilibrium position *(A)* approximately 1 cm. above the surrounding level *(B)*. The pressure head was measured from the equilibrium position rather than from the level of the surrounding liquid. For the finer capillaries the flow took place very slowly so that the equilibrium position was not attained until the elapse of 20 to 30 min. In order to carry out the

---

[1] *Manuscript received September 7, 1939.*
Contribution from the McLennan Laboratory, Department of Physics, University of Toronto, Toronto, Canada.

[2] *Holder of a Studentship under the National Research Council of Canada.*

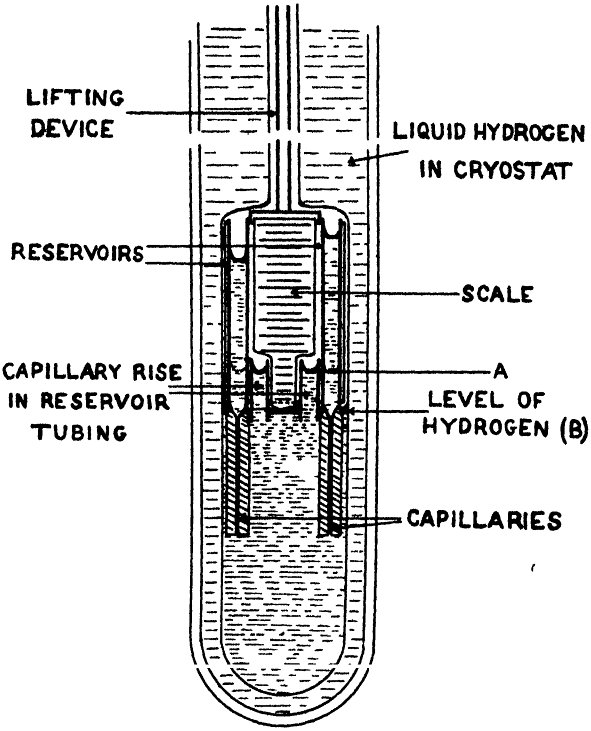

FIG. 1. *Diagram of apparatus.*

experiment more quickly, in this case, a piece of reservoir tubing open at both ends was placed beside the other reservoirs, so that the capillary rise could be measured directly. The pressure heads were then measured from the level in the open tube *(A)*. To insure complete "wetting" of the reservoirs by the hydrogen, readings were always taken with the liquid flowing out of the reservoirs to the bath, that is, in the position shown in Fig. 1. In the earlier work on liquid helium, the capillary rise was found to be negligible, and no correction was necessary.

The measurements with tubes I *a*, *b*, *c*, were made photographically as described in the previous publication (1) and the pressure head was measured from the equilibrium position finally attained. For tubes II *a* and III *a*, *b*, *c*, the pressure head was measured from the surface in the open reservoir by means of a cathetometer, the time being recorded on a chronograph; the measurements could be made in this way much more accurately, and down to smaller pressure heads. Therefore the results for tubes II and III have been given weight 1 in comparison with weight ½ for tubes I.

The pressure heads were usually measured from about 5 cm. down to 0.1 cm. When the pressure head was plotted against the time on semilogarithmic paper it was frequently found that the points lay on a straight line over a range from 5 cm. to about 0.5 cm. and then curved slightly up or down for the lower pressure heads. It seemed probable that this was due to an error in the correction for capillarity. This is confirmed by the fact that the graphs were easily rectified by adding to, or subtracting from, the pressure heads small amounts (usually less than 0.01 cm.) For some of the capillaries the pressure head was corrected for the kinetic energy of efflux but in no case was this greater than ½ of 1%. When these corrections were made the slopes of the graphs could be determined to better than 1%.

Results

The viscosity was determined by the use of 7 capillary tubes whose dimensions are given in Table I. The probable errors of the average length and diameter of the capillaries, and of the diameter of the reservoirs were all about 0.2%, so that the results for any one tube had a probable error due to this cause of about 0.9%. The slopes of the graphs could be determined with a

TABLE I

DIMENSIONS OF CAPILLARY TUBES

Tube	Length of capillary, cm.	Diameter of capillary, cm.	Diameter of reservoir, cm.
I*a*	5.93	0.01676	0.1428
I*b*	4.36	0.01205	0.1596
I*c*	9.50	0.02340	0.1838
II*a*	5.86	0.01590	0.1415
III*a*	3.83	0.01588	0.1415
III*b*	4.38	0.01679	0.1412
III*c*	1.627	0.01196	0.1405

TABLE II

TEMPERATURE, DENSITY, AND CALCULATED VISCOSITY

Tube	Temperature °K	Density, gm./cm.^{3}	Viscosity, 10^{-6} c.g.s. units	Tube	Temperature °K	Density gm./cm.^{3}	Viscosity, 10^{-6} c.g.s. units
III*a*	20.71	0.07049	136.2	III*a*	18.77	0.07260	160.0
I*a*	20.64	0.07056	134.7	III*a*	18.43	0.07295	166.5
I*b*	20.64	0.07056	136.0	II*a*	18.41	0.07298	165.1
I*c*	20.64	0.07056	139.0	III*c*	18.38	0.07295	165.0
III*b*	20.63	0.07058	134.8	III*b*	18.36	0.07303	163.7
III*a*	20.62	0.07059	137.0	II*a*	17.96	0.07342	170.2
III*c*	20.29	0.07099	140.5	III*a*	17.80	0.07358	177.2
III*a*	20.28	0.07098	138.7	I*a*	17.64	0.07374	172.0
III*b*	20.28	0.07098	140.0	I*b*	17.64	0.07374	174.2
I*a*	20.10	0.07118	141.1	I*c*	17.64	0.07374	176.0
I*b*	20.10	0.07118	141.1	III*a*	17.32	0.07405	185.0
I*a*	19.61	0.07171	145.5	III*a*	16.98	0.07448	191.4
I*b*	19.61	0.07171	146.5	III*a*	16.22	0.07510	204.6
I*c*	19.61	0.07171	144.8	I*a*	16.16	0.07516	201.0
III*a*	19.61	0.07171	147.4	I*b*	16.16	0.07516	204.6
III*b*	19.21	0.07213	151.9	III*a*	15.68	0.07560	217.6
III*c*	19.17	0.07218	151.3	III*a*	15.09	0.07613	229.3
III*a*	19.15	0.07220	152.7	III*a*	14.60	0.07656	238.7
I*a*	18.98	0.07238	153.2	I*a*	14.60	0.07656	236.8
I*b*	18.98	0.07238	150.0	I*b*	14.58	0.07658	241.5
I*c*	18.98	0.07238	154.2	III*a*	14.29	0.07683	246.6

probable error of about 0.6%, and thus the individual viscosity measurements might be expected to have a probable error of about 1.1%.

Table II contains the temperature, density, and calculated viscosity values for a large number of measurements. These results are also shown in Fig. 2, where a smooth graph has been drawn through the average position of the points. For convenience values taken from the smooth graph are given in Table III. The probable error of an individual measurement was also calculated from the deviations of measurements made at approximately the same temperature, and amounted to not more than 1%. This showed that the measurements with different tubes are consistent. The probable error of the average found in this way was about 0 3%.

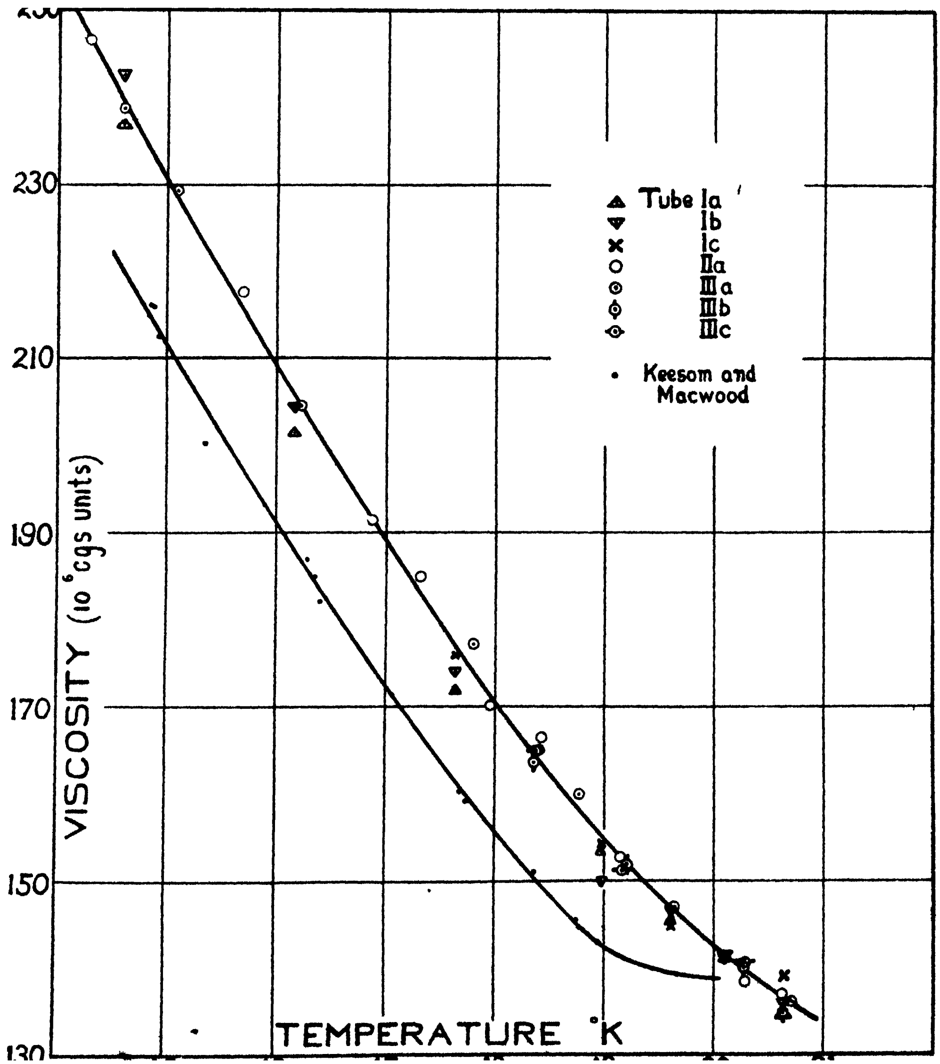

Fig 2 *Relation between the viscosity of liquid hydrogen and the temperature.*

For comparison the results of Keesom and Macwood are illustrated graphically in Fig. 2, and smoothed values are given in Table III. It can be seen that the variation with temperature for the two results is approximately the same except for the higher temperatures, but that the results obtained by means of the oscillating disc are about 10% lower than those obtained by the author.

TABLE III

VALUES OF VISCOSITY ESTIMATED FROM CURVES (FIG. 2)

Temperature, °K.	Viscosity, 10^{-6} c.g.s. units	
	Flow method	Oscillating disc
20.6	136.5	
20.41	138.4	
20.0	142.5	138.8
19.0	154.6	142.6
18.0	170.5	155.7
17.0	189.1	172.3
16.0	209.0	191.0
15.0	230.3	211.4
14.5	241.8	

Fig. 3 shows that the relation between log η and $1/T$ is linear for the higher temperatures and that the slope $d \log \eta / d(1/T)$ gradually decreases as the

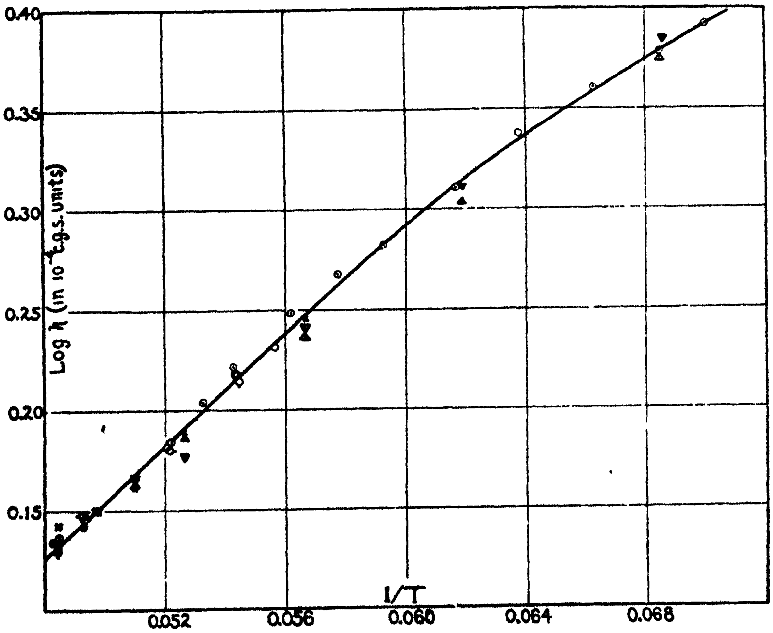

FIG. 3. *Relation between the logarithm of the viscosity and the reciprocal of the absolute temperature.*

temperature decreases. The linear portion of the graph between log η and $1/T$ leads to a viscosity relation of the familiar form

$$\eta = A \exp (E/RT),$$

where the activation energy $E = 64.6$ cal. per mole. The dependence of the viscosity of liquid hydrogen on temperature is therefore quite normal.

Acknowledgments

The author would like to thank Prof. E. F. Burton for his guidance and Prof. H. Grayson Smith and Prof. J. O. Wilhelm for their assistance in this research.

References

1. JOHNS, H. E., WILHELM, J. O., and SMITH, H. GRAYSON. Can. J. Research, A, 17 : 149-163. 1939.
2. KEESOM, W. H. and MACWOOD, G. E. Physica 5(8) : 737:744. 1938.
3. KEESOM, W. H. and MACWOOD, G. E. Physica 5(8) : 745-748. 1938.

EXPERIMENTAL COMPARISON OF SHUNT- AND SERIES-EXCITATION OF A HIGH, UNIFORM CROSS-SECTION, VERTICAL RADIATOR[1]

By K. A. MacKinnon[2]

Abstract

This paper presents the results of experiments with shunt- and series-excitation of a 0 55 wave, uniform cross-section, vertical radiator. Both unattenuated field strength at one mile and fading characteristics at remote points were determined for each mode of excitation. Whilst Morrison and Smith have already done similar work with a non-uniform cross-section tower, this is the first attempt to examine the fading of a uniform cross-section tower excited in the two modes.

Introduction

The shunt-excited antenna was introduced by Morrison and Smith (2) in 1936. To check the performance of the design against the ordinary series-excitation method they conducted experiments with the WWJ-Detroit uniform cross-section tower of about 0.38 wave-length physical height for ground-wave efficiency, and with the WSM-Nashville double-tapered tower of 0.58 wave-length for fading characteristics. Their results indicated no substantial difference between the performances of the two modes of excitation.

The fact that the double-tapered type of tower has a current distribution which produces considerably more sky-wave at zenith angles around 30° than does a sinusoidal current distribution (1) suggested the desirability of examining the fading characteristics of a shunt-excited, high, uniform cross-section tower, along which the current distribution when series-excited is approximately sinusoidal. Furthermore, as the WWJ uniform tower is only 0.38 wave-length high it was also considered worth while to compare the ground waves of a high tower using the two modes. The installation of the 50 kw. broadcast transmitter CBF provided an excellent opportunity for these experiments, as it had a shunt-excited uniform cross-section tower of 0.55 wave-length height with an insulated base which of course was short-circuited for shunt-excitation.

Ground-wave Comparison

The first experiments (February, 1938) were devoted to a comparison of the ground-wave of the CBF tower when shunt-excited with that when series-excited. A low power transmitter of 13 watts was used to excite the tower,

---

[1] *Manuscript received August 22, 1939.*

Contribution from the Engineering Division, Canadian Broadcasting Corporation, Montreal, Quebec, Canada. This paper was presented before a joint meeting of the American Section, International Scientific Radio Union and the Institute of Radio Engineers, held at Washington, April 28, 1939.

[2] *Transmission and Development Engineer, Canadian Broadcasting Corporation.*

and radial field strength measurements were made in various directions over the frozen surface of the St. Lawrence River, beside which CBF is built.

The results indicated that the series-excitation gave about 15% more ground-wave (unattenuated field strength at one mile per kilowatt input) than the shunt-excited. It should be pointed out here however that the power input in the series case was that into the base of the tower, whereas in the shunt case it was the power into the concentric transmission line. Thus the 15% figure should be decreased by an amount dependent on the losses in the line and output terminal equipment. This figure seemed reliable because no absolute values were necessary—the same antenna meter was used at about the same part of the scale in each case, and also the ground-wave was measured along the same radials with the same field strength gear.

The other disturbing feature was the fact that the absolute values found were much too low (212 mv./m./mile/kw. for shunt, 244 for series), whereas figures of the order of 260 should be expected. As a check on this, measurements were repeated with 50 kw. input shunt-excited, and a figure of 224 was obtained. As this was within 6% of the 13 watt shunt measurement, and considering the use of different antenna meters and the great difference in field strengths resulting from the widely different powers, it was felt that the agreement was satisfactory.

The low absolute field of the series-excitation indicated some defect in the ground system. This was further suggested by the much lower figure for shunt-excitation, because it was known that the base current in this mode of operation is much greater than in series-excitation.

No fading comparisons were carried out at this time because of the cold weather.

The following summer, imorovements were made to the ground system at the base of the tower and last fall the ground-wave comparison measurements were repeated, using 50 kw. in both cases.

The use of high power in the series-excitation case involved the installation of a two-wire line between the end of the concentric line and the base of the tower with impedance matching equipment at both ends, as well as tower lighting chokes. Fig. 1 indicates the connections and the point where the antenna resistance and current were measured in each case in order to determine the power input. Figs. 2 and 3 give views of the experimental setup at the base of the mast.

The result with the ground system improvements gave a ground-wave for series-excitation of 250 mv./m./mile/kw.; and for shunt-excitation 242, a difference of only 3%. The improvement in per cent due to the ground system changes was thus for series-excitation 250/244 or 2.5% gain, for shunt-excitation 242/212 or 14% gain.

At this point it is interesting to examine the decrease in lumped ground resistance, ohms due to the alterations. By inserting an ammeter in the ground strap across the insulated base of the tower it was possible to measure

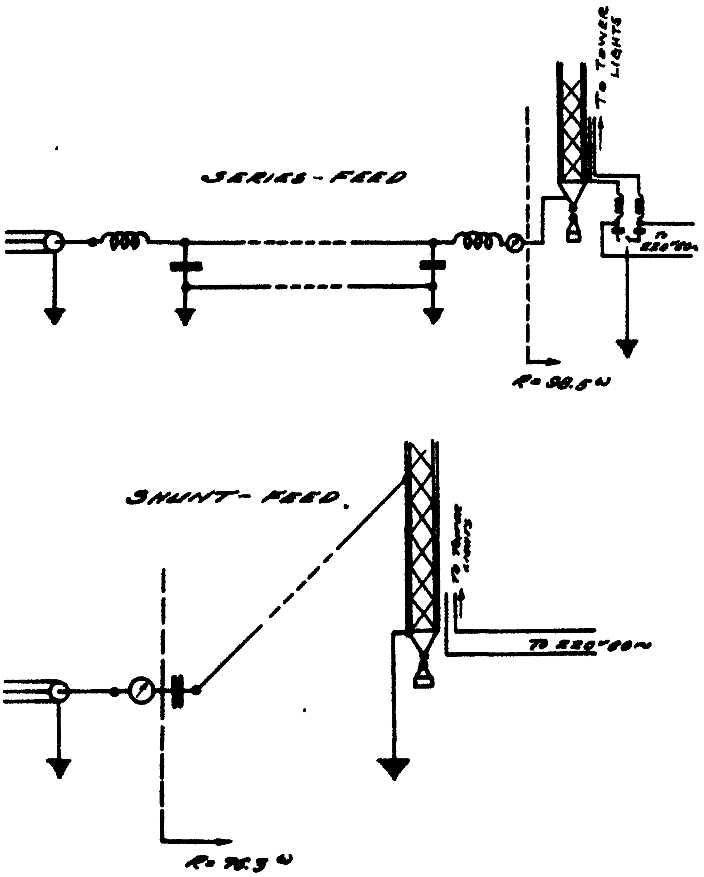

FIG. 1

during shunt-excitation simultaneously both the current in the slanting feed wire and that at the base of the tower. The base current was found to be 2.5 times the current at the bottom end of the feed wire.

These figures permit some simple calculations to be made of the extent of the ground system improvements. For shunt-excitation and 50 kw. into the feed wire (76.3 ohms; see Fig. 1), the feed wire current was 25.6 amp. and thus the base current $2.5\times25.6=64$ amp. A 14% loss in ground-wave efficiency means 13 kw. in 50 kw., and thus the ground system changes must have reduced the loss ohms by R_1 where $(64)^2\ R_1=13000$ or $R_1=3.2$ ohms.

Similarly, the base current in series-excitation (98.5 ohms; see Fig. 1) was 22.5 amp. A 2.5% loss in efficiency is equivalent to 2.5 kw. in 50 kw., and thus the ground system changes reduced the loss ohms by R_2 where $(22.5)^2R_2=2500$ or $R_2=4.9$ ohms.

If the radiating system could be considered as actually having a lumped loss resistance it might be expected that R_1 and R_2 would agree more closely. On the other hand, it should be remembered that the change in power loss

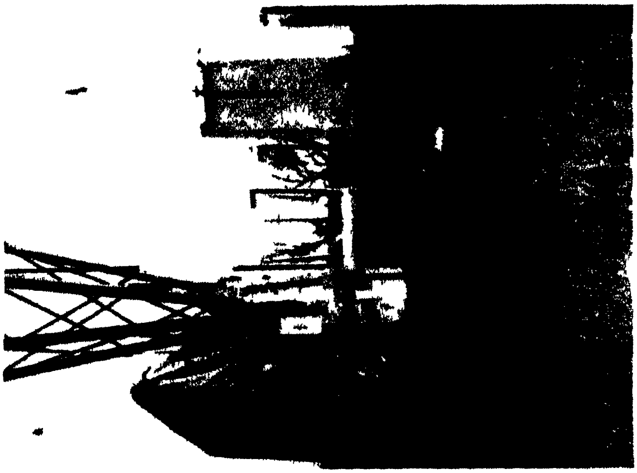

Fig. 2

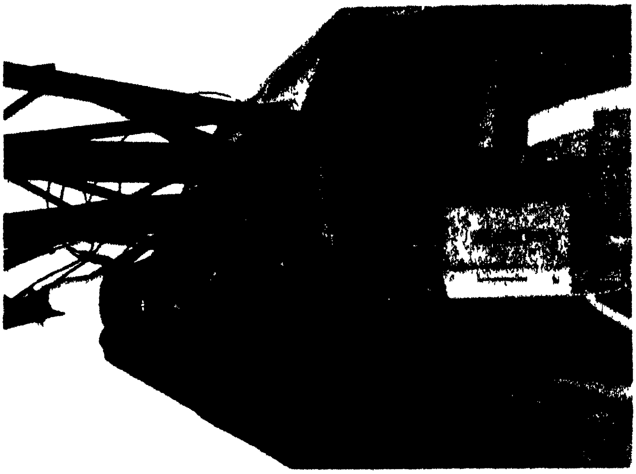

Fig. 3

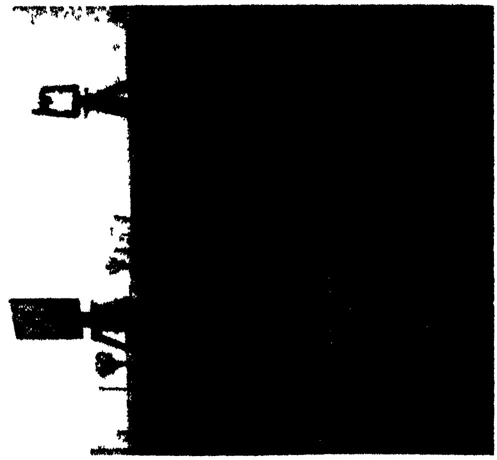

Fig 4

in these equations has been calculated from field strength measurements. This immediately brings into the picture a number of other unknown factors, such as a possible variation in the polar radiation pattern of the shunt-fed mast due to resistance changes at the mast base causing mismatching of some sort. Nevertheless, this digression indicates the greater need for adequate grounding at the tower base when shunt-excitation is used.

Discussion of Measuring Methods

There are four factors involved in the determination of ground-wave efficiency (unattenuated field strength at one mile per kw. input to mast); viz.,

(1) Antenna resistance,
(2) Antenna current,
(3) Field strength at given point,
(4) Linear distance from point to mast.

The procedure adopted to determine each of these will now be discussed in detail.

Antenna Resistance

This was measured across the base insulator for series-excitation, and between the line terminal of the impedance matching capacity connected to the slanting feed wire and ground for shunt-excitation.

Each resistance was measured by two methods—one using the CBC Antenna Measuring gear which balances two meter readings, and the other using the General Radio R. F. Bridge with its null indication. Each pair of measurements checked within ½%, which was very satisfying, as different operating principles are used in the above instruments.

Antenna Current

For convenience in changing over from one mode of excitation to the other, a separate antenna meter was used for each connection. In order to check these against each other, they were put in series and compared at the operating frequency (910 kc.), and the ambient temperature (40° F.).

Field Strength

All the field strength measurements were made with the same Jansky and Bailey instrument with loop on a tripod (see Fig. 4), whose absolute calibration had been checked by the makers some months previously. During the experiments the relative accuracy of the gear over a wide range of field strengths was rechecked.

At all inland points the gear was set up with the tripod. However, at all shore points the gear was set up in a small motorboat, with the tripod feet at water level.

Linear Distance to the Mast

Linear distance to the mast from the point of measurement was determined by means of a transit. This measured the angular elevation to the top of the mast, as well as the elevation of the measuring point. The height of the top of the tower and the elevation of its base being known, the distance to the tower could readily be calculated to a much greater accuracy than that of the other three factors required in the ground-wave efficiency determination.

The distances of points more than one mile from the tower were determined by reference to the National Defence map of the area (scale 1 in. = 1 mile). The tower was accurately located thereon by means of azimuth bearings taken on various lighthouses and church steeples visible from CBF.

Estimated Accuracy

For the relative accuracy, that is the comparison of shunt-excitation ground-wave with that of series-excitation, one should note that:—

(1) Resistance determinations checked by different methods within ½%;

(2) The antenna meters were compared in a series circuit at the operating frequency and temperature, so that the inaccuracies here might be 1% owing to modulation variations;

(3) The same field strength gear was used throughout;

(4) The linear distance factor was eliminated by measuring at identical points.

Accordingly, it appears safe to assume a relative accuracy of about 1 or 2% in the ground-wave comparison.

In considering the probable absolute accuracy one has more difficulty in allocating possible errors. The resistance measurement seems likely to be within ½%, as different methods and instruments used gave readings within this value. The antenna meters when compared in a series circuit read within 3% of each other and it is thus probable that the absolute meter error is of half this order. The absolute error of field strength gear is always open to question and in this case one is likely rather optimistic to expect an error of no more than 6% absolute. Linear distance measurement error with the transit was of course of so much higher accuracy than any of the above items that it may be neglected.

Therefore, it appears that the absolute error of the various ground-wave measurements is probably no less than 10%.

Sky-wave Comparison

The procedure in these sky-wave tests was to operate with 50 kw. into the mast for quarter-hour periods now with shunt-excitation and then with series-excitation. The change-over from one mode to the other was done as rapidly as possible, the time required varying from 10 to 15 min. Time recordings of the resultant field strengths were made simultaneously at various points from 70 to 130 miles from the mast.

The essence of this method of course is to make the change from one mode of excitation to the other rapidly enough to be confident that sky-wave conditions have not themselves altered in the interval. This state can be assumed if the recordings for at least two consecutive intervals of operation with the same mode are found to be of the same character.

Figs. 5, 6, and 7, of sections of the recordings, show samples of such sky-wave constancy. These are sufficient to indicate that there is no doubt the shunt-excitation method produces much more sky-wave than does the series-excitation. In fact this 0.58 wave tower when shunt-excited behaves from this viewpoint as though it were not much more than half its actual height.

This work was beset with many difficulties, chief of which was the presence on the CBF frequency of a strong Mexican Transmitter, XENT, 150 kw. This interfering station was operating every morning until after daybreak. On most of the nights when strong sky-waves were being received the signal from this station was sufficient to spoil all the recordings. On the other hand, when XENT was weak enough to permit a good recording of CBF, the sky-waves were usually too weak to cause noticeable fading.

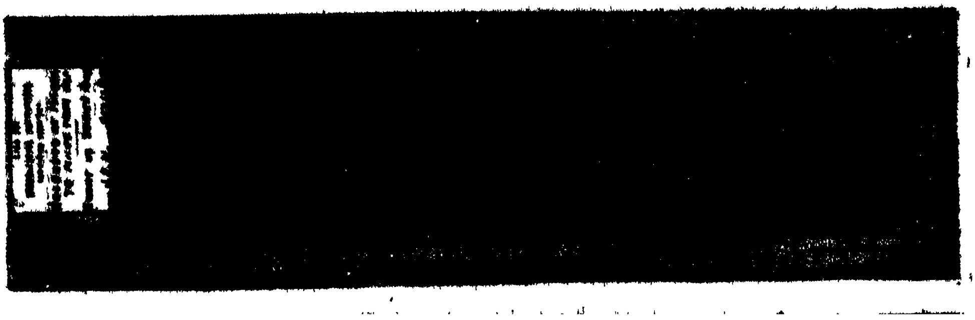

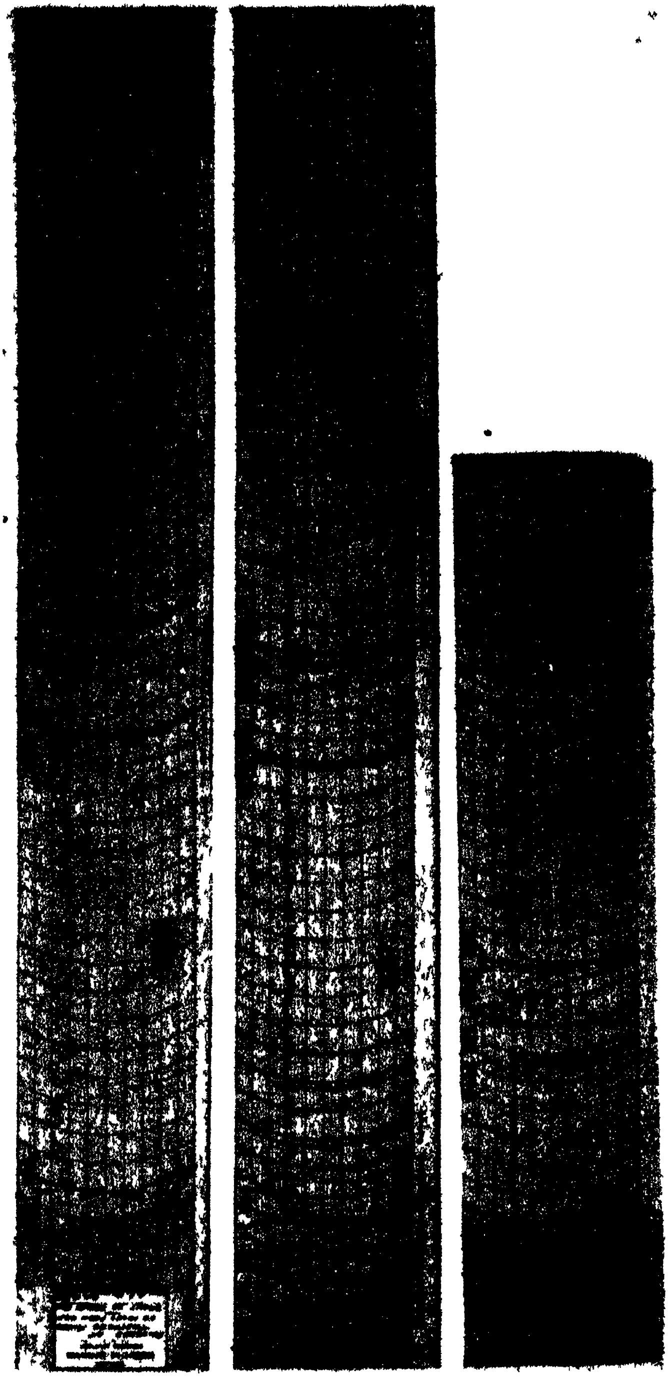

FIG

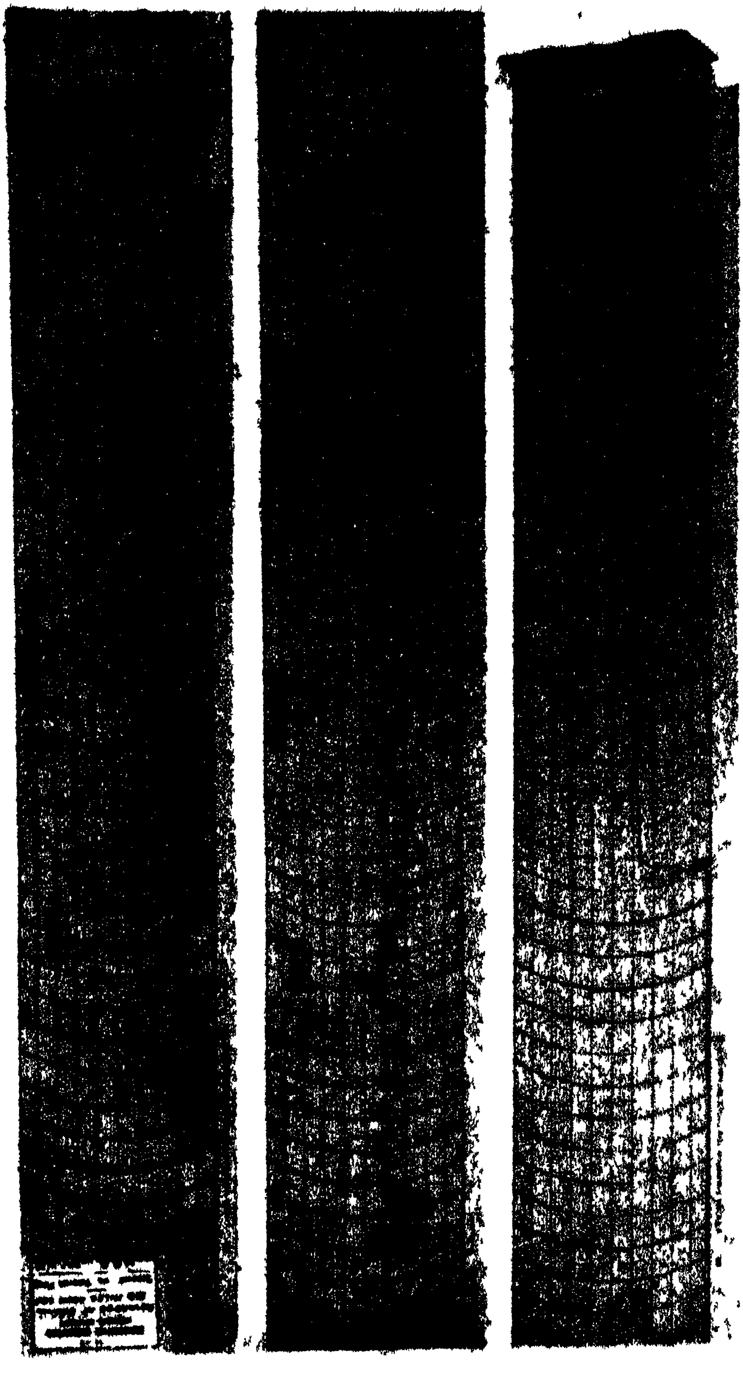

Fig. 7

Conclusions

To summarize, it may be said that these experiments with the 0.55 wavelength, uniform cross-section tower of CBF have shown that:—

(1) The ground-wave of this type of tower when shunt-excited can be within 3% of the ground-wave when series-excited, providing that adequate grounding arrangements are made around the tower base;

(2) The sky-wave suppression when shunt-excited is much less satisfactory than when series-excited.

In the choice between a high mast (say 0.55 wave) and a low mast (0.25 wave) for a high power station there are several factors to be considered:—

(1) Greater cost of high tower,

(2) Greater ground-wave efficiency of high tower,

(3) Greater sky-wave suppression of high tower (when series-excited).

In the basic engineering coverage scheme as announced by the Canadian Broadcasting Corporation, the attainment of a *national* service is considered as the paramount aim. Every extra bit of Canadian territory that gets fading-free service is counted as a gain. Consequently, sky-wave suppression is as important to the CBC as ground-wave efficiency.

There is another aspect to fading which is of importance to the use of our present so-called "clear" channels. The matter of fading is of great moment when strong interfering stations are on the same channel. On 910 kc., for instance, there are CBF—Montreal, 50 kw.; CKY—Winnipeg, 15 kw.; XENT—Nuevo Laredo, 150 kw. Deep fades whether slow or rapid, while readily handled by Automatic Volume Control satisfactorily on clear channels, give poor service on a channel like the above. Each time the signal of CBF fades deeply, XENT bursts in with consequent loss of service. On the other hand, a signal with less fading, such as the records indicate for series-excitation, tends to hold down the interference, thus rendering the service more tolerable.

Accordingly, it is considered that these experiments indicate the unsuitability of shunt-excitation for the high power national outlets of the CBC.

However, for high double-tapered towers, or masts no higher than quarter-wave, it appears that there is little to choose between series- and shunt-excitation from the point of view of ground-wave or sky-wave.

Acknowledgments

This work was carried out with the able assistance of W. G. Richardson and J. E. Hayes of the CBC Engineering Department. The ready help and co-operation of the CBF transmitter staff were also invaluable. Special thanks are due the Northern Electric Company for the loan of equipment, calibration of meters, and general interest and help given during the experiments.

References

1. MacKinnon, K. A. Can. J. Research, A, 13 : 60-71. 1935.
2. Morrison, J. F. and Smith, P. H. Bell Telephone Monograph B—938.

Section A

INDEX TO VOLUME 17

Authors

Allcut, E. A. and Ewens, F. G.—Thermal conductivity of insulating materials, 209.

Allen, F.—See Brisbin, G. W. F.

Babbitt, J. D.—The diffusion of water vapour through various building materials, 15.
A large-scale thermal conductance apparatus for the testing of building materials, 164.

Brisbin, G. W. F. and Allen, F.—The elastic extensibility of muscle, 33.

Cornish, W. E.—See Morrison, I. F.

Demers, P.—Une électrode argent-carbonate d'argent obtenue par électrolyse, 77.

Ewens, F. G.—See Allcut, E. A.

Field, G. S.—Dispersion and selective absorption in the propagation of ultrasound in fluids contained in tubes, 197.
The resonant radial frequencies of a cylinder of any wall thickness, 141.

Field, G. S.—See Johnson, J. S.

Field, R. H.—Note on the permanence of standards of length, 71.

Hay, G. E.—The equilibrium of a thin compressible membrane, 106.
The equilibrium of a thin compressible membrane with application to the periodontal membrane, 123.

Hillier, J. -The effect of chromatic error on electron microscope images, 64

Hillier, J.—See Prebus, A.

Johns, H. E.—The viscosity of liquid hydrogen, 221.

Johns, H. E., Wilhelm, J. O., and Smith, H. G.—The flow and viscosity of liquid helium, 149.

Johnson, J. S. and Field, G. S.—An apparatus for the detection of magnetic materials, 194.

McKinley, D. W. R.—Measurement of small optical activities with the quartz crystal light modulator, 202.

MacKinnon, K.—Experimental comparison of shunt- and series-excitation of a high, uniform cross section, vertical radiator, 227.

Morrison, I. F. and Cornish, W. E.—Description of a pressure cell for the measurement of earth pressure, 216.

Prebus, A. and Hillier, J.—The construction of a magnetic electron microscope of high resolving power, 49.

Ruedy, R.—Vibrations on power lines in a steady wind. VI. Forced vibrations of uniform strings and of strings with strengthened ends under the action of uniform periodic forces, 1.

Sanders, F. H.—Transmission of sound through thin plates, 179.

Sargent, B. W.—The β- and γ-rays of actinium B and C″, 82.
The half-periods of actinium B, actinium C″, and uranium X_1, 103.

Smith, H. G.—See Johns, H. E.

Wilhelm, J. O.—See Johns, H. E.

Section A

INDEX TO VOLUME 17

Subjects

Absorption
of β-rays of actinium B and actinium C'', 97.
Selective, in the propagation of ultrasound in fluids contained in tubes, 197.

Absorption method of finding the end-point of a β-ray spectrum, Improvement of, 82.

Actinium active deposit. Growth curves of,
Experimental, 93.
Theoretical, 92.

Actinium B
β- and γ-rays of, 82.
Half-period of, 103.

Actinium (B+C), γ-Rays of, 98.

Actinium C''
β- and γ-rays of, 82.
Half-period of, 104.

Aluminium covered fibreboard, Thermal conductance of, 174.

Asphalt felt, Moisture diffusion coefficient of, 22.

Beta-ray intensities, Measurements of, in the determination of the half-periods of actinium B, actinium C'', and uranium X_1, 103.

Beta-rays of actinium B and of actinium C'', Absorption of, 97.

Beta-spectra, Range method of determining maximum energies of, 87.

Brass plates, Transmission of high frequency sound through, 183.

Broadcasting, See Radiator.

Building materials
Large-scale thermal conductance apparatus used for testing, 164.
Thermal conductivity of, 209.
Various, Diffusion of water vapour through, 15.

Canadian legal standards of length, Permanence of, 73.

Conductance, Thermal, and conductivity of insulating materials, 209.

Conduction, Heat, See Thermal conductivity.

Convection, See under Thermal conductivity.

Chromatic error, Effect of, on electron microscope images, 64.

Cork, Rock, Thermal conductance of, 175.

Corkboard, Pressed, Moisture diffusion coefficient of, 22.

Cylinder of any wall thickness, Resonant radial frequencies of a, 141.

Density, temperature, and calculated viscosity of liquid hydrogen, 223.

Detector, An apparatus for the detection of magnetic materials, 194.

Diffusion of water vapour through various building materials, 15.
coefficient, moisture
Explanation of, 17.
Measurement of, 18.
Use of, 26.

Dispersion and selective absorption in propagation of ultrasound in fluids contained in tubes, 197.

Earth pressure, A pressure cell for the measurement of, 216.

Elastic extensibility of muscle, 33.

Electrode, Silver–silver-carbonate, obtained by electrolysis, 77.

Electrolysis, Silver–silver-carbonate electrode obtained by, 77.

Electron microscope, Magnetic, of high resolving power,
Applications of, 54.
Construction of, 49.

Electron microscope images, Effect of chromatic error on, 64.

Electron supermicroscope, 49

Equilibrium of a thin compressible membrane, 106.
with application to the periodontal membrane, 123.

Excitation, Shunt- and series-, of a high, uniform cross-section, vertical radiator, Experimental comparison of, 227.

Fibreboard
  Aluminium covered, Thermal conductance of, 174.
  Conductivity, resistance, and thickness of, 210.
  Moisture diffusion coefficient of, 21.

Flow and viscosity of liquid helium, 149.
  Helium I, 155.
  Helium II, 156.

Force(s)
  Arbitrary non-uniform alternating, Response of a strengthened string to, 13.
  Constant periodic, Action of, upon a damped string of uniform cross section, 1.
  Uniform alternating, Response of a strengthened damped string to, 9.

Frequencies, Resonant radial, of a cylinder of any wall thickness, 141.

Gamma-rays of actinium (B+C), 98.

Heat conduction, See Thermal conductivity.

Helium, Liquid, Flow and viscosity of, 149.

High frequency sound, Transmission of, through thin plates, 179.

Hot-box
  and hot-plate thermal conductivity apparatus, Comparison of, 170.
  Description of, 165.

Hot-plate and hot-box thermal conductivity apparatus, Comparison of, 170.

Hydrogen, Liquid, Viscosity of, 221.

Images, Electron microscope, Effect of chromatic error on, 64.

Imperial Standard Yard, Permanence of, 72.

Insulating materials, Thermal conductivity of, 209.

International Metre, Permanence of, 71.

Iron-nickel length standards, Permanence of, 74.

Kraft paper, Moisture diffusion coefficient of, 22.

Legal standards of length, Canadian, Permanence of, 73.

Length, Permanence of standards of, 71.

Lens, Magnetic, Resolving limit of a, 50.

Light modulator, Quartz crystal, Measurement of small optical activities with the, 202.

Liquid helium, Flow and viscosity of, 149.

Magnetic electron microscope of high resolving power, Construction of a, 49.
  Applications, 54.

Magnetic lens, Resolving limit of a, 50.

Magnetic materials, An apparatus for the detection of, 194.

Membrane, Equilibrium of a thin compressible, 106.
  Application to the periodontal membrane, 123.

Metal detectors, An apparatus for the detection of magnetic materials, 194.

Metre, International, Permanence of the, 71.

Microscope, Magnetic electron, of high resolving power, Constructior of, 49.
  Applications, 54.

Microscope images, Electron, Effect of chromatic error on, 64.

Moisture
  Condensation of, in walls and roofs, 15.
  Diffusion of, through various building materials, 15.

Muscle, Elastic extensibility of, 33.

Nerve tissue, Elastic extensibility of, 33.

Nickel-iron length standards, Permanence of, 74.

Nickel plates, Transmission of high frequency sound through, 186.

Optical activities, Small, Measurement of, with the quartz crystal light modulator, 202.

Periodontal membrane, Equilibrium of a thin compressible membrane with application to the, 123.

Pine wood, Moisture diffusion coefficient of, 21.

Plaster, Moisture diffusion coefficient of, 22.

Plaster board, Moisture diffusion coefficient of, 22.

Plates, Thin, Transmission of high frequency sound through, 179.

Power lines, See Vibrations on power lines in a steady wind.

Presdwood, Masonite, Moisture diffusion coefficient of, 22.

Pressure, Earth, A pressure cell for the measurement of, 216.

Pressure, Relations between time, volume, and, for flow experiments with liquid helium, 155.

Pressure cell for the measurement of earth pressure, 216.

Quartz crystal light modulator, Measurement of small optical activities with the, 202.

Radial frequencies, Resonant, of a cylinder of any wall thickness, 141.

Radiator, Vertical, high, uniform cross-section, Experimental comparison of shunt- and series-excitation of a, 227.

Radio, See Radiator.

Radioactivity
- β- and γ-rays of actinium B and actinium C'', 82.
- Half-periods of actinium B, actinium C'', and uranium X_1, 103.

γ-Rays of actinium (B+C), 98.

Resonant radial frequencies of a cylinder of any wall thickness, 141.

Rock cork, Thermal conductance of, 175.

Rock wool
- Moisture diffusion coefficient of, 22.
- Thermal conductivity of, 211.

Roofs, Condensation of moisture in, 15.

Rubber, Black vulcanized, and plasticized rubber hydrochloride, Moisture diffusion coefficient of, 22.

Scutan, Various samples of, Moisture diffusion coefficient of, 22.

Selective absorption, See Absorption, Selective.

Series- and shunt-excitation of a high, uniform cross-section, vertical radiator, Experimental comparison of, 227.

Shredded Redwood bark, Thermal conductivity of, 215.

Shunt- and series-excitation of a high, uniform cross-section, vertical radiator, Experimental comparison of, 227.

Silver-silver-carbonate electrode obtained by electrolysis, 77.

Slag wool, Thermal conductivity of, 21 .

Sound
- Calculation of shape of standing waves produced by a plane wave of, or by a steady wind, 1.
- High frequency, Transmission of, through thin plates, 179.
- waves, Longitudinal, in a fluid-filled tube, 197.

β-Spectra, Range method of determining maximum energies of, 87.

Spruce wood, Moisture diffusion coefficient of, 21.

Standards of length, Permanence of, 71.

Strings, Uniform and with strengthened ends, Forced vibrations of, under the action of uniform periodic forces, 1.

Temperature
- and vapour gradient through a wall
  - with vapour barrier, 27.
  - without vapour barrier, 31.
- density, and calculated viscosity of liquid hydrogen, 223.
- Relation between the viscosity of liquid helium and, 160.

Temperature gradients in insulating materials, 27, 211, 213.

Thermal conductance and conductivity of insulating materials, 209.

Thermal conductance apparatus, Large-scale, used for testing building materials, 164.

Thermal conductivity
- and conductance, 209.
- of building materials, Large-scale apparatus for measurement of, 164.
  - Comparison of hot-box and hot-plate apparatus, 170.
- of insulating materials, 209.
  - convection effects, 212.
  - surface resistance, 210.

Tissue, Muscle and nerve, Elastic extensibility of, 33.

Tooth, Periodontal membrane between jawbone and, Equilibrium of a thin compressible membrane with application to the, 123.

Ultrasound in fluids contained in tubes, Dispersion and selective absorption in the propagation of, 197.

— V —

Uranium X_1, The half-period of, 104.

Vapour gradient through a wall, 27, 31.

Vertical radiator, See Radiator, Vertical.

Vibrations on power lines in a steady wind
- VI. Forced vibrations of uniform strings and of strings with strengthened ends under the action of uniform periodic forces. 1.

Viscosity of
- liquid helium, 155.
- liquid hydrogen, 221.

Walls, Condensation of moisture in, 15.

Water vapour, The diffusion of, through various building materials, 15.

Waves
- Sound, Transmission of, down a fluid-filled tube, 197.
- Standing, produced by plane wave of sound or by a steady wind, Calculation of shape of, 1.

Wind, See Vibrations on power lines in a steady wind.

Wood, Diffusion of water vapour through, 21.

Yard, Imperial Standard, Permanence of the, 72.

I.A.R.I. 75

INDIAN AGRICULTURAL RESEARCH
INSTITUTE LIBRARY, NEW DELHI.

Date of Issue	Date of Issue	Date of Issue
10-7-58		

GIPNLK—H-40 I.A.R.I.—29-4-5—15,000